AD-A061 099 NEW YORK UNIV N Y DEPT OF PHYSICS F/G 7/4
THEORETICAL STUDIES RELATING TO THE INTERACTION OF RADIATION WI--ETC(U)
OCT 78 P R BERMAN, E J ROBINSON N00014-77-C-0553

UNCLASSIFIED NL

1 OF 2
ADA
061099

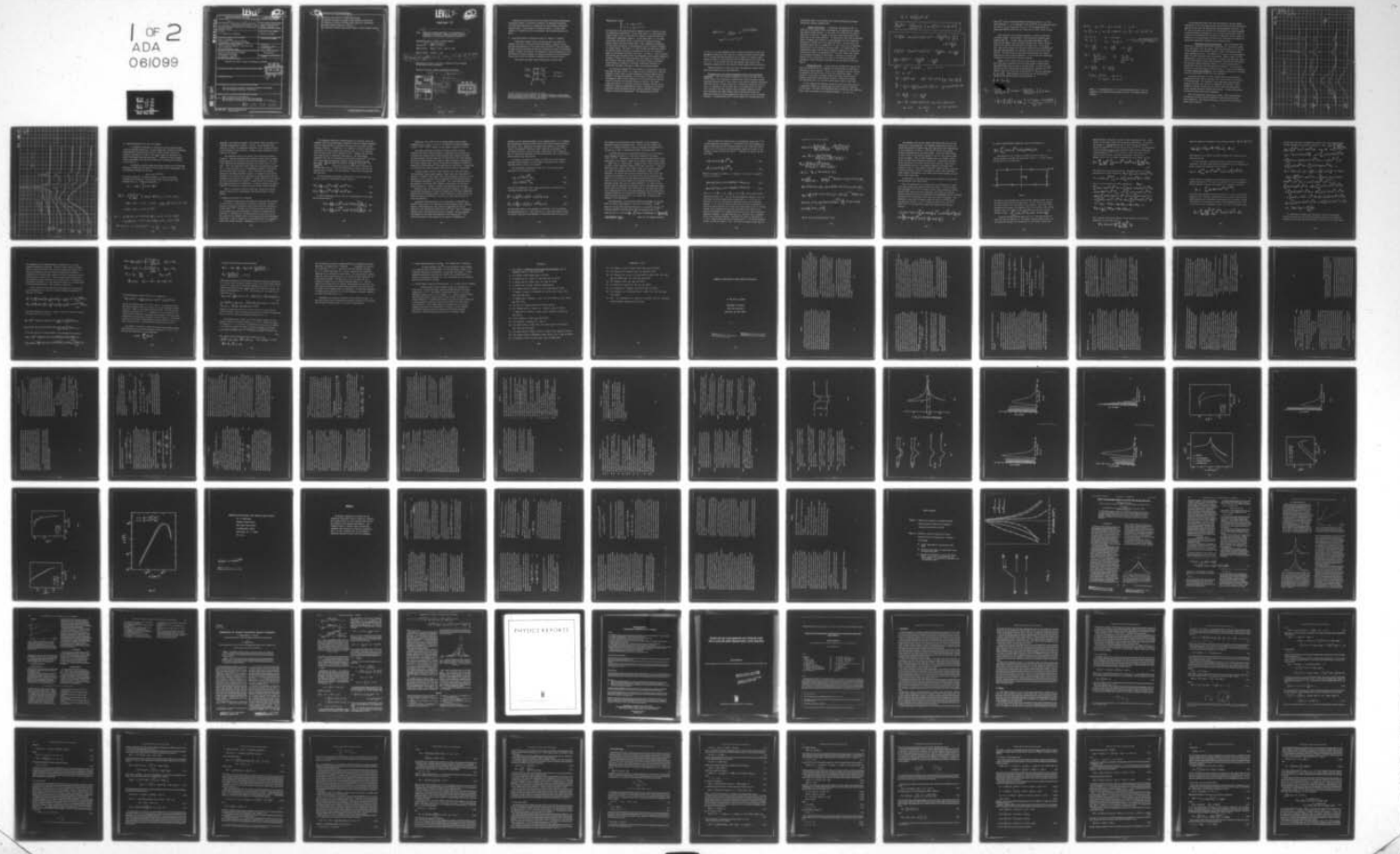

LEVEL II

SECURITY CLASSIFICATION OF THIS PAGE (When [illegible])

REPORT DOCUMENTATION PAGE

READ INSTRUCTIONS BEFORE COMPLETING FORM

1. REPORT NUMBER: AR 1	2. GOVT ACCESSION NO.
3. RECIPIENT'S CATALOG NUMBER	
4. TITLE (and Subtitle): Theoretical Studies relating to the Interaction of Radiation with Matter: Atomic Collision Processes Occurring in the Presence of Radiation Fields	5. TYPE OF REPORT & PERIOD COVERED: Annual Report (Interim) 8/1/77 - 7/31/78
	6. PERFORMING ORG. REPORT NUMBER
7. AUTHOR(s): P.R. Berman, E.J. Robinson	8. CONTRACT OR GRANT NUMBER(s): N00014-77-C-0553
9. PERFORMING ORGANIZATION NAME AND ADDRESS: Prof. P.R. Berman, Physics Dept. - New York University, 4 Washington Pl., New York, N.Y. 10003	10. PROGRAM ELEMENT, PROJECT, TASK AREA & WORK UNIT NUMBERS
11. CONTROLLING OFFICE NAME AND ADDRESS: Office of Naval Research - Code 613C: MAK, 800 N. Quincy St., Arlington, Virginia 22217	12. REPORT DATE: October 1, 1978
	13. NUMBER OF PAGES: 111
14. MONITORING AGENCY NAME & ADDRESS (if different from Controlling Office): Office of Naval Research Resident Representative New York, 715 Broadway - 5th Floor, New York, N.Y. 10003	15. SECURITY CLASS. (of this report): Unclassified
	15a. DECLASSIFICATION/DOWNGRADING SCHEDULE

16. DISTRIBUTION STATEMENT (of this Report)

Approved for public release; distribution unlimited

17. DISTRIBUTION STATEMENT (of the abstract entered in Block 20, if different from Report)

18. SUPPLEMENTARY NOTES

19. KEY WORDS (Continue on reverse side if necessary and identify by block number)

Laser Spectroscopy, Optical Collisions, Radiative Collisions, Velocity-Changing Collisions, Photon Echo

20. ABSTRACT (Continue on reverse side if necessary and identify by block number)

Work is reported in the areas of
Contents: (1) Collisional studies using laser spectroscopy,
(2) The nature and validity of collision kernels, → next page

DDC RECEIVED NOV 9 1978 D

AD A061099

DDC FILE COPY

78 10 26 036

DD FORM 1 JAN 73 1473 EDITION OF 1 NOV 65 IS OBSOLETE
S/N 0102-LF-014-6601

SECURITY CLASSIFICATION OF THIS PAGE (When Data Entered)

(3) Strong field effects in laser spectroscopy;
(4) Optical collisions including a model potential calculation;
(5) Radiative collisions including model potential calculations;
(6) Laser assisted heating or cooling; and
(7) Collisional studies using photon echoes or Optical Ramsey Fringes.

LEVEL II

12

Annual Report (AR1)

(6)

Title: "Theoretical Studies Relating to the Interaction of Radiation with Matter: Atomic Collision Processes Occurring in the Presence of Radiation Fields"

Supported by the U.S. Office of Naval Research

(15) Contract No.: N00014-77-C-0553

Report Period: August 1, 1977 - July 31, 1978

Date of Report: October 1, 1978

(9) Annual repts. no. 1, 1 Aug 77-31 Jul 78,

(10) P. R. / Berman
E. J. / Robinson

(11) 1 Oct 78

(12) 134p.

Research has been carried out in the areas of (1) Laser Spectroscopic Collisional Studies, (2) Optical Collisions, (3) Radiative Collisions, (4) Laser Assisted Cooling or Heating and (5) Photon Echoes and Optical Ramsey Fringes. These subjects are described below. In cases where preprints or reprints are not yet available, more detailed accounts are given.

1. Laser Spectroscopic Collisional Studies (P. Berman, J. LeGouet)

Three-level systems offer an interesting and novel means for studying collisions in atomic and molecular systems. Our work in this area has been summarized in two recent review articles[1,2*] with the latter of these articles stressing the physical principles involved in three-level systems. Current work involves the extension of these calculations to allow for different collision models, to include the effects of strong radiation fields, and to test the validity of generally used collision kernels.

The three-level system under consideration is shown below

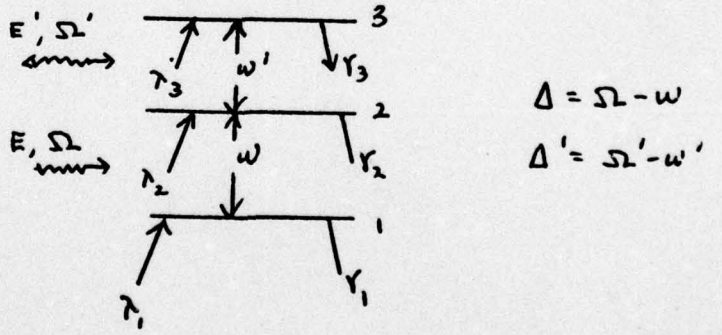

* Stars indicate articles published or submitted during the report period which are appended to this report. The reader is referred to these articles for detailed discussions of the subject matter.

Monochromatic fields

$$\vec{E} = \hat{\imath}\, E \cos(kz - \Omega t)$$
$$\vec{E}' = \hat{\imath}\, E' \cos(k'z - \Omega' t)$$

are incident on the system detuned by amounts Δ and Δ' from the 1-2 and 2-3 transitions respectively. If the "pump field" E is tuned within the Doppler width of the 1-2 transition, it excites a subset of atoms with a particular longitudinal velocity. On the other hand, if it is tuned well outside the Doppler width, it excites all velocity subclasses equally (albeit with small probability). Thus, depending on detuning, one can either selectively or non-selectively excite velocity subclasses in a given system. The field E' is used to probe the population density (in velocity space) excited by the pump field as well as to provide a means for two-quantum absorption from state 1 to state 3. Since collisions with foreign gas perturbers affect the absorptive and dispersive properties of media, a study of the probe absorption line shape as a function of Δ' for different fixed pump detunings Δ can provide valuable information (cross sections, strengths of collision, interatomic potential) on collisional processes occurring in atomic and molecular systems.

Our previous treatments[1,2] have utilized (1) perturbation theory for both pump and probe fields, (2) a model in which collisions are velocity-changing in their effect on level populations (diagonal density matrix elements) and phase-interrupting in their effort on optical coherences (off-diagonal density matrix elements) (3) the Keilson-Storer collision kernel[3] to describe the velocity-changing collisions. The phase - interrupting nature of collisions on optical coherences (giving rise to traditional pressure broadenings and shifts) is appropriate if the two transition levels associated with the optical coherence experience different collisional interactions.[2] The Keilson-Storer kernel[3]

$$W(\vec{v}' \to \vec{v}) = \frac{1}{(\pi u^2)^{3/2}} e^{-(\vec{v} - \alpha \vec{v}')^2/(\Delta u)^2}$$

$$(\Delta u)^2 = (1 - \alpha^2) u^2$$

($0 \leq \alpha \leq 1$; u = most probable speed of thermal distribution) giving the probability density per unit time for a collision induced velocity change $\vec{v}' \to \vec{v}$ is valid for weak collisions, but is suspect for strong or hard sphere collisions if the perturber to active atom mass ratio is large and if $v' \gtrsim u$. It is a kernel that has been commonly used owing to its analytical properties, but has received limited experimental verification.

Several situations in which the above approximations became invalid have been explored and are discussed below.

Collisions which are velocity-changing in their effect on optical coherences[4*]. When the collision interaction is nearly the same for two levels involved in a transition, collisions are velocity-changing (rather than phase-interrupting) in their effect on the optical coherence associated with those levels. We have carried out a theoretical calculation for this case. In particular, we have shown that, if the populations in levels 1 and 2 are nearly the same, owing to some incoherent pumping, then the probe absorption line shape clearly reflects whether collisions are phase-interrupting or velocity-changing in their effect on the 1-3 optical coherence. An experimental test[5] of these results for excited state rare

gas systems seems to be consistent with phase-interrupting collisions rather than velocity changing ones.

Transit-time effects. In analyzing experimental data[5] in which one of the energy levels is metastable, the importance of transit time effects became evident. In this case, the lifetime of the atom is determined by the time it spends in the laser field rather than by the decay time of the levels involved. We were able to show that a simplified model of transit time effects is in good agreement with more extensive calculations[6] carried out in the weak field limit. In this model, the metastable decay rate γ is replaced by $\gamma + v_t/R$ where v_t is a transverse velocity and R is the radius of the light beam. The transit time can significantly affect the saturation parameter (important in strong field calculations) which is proportional to γ^{-1} and this simple model allows for an adequate treatment of this effect. Inclusion of transit time effects led to a correction to the value of the saturation papameter measured by linear absorption techniques on excited states in the rare gases.[5]

Strong pump field. In many cases of experimental interest, the pump field exciting the 1-2 transition is strong enough to invalidate a perturbation theory approach. Thus it is of important practical interest to generalize our earlier work to allow for strong pump fields. In the absence of collisions, line shape formulas have been derived[7] which, although algebraically complicated, are easily evaluated on computer. Line splittings due to the ac Stark effect may be seen in some cases.

We have obtained the equations giving the probe field absorption in a three-level system with a strong pump field and collisions occurring in the system. The probe field absorption may be written as (for simplicity level 1 only is assumed to be incoherently pumped - $\lambda_2 = \lambda_3 = 0$)

$$I \propto Im \int \tilde{e}_{23}(\vec{v})\, d\vec{v}$$

$$\tilde{e}_{23}(\vec{v}) = \frac{-i\chi'}{\mu_{13}\mu_{23} + \chi^2}\left[\mu_{13}\, e_{22}^{(0)}(\vec{v}) + i\chi\, e_{12}^{(0)}(\vec{v})\right]$$

$$\Gamma_1^t\, \bar{e}_{11}^{(0)}(\vec{v}) - \int W_{11}(\vec{v}'\to\vec{v})\, \bar{e}_{11}^{(0)}(\vec{v}')\, d\vec{v}' = \frac{2\tilde{\gamma}_{12}\chi^2 N_0}{\tilde{R}^2}\left(1 - \frac{\gamma_2'}{\Gamma_2^t}\right) + \tilde{f}\,\frac{2\tilde{\gamma}_{12}\chi^2}{\tilde{R}^2}$$

$$\Gamma_2^t\, e_{22}^{(0)}(\vec{v}) - \int W_{22}(\vec{v}'\to\vec{v})\, e_{22}^{(0)}(\vec{v}')\, d\vec{v}' = -\frac{2\tilde{\gamma}_{12}\chi^2 N_0}{\tilde{R}^2} - \tilde{f}\,\frac{2\tilde{\gamma}_{12}\chi^2}{\tilde{R}^2}$$

$$\tilde{e}_{12}^{(0)}(\vec{v}) = \tilde{e}_{21}^{(0)}(\vec{v})^* = \frac{i\chi\mu_{12}^* N_0}{\tilde{R}^2} + \frac{i\chi\mu_{12}^*}{\tilde{R}^2}$$

$$\bar{e}_{11}^{(0)} = e_{11}^{(0)} - N_0 W_0(\vec{v}) \quad ; \quad N_0 = \Gamma_1/\gamma_1$$

$$\Gamma_i^t = \gamma_i + \Gamma_i^{vc}$$

$$\tilde{R}^2 = (\gamma_{12}^B)^2 + \Delta^2 \qquad (\gamma_{12}^B)^2 = \tilde{\gamma}_{12}^2 + 2\chi^2\tilde{\gamma}_{12}\left[\frac{1}{\Gamma_2^t} + \frac{1}{\Gamma_1^t}\left(1 - \frac{\gamma_2'}{\Gamma_2^t}\right)\right]$$

$$\tilde{f} = \frac{1}{\Gamma_2^t}\left(1 - \frac{\gamma_2'}{\Gamma_1^t}\right)\int W_{22}(\vec{v}'\to\vec{v})\, e_{22}^{(0)}(\vec{v}')\, dv' - \frac{1}{\Gamma_1^t}\int W_{11}(\vec{v}'\to\vec{v})\, \bar{e}_{11}^{(0)}(\vec{v}')\, d\vec{v}'$$

$$\chi = \frac{\rho_{12}E}{2\hbar} \quad ; \quad \chi' = \frac{\rho_{23}E'}{2\hbar}$$

$$\mu_{13} = \tilde{\gamma}_{13} + i(\Delta + \Delta' + (k-k')v) \quad ; \quad \mu_{23} = \tilde{\gamma}_{23} + i(\Delta' - k'v)$$

$$k = \omega/c \qquad k' = \omega'/c \qquad \mu_{12} = \tilde{\gamma}_{12} + i(\Delta - kv)$$

where Γ_i^{vc} = rate of velocity-changing collisions in level i; χ,χ' are field strengths E , E' in frequency units; $W_{ii}(\vec{v}'\to\vec{v})$ is the collision kernel for state i; γ_{ij} is decay rate of ρ_{ij} $(i \neq j)$ including effects of phase-interrupting collisions; γ_2' = decay rate of level 2 back to level 1.

These equations are virtually impossible to solve for arbitrary collision kernels. A key quantity is the saturation broadened homogeneous width γ_{12}^B . In most laser spectroscopy experiments, γ_{12}^B is less than the Doppler width and γ_{12}^B/k represents the width of the hole burnt in the velocity distribution by the pump field. If $k\Delta u \lesssim \gamma_{12}^B$ (Δu = rms velocity change per collision) collisions are relatively weak and a good approximation is to take the collision kernel of the form $W(\vec{v}'-\vec{v})$. For this kernel we have solved the equations and obtained solutions in terms of Bessel functions. As yet we have not numerically evaluated the line profiles that were obtained.

Another case of interest which we have solved is that in which $k\Delta u > \gamma_{12}^B$; <u>i.e.</u> collisions which are strong enough to remove atoms from the velocity hole created by the pump field. In that limit, the $\mathcal{F}$ terms in the equations may be dropped and the equations for $\rho^{(0)}$ reduce to the form of the weak field equations[1,2] with the replacement of γ_{12} by γ_{12}^B. These equations were solved for the Keilson-Storer Kernel and the resulting probe field absorption is

$$I \propto \mathrm{Im}\,\tilde{\rho}_{23}$$

$$\tilde{\rho}_{23} = \frac{\chi^2\chi' N_0}{k_{12}k_{23}k_{13}u^3}\sum_{j=1}^{4} A_j Z_j(\pi_j) - \frac{2\tilde{\gamma}_{12}\chi^2\chi' N_0}{\Gamma_2^t k_{12}^2 k_{23} u^3}\left\{\sum_{j=1}^{4} D_j Z_j(\pi_j)\right.$$

$$\left. + \sum_{j=1}^{2} B_j \sum_{n=1}^{\infty}\left(\frac{\Gamma_2^{vc}}{\Gamma_2^t}\right)^n \frac{1}{\sqrt{\pi}}\frac{1}{\sqrt{1-\alpha^{2n}}}\int_{-\infty}^{\infty}\frac{e^{-x^2} Z_j\left[(\pi_j-\alpha^n x)\frac{1}{\sqrt{1-\alpha^{2n}}}\right]}{|\pi_3 - x|^2}\right\}$$

$$k_{12} = k \; ; \quad k_{23} = \epsilon k' \; ; \quad k_{13} = k + \epsilon k' \; ; \quad \epsilon = \pm 1$$

$$\eta_{12} = \tilde{\gamma}_{12} + i\Delta \; ; \quad \eta_{13} = \tilde{\gamma}_{13} + i(\Delta + \Delta') \; ; \quad \eta_{23} = \tilde{\gamma}_{23} + i\Delta' \; ; \quad \eta_{12}^{B} = \gamma_{12}^{B} + i\Delta$$

$$\pi_1 = a_1 + c \qquad a_1 = -i\eta_{13}/k_{13}u$$

$$\pi_2 = b_1 - c \qquad b_1 = -i\eta_{23}/k_{23}u$$

$$c = \frac{b_1 - a_1 - \sqrt{(b_1-a_1)^2 + 4\alpha^2/(k_{12}k_{23}u^2)}}{2}$$

$$\pi_3 = \frac{i\eta_{12}^{B} + \alpha}{k_{12}u} \qquad \pi_4 = \frac{-i\eta_{12}^{B}}{k_{12}u} \qquad \pi_5 = \frac{i\eta_{12} + \alpha}{k_{12}u}$$

$$A_i = \frac{\pi_5 - \pi_i}{\prod_{\substack{j=1,4 \\ j\neq i}} (\pi_j - \pi_i)} \qquad D_i = \frac{a_1 - \pi_i}{\prod_{\substack{j=1,4 \\ j\neq i}} (\pi_j - \pi_i)}$$

$$B_1 = \frac{a_1 - \pi_1}{\pi_2 - \pi_1} \qquad B_2 = \frac{a_1 - \pi_2}{\pi_1 - \pi_2}$$

$$Z_j(\pi_j) = \begin{cases} Z(\pi_j) & \mathrm{Im}\ \pi_j > 0 \\ -Z(-\pi_j) & \mathrm{Im}\ \pi_j < 0 \end{cases}$$

where $\epsilon = 1$ (copropagating) or -1 (counter-propagating waves), α is the parameter in the Keilson-Storer kernel, and Z is the Plasma Dispersion function.

In the weak field limit, the first sum reduces to the two-quantum contribution to the line shape and the second to the step wise contribution from atoms which have not experienced velocity-changing collisions. The n^{th} term in the third sum provides the contribution from atoms undergoing n velocity-changing collisions in level 2 before being excited to level 3. We have not yet analyzed the line profile in detail to see the effects of collisions on line splittings, but have so far restricted our analysis to particular experimental situations to be discussed below.

Experiment of Liao and Bjorkholm. Liao and Bjorkholm have carried out a saturation spectroscopy experiment on a three-level system in Na perturbed by the rare gases. Using pump detunings of 4.0 GHz and 1.6 GHz (compared with a Doppler FWHM of 1.7 GHz), they obtained probe field absorption profiles. The analysis of the data is at the preliminary stage, but some conclusions have been reached. Typical large (4.0 GHz) detuning data is shown on the next page. At these large detunings, there is no velocity-selection and velocity-changing collisions are unimportant. The collision induced absorption about $\Delta' = 0$ is the "collisional redistribution term" that has been described elsewhere[1,2] and is also referred to as excitation via an optical collision. A fit of the experiment to theory with no free parameters (all broadening parameters are available from other experiments) yields very good agreement.

At smaller detunings (1.6 GHz), velocity-selection and velocity-changing collisions play an important role as can be seen in the data on the following page. The "shoulder" in the data arises from velocity-changing collisions and increases in magnitude with pressure. First attempts to analyze the data seem to indicate that the Keilson-Storer kernel does not adequately explain these results. We shall test whether a hard-sphere model gives better agreement.

Thus, this experiment offers great promise. With large detunings, one measures collision induced absorption and the various width and shift parameters. With smaller detunings, the nature of the collision kernel can be studied.

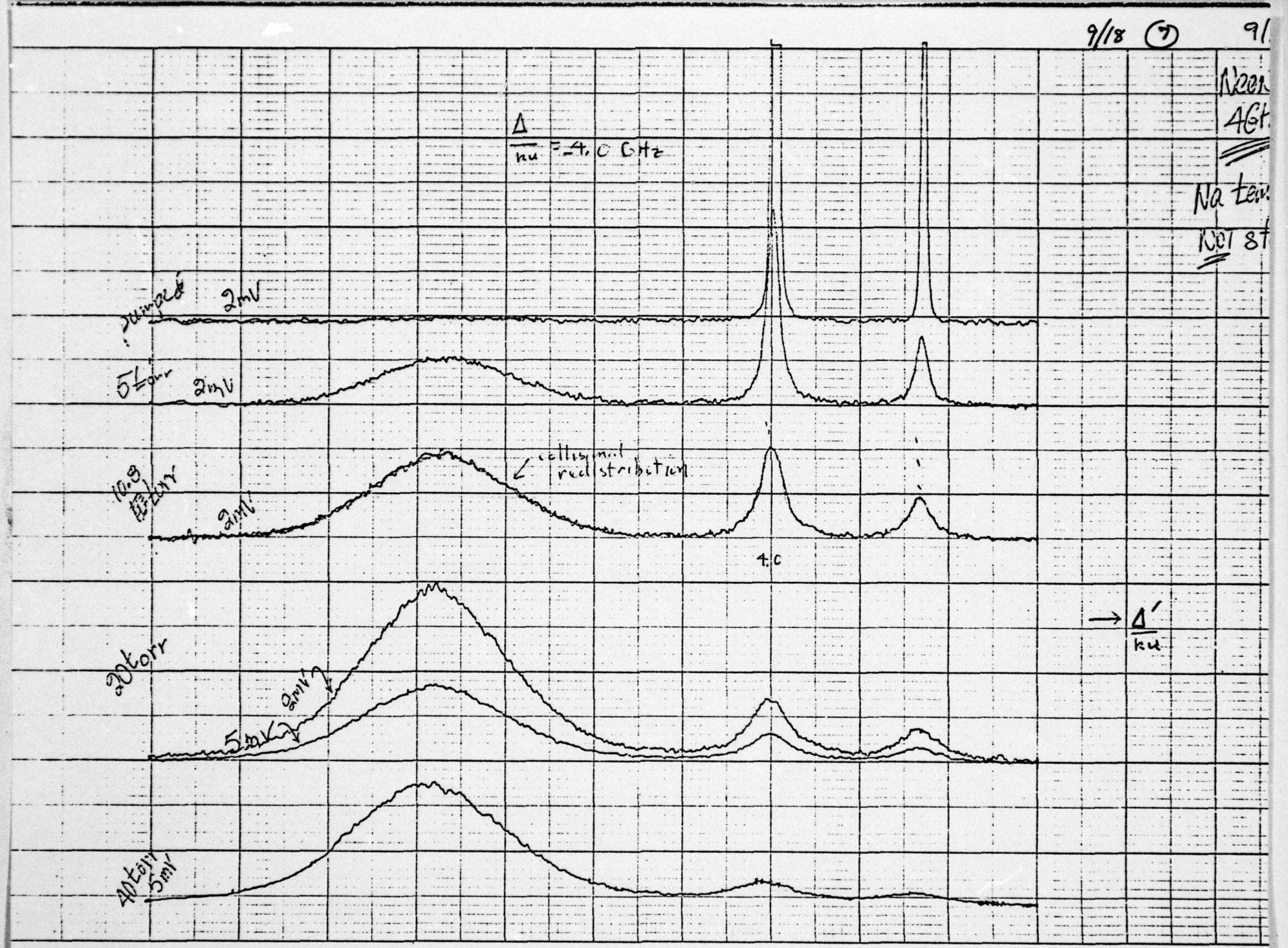
9/18 (7)
Δ/ku = 4.0 GHz
2mV
2mV
2mV
4.0
Δ'/ku
2mV
5mV
5mV

9/18 (5)

Neon
1.6 GHz

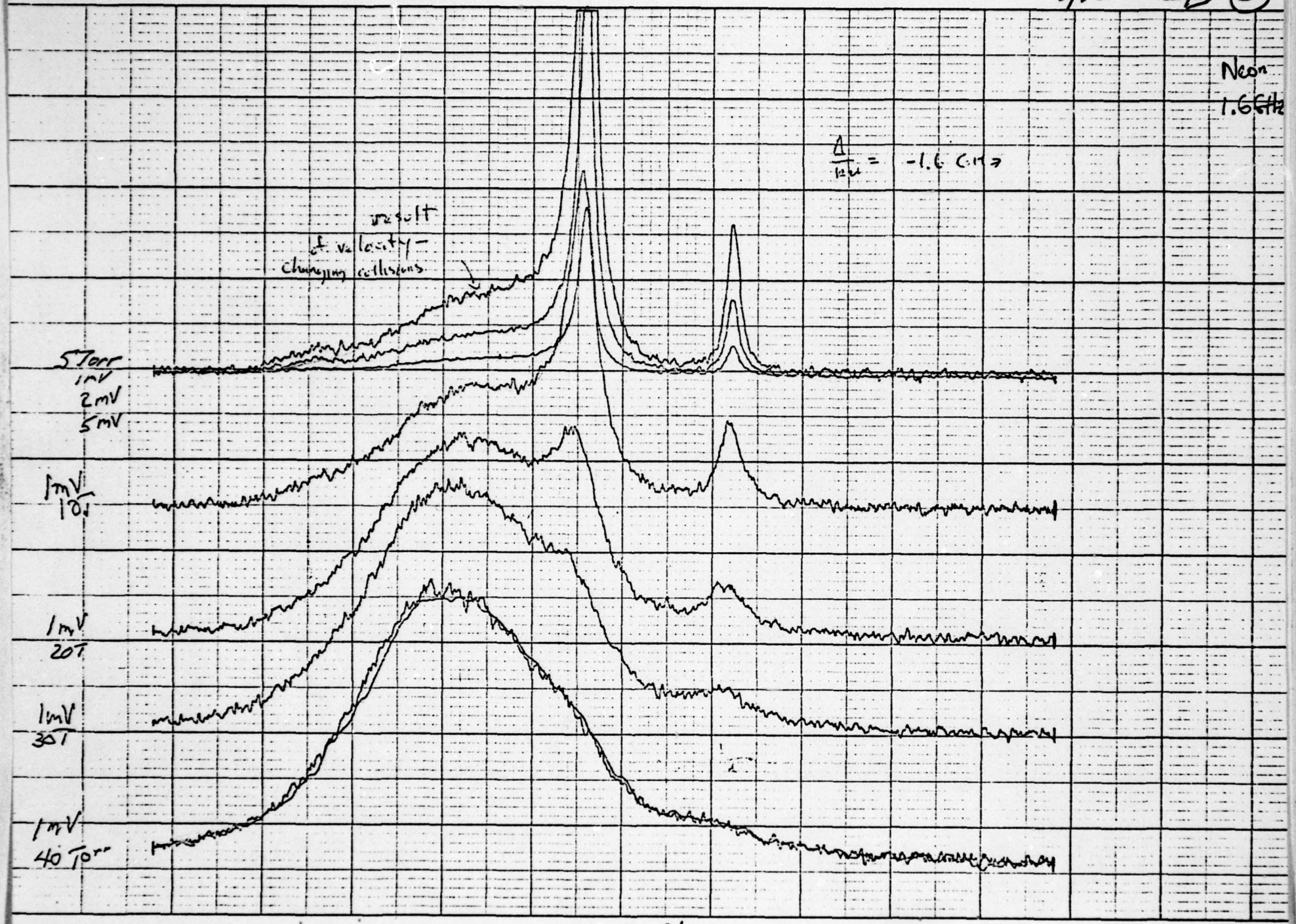

2. Optical Collisions (S.D. Yeh, P.R. Berman)

In "optical collisions", a collision is used to provide energy to aid in radiative excitation. We have termed such a process "Collisionally Aided Radiative Excitation (or Emission)" (CARE) and have carried out numerical calculations of CARE) in two level systems for attractive, repulsive andLennard-Jones type potentials.[8*] Saturation effects, dressed states, bare states, and collision induced level crossings are discussed in our article.[8]

In addition, a model problem was solved with the goal of obtaining additional insight into the nature of the results in CARE calculations. For an interatomic potential of the form

$$V(t) = A(b)\, e^{-|t|/\tau(b)}$$

(b = impact parameter), an analytic solution in terms of tabulated functions may be obtained. This solution, valid for arbitrary field strengths gives an excitation probability P

$$P = 2\pi \eta v \int_0^\infty b\, db\, P(b)$$

$$P(b) = \frac{\chi^2 \Delta^2 A^2 \tau^2}{\sigma^2 |D|^2} \Big| \frac{1}{1 - i\sigma\tau} \Phi(i\mu_2\tau,\, 1 + i\sigma\tau,\, iA\tau)$$

$$\times \Phi(1 - i\mu_2\tau,\, 2 - i\sigma\tau,\, -iA\tau) + \frac{1}{1 + i\sigma\tau} \Phi(-i\mu_2\tau,\, 1 - i\sigma\tau,\, iA\tau)$$

$$\times \Phi(1 + i\mu_2\tau,\, 2 + i\sigma\tau,\, iA\tau) \Big|^2$$

$$D = \mu_1 \Phi(i\mu_2\tau,\, 1 + i\sigma\tau,\, iA\tau)\, \Phi(1 + i\mu_1\tau,\, 1 + i\sigma\tau,\, iA\tau)$$

$$- \mu_2 \Phi(i\mu_1\tau,\, 1 + i\sigma\tau,\, iA\tau)\, \Phi(1 + i\mu_2\tau,\, 1 + i\sigma\tau,\, iA\tau)$$

$$\Delta = \Omega - \omega\,; \quad \sigma = (\Delta^2 + 4\chi^2)^{1/2}\,; \quad \chi = \frac{\rho E}{2\hbar}\,; \quad \mu_{1,2} = \frac{\Delta \pm \sigma}{2}$$

where $\mathcal{N}$ is the perturber density, v the relative speed, and $\phi(a,b,c)$ a confluent hypergeometric function. We have not yet analyzed this solution in detail; the asymptotic properties of the ϕ function are not fully developed in the literature. However, certain properties of the solution are apparent.

The asymptotic solution for larege "red" detunings (attractive potential - negative detuning) where collision induced level crossings occur agrees well with results using power law potentials.[9] For large "blue" detunings the exponential and power law results differ in two ways. First, the potential we have chosen has a discontinuity in slope at t = 0 and this gives rise to an additional asymptotic contribution not found with smooth potentials. Even if this term is discarded, however, the remaining asymptotic solution, on integration over impact parameter, has an inverse power dependence on detuning rather than the exponential one found by other authors.[9] Further analysis of our results as well as those obtained by others[9] is needed before the usefulness of this model potential can be determined. A similar potential was used by Crothers[10] for radiative collisions and may possess similar drawbacks.

Work is continuing on CARE in three-level systems with special emphasis being given to understanding interference effects in these systems.

3. Radiative Collisions (E.J. Robinson)

Considerable experimental and theoretical attention has been paid in recent years to the problem of "radiative collisions", inelastic processes in which two dissimilar atoms collide under the influence of a laser field.[11-18] One atom, A is initially excited, the other, B in its ground state, and the radiation is (nearly) resonant with the difference in excitation of the initial state of A and a level of B. As a result of the combined effect of the collision and the light-matter interaction, A makes a transition to its ground state, B to an excited state, and a photon absorbed. Dynamically, $A^* + B + h\nu \rightarrow A + B^{**}$.

The customary theoretical formulation, which we followed, treats the radiation field and nuclear motion classically (with the further assumption that the latter consists of straight line paths for both atoms) and the electrons quantally. In addition, it is possible to reduce the problem to an effective two level system, where initial state $|1\rangle$ is the composite (A*B) and final state $|2\rangle$ is composite (A,B**). Assuming that the atom-atom potential may be adequately represented by its dipole-dipole asymptotic form (see the references and the enclosed preprint[11*]) and that the rotating wave approximation holds the effective Hamiltonian is

$$H_{eff} = H_a + \sum_{i=1}^{2} |i\rangle\langle i| \left(Q_i R^{-6} + C_i E^2/2\right) + \frac{EB}{2} R^{-3} \left\{ |2\rangle\langle 1| e^{i\Delta t} + |1\rangle\langle 2| e^{-i\Delta t} \right\},$$

where $Q_i C_i$ are the van der Waals' and Stark coefficients for state $|i\rangle$, and B an angle-averaged constant sum over off-diagonal matrix elements. Δ is the detuning. Atomic units are employed here and below.

The time-dependent Schroedinger equations for the state amplitudes α_1 and α_2 become the simultaneous linear equations

$$i\dot{\alpha}_1 = \frac{EB}{2R^3} \alpha_2 e^{i\Delta t} + \left(\frac{C_1 E^2}{2} + Q_1 R^{-6}\right) \alpha_1, \tag{1a}$$

$$i\dot{\alpha}_2 = \frac{EB}{2R^3} \alpha_1 e^{-i\Delta t} + \left(\frac{C_2 E^2}{2} + Q_2 R^{-6}\right) \alpha_2, \tag{1b}$$

A useful alternative form is given by a transformation to the interaction representation.[13]

$$i\dot{\alpha}_1 = \frac{EB}{2R^3} \alpha_2 e^{i\Delta t} \exp\left\{ i(Q_1 - Q_2) \int_0^t \frac{ds}{R^6(s)} \right\}, \tag{2a}$$

$$i\dot{\alpha}_2 = \frac{EB}{2R^3} \alpha_1 e^{-i\Delta t} \exp\left\{ i(Q - Q_2) \int_0^t \frac{ds}{R^6(s)} \right\}. \tag{2b}$$

Either Eqs. (1) or (2) are to be solved subject to the initial condition at $t = -\infty$, $\alpha_1 = 1$, $\alpha_2 = 0$. In terms of the impact parameter ρ, $R(t) = (v^2t^2 + \rho^2)^{1/2}$, where v is the relative velocity of A and B.

Our initial plan was to exploit the simple structure of this effective two level problem by solving it numerically on a machine, and to present the results without being concerned about analytic solutions. We found, however, that the step size in time required for large detuning and/or small impact parameters tended to produce extremely time-consuming and costly computer jobs. We also found that the asymptotic methods discussed by the Soviet authors[14] were quantitatively unreliable. Consequently, we elected to seek model problems which could be solved in closed form.

A useful, simpler version of the problem is the weak field limit. (In the context of the present problem, "weak" means less than about 10^7 watt/cm^2.) Geltman[15] and Knight[16] have obtained analytic solutions to this problem in the low intensity case by ignoring the level-shifting term in the effective Hamiltonian, $V_{LS} = (Q_1 - Q_2)/R^6$. This simplification enables the problem to be reduced to an integral representation of a modified Bessel function K_1. However, it yields some unphysical results, e.g., lineshapes which are symmetrical about exact resonance. It also fails to generate oscillations of transition probabilities for impact parameters smaller than the Weisskopf radius. These omissions are quite serious, and lead us to prefer calculations in which V_{LS} is taken into account, at least approximately.

An immediate generalization of the calculations of Geltman[15] and Knight[16] may be made if one replaces the actual asymptotic level shifting term by a delta-function in time, where the coefficient of $\delta(t)$ is adjusted to the actual phase induced by the R^{-6} term. The R^{-3} transition-inducing term is included exactly in this treatment. We have completed our analysis of this model and submitted it for publication.[11] The closed form nature of the solution of the earlier investigators is

retained, but the spurious symmetry of the spectrum about $\Delta = 0$ is removed. The oscillations referred to above, which arise from interference effects, are present, also. Curiously, the impact model predicts a line shape closer to experiment[12] than does "exact" numerical calculations.[13] We are unable to account for this apparent "superiority", and it might be due to a fortuitous cancellation of errors applicable only to the specific atoms studied by the Harris group.

It would be of interest to extend the impact level shift model to arbitrary field strengths. We were unable to accomplish this without some modification, which we now discuss.

The interaction representation form, Eqs. (2), of the two level equations is of the general form

$$i\dot{\alpha}_1 = V^*(t)e^{i\Delta t}\alpha_2, \tag{3a}$$

$$i\dot{\alpha}_2 = V(t)e^{-i\Delta t}\alpha_1. \tag{3b}$$

The pair of simultaneous first order equations may be replaced by two non-coupled second order equations[19]

$$\ddot{\alpha}_1 - \left[\left(\frac{\dot{V}}{V}\right)^* + i\Delta\right]\dot{\alpha}_1 + |V|^2\alpha_1 = 0, \tag{4a}$$

$$\ddot{\alpha}_2 - \left[\left(\frac{\dot{V}}{V}\right) - i\Delta\right]\dot{\alpha}_2 + |V|^2\alpha_2 = 0. \tag{4b}$$

For arbitrary fields, it is necessary to solve Eqs. (3) or (4) without the approximation $\alpha_1 \cong 1$. Even with $V_{LS} = 0$, I have been unable to find an analytic solution to this equation. (Since there does not seem to be

any reference to the solution to this equation in the literature, apparently neither has anybody else). If Eqs. (4) were solvable for $V_{LS} = 0$, it would be possible to obtain an immediate generalization to the case $V_{LS} = A\delta(t)$, a strong field impact level shift model.

A problem that has been solved exactly with $V_{LS} = 0$ is the Rosen-Zener problem, for which $V = K \operatorname{sech} \pi t/T$, instead of the present $(v^2t^2 + \rho^2)^{-3/2}$. (Presumably, this arises from the milder nature of the singularity in the complex t plane for the former compared to the latter - - simple pole vs. branch point). Along the real t axis, however, there is quite a close resemblance between $R^{-3}(t)$ and $K \operatorname{sech} \pi t/T$ - - that is, there should be, at most, only a small change in the numbers generated by a power law coupling potential and a hyperbolic secant coupling potential. We verified this in the weak-field impact level shift case, choosing the parameters of $K \operatorname{sech} \pi t/T$ so that the two potentials are equal at $t = 0$, and gave the same transition amplitude at zero detuning. (Since we work in the time domain, the constants characterizing the hyperbolic secant vary with the impact parameter). It turns out that not only does the hyperbolic secant-impact level shift (HSILS) model agree exactly with the R^{-3}-impact level shift model at zero detunings, (this is by construction) but also for large detunings, with the greatest discrepancy between the two occurring at intermediate values of Δ, where we found cross-sections differing by up to about 10%. We consider this situation to be satisfactory.

For completeness, the weak-field transition amplitude in the HSILS model is given by the quadrature, $|\alpha_2(+\infty)| = 2K\left|\cos\frac{\phi}{2}\int_0^\infty \operatorname{sech}\frac{\pi t}{T}\cos\Delta t\, dt + \sin\frac{\phi}{2}\int_0^\infty \operatorname{sech}\frac{\pi t}{T}\sin\Delta t\, dt\right|$, where ϕ is defined as for the R^{-3} coupling potential (see preprint), and the integrals given by $\int_0^\infty \cos ax \operatorname{sech} Bx\, dx = \pi/2B \operatorname{sech}\frac{a\pi}{2B}$, $\int_0^\infty \sin ax \operatorname{sech} Bx\, dx = -\frac{\pi}{2B}\tanh\frac{a\pi}{2B} + \frac{1}{B}\operatorname{Im}\psi\left(\frac{1}{4} + \frac{ia}{4B}\right)$, where ψ is the digamma function.

Thus we regard the substitution of the hyperbolic secant for R^{-3} as a minor additional approximation. Our motivation for the replacement is that the HSILS model may be directly extended to the strong field limit, which, for $t \neq 0$, obeys the same differential equations as apply to the classical problem of Rosen and Zener.[20] Equations (3) become, for non-zero times

$$i\dot{\alpha}_1 = K \operatorname{sech} \frac{\pi t}{T} e^{i\Delta t} \alpha_2, \tag{5a}$$

$$i\dot{\alpha}_2 = K \operatorname{sech} \frac{\pi t}{T} e^{-i\Delta t} \alpha_1. \tag{5b}$$

Making the change of variable, $z = (\tanh \pi t/T + 1)/2$, Eqs. (4) become[19], for $t \neq 0$ ($z \neq 1/2$)

$$z(z-1)\alpha_1'' + [C_1 - (1+a+b)z]\alpha_1' - ab\alpha_1 = 0, \tag{6a}$$

$$z(z-1)\alpha_2'' + [C_2 - (1+a+b)z]\alpha_2' - ab\alpha_2 = 0, \tag{6b}$$

where $a = -b = \frac{kT}{\pi}$, $C_1 = \frac{1}{2} - i\frac{\Delta t}{2\pi}$, $C_2 = \frac{1}{2} + i\frac{\Delta t}{2\pi}$. Primes denote differention with respect to z. This is the hypergeometric equation. Eqs. (6) are subject to the indicated initial conditions at $t = \alpha$ ($z = 0$), so that for $z < 1/2$, the solutions are identical to the pure Rosen-Zener problem. At $z = 1/2$, the level-shifting delta function is switched on. Taking the delta function to act only in the upper state (this may be done without loss of generality since only the relative level shift is of physical significance), it changes the phase of α_2 by ϕ, while leaving the magnitude unchanged. The amplitude factor α_1, and hence α_2' is unchanged by the level shifting potential. Therefore the latter is continuous at $z = 1/2$. These provide new initial conditions at $z = 1/2$ for the solution of Eqs. (6) for the region $z > 1/2$. Our desired solution is the value of

a_2 at $z = 1$ ($t = +\infty$), to wit

$$\alpha_2(z=1) = \frac{\bar{A}_2 (\Gamma(c_2))^2}{\Gamma(c_2-a)\,\Gamma(c_2+a)} + \frac{\bar{B}_2 (\Gamma(2-c_2))}{\pi b \csc b} \tag{7}$$

where $\bar{A}_2 = \dfrac{-2H_2 T K A_1 G_1}{\pi(G_2 P_2(1-e^{\phi})) - H_2 Q_2)}$,

$$\bar{B}_2 = \frac{2T G_2 (1-e^{\phi}) K A_1 G_1}{\pi (G_2 P_2 (1-e^{\phi})) - H_2 Q_2)},$$

$A_1 = 1$, $G_2 = F(a, b, c_2, \frac{1}{2})$

$A_2 = \dfrac{KT}{\pi |(1-c_2)|}$, $H_2 = \left(\frac{1}{2}\right)^{1-c_2} F(a-c_2+1, b-c_2+1, 2-c_2, \frac{1}{2})$,

$G_1 = F(a, b, c, \frac{1}{2})$, $H_1 = F(a-c_1+1, b-c_1+1, 2-c_1, \frac{1}{2})$,

$Q_2 = \dfrac{ab}{c_2} F(a+1, b+1, c_2+1, \frac{1}{2})$, $P_2 = \{\frac{1}{2}^{1-c_2} F(a-c_2+1,$

$b-c_2+1, 2-c_2, \frac{1}{2}) + (1-c_2)(\frac{1}{2})^{-c_2} \dfrac{ab}{c_2} F(a-c_2+2,$

$b-c_2+2, 3-c_2, \frac{1}{2})\}$.

The F's are Gauss hypergeometric series.

The numerical work for the strong field HSILS model has been completed and is being analyzed. Our findings indicate that there is no perceptible difference between weak field and strong field formulations up to an intensity of about 2×10^6 watt/cm^2 for the Ca-Sr system studied experimentally by the Harris group. Above that power density, we find a shift of the spectral maximum to the red, and a small change in the lineshape. Also, as the intensity rises, the relative contribution of small impact parameters diminishes. Consequently, the shift in the peak seems to be almost entirely due to the A.C. Stark effect. That part of the shift due to the exact treatment of the Ksech $\pi t/T$ coupling, which is in the opposite direction toward the blue, seems not to have much effect, since it is greatest at small impact parameters, whose relative contribution to the total cross section becomes less and less at high intensities.

A paper based on the HSILS model should be completed and submitted for publication in the near future.

Thus, the simulation of an inverse power law potential by a hyperbolic secant seems to be well-motivated and useful. On the other hand, the replacement of $R^{-6}(t)$ by a delta function, while yielding an exactly solvable model seems to be less convincing, even though it generates spectral properties known to be consistent with experiment, and is a distinct improvement over calculations which omit level shifts altogether. Consequently, we were led to explore a model in which the potentials are pure hyperbolic secant, i.e., R^{-3} replaced by Ksech $\pi t/T$, and R^{-6} by Psech^2 $\pi t/T$. In the weak field limit, this means that we need the integral

$$i\alpha_2(t=+\infty) = K\int_{-\infty}^{\infty} dt\, \operatorname{sech}\frac{\pi t}{T}\, e^{i\delta t} \exp\left\{iP\int_0^t \operatorname{sech}^2\frac{\pi s}{T}\, ds\right\}$$

$$= K\int_{-\infty}^{\infty} dt\, \operatorname{sech}\frac{\pi t}{T}\, e^{i\delta t} \exp\left\{\frac{iPT}{\pi}\tanh\frac{\pi t}{T}\right\}. \qquad (8)$$

In terms of dimensionless parameters, this is proportional to

$$I = \int_{-\infty}^{\infty} \operatorname{sech} x \, e^{i\beta x} \exp\{i\mu \tanh x\} \, dx. \qquad (9)$$

The integral in Eq. (9) may be formally written in terms of a contour integral. Consider the path shown in Fig. 1. We first consider the case of $\mu = 0$ for simplicity.

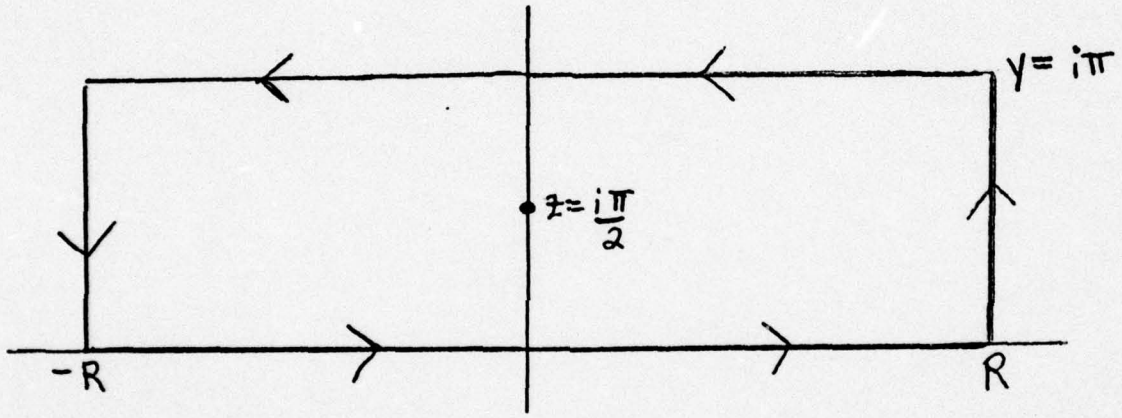

Figure 1

For large R, the contributions to the contour integral arising from the vertical sections vanishes exponentially. The two horizontal sections are easily shown to be proportional to one another. Thus, apart from a multiplicative constant, the integral of Eq. (9) is given by the residue theorem. For $\mu = 0$, there is only the simple pole at $i\pi/2$, and the integral becomes $\int_{-\infty}^{\infty} \operatorname{sech} x \, e^{i\beta x} dx = I = \pi \operatorname{sech} \frac{\pi\beta}{2}$.

A similar procedure should apply for $\mu \neq 0$. The same contour is used, the vertical segments of the contour integral vanish as $R \to \infty$, and the horizontal segments are proportional to one another, leaving the

desired integral expressible in terms of the singularity at $i\pi/2$. This, however, is no longer a pole, but an essential singularity. To evaluate the residue in a straightforward way, we would require the Laurent series for $\text{sechx}e^{i\mu\tanh x}$ and the Taylor series for $e^{i\beta x}$ in the neighborhood of the non-analytic point, which ordinarily would involve, among other things, expanding $e^{i\mu\tanh x}\, e^{\beta x}$, and sechx. This gives a mess, and it turns out that a simpler procedure is available. Writing the integral in Eq. (9) in a series representation at the outset, we have

$$I = \sum_{k=0}^{\infty} \frac{(i\mu)^k}{k!} \int_{-\infty}^{\infty} \operatorname{sech} x\, e^{i\beta x} \tanh^k x\, dx = \sum_{k=0}^{\infty} \frac{(i\mu)^k}{k!} I_k. \tag{10}$$

The zeroth term has already been given. The coefficient of μ^1 may be calculated via a parts integration $I_1 = \int_{-\infty}^{\infty} \operatorname{sech} x \tanh x\, e^{i\beta x} dx$

$$= -\operatorname{sech} x\, e^{i\beta x}\Big|_{-\infty}^{\infty} + i\beta \int_{-\infty}^{\infty} \operatorname{sech} x\, e^{i\beta x} dx = i\beta I_0.$$

For $k \geq 2$, we have again, via parts integration, $I_k =$

$$\int_{-\infty}^{\infty} \operatorname{sech} x \tanh^k x\, e^{i\beta x} dx = \int_{-\infty}^{\infty} (\operatorname{sech} x \tanh x) \tanh^{k-1} x\, e^{i\beta x} dx =$$

$$-\operatorname{sech} x \tanh^{k-1} x\, e^{i\beta x}\Big|_{-\infty}^{\infty} + i\beta \int_{-\infty}^{\infty} \operatorname{sech} x \tanh^{k-1} x\, e^{i\beta x} dx$$

$$+(k-1)\int_{-\infty}^{\infty} \operatorname{sech}^3 x \tanh^{k-2} x\, e^{i\beta x} dx = i\beta \int_{-\infty}^{\infty} \operatorname{sech} x \tanh^{k-1} x\, dx$$

$$+\int_{-\infty}^{\infty} \operatorname{sech} x \tanh^{k-2} x\, e^{i\beta x} dx - (k-1)\int_{-\infty}^{\infty} \operatorname{sech} x \tanh^{k} x\, e^{i\beta x} dx,$$

$$\text{or, } I_k = i\beta I_{k-1} + (k-1)I_{k-2} - (k-1)I_k, \text{ or}$$

$$I_k = \frac{1}{k}\left[i\beta I_{k-1} + (k-1)I_{k-2}\right].$$

Thus, instead of explicitly working out the residue at the essential singularity, we have the series

$$I = \pi \operatorname{sech} \frac{\pi\beta}{2} \sum_{k=0}^{\infty} \frac{(i\mu)^k}{k!} J_k,$$

where the terms are obtainable via the recursion formula $J_0 = 1$, $J_1 = i\beta$,

$$J_k = \frac{1}{k}\left[i\beta J_{k-1} + (k-1) J_{k-2} \right], \quad k \geq 2.$$

This appears to be a simple, tractable procedure and numerical work is being carried out.

It is noted that a similar trick works in the case of optical collisions. The weak field transition probability, in the dressed atom basis, requires the evaluation of the integral

$$\alpha_2 = A \int_{-\infty}^{\infty} dt\, R^{-6}(t) e^{i\Delta t} \exp\left\{ iQ \int_0^t ds\, R^{-6}(s) \right\}.$$

We may construct a hyperbolic secant model analogous to the radiative caseby replacing the $R^{-6}(t)$ term by a $\mathrm{sech}^2 \pi t/T$ in both the exponential and its prefactor, reducing the problem to an integral of the form

$$I = \int_{-\infty}^{\infty} dx\, \mathrm{sech}^2 x\, e^{i\beta x} e^{i\mu \tanh x}.$$

We use the same contour as previously (Fig. (1)). Again, the vertical segments give a vanishing contribution to the integral, and the horizontal segments give contributions proportional to each other, leaving the integral to be expressed in terms of the singularity at $i\pi/2$. For $\mu = 0$, this is now a second-order pole. For $\mu \neq 0$, we have the series

$$I = \sum_{k=0}^{\infty} \frac{(i\mu)^k}{k!} \int_{-\infty}^{\infty} e^{i\beta x} \mathrm{sech}^2 x \tanh^k x\, dx,$$

and may avoid the need to evaluate the residue at an essential singularity by again formulating the problem recursively. Thus, $I = \sum_{k=0}^{\infty} \frac{(i\beta)^k}{k!} I_k$, $I_k = \int_{-\infty}^{\infty} e^{i\beta x} \operatorname{sech}^2 x \tanh^k x \, dx$. Using the contour of Fig. 1, $I_0 = \pi\beta \operatorname{csch} \frac{\pi\beta}{2}$, $I_1 = \int_{-\infty}^{\infty} \operatorname{sech}^2 x \tanh x \, e^{i\beta x} dx$

$= \int_{-\infty}^{\infty} (\operatorname{sech} x \tanh x) \operatorname{sech} x \, e^{i\beta x} dx = -\operatorname{sech}^2 x \, e^{i\beta x} \Big|_{-\infty}^{+\infty} + i\beta \int_{-\infty}^{\infty} \operatorname{sech}^2 x e^{i\beta x} dx - \int_{-\infty}^{\infty} \operatorname{sech}^2 x \tanh x \, e^{i\beta x} dx$, or

$I_1 = i\beta I_0 - I_1$, $I_1 = i\frac{\beta I_0}{2} = i\frac{\beta^2 \pi}{2} \operatorname{csch} \frac{\pi\beta}{2}$. For $k \geq 2$,

$I_k = \int_{-\infty}^{\infty} e^{i\beta x} \operatorname{sech}^2 x \tanh^k x \, dx = \int_{-\infty}^{\infty} (\operatorname{sech} x \tanh x)(\operatorname{sech} x \tanh^{k-1} x) e^{i\beta x} dx = -\operatorname{sech}^2 x \tanh^{k-1} x \, e^{i\beta x} \Big|_{-\infty}^{+\infty} + \int_{-\infty}^{\infty} \operatorname{sech}^2 x \tanh^k x \, e^{i\beta x} dx + (k-1) \int_{-\infty}^{\infty} \operatorname{sech}^4 x \tanh^{k-2} x \, e^{i\beta x} dx + i\beta \int_{-\infty}^{\infty} \operatorname{sech}^2 x \tanh^{k-1} x \, e^{i\beta x} dx$

$= \int_{-\infty}^{\infty} \operatorname{sech}^2 x \tanh^k x \, e^{i\beta x} dx + (k-1) \int \operatorname{sech}^2 x \tanh^{k-2} x \, e^{i\beta x} dx - (k-1) \int_{-\infty}^{\infty} \operatorname{sech}^2 x \tanh^k x \, e^{i\beta x} dx + i\beta \int_{-\infty}^{\infty} \operatorname{sech}^2 x \tanh^{k-1} x \, e^{i\beta x} dx$,

Or, $I_k = I_{k-2} + \frac{i\beta I_{k-1}}{k-1}$.

In contrasting the weak-field integration required for hyperbolic function coupling and level shifting potentials with the R^{-n} potentials occurring in the actual atom-atom system, we note that in the former case,

the singularity in the complex plane is a pole for $\mu = 0$, and an essential singularity otherwise. In the R^{-3} case, there is a branch point for zero level shift while when level shifts are present, the integrand decomposes into one term which possesses an essential singularity and a second which consists of a sum of functions, each of which possesses a branch point. The relatively milder pathology for the hyperbolic secant case leads one to suspect that it is possible to successfully formulate it in the strong field case as a generalization of the Rosen-Zener problem. This proves to be the case.

We now consider the strong field generalization of this problem. In the notation of Eqs. (3), $V(t) = \{K\,\mathrm{sech}\,\pi t/T\}\exp(-i\mu\tanh\pi t/T)$, so that Eqs. (4) become

$$\ddot{\alpha}_1 + \left[\frac{\pi t}{T}\tanh\frac{\pi t}{T} + i\frac{\mu\pi}{T}\mathrm{sech}^2\frac{\pi t}{T} - i\Delta\right]\dot{\alpha}_1 + K^2\mathrm{sech}^2\frac{\pi t}{T}\alpha_1 = 0 \tag{11a}$$

$$\ddot{\alpha}_2 + \left[\frac{\pi t}{T}\tanh\frac{\pi t}{T} - i\frac{\mu\pi}{T}\mathrm{sech}^2\frac{\pi t}{T} + i\Delta\right]\dot{\alpha}_2 + K^2\mathrm{sech}^2\frac{\pi t}{T}\alpha_2 = 0 \tag{11b}$$

Using the Rosen-Zener problem as a model, we make the change of variable $z = (\tanh \pi t/T + 1)/2$, so that

$$z(1-z)\alpha_1'' - \left[(z-\tfrac{1}{2}) - 2i\mu z(1-z) + \frac{iT\Delta}{2\pi}\right]\alpha_1' + \frac{T^2}{\pi^2}K^2\alpha_1 = 0, \tag{12a}$$

$$z(1-z)\alpha_2'' - \left[(z-\tfrac{1}{2}) + 2i\mu z(1-z) - \frac{iT\Delta}{2\pi}\right]\alpha_2' + \frac{T^2}{\pi^2}K^2\alpha_2 = 0 \tag{12b}$$

If we cast this into a form analogous to the hypergeometric equation

$$z(1-z)\alpha_1'' + \left[(a_1+b_1+1)z - c_1 + 2d_1z^2\right]\alpha_1' + (a_1b_1 + e_1z)\alpha_1 = 0, \tag{13a}$$

$$z(1-z)\alpha_2'' + \left[(a_2+b_2+1)z - c_2 + 2d_2z^2\right]\alpha_2' + (a_2b_2 + e^2z)\alpha_2 = 0, \tag{13b}$$

where $a_1 = i\nu\left[1 - \sqrt{1 - \frac{T^2k^2}{\mu^2\pi^2}}\right]$, $a_2 = -a_1$,

$b_1 = i\nu\left[1 + \sqrt{1 - \frac{T^2k^2}{\mu^2\pi^2}}\right]$, $b_2 = -b_1$,

$c_1 = \frac{1}{2} - \frac{i\Delta T}{2\pi}$, $c_2 = c_1^*$,

$d_1 = i\nu$, $d_2 = -d_1$, $e_1 = e_2 = 0$.

The hypergeometric equation (HGE), is, by comparison

$$z(1-z)F'' + [(a+b+1)z - c]F' + abF = 0.$$

The HGE has regular points at z = 0, 1, and ∞. Our equation retains the regular singular points at 1 and 0, but has an irregular singular point at ∞. That is, the general solution of Eqs. (13) will have an essential singularity at z = ∞. Comparing the z and t planes, it is obvious that the essential singularity that appeared in the weak field integrand has been mapped to infinity in the new variable. The general solution at the finite singular points will have either a pole or a branch point, however, a situation that persists even for $\mu \neq 0$.

We attempt to solve Eqs. (13) by the power series method, looking particularly for one solution that goes to unity at z = 0 (t = - ∞). Writing (the subscripts 1, 2 are suppressed)

$$\alpha = \sum_{s=0}^{\infty} A_s z^s,$$

we obtain the three term recursion relation

$$A_0 = 1, \quad A_1 = \frac{ab}{c}, \quad A_{s+1} = A_s \frac{(a+s)(b+s)}{(s+c)(s+1)} +$$

$$A_{s-1} \frac{e+2d(s-1)}{(s+c)(s+1)}, \quad s \geq 2.$$

This gives a solution of the relevant differential equation, analytic at $z = 0$, and, since the nearest singular point of the differential equation is at $z = 1$, must also be convergent throughout the circle $|z| < 1$. We require the second solution, looking again at the HGE for guidance. We make the transformation $\alpha = z^{1-c}\beta$. The equation for β is again of the same form, to wit,

$$z(z-1)\beta'' + [(\bar{a}+\bar{b}+1)z - \bar{c} + 2\bar{d}z^2]\beta' + (\bar{a}\bar{b} + \bar{e}z)\beta = 0, \tag{14}$$

where $\bar{a}+\bar{b} = a+b+2-2c$, $\bar{a}\bar{b} = ab + (a+b+1)(1-c) + c(c-1)$, $\bar{c} = 2-c$, $\bar{d} = d$, $\bar{e} = e + 2(1-c)d$.

Clearly, an analogous series for β may be written, with the same recursion formulae. Thus a complete solution has been found in a convenient form. We seek a second generalization tractable at $z = 1$.

To accomplish this, we make use of the symmetry inherent in the equation between the singular points at $z = 0$ and 1. Making the change of variable $u = 1 - z$, we obtain a differential equation in the variable u in which the roles the two finite singular points are interchanged

$$u(u-1)\alpha'' + [(\hat{a}+\tilde{b}+1)u - \tilde{c} + 2\hat{d}u^2]\alpha' + [\hat{a}\tilde{b} + \tilde{e}u]\alpha = 0, \tag{15}$$

where primes denote differential with respect to u, and

$$\hat{a}+\tilde{b} = a+b+4d, \quad \hat{a}\tilde{b} = ab + e \quad \tilde{c} = a+b+1-c-2d$$

$$\hat{d} = -d, \quad \tilde{e} = -e.$$

The two solutions in the new representation may be immediately written down from our original pair. These are convergent (in terms of z) in the range $0 < z \leq 1$. Since one of the new solutions vanishes at $z = 1$, and the other goes to 1, all we require for the transition amplitude is the coefficient of the latter. We thus proceed at follows. Using the series centered around $z = 0$, and the initial conditions, we write down a solution. For the point $z = 1/2$, we write also the solution in terms of the two series centered around $z = 1$. The two forms of the solution must be analytic continuations of each other, and the values of functions and first derivatives must be the same for the two forms in their common domain of analyticity. We use this information to evaluate the coefficients of the two independent solutions evaluated in series form relative to $z = 1$.

Preparation for numerical analysis of this model have begun. It also seems likely that an analogous differential equation may be written for the optical collision case. This will be investigated.

4. Laser Assisted Heating or Cooling - (P.R. Berman with S. Stenholm).

We have proposed a plan[21*] to use collisions in the presence of a radiation field to either take up or provide kinetic energy in the absorptive process and, consequently, cool or heat the sample. A recent successful experiment using ions in a trap[22] uses a method similar in spirit to our proposal, although it is the trap rather than the collision partners which absorb the energy.

5. Optical Ramsey Fringes and Photon Echoes - (J. Le Gouet and P.R. Berman).

We have begun a study of photon echoes in a standing wave laser field. It turns out that, using two strong standing wave pulses separated by a time τ, one obtains a true photon echo at $t = 2\tau$ plus additional signals at $t = n\tau$ (n = integer > 2). These subsequent signals are equivalent to the Optical Ramsey Fringes recently discussed by several authors.[23] An interesting feature of the strong field calculation is that population pulsations appear at $\exp(2ikvt)$ for atoms moving with velocity v. Thus, small changes in velocity owing to velocity-changing collisions can be magnified by a factor n so that standing wave echoes may prove useful for studying weak velocity-changing collisions. Our theoretical results are at a preliminary stage.

References

1. P.R. Berman, in Advances in Atomic and Molecular Physics, 13, 57 (Academic Press Inc., New York, 1978).
2. P.R. Berman, Physics Reports 43, 101 (1978).
3. J. Keilson and K.E. Storer, Q. Appl. Math. 10, 243 (1952).
4. J. LeGouet and P.R. Berman, Phys. Rev. A17, 52 (1978).
5. J. LeGouet and R. Vetter, (private communication).
6. S.G. Rautian and A.M. Shalagin, Sov. Phys.-JETP 31, 518 (1970); J. Thomas, M. Kelley, J. Mouchalin, N.A. Kurnit and A. Javan, Phys. Rev. A15, 2356 (1977).
7. S. Salomaa and S. Stenholm, J. Phys. B 8, 1795 (1975); 9, 1221 (1976); 10, 3005 (1977).
8. S.D. Yeh, P.R. Berman-submitted to Physical Review.
9. S.D. Tvorogov and V.V. Fomin, Opt. i Spectrosc. 30, 228 (1971); J. Szudy and W.E. Baylis, J. Quant. Spectr. Radiative Transfer 15, 641 (1975).
10. D.S.F. Crothers, J. Phys B 11, 1025 (1978).
11. E.J. Robinson - submitted to J. Phys. B.
12. S.E. Harris and D.L. Lidow, Phys. Rev. Lett. 33, 674 (1974); Phys. Rev. Lett. 34, 172 (1975).
13. S.E. Harris and J.C. White, I.E.E.E. J. Quant. Elect. QE13, 972 (1977).
14. V.S. Lisitsa and S.E. Yakovlenko, Soviet Physics J.E.T.P. 39, 759 (1974).
15. S. Geltman, J. Phys. B: Atom. Molec. Phys. 9, L569 (1976).

References - Con't.

16. P.L. Knight, J. Phys. B: Atom. Molec. Phys. 10, L195 (1977).

17. M.G. Payne and M.N. Nayfeh, Phys. Rev. A13, 596 (1976).

18. R.W. Falcone, W.R. Green, J.C. White and S.E. Harris, Phys. Rev. Lett. 36, 462 (1976); Phys. Rev. Lett. 37, 1590 (1976).

19. R.T. Robiscoe, Phys. Rev. A17, 247 (1978).

20. N. Rosen and C. Zener, Phys. Rev. 40, 502 (1932).

21. P.R. Berman and S. Stenholm, Optics Comm. 24, 155 (1978).

22. D.J. Wineland, R.E. Drullinger and F.L. Walls, Phys. Rev. Lett. 40, 1639 (1978).

23. See V.P. Chebotayev, N.M. Dyuba, M.I. Skvortsov, and L.S. Vasilenko, Applied Physics (Germany) 15, 319 (1978).

THEORY OF COLLISIONALLY AIDED RADIATIVE EXCITATION

S. Yeh and P.R. Berman

Department of Physics

New York University

New York, New York 10003

Supported by the U.S. Office of Naval Research under Contract No. N00014-77-C-0553.

ABSTRACT

The excitation of a two-level active atom by a radiation field in the presence of a low density perturber bath is studied. In particular, the collisional enhancement of the absorption cross section is investigated. Features of the absorption line profiles are predicted on physical grounds using a dressed atom approach and verified by detailed numerical calculations for attractive, repulsive and Lennard-Jones type interatomic potentials. Complete spectra of the absorption cross section both as a function of detuning and as a function of field strength are given. In the weak field limit, the results are compared with those of traditional pressure broadening theory and to the recent experimental results of Carlsten et al. In the strong field limit, the results display a saturation behavior consistent with the predictions of Lisitsa and Yakovlenko.

I. Introduction

With the development of high intensity laser sources, there has been renewed interest in the study of atomic collisions in the presence of radiation fields.[1-15] Both Collisionally Aided Radiative Excitation (or Emission) (CARE), sometimes referred to as "optical collisions",[1-3] and Radiatively Aided Inelastic Collisions (RAIC), sometimes referred to as "radiative collisions",[5-10] have been examined by a number of authors. The discussion in this paper is limited to CARE although RAIC can be studied by the same methodology to be presented here.

To put the CARE problem into some perspective, consider a two-level active atom with level separation ω_o subjected to an applied radiation field of frequency ω. The active atoms also undergo collisions with structureless perturbers at some rate Γ and one wishes to calculate the absorption cross section as a function of detuning $\Delta = \omega - \omega_o$. The field amplitude E in frequency units is given by $\chi = \mu E/2\hbar$, where μ is the dipole moment matrix element of the transition.

If the detuning is greater than both the Doppler width and power broadened homogeneous width, i.e. $|\Delta|$ > Doppler width $\gtrsim \chi$, the absorption cross section is negligible in the absence of collisions and can be enhanced by collisional processes. Consequently, the study of CARE is restricted to detunings $|\Delta|$ > Doppler width $\approx 10^{10}$ sec^{-1}. In situations where lasers with limited tunability are employed so that large $|\Delta|$ can not be avoided, CARE may provide a means for increasing the absorption of the sample.

The case of large field strengths $\chi > |\Delta| > 10^{10}$ sec^{-1} requires some additional discussion. Such field strengths can be attained only with pulsed lasers. For pulse rise times longer than $|\Delta|^{-1} \lesssim 10^{-10}$ sec the atomic excitation would adiabatically follow the field in the absence of collisions, and the atom would return to its ground state following[16] the pulse. However, collisions interfere with the adiabatic following and give rise to some net absorption following the radiation pulse. In this limit, collisions are essential for absorption to occur. On the other hand CARE is less important if the pulse rise time is faster than $|\Delta|^{-1}$ since, in this limit, there can be substantial absorption in the absence of collisions.

Thus, the conditions of interest for CARE are

$$|\Delta| > \text{Doppler width} \gtrsim \chi \qquad (1a)$$

or

$$[\chi > |\Delta| > \text{Doppler width}] \text{ .AND. } [\text{radiation pulse rise time} > |\Delta|^{-1}] \qquad (1b)$$

For the remainder of this paper we assume that condition (1a) or (1b) is satisfied although the calculations presented in Secs. III, IV isolate the CARE contribution to the absorption even if these conditions do not hold.

If conditions (1) are satisfied, the atomic dipole oscillates with a period $\tau \lesssim |\Delta| < 10^{-10}$ sec in a reference frame rotating at frequency ω_0. Thus the time scale of importance in the problem is

$\tau \lesssim 10^{-10}$ sec - any processes slower than that can not cancel the rapid oscillation of the dipole. It is assumed that $\Gamma << |\Delta|$, i.e. the perturber density is such that at most one collision occurs in the interval τ (typically, valid for pressures < 1.0 atmosphere). The condition $\Gamma << |\Delta|$ is equivalent to taking the CARE rate to be linear in the perturber density. One can calculate the CARE contribution for a single collision and than average over all possible collisions to obtain the CARE rate.

In the limit of weak fields [Eq. (1a)], the study of CARE is essentially that of pressure broadened linear absorption. This area of research enjoys a long history[17-23], but there are few papers that present detailed numerical calculations for the entire range of detuning, although asymptotic formulas are available in various limits.[18-21] For strong fields, there have been some numerical studies of radiatively aided inelastic collisions[2,3,5,6], but most of these calculations have concentrated on obtaining analytic approximations for various limits of detunings and field strengths. Moreover, most strong field CARE and RAIC calculations have utilized somewhat unphysical potentials, i.e. of the form $-|c|/R^n$.

It is our purpose to present a physical picture of CARE for attractive, repulsive, and Lennard-Jones type interatomic potentials. General features of the results are predicted on the basis of simple physical arguments and detailed numerical calculations are presented to verify the predictions. This paper also forms the basis for future work that will

consider level schemes more complicated than the two-level systems discussed below.

II. General Considerations

Consider a collision between a two-level active atom and a ground state perturber. The active atom's energy levels are shifted during a collision and this shift is shown schematically in Fig. 1 for some specific collision impact parameter b and relative velocity v. The shift of level 2 relative to level 1 determines whether collisions increase or decrease the 1-2 transition frequency relative to its unperturbed value ω_o. In the case shown, the frequency shift is towards the red and one speaks of an attractive (relative) potential. Conversely, for a relative shift towards the blue, one speaks of a repulsive potential. Collision energies are assumed to be larger than the detuning $|\Delta|$, but not sufficient to couple the levels in the absence of applied fields. (We have set $\hbar = 1$ and measure energy in frequency units.)

If, for some t during the collision, the instantaneous transition frequency $\omega_o(t)$ equals the frequency of the applied field, there is an "instantaneous resonance" for this interaction. For the case shown in Fig. 1, "instantaneous resonances" occur for a range of red detunings, but not for any blue detunings. As is described below, the presence of instantaneous resonances can greatly enhance the absorption cross section, especially in the case of large detunings.

The picture presented above is best used when the applied radiation fields are weak. For the case of strong external fields, a dressed

atom[24] approach provides additional insight. The dressed atom approach can be used for weak as well as strong external fields. In this approach, the unperturbed Hamiltonian H_o is taken to consist of the free atomic Hamiltonian + free field Hamiltonian + atom-field interaction. In the absence of spontaneous emission, and in the rotating wave approximation, the two dressed states (eigenstates of H_o) are the linear combinations of the two bare states $|1,n\rangle, |2,n-1\rangle$, given by

$$|I\rangle = \frac{1}{\sqrt{2}}\left(1+\frac{\Delta}{\Omega}\right)^{1/2}|1,n\rangle + \frac{1}{\sqrt{2}}\left(1-\frac{\Delta}{\Omega}\right)^{1/2}|2,n-1\rangle \qquad (2)$$

$$|II\rangle = \frac{1}{\sqrt{2}}\left(1-\frac{\Delta}{\Omega}\right)^{1/2}|1,n\rangle - \frac{1}{\sqrt{2}}\left(1+\frac{\Delta}{\Omega}\right)^{1/2}|2,n-1\rangle$$

where the bare states are labelled by both the field and atomic variables with n being the number of photons in the field and

$$\Omega = \left(\Delta^2 + 4\chi^2\right)^{1/2}$$

is the Rabi frequency with χ the field strength in frequency units. The energies of these eigenstates are

$$E_I = E_1 + n\omega - \tfrac{1}{2}\Delta \mp \tfrac{1}{2}\Omega \qquad (3)$$

$$E_{II} = E_1 + n\omega - \tfrac{1}{2}\Delta \pm \tfrac{1}{2}\Omega \quad ;$$

the upper signs are used for positive Δ and the lower signs for

negative Δ so that

$$E_{II} - E_I = \pm \Omega \qquad (4)$$

In the absence of collisions, the dressed states are separated by Ω, with $E_{II} > E_I$ for $\Delta < 0$ and $E_{II} < E_I$ for $\Delta > 0$.

In contrast to the classical field picture (Fig. 1) in which the only effect of collisions is to shift the energy levels, collisions both shift and couple the dressed states. The amount of the shift of each dressed state is determined by the proportion of bare states it contains. For example if state $|II\rangle$ is composed mostly of bare state $|2,n-1\rangle$ then it will shift in the same way as state $|2\rangle$ of Fig. 1. On the other hand if $|II\rangle$ consists of an almost equal admixture of bare states $|1,n\rangle$ and $|2,n-1\rangle$ it will shift as the average of the the shifts of the states $|1\rangle$ and $|2\rangle$ of Fig. 1. The role of collisions on the dressed states is best illucidated by examining the weak and strong field limits.

Weak fields - $\chi << |\Delta|$. In this limit, state $|II\rangle$ is separated from state $|I\rangle$ by Δ [see Eq. (3)] and the dressed states are approximately equal to the bare ones. Consequently the collisional shift of the levels is the same as for the two atomic states. The instantaneous energy levels of the dressed states during a collision are shown in Figs. 2a and 2b for negative and positive Δ, respectively, assuming an attractive potential. The "instantaneous resonances" of the classical field picture are transformed into "crossing points" in the dressed atom approach. As is evident from Figs. 2a, 2b crossing points can occur for red detunings but will never occur for blue ones.

Strong fields - $\chi >> |\Delta|$. In the strong field limit, the dressed states are separated by 2χ and are given by $|I\rangle$, $|II\rangle = \frac{1}{\sqrt{2}}(|1,n\rangle \pm |2,n-1\rangle)$. Since the relative populations of the bare states is the same in each of the dressed states, the collisional shift for the dressed states is identical[25] as shown in Fig. 2c. Hence the relative shift of the dressed states is zero and it is impossible to have a crossing, regardless of the sign of Δ, provided $|\Delta| << \chi$.

For intermediate field strengths $\chi \approx |\Delta|$, features of both the weak and strong field cases are present.

Since crossings can occur only for the weak field limit $\chi < |\Delta|$, it is of some interest to determine the additional conditions needed to ensure a crossing. A crossing occurs if, the collisional level shift equals Δ at some time during the collision [or, equivalently, if the applied frequency equals the instantaneous separation $\omega_o(t)$ of the two atomic states]. Instead of using the time t, one can easily as well parameterize the collisional shifts by the internuclear separation R which, in turn, depends on t for a given collision. In Fig. 3 are shown the collisional shifts as a function of internuclear separation for the cases of (1) attractive potential, (2) repulsive potential, (3) Lennard-Jones type[26] potential.

Crossings occur if there is some $R(t_c)$ during a collision for which Δ equals the collisional shift. Clearly, crossings do not occur in case (1) if $\Delta > 0$, in case (2) if $\Delta < 0$ and in case (3) if both $\Delta < 0$ and $|\Delta| > |W_{LJ}|$ ($|W_{LJ}|$ = well depth of the Lennard-Jones potential).

For all other values of Δ, crossings occur for some range of impact parameters and relative velocities, although rather high relative velocities would be needed to ensure a crossing with repulsive potentials and $\Delta \geq$ thermal energy. If both $\Delta > 0$ and $\Delta < 0$ crossings occur in case (3), the $\Delta > 0$ crossing occurs for a smaller range of impact parameters.

We have not yet indicated the manner in which the presence or absence of crossings affects the absorption cross section. In order to do so, it is convenient to introduce the "optical collision impact parameter" b_c[27], defined as the impact parameter for which $\int_{-\infty}^{\infty} [\omega_0(t') - \omega_0]\, dt' = 1$. The parameter b_c is the characteristic impact parameter for the weak field case, producing a change sufficient to significantly disturb the phase of the atomic dipole. The collision time $\tau_c = b_c/v$ and $\omega_c = 1/\tau_c$. The collision interaction possesses frequency components $\omega \lesssim \omega_c$. The importance of crossings then depends on whether $\Omega\tau_c = (\Delta^2 + 4\chi^2)^{1/2}\tau_c \ll 1$ (impact limit) or $\Omega\tau_c > 1$.

If $\Omega\tau_c \ll 1$, the collision possesses sufficient frequency components to compensate for the detuning, i.e. $\omega_c/|\Delta| \gg 1$. In this case, the sign of the detuning is relatively unimportant, indicating that crossing points do not play a significant role in the process. Another way to view this result is as follows: Crossing points are points of stationary phase for the dipole oscillator. Only if the oscillator's phase is rapidly varying in the <u>absence of collisions</u> does the point of stationary

phase produce the major contribution in the absorption process. In the impact limit $\Omega\tau_c \ll 1$, the phase is <u>not</u> rapidly varying in the absence of collisions, and crossings are irrelevant. In the weak field limit the absorption cross section varies as Δ^{-2} in the impact region.

If $\Omega\tau_c \gg 1$, the oscillator's phase is rapidly varying in the absence of collisions. Collision induced crossings can greatly enhance the absorption cross section. In the weak field limit, the absorption cross section will vary as $|\Delta|^{-p}$ $(p > 0)$ if crossings occur and as some power of $|\Delta|$ times $\exp[-\alpha|\Delta\tau_c|^q]$ $(q > 0)$ if no crossings occur.[19-21] This difference in dependence on Δ indicates the importance of crossings when $\Omega\tau_c > 1$. In the strong field case no crossings occur and the cross section falls as $\exp[-\beta(\chi\tau_c)^{q'}]$ as a function of the field strength[1]. In the above α and β are constants.

In reference to the specific potentials of Fig. 2, general conclusions can be reached:

i) In the impact limit $\Omega\tau_c \ll 1$, absorption cross section go as Δ^{-2} for all potentials.

ii) If $\Omega\tau_c \gtrsim 1$ and $\chi > |\Delta|$, the absorption cross section is approximately independent of $|\Delta|$ for a fixed χ and is an exponentially decreasing function of χ for a fixed Δ.

iii) If $\Omega\tau_c > 1$ and $|\Delta| > \chi$, the cross sections fall as $|\Delta|^{-p}$ if a crossing occurs ($\Delta < 0$ - attractive, $\Delta > 0$ - repulsive, $\Delta > 0$ - Lennard-Jones and $\Delta < 0$ if also $|\Delta| < |W_{LJ}|$ - Lennard-Jones), and as some power of $|\Delta|$ times $\exp(-\alpha|\Delta\tau_c|^q)$ if no crossing occurs. For

attractive potentials the profile goes as $|\Delta|^{-p}$ for red detunings and exponentially for blue ones. For repulsive potentials the profile goes as Δ^{-p} for blue detunings and exponentially for red ones. For Lennard-Jones type potentials, there are two regions. For $|\Delta| < |W_{LJ}|$ for both blue and red detunings the profile has a power law dependence in $|\Delta|$ (the cross section is larger on the red side since red crossings occur for a larger range of impact parameters). For $|\Delta| > |W_{LJ}|$, the blue side still goes as a power law in $|\Delta|$, but the red side falls off exponentially. Thus for very large $|\Delta|$, the absorption cross section on the blue side will be larger than that on the red.

These features will be verified by the numerical calculations of the next two sections. One can conclude that, if $|\Delta|\tau_c > 1$, the optimum external field strength to use for CARE is $\chi \gtrsim |\Delta|$, since higher fields give an exponential fall off in the cross section.

III. The Equations of Motion

The Hamiltonian for a two-level active atom interacting with a radiation field and a perturber atom can be written as

$$H = H_A + H_R + H_{AR} + V(t) = H_o + V(t) \tag{5}$$

where (i) the free atomic Hamiltonian, H_A, has two eigenstates $|1\rangle$, $|2\rangle$, with eigenenergies E_1, E_2, $E_2-E_1 = \omega_o$; (ii) $H_R = \omega a^+ a$ is the quantized free field Hamiltonian describing a single-mode field with ω the photon energy; (iii) the active-atom-field interaction is given in the rotating wave approximation by $H_{AR} = \chi'(aR^+ + a^+R)$, where a and a^+ are the usual annihilation and creation operators respectively for photons of frequency ω, R^+ and R are the raising and lowering operators for the two atomic states, and χ' is the coupling constant, relating to χ by $\chi = \sqrt{n}\chi'$ with n the number of photons, (iv) the effective interaction with the perturber, $V(t)$, is taken to be time-dependent since the internuclear motion is not quantized, and is diagonal in the basis of bare states $|1,n\rangle$, $|2,n-1\rangle$ (eigenstates of $H_A + H_R$),

$$\begin{aligned} V_1(t) &= \langle 1,n|V(t)|1,n\rangle \\ V_2(t) &= \langle 2,n-1|V(t)|2,n-1\rangle \\ \langle 1,n|V(t)|2,n-1\rangle &= \langle 2,n-1|V(t)|1,n\rangle = 0 \end{aligned} \tag{6}$$

owing to the absence of inelastic collisions. This is in general a good approximation for electronic and vibrational transitions where the thermal energy is not high enough to excite the atom.

The calculation is carried out in a dressed state basis composed of the eigenstates, $|I\rangle$, $|II\rangle$ of $H_o = H_A + H_R + H_{AR}$ given in Eq. 2. Defining

$$V_s(t) = V_1(t) + V_2(t);\ V_d(t) = V_2(t) - V_1(t) \tag{7}$$

writing

$$|\psi\rangle = [C_I(t)\,|I\rangle + C_{II}(t)\,|II\rangle]\, e^{-i/2 \int_{-\infty}^{t} V_s(t')dt'}$$

attractive potentials the profile goes as $|\Delta|^{-p}$ for red detunings and exponentially for blue ones. For repulsive potentials the profile goes as Δ^{-p} for blue detunings and exponentially for red ones. For Lennard-Jones type potentials, there are two regions. For $|\Delta| < |W_{LJ}|$ for both blue and red detunings the profile has a power law dependence in $|\Delta|$ (the cross section is larger on the red side since red crossings occur for a larger range of impact parameters). For $|\Delta| > |W_{LJ}|$, the blue side still goes as a power law in $|\Delta|$, but the red side falls off exponentially. Thus for very large $|\Delta|$, the absorption cross section on the blue side will be larger than that on the red.

These features will be verified by the numerical calculations of the next two sections. One can conclude that, if $|\Delta|\tau_c > 1$, the optimum external field strength to use for CARE is $\chi \gtrsim |\Delta|$, since higher fields give an exponential fall off in the cross section.

III. The Equations of Motion

The Hamiltonian for a two-level active atom interacting with a radiation field and a perturber atom can be written as

$$H = H_A + H_R + H_{AR} + V(t) = H_o + V(t) \tag{5}$$

where (i) the free atomic Hamiltonian, H_A, has two eigenstates $|1\rangle$, $|2\rangle$, with eigenenergies E_1, E_2, $E_2-E_1 = \omega_o$; (ii) $H_R = \omega a^+ a$ is the quantized free field Hamiltonian describing a single-mode field with ω the photon energy; (iii) the active-atom-field interaction is given in the rotating wave approximation by $H_{AR} = \chi'(aR^+ + a^+R)$, where a and a^+ are the usual annihilation and creation operators respectively for photons of frequency ω, R^+ and R are the raising and lowering operators for the two atomic states, and χ' is the coupling constant, relating to χ by $\chi = \sqrt{n}\chi'$ with n the number of photons, (iv) the effective interaction with the perturber, V(t), is taken to be time-dependent since the internuclear motion is not quantized, and is diagonal in the basis of bare states $|1,n\rangle$, $|2,n-1\rangle$ (eigenstates of $H_A + H_R$),

$$\begin{aligned} V_1(t) &= \langle 1,n|V(t)|1,n\rangle \\ V_2(t) &= \langle 2,n-1|V(t)|2,n-1\rangle \\ \langle 1,n|V(t)|2,n-1\rangle &= \langle 2,n-1|V(t)|1,n\rangle = 0 \end{aligned} \tag{6}$$

owing to the absence of inelastic collisions. This is in general a good approximation for electronic and vibrational transitions where the thermal energy is not high enough to excite the atom.

The calculation is carried out in a dressed state basis composed of the eigenstates, $|I\rangle$, $|II\rangle$ of $H_o = H_A + H_R + H_{AR}$ given in Eq. 2. Defining

$$V_s(t) = V_1(t) + V_2(t);\ V_d(t) = V_2(t) - V_1(t) \tag{7}$$

writing

$$|\psi\rangle = [C_I(t)\ |I\rangle + C_{II}(t)\ |II\rangle\ ]\ e^{-1/2\ i\int_{-\infty}^{t} V_s(t')dt'}$$

and using Schrödinger equation together with Eqs. 2, 3 and 6, we obtain the equations for the probability amplitudes

$$\begin{aligned} i\dot{C}_I &= [E_I - \tfrac{\Delta}{2\Omega} V_d(t)]\, C_I + \frac{(1-\Delta^2/\Omega^2)^{1/2}}{2} V_d(t) C_{II} \\ i\dot{C}_{II} &= \frac{(1-\Delta^2/\Omega^2)^{1/2}}{2} V_d(t)\, C_I + [E_{II} + \tfrac{\Delta}{2\Omega} V_d(t)]\, C_{II} \end{aligned} \tag{8}$$

In the dressed basis, V(t) is no longer diagonal; C_I and C_{II} are coupled through off-diagonal matrix elements which are nonzero only during a collision. This makes the dressed state basis a favorable choice in numerical calculations, since we can limit the integration within the short range of a collision. If $C_I(t=-\infty) = 1$ and $|\Delta|\cdot$(radiation pulse rise time) > 1 (as is implicitly assumed throughout this work), C_{II} goes to zero as $t \to +\infty$ in the absence of collisions. Thus, $|C_{II}(t=\infty)|^2$ represents the contribution of CARE. Note that the probabilities $|C_I|^2$, $|C_{II}|^2$ depend only on the difference potential.

To solve Eqs. (7), we assume that the atoms follow straight line trajectories and take two model potentials, an attractive van der Waals' potential,

$$V_d^{VDW}(t) = \frac{C_6^{VDW}}{(b^2+v^2t^2)^3} \tag{9}$$

with $C_6^{VDW} < 0$ an effective van der Waals constant, and a Lennard-Jones potential,

$$V_d^{LJ}(t) = \frac{C_6^{LJ}}{(b^2+v^2t^2)^3} + \frac{C_{12}^{LJ}}{(b^2+v^2t^2)^6} \tag{10}$$

with $C_{12}^{LJ} > 0$. In Eqs. (9) and (10), b is the impact parameter and the point of

closest approach is taken at t = 0.

All relaxation rates are neglected in Eq. (8) owing to conditions (1). As discussed in the introduction, it suffices to consider a single collision with impact parameter b and relative velocity v. The total CARE cross section is given by

$$\sigma = 2\pi \int_0^\infty |C_{II}(b,\infty)|^2 b\,db \tag{11}$$

No average over the velocity will be attempted.

For a Hamiltonian that is an even function of time, one can show[28] that

$$\begin{aligned} &C_{II}(t)\, C_I^*(-t) - C_I(t)\, C_{II}^*(-t) = C_{II}(0)\, C_I^*(0) - C_I(0)\, C_{II}^*(0) \\ &C_I(t)\, C_I(-t) + C_{II}(t)\, C_{II}(-t) = C_I^2(0) + C_{II}^2(0) \end{aligned} \tag{12}$$

In addition, unitarity is maintained

$$|C_I(t)|^2 + |C_{II}(t)|^2 = 1 \tag{13}$$

Since the integration of Eqs. (8) can be very time consuming, Eqs (12) and (13) can be used to reduce the range of integration to $-\infty < t \leq 0$. The integration is conveniently done using a subroutine called DVERK in IMSL which uses a Runga-Kutta method based on Verner's fifth and sixth order formulas[29].

IV. Results

A. van der Waals' Potential

In the following, the van der Waals constant C_6^{VDW} is taken to be $-1.26 \times 10^{18} \frac{\text{Å}^6}{\text{sec}}$ and $v = 10^5$ cm/sec.

(i) Weak field case, $\chi \ll |\Delta|$.

The variation of the probability, $|C_{II}(b,\infty)|^2$, as a function of impact parameter b is represented in Fig. 4a for red detuning and Fig. 4b for blue detuning for values $\chi = 10^8$/sec, $|\Delta| = 5 \times 10^{11}$/sec. The probability $|C_{II}(b,\infty)|^2$ is an oscillating function of b with an envelope increasing with increasing b on the red side and decreasing with increasing b on the blue side. The oscillations start at some finite b and get faster as b is decreased. The results at this low detuning, $|\Delta|\tau_c = .5$, can be compared with the impact approximation ($|\Delta|\tau_c \ll 1$). In the impact approximation, the equations are easily solved to yield the standard result of impact pressure broadening theory,

$$|C_{II}(b,\infty)|^2 = P(b) = \frac{2\chi^2}{\Delta^2}(1 - \cos\theta) \tag{14}$$

with

$$\theta = \int_{-\infty}^{\infty} \frac{C_6^{VDW}}{(b^2+v^2t^2)^3}\,dt = \frac{3\pi}{8}\frac{C_6^{VDW}}{b^5 v} \tag{15}$$

For the parameters chosen, P(b) oscillates at a constant amplitude $.16 \times 10^{-6}$, irrespective of blue or red detuning. The impact approximation underestimates the transition probability on the red side, overestimates it on the blue side, but still provides a fair approximation at this detuning. For detunings $|\Delta|\tau_c < 1$ the presence of crossings is seen to be relatively unimportant, as predicted in Sec. II. The behavior of $|C_{II}(b,\infty)|^2$ for larger detunings $|\Delta|\tau_c > 1$ is shown in Figs. 5a, 5b, for $|\Delta| = 6\times10^{12}$/sec., $\chi = 10^8$/sec. On the red side, the probability envelope is considerably greater than the impact value $.11 \times 10^{-8}$. Crossings provide stationary phase points to

eliminate some of the rapid oscillations owing to large $|\Delta|$. The maximum contribution is centered about the largest b giving rise to a crossing in agreement with calculations using a uniform approximation[30] that consider this region. On the blue side, the rapid phase variation due to detuning further diminishes the probability from its impact value. On both sides, the positions of maxima are shifted to smaller impact parameters, since higher frequency components (consequently smaller b) are needed to compensate for larger $|\Delta|$. In this range of detuning, the crossing point on the red side greatly enhances the cross section relative to that on the blue, in agreement with the discussion of Section II.

The oscillation of $|C_{II}(b,\infty)|^2$ has been interpreted as the phased cancellation or enhancement of the transition amplitudes from the incoming and outgoing crossings during the collision. This interpretation is applicable only for large detunings on the red side. It is not an appropriate interpretation on the blue side where no crossings occur nor for detunings $|\Delta|\tau_c < 1$ where crossing points do not provide the major contributions to the absorption.

Eq. (11) is integrated numerically from a given impact parameter, $b_o = 5\text{Å}$ say, to infinity, and the contribution from 0 to b_o is estimated. The region of small b is particularly troublesome owing to the fast oscillations involved. Fortunately, the contribution from small impact parameters is relatively unimportant owing to the nature of the envelope function and to the weighting factor bdb.

A line profile is shown in Fig. 6 and is in agreement with the qualitative discussion of Sec. II. For small detunings, $|\Delta|\tau_c \ll 1$, the cross section falls off as Δ^{-2} on both the red and the blue sides. For large detunings, $|\Delta|\tau_c \gg 1$ on the red side, it falls off as $\Delta^{-3/2}$ in agreement with the quasistatic results of classical pressure broadening theories[19-21]. On the blue side, the cross section goes approximately as $\Delta^{-7/3}\exp(-\alpha\Delta^{5/6})$ with α a constant. This has the same Δ dependence as the asymptotic results of Tvorogov and Fomin[31],

although their results differ from ours by a multiplicative factor. The results of Vainshtein et al[32] are also shown in Fig. 6, and are seen to differ from our results in both their absolute magnitude and Δ dependence.

(ii) Intense field case $|\Delta| \ll X$

There is no additional difficulty in numerically integrating Eqs. (8) in the case of strong fields. As discussed in Sec. II, there are no crossings if $X \gg |\Delta|$. For $X\tau_c < 1$, the criteria for the impact limit are satisfied and one obtains the results of impact limit; for $X\tau_c > 1$, absorption cross sections are expected to be exponentially small (in the factor $X\tau_c$) in both the blue and red wings, owing to the absence of crossings.

The numerical results confirm these conclusions. For $X\tau_c < 1$, the probability $|C_{II}(b,\infty)|^2$ is an oscillating function in b with constant amplitudes (impact results), while for $X\tau_c \gg 1$, it has the characteristic shapes shown in Figs. 4b and 5b, indicating the absence of a crossing irrespective of the sign of the detuning. For $X\tau_c \ll 1$ and $|\Delta| < X$, the impact theory is valid and one obtains a symmetric absorption profile with a Δ^{-2} dependence.

(iii) $\sigma(\Delta)$ for $X\tau_c \gtrsim 1$

One can combine subsections (i) and (ii) above to obtain the spectrum for $X\tau_c \gtrsim 1$, and a typical spectrum is shown in Fig. 7. For $|\Delta| \ll X$, there are no crossings and the absorption cross section is approximately constant with $|\Delta|$. For $|\Delta| \gg X$, one regains the limiting condition of subsection (i) above with the corresponding line wings decreasing as $|\Delta|^{-3/2}$ on the red side and as $\Delta^{-7/3}\exp[-\alpha\Delta^{5/6}]$ on the blue side. On the red side the profile passes through a maximum at $|\Delta| \gtrsim X$, indicating the transition from the no crossing ($X > |\Delta|$) to the crossing ($X < |\Delta|$) case. On the blue side, the fall off is monotonic owing to the monotonically increasing separation of the dressed state energies with increasing Δ.

For a given X, maximum excitation is achieved for a red detuning of $X \gtrsim |\Delta|$.

(iv) $\sigma(X)$ for fixed $|\Delta|$

The absorption cross section as a function of X for fixed $|\Delta|$ is shown in Fig. 8. The cross section varies as X^2 in both the red and blue wings provided either $X\tau_c \ll 1$ or $X \ll |\Delta|$. However, for field strengths $X \gg |\Delta|$ and $X\tau_c > 1$ saturation occurs and the cross sections fall off approximately as $\exp(-\beta X^{5/6})$ consistent with the result of Lisitsa and Yakovlenko.[1] At these large field strengths, the dressed states never cross [Fig. 2c] and their separation is dominated by X rather than $|\Delta|$. This saturation effect is not at all related to unitarity, since it has been implicitly assumed that the excited state probability remains small in comparison with unity. The saturation mechanism is simply the one discussed in connection with Fig. 2c of Sec. II.

(B) Lennard-Jones Potential

The difference potential shown in Fig. 3 is plotted with $C_6^{LJ} = -1.03\times10^{18} \frac{\text{Å}^6}{\text{sec}}$, $C_{12}^{LJ} = 2.23\times10^{23} \frac{\text{Å}^{12}}{\text{sec}}$, which are given by Kielkopf et al[33] for Cesium $6\,S_{\frac{1}{2}} \rightarrow 7\,P_{\frac{1}{2}}$ transition perturbed by Xe.

(i) Weak field case, $X \ll |\Delta|$

Fig. 9 shows $|C_{II}(b,\infty)|^2$ as a function of b, with $|\Delta| = 3\times10^{10}$/sec, $X = 10^9$/Sec. At this detuning, the impact approximation is very good. One can see oscillations with constant amplitude (except for one additional peak at b = 8.24Å) with positions of maxima (and minima) and their heights matched by the results of the impact approximation. The extra peak is characteristic of Lennard-Jones potentials. The impact phase for a Lennard-Jones potential is

$$\theta_{LJ} = \int_{-\infty}^{\infty} \left(\frac{C_6^{LJ}}{(b^2+v^2t^2)^3} + \frac{C_{12}^{LJ}}{(b^2+v^2t^2)^6} \right) dt = \frac{3\pi C_6^{LJ}}{8b^5 v} + \frac{63\pi C_{12}^{LJ}}{256 b^{11} v} \qquad (11)$$

In addition to $b = \infty$, $\theta_{LJ} = 0$ at $b_1 = (-\frac{21}{32}\frac{C_{12}^{LJ}}{C_6^{LJ}})^{1/6}$. Since the minima of $|C_{II}(b,\infty)|^2$ are determined by $\theta_{LJ} = 2n\pi$, $n = 0, 1, 2, \ldots$, in the impact region, the extra zero results in an additional peak with its height determined by the maximum phase $|\theta_{LJ}|$ in the interval (b_1,∞).

For larger red detunings, $|C_{II}(b,\infty)|^2$ follows a typical crossing behavior (Figs. 4a, 5a) if $|\Delta| < |W_{LJ}|$ and non-crossing behavior (Figs. 4b, 5b) if $|\Delta| > |W_{LJ}|$ in agreement with the discussion of Sec. II. There is always a crossing on the blue side, regardless of detuning, and $|C_{II}(b,\infty)|^2$ displays the type of crossing behavior shown in Figs. 4a, 5a.

The absorption profile is shown in Fig. 10 for $\chi = 10^9$/sec. At detunings $< 10^{11}$/sec., the impact approximation is valid and absorption falls as $|\Delta|^{-2}$. For $|\Delta|\tau_c \gtrsim 1$, but $|\Delta| < |W_{LJ}|$ there are crossings for both red and blue detunings. Excitation is greater for red than blue detunings, owing to the larger range of impact parameters giving rise to the crossings on the red side as discussed in Sec. II. As $|\Delta|$ is further increased such that $|\Delta| > |W_{LJ}|$, there is no longer a crossing for red detunings and the red wing begins to fall off rapidly. The change in dependence from power law to exponential fall off with detuning on the red side is the well known satellite feature of potentials possessing minima. For blue detunings, the $|\Delta|$ dependence approaches $|\Delta|^{-1.25}$, typical for the far wings of a power law potential going as R^{-12}. For large $|\Delta|$, the blue wing eventually exceeds red wing absorption. The line shape has the same qualitative features observed by Carlsten et al[9] in a Sr-Ar system. The results differ quantitatively in the specific $|\Delta|$ dependence of the cross sections as well as in the ratio of red to blue absorption for a given $|\Delta|$. These discrepancies may be attributed to differences between the Ar-Sr and Cs-Xe interatomic potentials.

(ii) $\sigma(\Delta)$ for $\chi\tau_c \gtrsim 1$

A profile $\sigma(\Delta)$ for $\chi = 10^{12}$/sec is shown in Fig. 11. Since $\chi\tau_c \gtrsim 1$, the presence or absence of crossing greatly affects the magnitude of the absorption cross section. For $|\Delta| \ll \chi$, the dressed states of Fig. (2c) do not cross and the cross sections for both red and blue detunings are approximately independent of Δ. For $|\Delta| \gtrsim \chi$ and $|\Delta| < |W_{LJ}|$, a crossing becomes possible on the red wing (since the χ chosen is less than $|W_{LJ}|$) and also on the blue wing. For the parameters chosen, the red wing increases slightly with increasing $|\Delta|$, owing to the presence of the crossing, but then begins to decrease exponentially as soon as $|\Delta| > |W_{LJ}|$. The blue wing decreases monotonically with increasing $|\Delta|$, asymptotically going as $|\Delta|^{-1.25}$.

If a value $\chi > |W_{LJ}|$ is chosen, there is never a crossing for red detunings and the red wing decreases monotonically. Figure 11 is consistent with the qualitative discussion of Sec. II. For a given χ, the optimal detuning for maximum excitation depends on the detailed nature of the potential.

(iii) $\sigma(\chi)$ for fixed $|\Delta|$

Finally, the line shape as a function of χ for fixed detuning, $|\Delta| = 10^{12}$/sec, is shown in Fig. 12. For $\chi\tau_c \ll |\Delta|\tau_c \approx 1$, the absorption goes as χ^2. There are crossings in both the red and blue wings since $|\Delta| < |W_{LJ}|$. As χ increases, the red crossing disappears at $\chi = \frac{1}{2}(W_{LJ}^2 - \Delta^2)^{\frac{1}{2}}$ and the blue wing crossing disappears at $\chi = \Delta$. The corresponding saturation of the spectrum is clearly seen in Fig. 12, with $\sigma(\chi)$ saturating at smaller χ in the red wing than the blue.

V. Summary

A physical picture of Collisionally Aided Radiative Excitation (or Emission) (CARE) has been given based on a dressed atom approach. This approach enabled us to obtain general predictions for both the detuning and field dependence of CARE. These predictions were compared with numerical solutions of the problem and were found to successfully explain the CARE line shape. Moreover, the results for a Lennard-Jones potential are qualitatively in agreement with the experimental data of Carlsten et al.

The numerical solutions, while costly, offer a much wider range of validity than the asymptotic formulas obtained by previous authors. Our methods can easily be extended to problems with arbitrary interatomic potentials and to other than straight line internuclear paths.

This work was supported by the U.S. Office of Naval Research through contract No. N00014-77-C-0553, and computational time was supported in part by DOE under contract E(11-1)-3077 at NYU and by the NYU Computer Center.

References

1. V.S. Lisitsa and S.I. Yakovlenko, Sov. Phys., JETP, 39, 759 (1974); Sov. Phys. JETP, 41, 233 (1975); S.P. Andreev and V.S. Lisitsa, Sov. Phys. JETP, 45, 38 (1977).
2. A.M.F. Lau, Phys. Rev. A13, 139 (1976); N.M. Kroll and K.M. Watson, Phys. Rev. A13, 1018 (1976).
3. W.H. Miller and T.F. George, J. Chem. Phys., 56, 5637 (1972); J.M. Yuan, J.R. Liang, and T.F. George, J. Chem. Phys., 66, 1107 (1977).
4. P.R. Berman in Adv. in Atomic and Molecular Phys., ed. by D.R. Bates and B. Bederson, Vol. 13 (Academic Press, New York) p. 57-112.
5. M.G. Payne and M.H. Nayfeh, Phys. Rev. A13, 596 (1976); M.H. Nayfeh and M.G. Payne, Phys. Rev., A17, 1695 (1978); M.G. Payne, C.W. Choi, and M.H. Nayfeh, unpublished.
6. R.W. Falcone, W.R. Green, J.C. White, J.F. Young, and S.E. Harris, Phys. Rev. A15, 1333 (1976); S.E. Harris and J.C. White, IEEE J. of Quant. Electr. QE-13, 972 (1977).
7. Ph. Cahuzac and P.E. Toschek, Phys. Rev. Lett. 40, 1087 (1978).
8. L.I. Gudzenko and S.I. Yokovlenko, Sov. Phys. JETP, 35, 877 (1972).
9. S. Geltman, J. Phys. B10, 3057 (1977).
10. P. Milonni, J. Chem. Phys. 66, 3715 (1977).
11. J.L. Carlsten, A. Szöke, and M.G. Rayner, Phys. Rev. A15, 1029 (1977).
12. A. Omont, E.W. Smith, and J. Cooper, Astrophys. J., 175, 185 (1972); J. Cooper, and R.J. Ballagh, unpublished.
13. G. Nienhuis, and F. Schuller, Physica, 92C, 397 (1977).
14. A. Ben-Reuven, J. Jortner, L. Klein, and S. Mukamel, Phys. Rev. A13, 1402 (1976).

15. A. Gallagher and T. Holstein, Phys. Rev. A16, 2413 (1977).

16. D. Grischkowsky, Phys. Rev. A7, 2096 (1973).

17. For an extensive list of papers, books and reviews, see P.R. Berman, Appl. Phys. 6, 283 (1975).

18. E. Lindholm, Arkiv för Matematik, Astronomi och Fysik 32A, 1 (1945).

19. P.W. Anderson, Phys. Rev. 86, 809 (1952); P.W. Anderson and J.D. Talman, Report of Bell Tel. Labs., unpublished.

20. J. Szudy and W.E. Baylis, J. Quant. Spectrosc. Radiat. Transfer, 15, 641 (1975).

21. S.D. Tvorogov and V.V. Fomin, Opt. Spectrosc. 30, 228 (1971).

22. J. Kielkopf, J. of Phys., B9, 1601 (1976); B11, 25 (1978).

23. K.M. Sando and J.C. Wormhoult, Phys. Rev. A7, 1889 (1973).

24. C. Cohen-Tannoudji, Cargése Lecture in Physics, Vol. 2, (Gordon and Breach, New York, 1968) p. 347.

25. The velocity changing effects are neglected throughout the calculation so that this picture is valid.

26. A Lennard-Jones potential is used because of its mathematical simplicity. For more realistic potentials, see W.E. Baylis, J. Chem. Phys., 51, 2665 (1969); J. Pascale and J. Vandeplanque, 60, 2278 (1974).

27. This was originally defined by V. Weisskopf, sometimes referred to as the Weisskopf radius.

28. C.F. Lebeda and W.R. Thorson, Can. J. of Phys. 48, 2937 (1970).

29. T.E. Hull, W.H. Enright, and K.R. Jackson, TR No. 100, Dept. of Computer Science, Univ. of Toronto, Oct. 1976

30. W. Fritsch and U. Wille, J. Phys. B, 11, L43 (1978). For a detailed account of the uniform approximation, see M.S. Child, Molecular Collision Theory (Academic Press, London and New York, 1974) p. 191-194.

31. Eq. 25 of Ref. 21.

32. Eqs. 30 and 31 in L. Vainshtein, L. Presnyakov, and I. Sobelman, Sov. Phys. JETP, 16, 370 (1963). In this paper, the authors studied a different problem, however, the integral they obtained (Eq. A.1) took the same form as an integral obtained in a perturbation calculation for the CARE problem.

33. J.F. Kielkopf, J.E. Davis, and J.A. Gwinn, J. Chem. Phys., 53, 2605 (1970).

Figure Captions

Figure 1 Variation of the atomic energy levels $E_1(t)$, $E_2(t)$ of a two-level atom during a collision in the classical field picture for an attractive potential. For the incident field frequency ω shown, instantaneous resonances occur at times t_1 and t_2 during the collision. Note that instantaneous resonances occur for a range of $\Delta = \omega - \omega_0 < 0$ but not if $\Delta > 0$.

Figure 2 (a) Variation of the dressed state energies of a two-level atom during a collision with an attractive potential and red detuning, $\Delta < 0$, in the weak field limit, $\chi \ll |\Delta|$. The level separation is $\Omega \approx |\Delta|$; t_1 and t_2 are crossing points corresponding to the two points of instantaneous resonance in Fig. 1.

(b) Variation of the dressed state energies of a two-level atom during a collision with an attractive potential and blue detuning, $\Delta > 0$, in the weak field limit. No crossing points occur.

(c) Variation of the dressed state energies of a two-level atom during a collision in the high intensity limit, $\chi \gg |\Delta|$. The level separation is $\Omega \simeq 2\chi$. If $\Delta < 0$, $E_{II} > E_I$; if $\Delta > 0$, $E_I > E_{II}$. No crossing is possible regardless of the sign of Δ.

Figure 3 Interatomic difference potentials. 1: Attractive van der Waals' potential, $C_6^{VDW} = -1.26 \times 10^{18}$ Å^6/sec. 2: Repulsive van der Waals' potential, $C_6^{VDW} = 1.26 \times 10^{18}$ Å^6/sec. 3: Lennard-Jones potential, $C_6^{LJ} = -1.03 \times 10^{18}$ Å^6/sec, $C_{12}^{LJ} = 2.23 \times 10^{23}$ Å^{12}/sec. The well depth is $W_{LJ} = -1.19 \times 10^{12}$/sec, and occurs at $R = 8.7$ Å.

Figure 4 (a) The probability $|C_{II}(b,\infty)|^2$ as a function of impact parameter b for the attractive van der Waals' potential and small red detuning. $\chi = 10^8$/sec ($\chi\tau_c = 1.08 \times 10^{-4} \ll 1$), $C_6^{VDW} = -1.26 \times 10^{18}$ Å^6/sec, $v = 10^5$ cm/sec, $\Delta = -5 \times 10^{11}$/sec ($|\Delta|\tau_c = .54 < 1$).

(b) The probability as a function of impact parameter for the attractive van der Waals' potential and small blue detuning, $\Delta = 5 \times 10^{11}$/sec ($\Delta\tau_c = .54 < 1$). Other parameters are the same as those in Fig. 4a.

Figure 5 (a) The probability as a function of impact parameter for the attractive van der Waals' potential and a large red detuning. $\chi = 10^8$/sec, $C_6^{VDW} = -1.26 \times 10^{18}$ Å^6/sec, $v = 10^5$ cm/sec, $\Delta = -6 \times 10^{12}$/sec ($|\Delta|\tau_c = 6.49 > 1$).

(b) The probability as a function of impact parameter for the attractive van der Waals' potential for a large blue detuning $\Delta = 6 \times 10^{12}$ sec^{-1} ($\Delta\tau_c = 6.49 > 1$). Other parameters are the same as in Fig. 5a.

Figure 6 Absorption cross section $\sigma(\Delta)$ for an attractive van der Waals' potential in the weak field limit with parameters as in Figs.4. ——— : this calculation; - - - - - - - - : Tvorogov and Fomin[31]; ——— – ——— – ——— – — : Vainshtein et al [32].

Figure 7 Absorption cross section $\sigma(\Delta)$ at a high intensity, $\chi = 10^{12}$/sec ($\chi\tau_c = 1.08 \gtrsim 1$), for the attractive van der Waals' potential. Other parameters are the same as in Figs.5. ———: red detuning; - - - - - - - - : blue detuning.

Figure 8 Absorption cross section $\sigma(\chi)$ for the attractive van der Waals' potential with a fixed detuning $|\Delta| = 3 \times 10^{12}$/sec. Other parameters are the same as in Fig. 5. ——— : red detuning; ------- blue detuning.

Figure 9 The probability as a function of impact parameter, b, for the Lennard-Jones potential. $\chi = 10^{9}$/sec ($\chi\tau_c = 1.02 \times 10^{-3} \ll 1$), $\Delta = 3 \times 10^{10}$/sec ($\Delta\tau_c = 3.06 \times 10^{-2} \ll 1$), $v = 10^{5}$ cm/sec, $C_6^{LJ} = -1.03 \times 10^{18}$ Å^6/sec, $C_{12}^{LJ} = 2.23 \times 10^{23}$ Å^{12}/sec.

Figure 10 $\sigma(\Delta)$ for a Lennard-Jones potential in the weak field limit, $\chi = 10^{9}$/sec ($\chi\tau_c = 1.02 \times 10^{-3} \ll 1$). Other parameters are the same as in Fig. 9. ———: red detuning; -------: blue detuning.

Figure 11 $\sigma(\Delta)$ at a high intensity, $\chi = 10^{12}$/sec ($\chi\tau_c = 1.02 \gtrsim 1$), for the Lennard-Jones potential. Other parameters are the same as in Fig. 9. ———: red detuning; ------: blue detuning.

Figure 12 $\sigma(\chi)$ for the Lennard-Jones potential with $|\Delta| = 10^{12}$/sec ($|\Delta|\,\tau_c = 1.02 \gtrsim 1$). Other parameters are the same as in Fig.9. ———— : red detuning; ------- : blue detuning. Saturation occurs at lower χ for the red wing than for the blue.

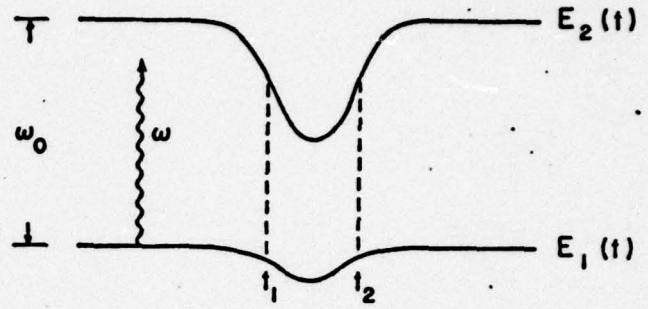

Fig. 1

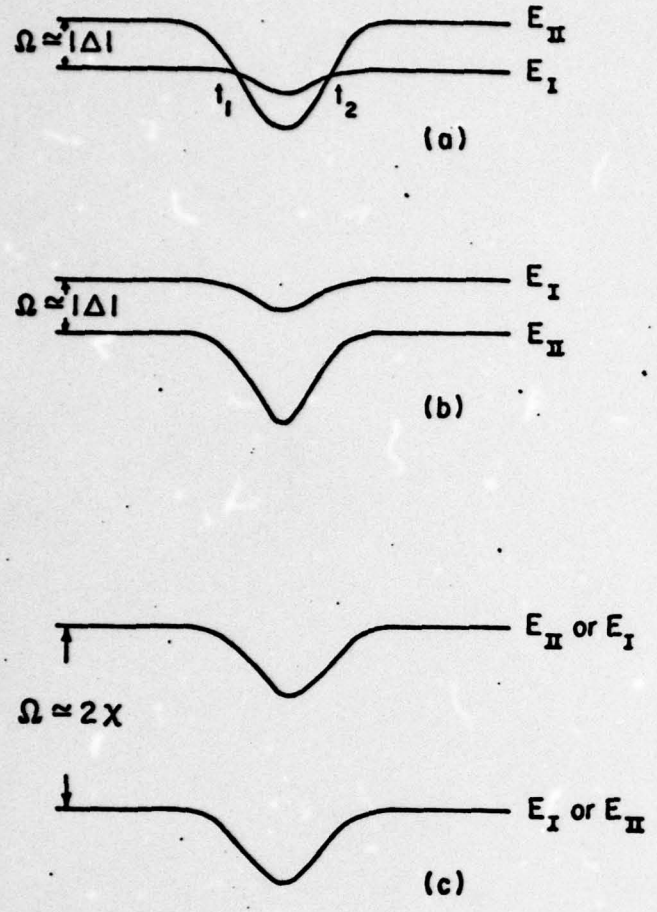
Ω ≃ |Δ|
E_II
E_I
t_1
t_2
(a)
Ω ≃ |Δ|
E_I
E_II
(b)
E_II or E_I
Ω ≃ 2χ
E_I or E_II
(c)

Fig. 2

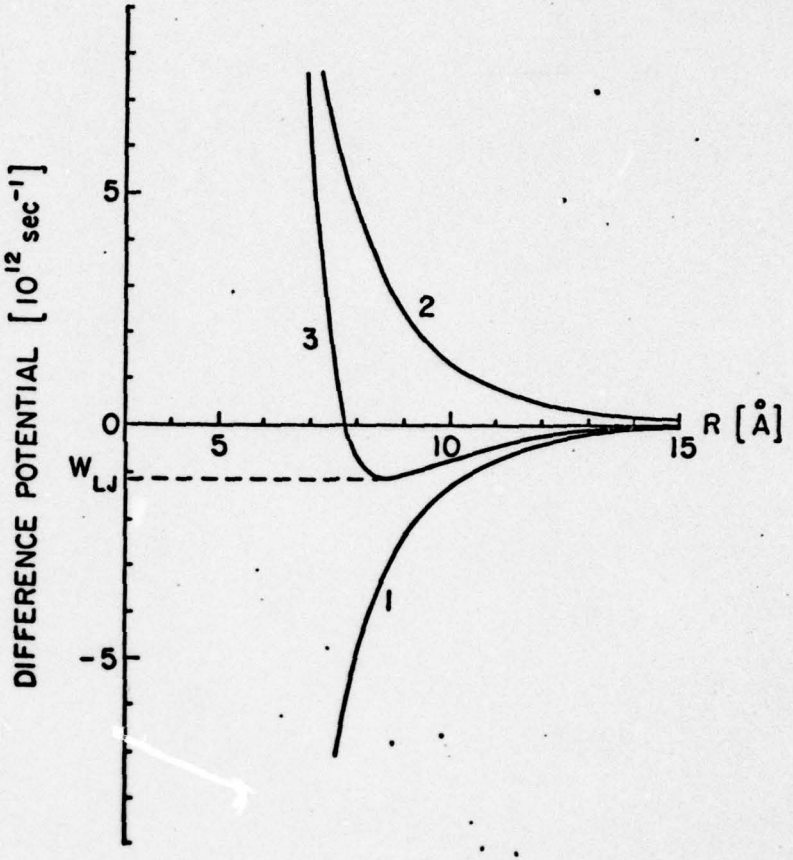
DIFFERENCE POTENTIAL [10^12 sec^-1]
5
0
-5
W_LJ
5
10
15
R [Å]
1
2
3

Fig. 3

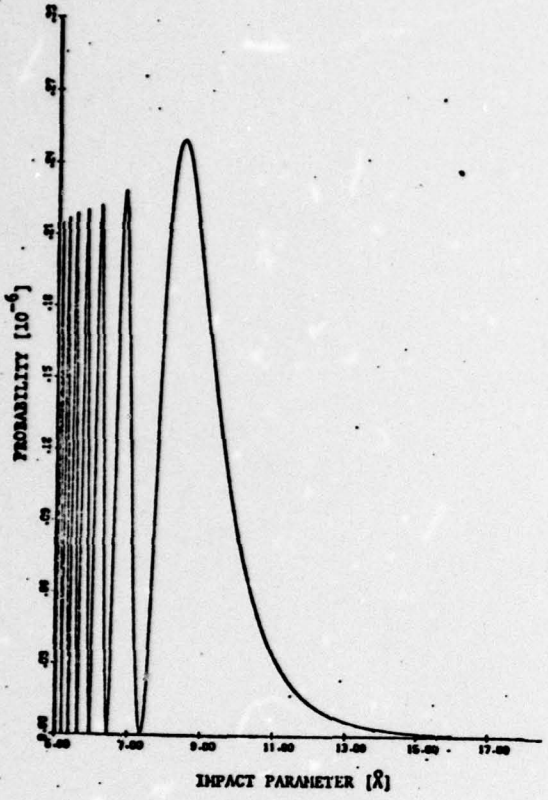
PROBABILITY [10^{-6}]
IMPACT PARAMETER [Å]

Fig. 4(a)

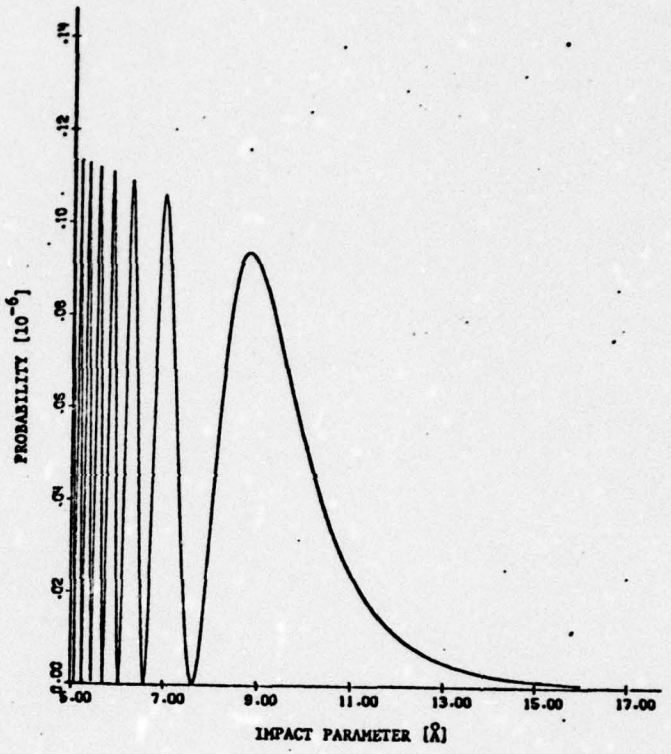
PROBABILITY [10^{-6}]
.00
.02
.04
.06
.08
.10
.12
.14
5.00
7.00
9.00
11.00
13.00
15.00
17.00
IMPACT PARAMETER [Å]

Fig. 4(b)

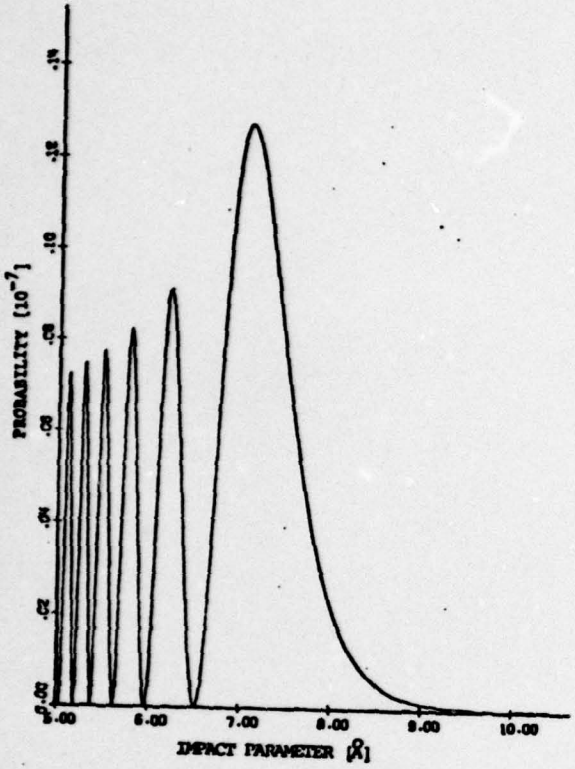
PROBABILITY [10^{-7}]
.00
.04
.08
.12
.16
5.00
6.00
7.00
8.00
9.00
10.00
IMPACT PARAMETER [Å]

Fig. 5(a)

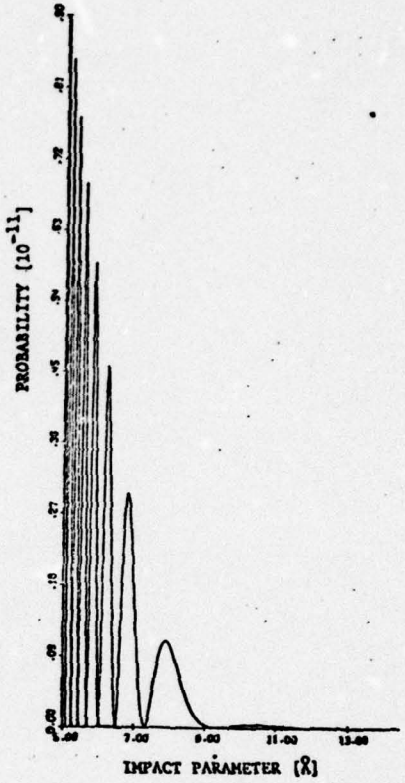
PROBABILITY [10^{-11}]
.00
.09
.15
.21
.27
.30
.36
.42
.45
.51
.57
.63
.69
.72
.78
.81
.87
.90
7.00
9.00
11.00
13.00
IMPACT PARAMETER [Å]

Fig. 5(b)

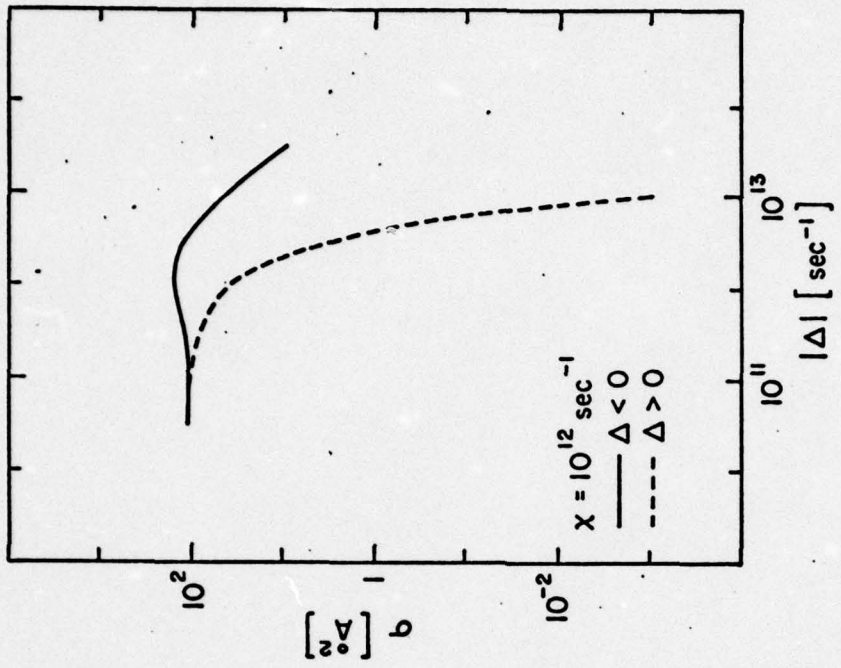
10^{13}
10^{11}
$|\Delta|$ [sec^{-1}]
$\chi = 10^{12}$ sec^{-1}
$\Delta < 0$
$\Delta > 0$
10^{2}
1
10^{-2}
q [Å^2]

Fig. 7

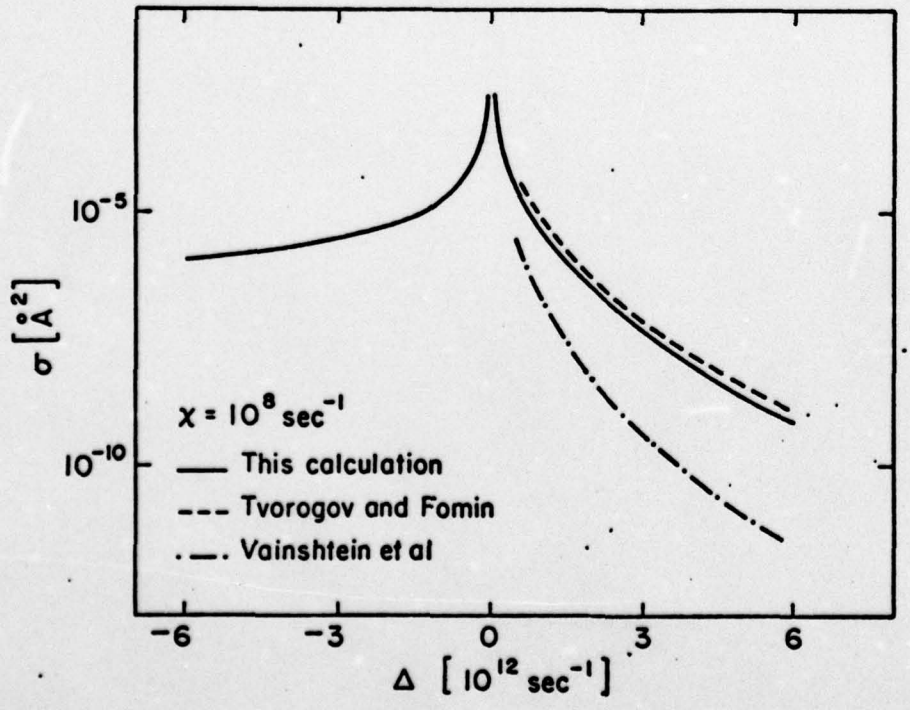
10^{-5}
10^{-10}
σ [Å^2]
$\chi = 10^{8}$ sec^{-1}
This calculation
Tvorogov and Fomin
Vainshtein et al
-6
-3
0
3
6
Δ [10^{12} sec^{-1}]

Fig. 6

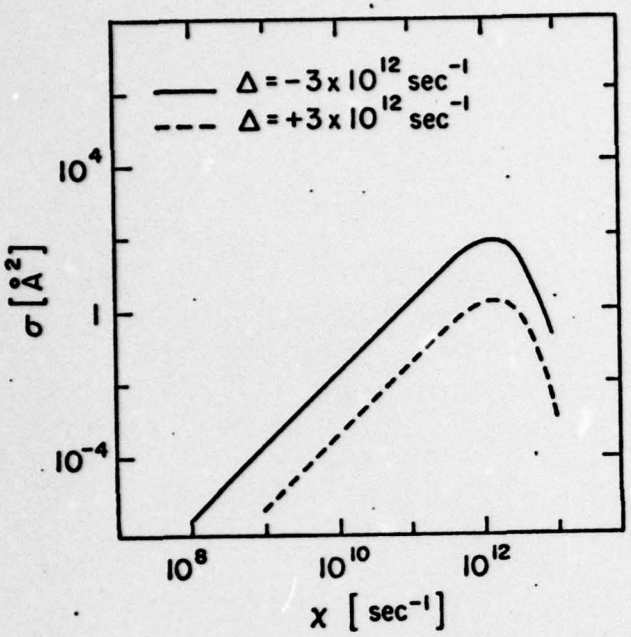
Δ = −3 x 10^12 sec^−1
Δ = +3 x 10^12 sec^−1
10^4
1
10^−4
σ [Å^2]
10^8
10^10
10^12
x [sec^−1]

Fig. 8

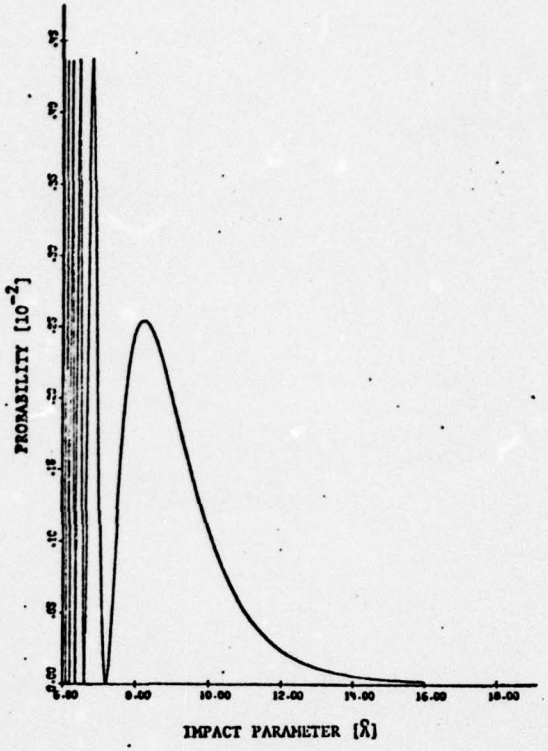
PROBABILITY [10^−2]
IMPACT PARAMETER [Å]

Fig. 9

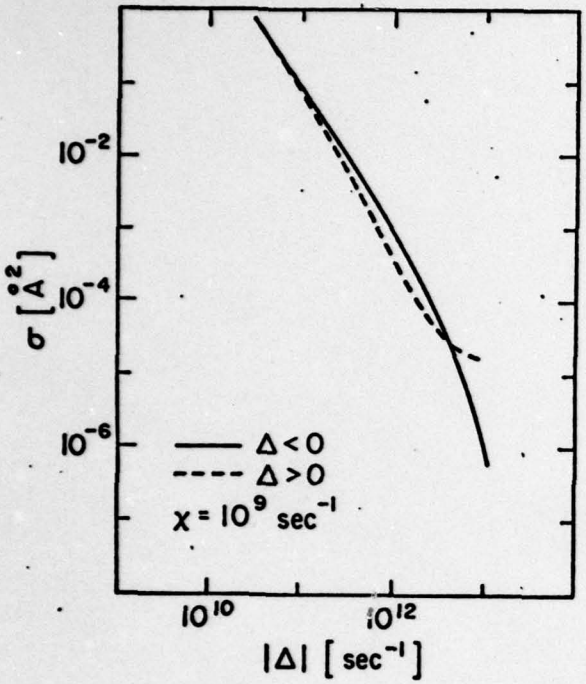
10^{-2}
10^{-4}
10^{-6}
σ [Å²]
Δ < 0
Δ > 0
χ = 10^{9} sec^{-1}
10^{10}
10^{12}
|Δ| [sec^{-1}]

Fig. 10

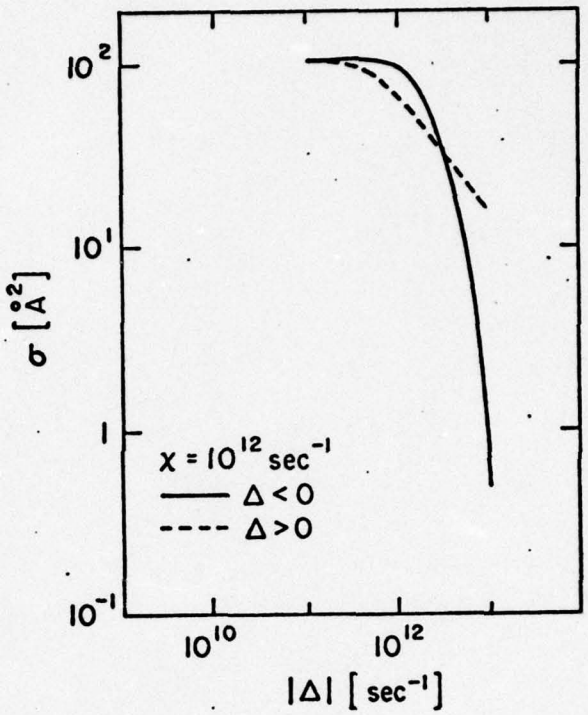
10^{2}
10^{1}
1
10^{-1}
σ [Å²]
χ = 10^{12} sec^{-1}
Δ < 0
Δ > 0
10^{10}
10^{12}
|Δ| [sec^{-1}]

Fig. 11

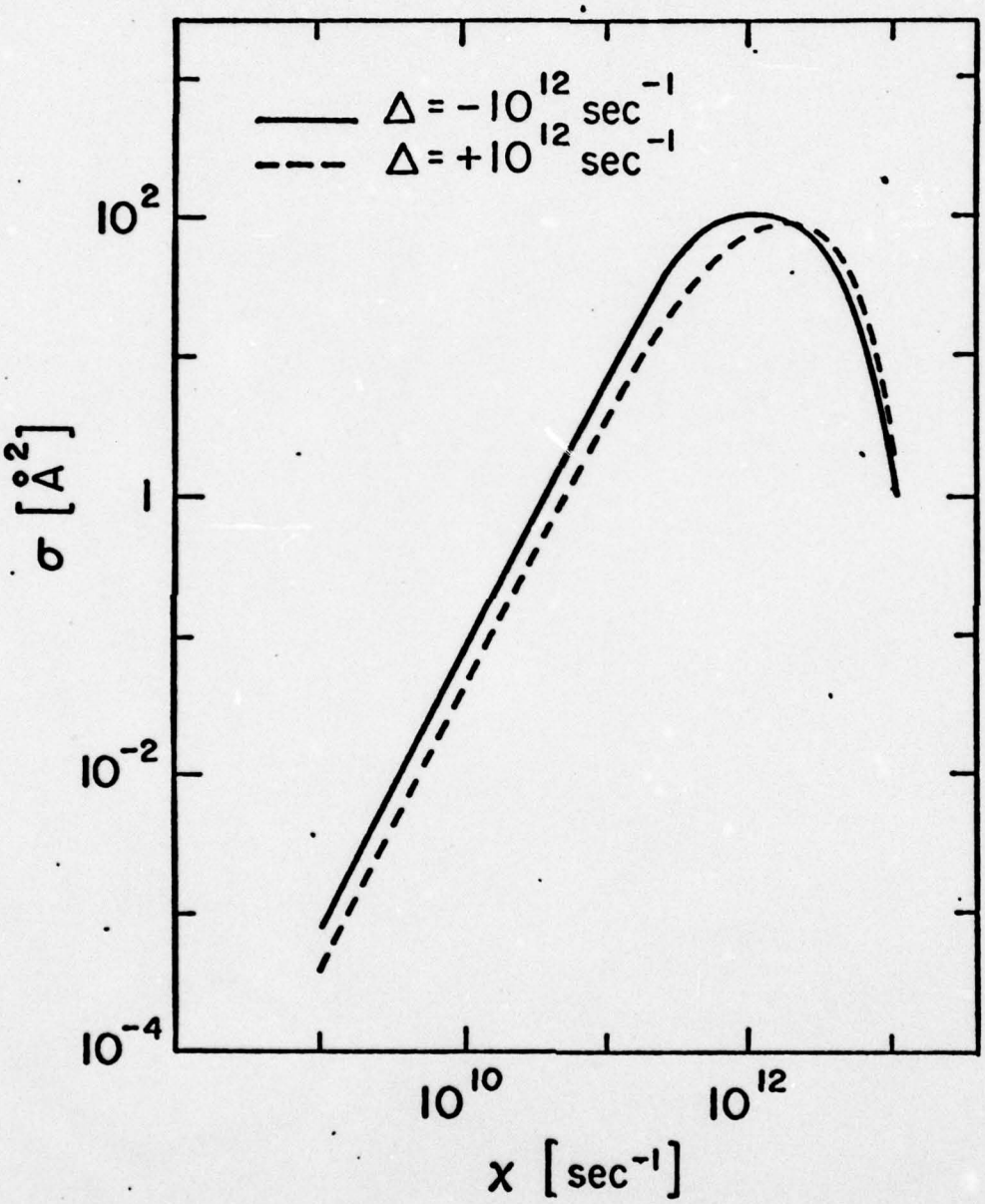

Fig. 12

RADIATIVE COLLISIONS WITH IMPACT LEVEL SHIFTS

E. J. Robinson

Physics Department

New York University

4 Washington Place

New York, N. Y. 10003

U. S. A.

Supported by the U.S. Office of Naval Research
under Contract No. N00014-77-C-0553

ABSTRACT

An analytic expression is derived for the transition probability during a radiative collision for a model problem in which induced level shifts are treated in the impulse approximation. The formulae predict a behavior that qualitatively resembles that obtained for realistic potentials, and is in fair agreement with the experimental lineshape obtained by Harris and his colleagues.

IMPACT MODEL FOR RADIATIVE COLLISIONS

A number of authors have, in recent years, reported on the novel excitation process known as radiative collisions. (Guzenko and Yakovlenko 1972, Lisitsa and Yakovlenko 1974, Harris and Lidov 1974, 1975, Falcone et al 1976a, 1976b, Harris and White 1977, Geltman 1976, Payne and Mayfeh 1976, Knight 1977.) These are scattering events in which energy is transferred between unlike atomic species in the presence of a laser field which is nearly resonant with the difference in excitation of the two atoms. Thus, if A and B are the two dissimilar systems, the reaction proceeds according to

$$A^* + B + h\nu \rightarrow A + B^* .$$

A portion of the appropriate energy level diagram is shown in figure 1. Excited atom A undergoes a collision with atom B initially in its state of lowest energy, while the system is subjected to a radiation field. The transition to the final state, where A is in its ground state and B is energized, involves the absorption of a photon. (Clearly an analogous process which is accompanied by stimulated emission could also be studied. In the present work, we consider only the absorptive case.) Since the process involves a change in the state of each atom, it cannot occur without the collision.

We adhere to the customary theoretical formulation, in which the radiation field and the nuclear motion are treated classically, and the electrons quantally, and where, in addition, the nucleii are assumed to travel along straight line paths. Hence, the only effect of the nuclear motion is to generate a time-dependent potential for the electrons, with the result that the energy of electrons + radiation field need not be conserved.

Assuming linearly polarized monochromatic light, the Hamiltonian for the problem is given by

$$H = H_a + V_c - e\vec{E} \cdot (\vec{r}_A + \vec{r}_B) \cos\omega t, \qquad (1)$$

where H_a is the electronic Hamiltonian, V_c is the ~~Coulomb~~ interatomic potential acting on the electrons at internuclear separation R, and where the third term gives the interaction between the electrons and radiation field. (The vectors $\vec{r}_A$ and $\vec{r}_B$ represent the sums of position operators for all the electrons in the respective atoms, measured with respect to the separate nucleii.) The nucleii are considered to be much closer than a wavelength during the interaction, so that phase differences between $\vec{E}(0)$ and $\vec{E}(\vec{R})$ are negligible.

The asymptotic form of the ~~Coulomb~~ interaction V_c behaves like R^{-3}, and we assume, following the cited references, that this form adequately represents the interaction between the atoms at all separations of interest.

By making the rotating wave approximation and treating the problem perturbatively through second order in E and V_c, it is possible to approximately reduce the problem to a two level system driven by the effective Hamiltonian

$$H_{eff} = H_a + \sum_{i=1}^{2} a_i^+ a_i \left(Q_i R^{-6} + \frac{C_i E^2}{2} \right) + \frac{EB}{2} R^{-3} \left(a_2^+ a_1 e^{-i\Delta t} + a_1^+ a_2 e^{+i\Delta t} \right). \qquad (2)$$

(Harris and White) Atomic units are used here and throughout the remainder of the article. The initial and final states (designated by the subscripts 1,2) are composites, i.e. in state 1 atom A is in level A_2 and

atom B in level B_1, and in state 2 atom A is in level A_2 and atom B is in level B_3. In equation (2), Q_i is the van der Waals R^{-6} coefficient for composite state i, C_i the composite A.C. Stark coefficient, and B an angle averaged sum over off-diagonal matrix elements, which is taken to be a constant here and in some references. (Lisitsa and Yakovlenko, Harris and White.) (Geltman and Knight follow the more rigorous procedure of retaining the angular dependence, and averaging the transition probability after completing the calculation. The form of the final result does not depend upon which method is used.) The operators a_i, a_i^+ annihilate and create the system in state i.

In this two level representation of the electronic motion, the time dependent Schroedinger equation becomes a pair of coupled, first-order differential equations for the state amplitudes α_1 and α_2, for detuning Δ

$$i\,\dot{\alpha}_1 = \frac{EB}{2R^3}\alpha_2 e^{i\Delta t} + \left(\frac{C_1E^2}{2} + Q_1R^{-6}\right)\alpha_1, \qquad (3a)$$

$$i\,\dot{\alpha}_2 = \frac{EB}{2R^3}\alpha_1 e^{-i\Delta t} + \left(\frac{C_2E^2}{2} + Q_2R^{-6}\right)\alpha_2 . \qquad (3b)$$

Equations (3a) and (3b) are to be solved subject to the initial conditions that $\alpha_1 = 1$, $\alpha_2 = 0$ as $t \to -\infty$.

We will restrict our attention to the weak field limit for the balance of the article, neglect the A.C. Stark shift, and solve for $\alpha_2(t = +\infty)$ with $\alpha_1 = 1$ for all t. Dropping the argument $(+\infty)$, the transition amplitude reduces to the integral

$$i\alpha_2 = \frac{EB}{2}\int_{-\infty} dt\, \exp[-i\Delta t - i\,(Q_1-Q_2)f(t)]/(V^2t^2+\rho^2)^{3/2}, \qquad (4)$$

where ρ is the impact parameter, V the relative velocity, and $f(t) = \int_{-\infty}^{t} \frac{ds}{(V^2s^2+\rho^2)^3}$. (The lower limit of the integral defining f is arbitrary to within an overall phase factor.) The integral in equation (4) cannot be evaluated in closed form. Geltman and Knight have utilized an approach that is equivalent to neglecting the level shifting term in the exponential, thereby reducing the problem to the evaluation of

$$i\alpha_2 = \frac{EB}{2}\int_{-\infty} dt\, \exp[-i\Delta t]/(V^2t^2+\rho^2)^{3/2} . \qquad (5)$$

The integral in equation (5) is proportional to a well-known representation of the modified Bessel function K_1. (Abramowitz and Stegun, 1964.) Thus, in this zero level-shift approximation, the transition amplitude becomes

$$\alpha_2 = -i\,\frac{BE|\Delta|}{V^2\rho}\,K_1\left(\frac{|\Delta|\rho}{V}\right) . \qquad (6)$$

The spectrum calculated with this formula reaches a maximum at $\Delta = 0$ and is manifestly symmetrical about the peak. This insensitivity of the total cross section to the sign of the detuning is contrary to experiment and also in disagreement with theoretical results in which the level shifting term f(t) is taken into account. (Lisitsa and Yakovlenko, Harris and White.) In a sense, too, the inclusion of the second order perturbative term bilinear in the interactions $\vec{E}\cdot(\vec{r}_A + \vec{r}_B)$ and V_c, while omitting terms quadratic in these potentials, appears to be somewhat inconsistent. Consequently, we tend to prefer results based on theories in which f(t) is included at least approximately. (For large impact parameters, $f(t)\to 0$ much more rapidly than the transition

amplitude, and its neglect in that limit is completely justified.) Unfortunately, for non-vanishing, realistic f(t) one can no longer express the answer in analytic form, and results in the references are obtained by numerical or asymptotic methods.

Numerical methods provide an essentially exact solution to the coupled equations that characterize this problem, and, superficially, it might seem that nothing more need be done once a functioning program is constructed. Unfortunately, for large detunings and/or small impact parameters, the step size required to preserve accuracy becomes so small that the quantity of computer time required to calculate lineshapes grows virtually without bound. Furthermore, the techniques of numerical analysis often fail to provide insight, since they can hide the explicit dependence of results on the relevant parameters. For these reasons, we have sought an analytically intregable model problem which includes both detuning and time-dependent level shifts.

The purpose of this work is to point out that the impact model, which is an extension of work which omits level shifts (Geltman, Knight) represents just such a soluble problem. We will derive an analytic expression for α_2 in this model, and, by choosing the parameters in a manner related to real atomic constants, apply the model to actual collisions.

In the impact model, the level-shifting potential is a delta function in time, so that f(t) becomes a step function, possessing the values f(t) = 0, t<0, and f(t) = ϕ, t>0, ϕ constant. Equation (4) then becomes, after taking advantage of even and odd integrands,

$$;\alpha_2 = EB \exp(-i\phi/2) \left\{ \cos(\phi/2) \int_0^\infty dt \cos\Delta t/(V^2t^2+\rho^2)^{3/2} + \sin\phi/2 \int_0^\infty dt \sin\Delta t/(V^2t^2+\rho^2)^{3/2} \right\} , \quad (7)$$

where we have now absorbed the factor Q_1-Q_2 into the definition of f(t).

The first integral in equation (7) is proportional to the same $K_1(\frac{\Delta\rho}{V})$ already obtained by Geltman and by Knight. The second integral may be expressed in terms of I_1 and L_{-1} (Abramowitz and Stegun), where I_1 is a modified Bessel function and L_{-1} a modified Struve function. Thus,

$$;\alpha_2 = \exp(-i\phi/2) \frac{EB}{V^2} \left\{ \frac{\cos\phi/2}{2} \pi^{1/2}\Delta K_1(\tfrac{\Delta\rho}{V})/\Gamma(\tfrac{3}{2})V + \sin\phi/2 \frac{\pi^{1/2}}{4\rho} \Gamma(-\tfrac{1}{2}) \Delta[I_1(\tfrac{\Delta\rho}{V}) - L_{-1}(\tfrac{\Delta\rho}{V})] \right\} . \quad (8)$$

This trivially reduces to equation (5) if ϕ = 0. We note immediately that the symmetry about the line center inherent in Geltman's and Knight's approximation is removed, with the maximum tending to be shifted toward negative detunings. (Our use of the terms "negative" and "positive" detunings, or equivalently "red" and "blue", is consistent with the assumption that the van der Waals force is more attractive in the final state. If the converse applies, the description is reversed.) It still turns out, however, that the line shape integrated over impact parameter will have a maximum at Δ = 0. These points are in agreement with experiment and with calculations incorporating realistic f(t). We note also that, at zero detuning, the amplitude for large impact parameters

falls off as ρ^{-2} and that, as a result of the asymptotic decay of K_1 and $I_1 - L_{-1}$, the contributions of large impact parameters constitute less at non-zero detuning than they do at exact resonance, again in agreement with the numerical calculations of Harris and White.

It is of interest to ask whether this impact ansatz for the level-shifting potential has any relevance for radiative collisions between real atoms. Certainly, one would expect a step function approximation to be valid if the rise time of f(t) is much less than the full width, half maximum of $(v^2t^2+\rho^2)^{-3/2}$. In the actual physical problem of interest, however, the phase integral varies over a characteristic time only somewhat faster than $R^{-3}(t)$, and one might question how well its behavior is represented by a step function. It turns out that if we make ϕ a function of impact parameter, choosing it to be the actual integrated phase induced by the R^{-6} interaction, the model yields an excellent approximation to α_2 for small detunings and impact parameters greater than R_W, the Weisskopf radius. Furthermore for values of $\rho<R_W$, the phase factor ϕ varies sufficiently rapidly with impact parameter to produce the characteristic oscillations generated in numerical solutions (Harris and White), although in quantitative disagreement with the positions and values of maxima. It is of interest to note that oscillation occurs here even though its standard explanation in terms of interference between the amplitudes generated at two curve crossings does not apply. Obviously, there is interference in the present problem, but it occurs because of different phase factors attached to the coefficients of negative and positive time contributions to α_2.

We also find oscillations on the blue side of zero detuning, where there is no curve crossing in the R^{-6} problem. We also find this in our own numerical calculations with the actual potential, and it appears that the assumption that level crossings are needed for interference is not correct.

Taking the impact ansatz to be an approximation method for real problems, we have applied our formulae to the Ca-Sr system investigated experimentally and theoretically by Harris and his colleagues. (Harris and Lidow 1974, 1975, Falcone et al 1976a, 1976b, Harris and White.)

In order to prevent the integral over impact parameter from diverging, it is necessary to set its lower limit at a value $\neq 0$, similar to cutoffs introduced by Geltman and by Knight. (The presence of the $\sin(\phi/2)$ term in equation (8) reduces the average contribution of the divergent term, but does not eliminate it.) Physically, such a cut-off is meaningful, also, since the repulsive core of the interatomic potential excludes contributions from small separations anyway. With this in mind, one should perhaps use an effective kinetic theory radius for the minimum impact parameter. Lacking reliable values, we arbitrarily chose 7 Å as our minimum impact parameter.

Our lineshape results are plotted in figure 2, together with those of the Harris group. We have performed our calculation for the rms relative velocity, ignoring the Maxwell-Boltzmann distribution. We do not anticipate that any major effect results from our failure to average over velocities.

Our integrated lineshape, while exhibiting the same red preference, is seen to be broader than that generated by finite difference solution

of the time-dependent two level equation. It is not, however as different from the experimental curve as the numerical work, especially in the blue. It is not clear why our impact results seem to produce a better approximation to the experimental curve than "exact" numerical methods. It is tempting to assert that the presence of the repulsive core in the actual system causes the potential to behave more impulse-like than a pure R^{-6} interaction, but that is pure speculation.

To summarize, we have presented analytic solutions for a model of radiative collisions, including the effect of time-dependent electronic level shifts. Our results are an extension of the work of Geltman and Knight, who neglect level shifts. The formulae make predictions for the variation of weak-field transition probabilities with impact parameter and detuning that qualitatively resemble the behavior of real systems. For unknown reasons, the line shape calculated with our equations seem to be in better accord with experimental curves than numerical calculations utilizing realistic potentials.

In a future article, we will report on efforts to extend this work to arbitrary field strengths.

The author wishes to thank Prof. Paul R. Berman for introducing him to the problem of radiative collisions, and for stimulating conversations.

This work was partially supported by the U.S. Office of Naval Research, through Contract Number N00014-77C-0553.

REFFRENCES

Abramowitz M and Stegun I A 1964 Handbook of Mathematical Functions (Washington D.C.: NBS)

Falcone R W, Green W R, White J C, and Harris S E 1976a Phys. Rev. Lett. 36 462

-----1976b Phys. Rev. Lett. 37 1590

Geltman S 1976 J. Phys. B: Atom. Molec. Phys. 9 L569

Gudzenko L I, and Yakovlenko S I 1972 Sov. Phys.-J E T P 35 877

Harris S E and Lidov D B 1974 Phys. Rev. Lett. 33 674

-----1975 Phys. Rev. Lett. 34 172

Harris S E and White J C 1977 I E E E J. Quant. Electr. QE-13 972

Knight P L 1977 J. Phys. B: Atom. Molec. Phys. 10 L195

Lisitsa V S and Yakovlenko S E 1974 Sov. Phys.-J E T P 39 759

Payne M G and Nayfeh M H 1976 Phys. Rev. A 13 596

Figure Captions

Figure 1: Energy Level diagram of composite system. System absorbs a photon and undergoes a transition from A2-B1 to A1-B3.

Figure 2: Radiative collision spectrum for Ca-Sr. Cross section for absorption as a function of detuning.

- α; Impact approximation calculation, this work.
- β; Smoothed graph based on experimental curve of Harris and White.
- λ; Numerical calculation of Harris and White. (Note: each curve is normalized to the same maximum. The ordinates, obviously, are in arbitrary units.)

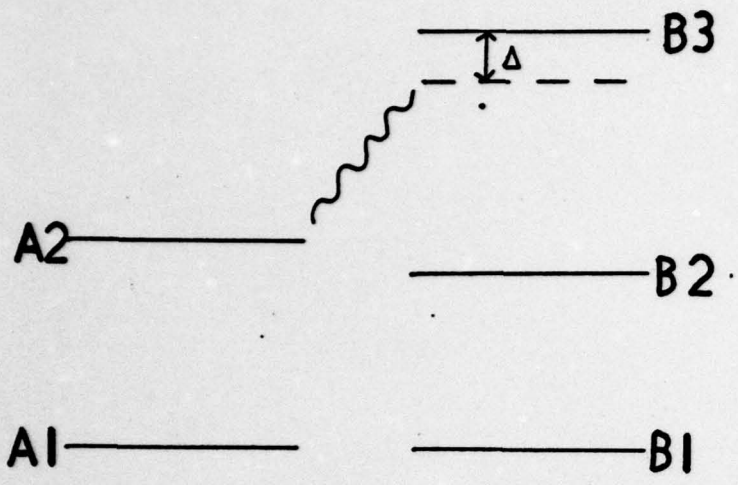

FIG. 1

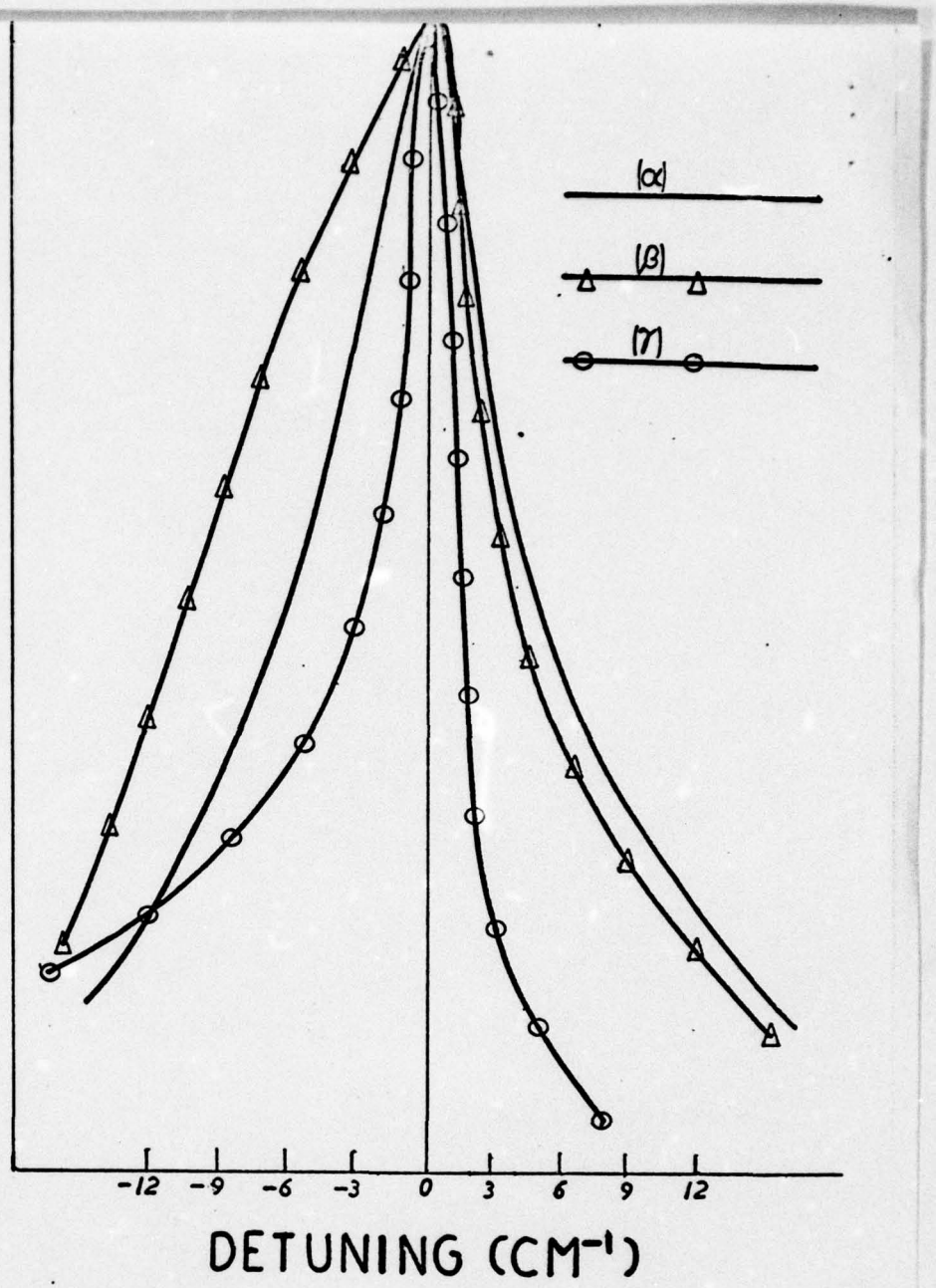

Study of velocity-changing collisions in excited Kr using saturation spectroscopy

C. Brechignac and R. Vetter
Laboratoire Aime Cotton, Centre National de la Recherche Scientifique II, Batiment 505, 91405-Orsay, France

P. R. Berman
Physics Department, New York University, 4 Washington Place, New York, New York 10003

(Received 28 September 1977)

A saturated-absorption experiment is used to measure the effects of velocity-changing collisions between Kr* metastable atoms ($4p^5 5s[3/2]_2$) and He and Ar perturbers. Comparison between experimental profiles and profiles calculated assuming hard-sphere collisions between Kr* and perturber atoms confirms the calculations of Borenstein and Lamb concerning the change of velocity associated with a collision. Furthermore it is found that the rate of velocity-changing collisions is consistent with the predictions of kinetic theory.

I. INTRODUCTION

We report the first systematic saturation spectroscopy study of velocity-changing collisions (VCC) between electronically excited active atoms and ground-state perturbers. By choosing a perturber–active-atom mass ratio less than unity, we are able to clearly isolate the effects of close-encounter collisions. As such, our analysis represents an initial step in obtaining specific information on the short-range part of excited-state interatomic potentials by monitoring VCC using saturation spectroscopy, and it indicates the potential of this method for studying scattering in short-lived excited states.

The study of velocity-changing collisions (VCC) in the ground and excited states of atoms or molecules using laser spectroscopic techniques has received increased attention over the past few years.[1-9] In a typical experiment one uses a narrow-band laser source of frequency Ω tuned near an atomic-transition frequency ω to selectively excite atoms with an axial velocity $v_z = (\Omega - \omega)/k$, $(k = \Omega/c)$; only atoms with this axial velocity will see a Doppler-shifted laser frequency in resonance with their own transition frequency. A probe laser beam is then used to monitor any velocity change undergone by these excited atoms. Although only one velocity component is studied by this technique, information on the nature of the collision interaction can be inferred from the results of such experiments. Theoretical aspects of the problem are examined in Refs. 10–12.

To date, experiments have been analyzed assuming collisions are of a "weak" or "strong" nature. Weak collisions involve relatively small velocity changes Δu ($\Delta u \ll u$ = width of the equilibrium velocity distribution) and presumably characterize collisions with large impact parameters. A strong collision usually refers to a collision which, on average, completely thermalizes the atom's velocity distribution ($\Delta u \approx u$) as might occur following a close collision between a heavy perturber and a light active atom. In a previous publication, we reported on the influence of collisions on saturated absorption profiles of the 557-nm line of Kr I[5]; Kr*-Kr and Kr*-Xe collisions were considered and interpreted in terms of a strong-collision model.

In this work, we study the effect of close-encounter collisions between Kr* atoms and He or Ar perturbers, for which both the strong-and weak-collision models are inadequate. Saturated-

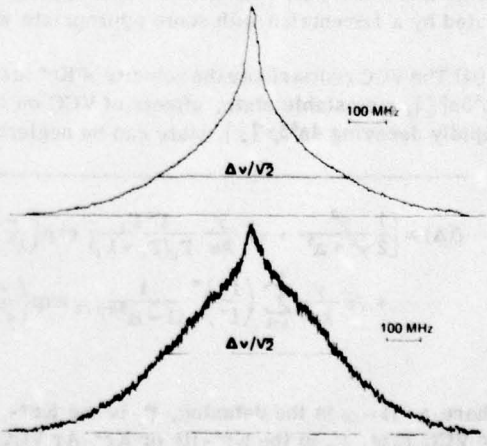

FIG. 1. Typical recording of the 557-nm line of Kr I in the presence of He and Ar perturbers. Upper trace: P_{Kr}, 8 mTorr; P_{He}, 260 mTorr. Lower trace: P_{Kr}, 8 mTorr; P_{Ar}, 220 mTorr. The horizontal line represents the Doppler width $/\sqrt{2}$. In this experiment the frequency scale is determined by Fabry-Perot fringes spaced by 83 MHz.

Supported by the U.S. Office of Naval Research under Contract No. N00014-77-C-0553.

absorption line shapes for the 557-nm transition $(4p^5 5s[\frac{3}{2}]_2 - 4p^5 5p'[\frac{1}{2}]_1)$ in Kr I were obtained using an experimental arrangement that has been described elsewhere.[8] The pressure of krypton was kept at a fixed value of 8 mTorr and the pressures of He and Ar perturbers were varied between 0 and 700 and 0 and 250 mTorr, respectively. Typical recordings of saturated-absorption profiles are shown on Fig. 1. Saturated-absorption profiles have shapes and widths varying with mass and pressure of perturbers; they could be consistently fit over the entire pressure ranges assuming they are the sum of a narrow resonance of width 2γ [full width at half maximum (FWHM)] and a broad background. The narrow component corresponds to atoms that have not undergone VCC, and the broad one corresponds to atoms that have experienced VCC. The shape of the background signals provides direct information characterizing the strength and cross-section for Kr*-Kr, Kr*-He, and Kr*-Ar collisions. In this paper we use a hard-sphere model to describe the collisions, but more detailed models could be used in the future.

II. THEORETICAL ASPECTS

The following assumptions, consistent with the experimental results, were used to arrive at a theoretical line shape.

(i) The narrow resonance in the line shape, as modified by phase-interrupting collisions, saturation broadening, weak VCC,[6,7,9-13] beam misalignment, and laser jitter can still be well approximated by a Lorentzian with some appropriate width 2γ.

(ii) The VCC redistribute the velocity of Kr* in the $4p^5 5s[\frac{3}{2}]_2$ metastable state; effects of VCC on the rapidly decaying $4p^5 5p'[\frac{1}{2}]_1$ state can be neglected.

(iii) Close-encounter Kr*-He or Kr*-Ar collisions can be characterized as hard-sphere collisions with a collision kernel of the Keilson-Storer type[14]

$$W(\vec{v}' \to \vec{v}) = \Gamma_2 [\pi(\Delta u)^2]^{-3/2} \times \exp[-(\vec{v} - \alpha\vec{v}')^2/(\Delta u)^2], \quad (1)$$

where $W(\vec{v}' \to \vec{v})$ is the probability density per unit time to have a velocity change from $\vec{v}'$ to $\vec{v}$,

$$\Delta u = (1-\alpha^2)^{1/2} u \quad (2)$$

is $\sqrt{2}$ times the rms velocity change per collision, u is the most probable speed of the equilibrium distribution, α is a parameter related to the strength of a collision, and Γ_2 is the rate of VCC. For hard-sphere collisions, Borenstein and Lamb[15] have calculated α as a function of perturber–active-atom mass ratio using a computer simulation of the collisions.

(iv) A single VCC is sufficient to remove atoms from the velocity holes created by the field, i.e., $\Delta u > 2\gamma/k$. This condition is satisfied in our experiment.

(v) The Kr*-Kr collisions can be approximated as "strong" collisions leading to a thermal distribution after a single average collision. Hard-sphere collisions between equal-mass atoms or excitation-exchange collisions are approximately described by such a collision model.[15] The data of Fig. 1 contain both the Kr*-Kr and Kr*-He or Ar contributions to the broad background.

Assuming that the field strengths are weak enough to justify a rate-equation approximation to the atom-field interaction and using the above collision model, one arrives at the saturated-absorption line shape[10-12] for equal pump and probe frequencies,

$$I(\Delta) \propto \left[\frac{1}{2}\frac{\gamma^2}{\gamma^2+\Delta^2} + \sqrt{\pi}\frac{\gamma}{ku}\frac{\Gamma'\Gamma_1}{\Gamma_0(\Gamma_0+\Gamma_1)}\exp\left(\frac{-\Delta^2}{k^2u^2}\right) + \sqrt{\pi}\frac{\gamma}{ku}\sum_{n=1}^{\infty}\left(\frac{\Gamma_2}{\Gamma'}\right)^n \frac{1}{(1-\alpha^{2n})^{1/2}}\exp\left(\frac{-\Delta^2}{k^2u^2}\,\frac{1+\alpha^n}{1-\alpha^n}\right)\right]\exp\left(\frac{-\Delta^2}{k^2u^2}\right) \quad (3)$$

where $\Delta = \Omega - \omega$ is the detuning, Γ_1 is the Kr*-Kr VCC rate, Γ_2 is the Kr*-He or Kr*-Ar VCC rate,

$$\Gamma_0 = \tau^{-1},$$

where τ is the lifetime of Kr* atoms in the laser beams (experimentally, since the natural lifetime of the metastable is very long, τ is determined by the transit time in the beams, which will be pressure dependent) and

$$\Gamma' = \Gamma_0 + \Gamma_1 + \Gamma_2.$$

The line shape (3) has a simple interpretation. The first term arises from atoms undergoing no VCC during the time τ, the second term arises from atoms undergoing at least one Kr*-Kr collision in the time τ leading to a complete thermalization and the final term corresponds to atoms undergoing no Kr*-Kr collisions and some Kr*-He or Kr*-Ar collisions in the time τ leading to a partial thermalization of the sample.

III. ANALYSIS OF THE DATA

Experimental profiles were compared to theoretical line shapes corresponding to expression (3) by making the following assumptions: For the fixed Kr pressure of 8 mTorr chosen in this experiment we have taken the rate Γ_1 for thermalizing Kr*-Kr collisions as $\Gamma_1 = 1.4\times10^5$/sec determined from our previous experiment.[8] We have used a hard-sphere model for the determination of α and Γ_2; α was chosen from the results of Borenstein and Lamb[15]: $\alpha = 0.936$ for Kr*-He and $\alpha = 0.6$ for Kr*-Ar. {A larger value of α implies a smaller Δu [cf. Eq. (2)]; for perturber–active atom mass ratios $\gg1$, $\alpha \approx 0$, and for perturber–active-atom mass ratios $\ll1$, $\alpha \approx 1$.} The rate Γ_2 was chosen from the kinetic theory of gases with the "radii" of atoms as indicated by Allen,[16] $\Gamma_2 = 1.0\times10^4 p$ sec^{-1} for Kr*-He and $\Gamma_2 = 0.53\times10^4 p$ sec^{-1} for Kr*-Ar, where p is the perturber pressure in mTorr. At each perturber pressure, the values of the two parameters γ and Γ_0 were varied so as to minimize the rms error of the fit of Eq. (3) to the data. Typical examples for He and Ar are shown on Fig. 2. For the entire pressure range studied the data could be fit very well (i.e. with a normalized rms error ≤ 0.05) by Eq. (3).

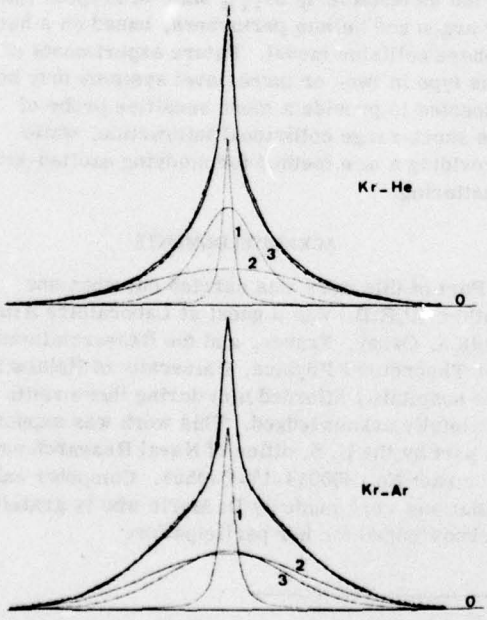

FIG. 2. Typical fits for He and Ar perturbers. Upper trace: P_{Kr}, 8 mTorr; P_{He}, 110 mTorr. Lower trace: P_{Kr}, 8 mTorr; P_{Ar}, 120 mTorr. The solid line corresponds to the recorded profile and large dots represent the calculated profiles corresponding to the best fit. The three dotted lines represent the contributions from the three terms of Eq. (3): Curve 1 corresponds to the narrow resonance (first term), curve 2 corresponds to the Gaussian background (second term) arising from Kr*-Kr collisions, and curve 3 corresponds to the contribution of VCC (third term) arising from Kr*-He and Kr*-Ar collisions.

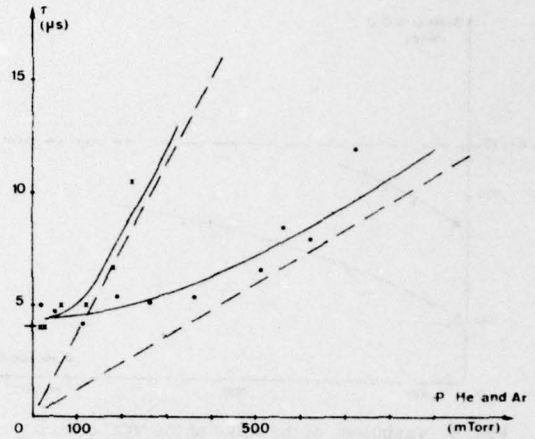

FIG. 3. Variations of the transit time τ vs perturber pressures. (Dots correspond to He-Kr* and crosses to Ar-Kr* data.) The broken lines correspond to the variations given by the classical law of diffusion.

The values of $\tau = \Gamma_0^{-1}$ obtained for the various perturber pressures are plotted on Fig. 3. There is an increase of τ with pressure similar to the one observed for Kr*-Kr collisions[8]; accordingly, we conclude that τ is determined by the transit times of atoms in the beams. The findings are consistent with the premise that heavier perturbers are more effective in increasing the transit time than lighter ones. The two curves converge to the same transit time at low pressure ($\tau_0 \approx 4$ μs) in accordance with the value measured in pure Kr at 8 mTorr; for the highest pressures they tend roughly to the linear variations given by the classical law of diffusion.[8]

The FWHM of the VCC contributions (third term in Eq. 3) as a function of perturber pressures is shown on Fig. 4. As may be seen, both widths approach the thermal-equilibrium value $\Delta\nu/\sqrt{2}$ = 510 MHz as the perturber pressure is increased. The heavier Ar atoms produce thermalization at a lower pressure than the lighter He ones (see also Fig. 1) consistent with the hard-sphere collision model. A value for these widths obtained at very low pressure can be deduced from Eq. (3) by taking the $n = 1$ term in the sum. These values are indicated in Fig. 4 by short-dashed lines.

We have tried various values of α around the values mentioned above, $\alpha = 0.93$ for Kr*-He and $\alpha = 0.6$ for Kr*-Ar. If α is chosen too small the

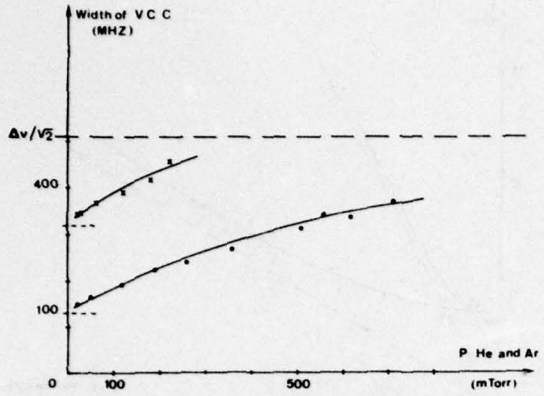

FIG. 4. Variations of the width of the VCC contributions [third term in Eq. (3) of text] vs perturber pressure (dots correspond to He and crosses to Ar perturbers). The horizontal dashed line corresponds to the thermal-equilibrium limit. The short horizontal dashed lines correspond to the width of the $n=1$ contribution in Eq. (3).

resulting Δu is too large to fit the data (for example, $\alpha = 0.85$ for He is a lower limit); on the other hand if α is chosen too large, the data could be fit only with unacceptably small values for 2_γ (for He, $\alpha = 0.98$ is an upper limit). We conclude that

$$\alpha = 0.93 \pm 0.03 \text{ for Kr*-He},$$

$$\alpha = 0.6 \pm 0.2 \text{ for Kr*-Ar},$$

where the error limits are obtained by those values of α leading to a normalized rms error of 0.2 in the fitting procedure.

The values of Γ_2 that we have chosen have been calculated using the ground-state kinetic-theory radii tabulated by Allen.[16] Values of Γ_2 determined in the same manner but by choosing for Kr* metastables a radius corresponding to the excited electron[17] have also been tried. Results are less consistent; first, the transit time takes on a nearly constant value ($\approx 3\ \mu$s) over the range of pressure and, second, the width of the narrow resonance is too small. Additional experiments with various perturber–active-atom mass ratios may help to clarify the manner in which the effective excited-state radius should be chosen.

We have tried also to fit the profiles by leaving free the three parameters γ, Γ_0, and Γ_2. For He the variations of Γ_2 with pressure showed, as expected, a linear increase at low pressure, but a decrease at high pressure ($p > 200$ mTorr). This deviation from the linear increase was attributed to the fitting procedure used since at high pressures VCC contribute well into the wings of the thermal distribution and it is difficult to distinguish between Kr*-Kr and Kr*-He contributions. The low-pressure regime gave $\Gamma_2 = 0.95 \times 10^4 p\ \text{sec}^{-1}$ confirming our choice for Γ_2 determined from kinetic theory and Allen's values.

IV. CONCLUSION

We have arrived at a consistent picture of VCC in the metastable $4p^5 5s[\frac{3}{2}]_2$ state of krypton caused by argon and helium perturbers, based on a hard-sphere collision model. Future experiments of this type in two- or three-level systems may be expected to provide a more sensitive probe of the short-range collisional interaction, while providing a new method for studying excited-state scattering.

ACKNOWLEDGMENTS

Part of this work was carried out when one author (P.R.B.) was a guest at Laboratoire Aimé Cotton, Orsay, France, and the Research Institute for Theoretical Physics, University of Helsinki; the hospitality afforded him during these visits is gratefully acknowledged. This work was supported in part by the U. S. office of Naval Research under Contract No. N00014-17-C-0553. Computer calculations were made by D. Merle who is gratefully acknowledged for her participation.

[1]T. W. Hänsch and P. E. Toschek, IEEE J. Quantum Electron. 5, 61 (1969); P. W. Smith and T. W. Hänsch, Phys. Rev. Lett. 26, 740 (1971); R. Keil, A. Schabert, and P. Toschek, Z. Phys. 261, 71 (1973); I. M. Beterov, Y. A. Matyugin, and V. P. Chebotaev, Zh. Eksp. Teor. Fiz. 64, 1495 (1973) [Sov. Phys.-JETP 37, 756 (1973)]; T. W. Meyer and C. K. Rhodes, Phys. Rev. Lett. 32, 637 (1974); R. G. Brewer, R. L. Shoemaker, and S. Stenholm, *ibid.* 33, 63 (1974); R. L. Shoemaker, S. Stenholm, and R. G. Brewer, Phys. Rev. A 10, 2037 (1974); J. Schmidt, P. R. Berman, and R. G. Brewer, Phys. Rev. Lett. 31, 1103 (1973); P. R. Berman, J. M. Levy, and R. G. Brewer, Phys. Rev A 11, 1668 (1975).

[2]T. Kan and G. J. Wolga, IEEE J. Quantum Electron. 7, 141 (1971).

[3]J. Brochard and Ph. Cahuzac, J. Phys. B 9, 2027 (1976).

[4]Ph. Cahuzac, O. Robaux, and R. Vetter, J. Phys. B 9, 3165 (1976).

[5]W. K. Bischel and C. K. Rhodes, Phys. Rev. A 14, 176 (1976).

[6]A. T. Mattick, N. A. Kurnit, and A. Javan, Chem. Phys. Lett. 38, 176 (1976).

[7]L. S. Vasilenko, V. P. Kochanov, and V. P. Chebotaev, Optics Commun. 20, 409 (1977).
[8]C. Brechignac, R. Vetter, and P. R. Berman, J. Phys. B 10, 3443 (1977).
[9]Ph. Cahuzac, E. Marie, O. Robaux, R. Vetter, and P. R. Berman, J. Phys. (to be published).
[10]A. P. Kolchenko, A. A. Pukhov, S. G. Rautian, and A. M. Shalagin, Zh. Eksp. Teor. Fiz. 62, 2097 (1972) [Sov. Phys. JETP 36, 619 (1973)].
[11]P. R. Berman, Phys. Rev. A 13, 2191 (1976).
[12]P. R. Berman, Adv. At. Mol. Phys. 13, 57 (1978).
[13]V. A. Alexseev, T. L. Andreeva, and I. I. Sobelman, Zh. Eksp. Teor. Fiz. 64, 813 (1973) [Sov. Phys.-JETP 37, 413 (1973)].
[14]J. Keilson and J. E. Storer, Q. Appl. Math. 10, 243 (1952).
[15]M. Borenstein and W. E. Lamb, Phys. Rev. A 5, 1311 (1972).
[16]C. W. Allen, *Astrophysical Quantities*, 2nd ed. (University of London, London, 1963), p. 45. These radii are approximately gas kinetic radii of monoatomic molecules and correspond to the distance of closest approach in the formation of molecules.
[17]M. Aymar (private communication).

Classification
Physics Abstracts
32.70 — 34.40

PERSISTENCE OF VELOCITY FOLLOWING ELASTIC COLLISIONS

C. BRÉCHIGNAC, R. VETTER

Laboratoire Aimé-Cotton, C.N.R.S. II, Bâtiment 505, 91405 Orsay Cedex, France

and

P. R. BERMAN (*)

Physics Department, New York University, 4 Washington Place, New York, N.Y. 10003, U.S.A.

(*Reçu le 21 avril 1978, accepté le 2 juin 1978*)

Résumé. — Une expérience d'absorption saturée à deux lasers conduite sur la raie de KrI à $\lambda = 557$ nm a permis l'étude des collisions élastiques Kr*-He. Pour une classe donnée d'atomes pompés hors résonance ($v_z \neq 0$) on peut mettre en évidence la persistance de la vitesse initiale après n collisions élastiques.

Abstract. — Elastic Kr*-He collisions have been studied using a two laser saturated-absorption experiment on the $\lambda = 557$ nm line of KrI. With the pump laser detuned from the atomic resonance, one can follow the collisional relaxation of Kr* atoms from a non-thermal distribution centred at $v_z \neq 0$ back towards a thermal distribution.

In saturated-absorption experiments, a probe beam monitors the longitudinal velocity distribution of active atoms that are selectively excited by a pump beam. Velocity-changing collisions (V.C.C.) alter this longitudinal velocity distribution and produce a corresponding modification of saturated-absorption profiles. *Strong* or *thermalizing* collisions give rise to a broad Gaussian background superimposed on the narrow resonance, i.e., following a collision, on average, the active atom's velocity is independent of its initial velocity, v_z, and is determined by the thermal distribution [1-4]. *Weak* collisions give rise to a distortion of the shape of the narrow resonance ; they are collisions with large impact parameters producing velocity changes smaller than the width of the hole burned in the velocity distribution [5-8]. Elastic hard sphere collisions between light perturbers and heavy active atoms lead to a non-Gaussian background signal owing to the velocity redistribution that they induce [9, 10]. The degree of thermalization following an average collision is sometimes referred to as the *persistence of velocity*.

In a previous publication [9], we studied the effect of V.C.C. on saturated-absorption profiles ($\lambda = 557$ nm of KrI) as a function of the active atom to perturber mass ratio. In that work the same laser was used to saturate and to probe the transition. During the scanning of the laser frequency, the saturator selects successive classes of velocity v_z ; V.C.C. drift and broaden the corresponding distributions of active atoms but their effect is necessarily detected by the probe at $-v_z$ only, hence symmetrical profiles centred around $v_z = 0$. To directly view the drift of active atoms, it is necessary to select them at a given $v_z \neq 0$ and to tune the probe over the velocity distribution as modified by V.C.C.

To this end, we have performed a two laser saturated-absorption experiment on the same transition of $Kr(4p^5\ 5s[3/2]_2\text{-}4p^5\ 5p'[1/2]_1)$ with the V.C.C. provided by the perturbers. The first dye laser, at frequency ν_1, is used to select by saturation a given class of longitudinal velocities far from zero ; to accomplish this, it is detuned from the atomic resonance at ν_0 by an amount comparable to the Doppler width ($\Delta\nu_D = 720$ MHz). The second-dye laser is used to probe both saturated-absorption (counter propagating waves) and linear absorption. Fabry-Perot fringes are used to calibrate the frequency scale of the probe. A typical recording is shown on figure 1. Trace I is the linear absorption profile, centred at ν_0. Trace II is a saturated-absorption profile obtained in pure krypton, for a detuning $\Delta = \nu_1 - \nu_0 = 600$ MHz

(*) Supported by the U.S. Office of Naval Research under Contract n° N 000 14 - 77-C-0553.

Supported by the U.S. Office of Naval Research under Contract No. N00014-77-C-0553.

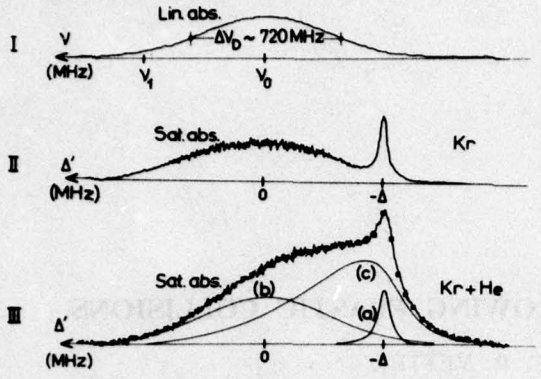

FIG. 1. — Trace I : Linear-absorption profile, centred at ν_0. Trace II : Saturated-absorption profile, obtained in pure krypton for a detuning $\Delta = 600$ MHz of the saturator. Trace III : Saturated-absorption profile, obtained in a mixture Kr-He ($P(\mathrm{Kr}) \simeq 10$ mtorr, $P(\mathrm{He}) \sim 450$ mtorr) for a detuning $\Delta = 600$ MHz. The squares represent a profile calculated from expression (2) with the values of the parameters indicated in the text. Trace (a) is the Lorentzian centred at $-\Delta$; Trace (b) is the contribution due to thermalizing Kr*-Kr collisions, centred at $\Delta' = 0$; Trace (c) is the contribution due to Kr*-He V.C.C.

of the saturator ; it shows a narrow resonance centred at $\Delta' = -\Delta$ and a Gaussian background centred at $\Delta' = 0$, and attributed to Kr*-Kr collisions. Trace III shows a saturated-absorption profile obtained in a mixture Kr-He, for the same detuning. The difference in shape between trace II and III is attributed to Kr*-He V.C.C. whose main contribution lies between $-\Delta$ and 0.

INTERPRETATION OF PROFILES. — To calculate the resulting profile in the presence of elastic collisions, one considers their effect on the phase of active dipoles (introduced *via* classical broadening constants) and their effect on the velocity associated with the atomic state populations (introduced *via* a *collision propagator* [11]). The propagator G which propagates a population density $n(v_z, 0)$ (v_z = longitudinal velocity) to the value $n(v'_z, t)$ *via*

$$n(v'_z, t) = \int G(v_z \to v'_z, t)\, n(v_z, 0)\, \mathrm{d}v_z$$

satisfies the equation :

$$\frac{\partial G}{\partial t}(v_z \to v'_z, t) = -\Gamma G(v_z \to v'_z, t) + \Gamma_1 \int W_1(v''_z \to v'_z)\, G(v_z \to v''_z, t)\, \mathrm{d}v''_z + \Gamma_2 \int W_2(v''_z \to v'_z)\, G(v_z \to v''_z, t)\, \mathrm{d}v''_z \quad (1)$$

with

$$G(v_z \to v'_z, 0) = \delta(v_z - v'_z)\,.$$

Both thermalizing and non thermalizing collisions are assumed to occur with rates Γ_1 and Γ_2 respectively. The quantity Γ is the total rate of population density loss, $\Gamma = \Gamma_0 + \Gamma_1 + \Gamma_2$ where Γ_0 is the inverse lifetime of the state population under consideration, which is here the time during which the atoms stay in the fields [9]. $W_1(v''_z \to v'_z)$ is the probability density for a thermalizing event to occur per unit time ;

$$W_1(v''_z \to v'_z) = W_1(v'_z) = \frac{1}{\sqrt{\Pi} u} \exp - (v'^2_z/u^2)$$

where u is the most probable speed of the thermal distribution. $W_2(v''_z \to v'_z)$ is the probability density for non-thermalizing events ; we choose the model of Keilson and Storer [12] to express :

$$W_2(v''_z \to v'_z) = \frac{1}{\sqrt{\Pi}\Delta u} \exp - [(v'_z - \alpha v''_z)^2/(\Delta u)^2]$$

where α is the mean *strength* of V.C.C. related to the r.m.s. change of velocity Δu by $(\Delta u)^2 = (1 - \alpha^2)\, u^2$. In this model Γ_2 can be fairly-well approximated by the rate of collisions in a hard sphere model and for a small ratio of perturber to active atom mass $m/M \ll 1$, $\alpha \approx 1 - \frac{4}{3}\frac{m}{M}$ [11].

Equation (1) can be solved by iteration and one obtains [10] :

$$\tilde{G}(v_z \to v'_z) = \frac{\delta(v_z - v'_z)}{\Gamma} + \frac{\Gamma_1\, W_1(v'_z)}{\Gamma_0(\Gamma_0 + \Gamma_1)} + \frac{1}{\Gamma} \sum_n \left(\frac{\Gamma_2}{\Gamma}\right)^n \frac{1}{\sqrt{\Pi}\,\Delta u_n} \exp - \left[\frac{v'_z - \alpha^n v_z}{\Delta u_n}\right]^2$$

where

$$(\Delta u_n)^2 = (1 - \alpha^{2n})\, u^2$$

and

$$\tilde{G}(v_z \to v'_z) = \int_0^\infty G(v_z \to v'_z, t)\, \mathrm{d}t\,.$$

Saturated-absorption profiles are given, in a two laser experiment (counter propagating beams) by the following expression (at very low saturation) [10]

$$I = I_0 \int \mathrm{d}v_z \int \mathrm{d}v'_z \frac{\tilde{\gamma}}{\tilde{\gamma}^2 + (\Delta - kv_z)^2}\, \tilde{G}(v_z \to v'_z) \times \frac{\tilde{\gamma}}{\tilde{\gamma}^2 + (\Delta' + kv'_z)^2}\, W_1(v_z)$$

where $\tilde{\gamma}$ is the homogeneous width (H.W.H.M.), Δ the detuning of the saturator and Δ' the detuning of the probe.

$\tilde{G}(v_z \to v'_z)$ is the sum of three terms, hence the total profile is also a sum of three terms ; it can be expressed in the Doppler limit ($\tilde{\gamma} \ll ku$) as :

$$I = I_a + I_b + I_c = I_0 \frac{\sqrt{\Pi}}{\Gamma} \frac{e^{-\Delta^2/k^2u^2}}{ku\tilde{\gamma}} \left\{ \frac{2\tilde{\gamma}^2}{4\tilde{\gamma}^2 + (\Delta + \Delta')^2} + \frac{\sqrt{\Pi}}{ku}\tilde{\gamma} \frac{\Gamma_1 \Gamma}{\Gamma_0(\Gamma_0 + \Gamma_1)} e^{-(\Delta'/ku)^2} + \right.$$

$$\left. + \frac{1}{\sqrt{\Pi}} \sum_n \left(\frac{\Gamma_2}{\Gamma}\right)^n \frac{\tilde{\gamma}}{k\,\Delta u_n} \int_{-\infty}^{+\infty} \frac{2\tilde{\gamma}_n}{4\tilde{\gamma}_n^2 + (\Delta' + \alpha^n \Delta + x)^2} \exp - \left(\frac{x}{k\,\Delta u_n}\right)^2 dx \right\} \quad (2)$$

where $2\tilde{\gamma}_n = \tilde{\gamma}(1 + \alpha^n)$.

The first term in (2) is a Lorentzian corresponding to atoms which have not undergone velocity changes; it is centred at $-\Delta$ with total width (F.W.H.M.) of $4\tilde{\gamma}$. The second term is a Gaussian corresponding to atoms which have undergone at least one thermalizing collision; it is centred at $\Delta' = 0$ and has the Doppler width. The third term is a sum of Voigt integrals and corresponds to atoms which have undergone velocity changes but no thermalizing event; it is asymmetrical and expresses the progressive loss of memory of the initial velocity following n collisions.

The profile shown on figure 1 has been compared to a theoretical one (expression (2)) by use of a least square fit. α has been chosen equal to 0.94 corresponding to the predicted value [11]; $\tilde{\gamma}$ has been evaluated at 18 MHz according to the experimental situation. Thus, profiles depend on two parameters only, Γ_2/Γ and $\Gamma_1\Gamma/\Gamma_0(\Gamma_0 + \Gamma_1)$ which determine the intensities of the two components due to V.C.C. compared to the intensity of the Lorentzian. Here we have chosen to fix Γ_2/Γ and we have looked for a value of $\Gamma_1\Gamma/\Gamma_0(\Gamma_0 + \Gamma_1)$ which gives account of the shape of the profile; the same procedure has been used for several different values of Γ_2/Γ, n being limited to sixty. The best fit, determined by the minimum value of the mean square deviation, has been obtained for a well-defined couple of parameters; in particular, the shape of the profile is very sensitive to the value of Γ_2/Γ.

An example of the fit is shown on figure 1; on trace III, dots represent the calculated profile, sum of the three terms of equation (2), each of them being represented by a *thin* curve (trace a, b, c). The asymmetry of the component due to Kr*-He V.C.C. shows the non-thermalizing nature of these collisions; this is better shown on figure 2, where different Voigt profiles related to different values of n are represented. A profile associated to n represents the contribution of atoms which have undergone a mean velocity change Δu_n after n collisions.

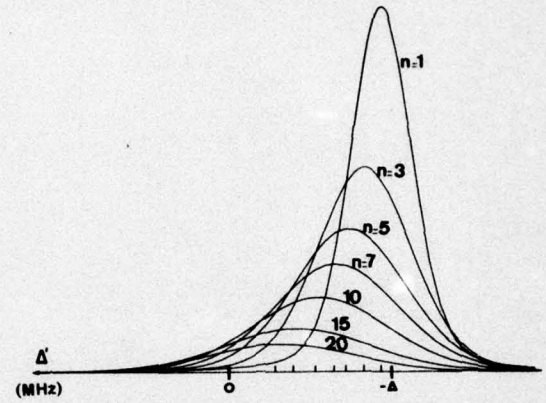

FIG. 2. — Contribution of different Voigt profiles with different n values to the component associated to Kr*-He V.C.C. (Trace (c) of figure 1). Positions of these different components are marked by dashes. Note that the profile for $n = 1$ is already shifted of an amount $k\,\Delta u$.

The fit yields the following values for the parameters : $\Gamma_1/\Gamma_2 = 0.04$ and $\Gamma_0/\Gamma_2 = 1.6$ in close agreement with those obtained in [9] on Kr saturated-absorption with one laser. However we can notice that the fit of the asymmetrical profile is much more sensitive to certain parameters; in particular, the spread of α values around 0.94 indicates that, actually, α is defined in a narrow range : $\alpha = 0.94 \pm 0.01$. Thus, our results indicate that a simple model of hard sphere collisions can consistently explain the effects of V.C.C. on saturated-absorption profiles.

D. Merle is warmly acknowledged for her contribution to computing.

References

[1] SMITH, P. W. and HÄNSCH, Th., *Phys. Rev. Lett.* **26** (1971) 740.
[2] KAN, T. and WOLGA, G. J., *I.E.E.E., Q.E.* **7** (1971) 141.
[3] CAHUZAC, Ph., ROBAUX, O. and VETTER, R., *J. Phys. B* **9** (1976) 3165.
[4] BRÉCHIGNAC, C., VETTER, R. and BERMAN, P. R., *J. Phys. B* **10** (1977) 3443.
[5] KOLCHENKO, A. P., PUKHOV, A. A., RAUTIAN, S. G. and SHALAGIN, A. M., *Sov. Phys. J.E.T.P.* **36** (1973) 619.
[6] BERMAN, P. R., *Phys. Rev. A* **13** (1976) 2191.
[7] VASILENKO, L. S., KOCHANOV, V. P. and CHEBOTAEV, V. P., *Opt. Commun.* **20** (1977) 409.
[8] CAHUZAC, Ph., MARIÉ, E., ROBAUX, O., VETTER, R. and BERMAN, P. R., *J. Phys. B* **11** (1978) 645.
[9] BRÉCHIGNAC, C., VETTER, R. and BERMAN, P. R., *Phys. Rev. A*, to be published.
[10] LE GOUËT, J.-L., submitted to *J. Phys. B*.
[11] BERMAN, P. R., *Adv. At. Mol. Phys.* **13** (1977) 57.
[12] KEILSON, J. and STORER, J. E., *Q. Appl. Math.* **10** (1952) 243.

PHYSICS REPORTS

NORTH-HOLLAND PUBLISHING COMPANY
AMSTERDAM

PHYSICS REPORTS
A review section of PHYSICS LETTERS (Section C)

PREPARATION OF MANUSCRIPTS

Manuscripts should be written in English. They should be typewritten originals with a wide margin and ample spaces between the lines. One extra copy will facilitate the editor's task.
Paper should be provided with an abstract not exceeding 200 words, a list of contents, a list of captions of figures and a list of references.
Footnotes should be given in the text between lines and not in the list of references. References should be numbered in the text between square brackets. Figures should be originals, drawn in India ink and with sufficiently large lettering to remain legible after the reduction by the printer.

SUBSCRIPTIONS

PHYSICS REPORTS is published as a review section of PHYSICS LETTERS (Section C). Each volume of PHYSICS REPORTS contains approximately 360 pp. PHYSICS REPORTS can be subscribed to separately. The price per volume amounts to Dfl. 150.00 postage included. Single copies of issues will be made available at a price which will depend on the size of the issue concerned.

How to order:

(i) Subscriptions to PHYSICS REPORTS can be ordered from booksellers and subscription agencies or directly from the Publisher: North-Holland Publishing Company, Journal Division, P.O. Box 211, Amsterdam, The Netherlands.
(ii) Single copies of issues can only be ordered from the Publisher and a check should be enclosed with the order. The price of each issue will be announced on publication.

CLAIMS FOR MISSING NUMBERS should be made within three months, following the date of publication. The Publisher expects to supply missing numbers free only when losses have been sustained in transit and when stock will permit.

Forwarding address of the Technical Editor of Physics Reports:
NORTH-HOLLAND PUBLISHING COMPANY, P.O. Box 103, Amsterdam, The Netherlands
Cables: Nohum-Amsterdam – Telephone: (020) 5153254 – Telex 16479 epc nl

Printed in the Netherlands
Published weekly

EFFECTS OF COLLISIONS ON LINEAR AND NON-LINEAR SPECTROSCOPIC LINE SHAPES

Paul R. BERMAN

Physics Department, New York University, 4 Washington Place, New York, New York 10003, USA

Supported by the U.S. Office of Naval Research under Contract No. N00014-77-C-0553.

NORTH-HOLLAND PUBLISHING COMPANY – AMSTERDAM

PHYSICS REPORTS (Section C of Physics Letters) 43, No. 3 (1978) 101–149. NORTH-HOLLAND PUBLISHING COMPANY

EFFECTS OF COLLISIONS ON LINEAR AND NON-LINEAR SPECTROSCOPIC LINE SHAPES*

Paul R. BERMAN

Physics Department, New York University, 4 Washington Place, New York, New York 10003, USA

Received December 1977

Contents:

Abstract:

A fundamental physical problem is the determination of atom–atom, atom–molecule and molecule–molecule differential and total scattering cross sections. In this work, a technique for studying atomic and molecular collisions using spectroscopic line shape analysis is discussed. Collisions occurring within an atomic or molecular sample influence the sample's absorptive or emissive properties. Consequently the line shapes associated with the linear or non-linear absorption of external fields by an atomic system reflect the collisional processes occurring in the gas. Explicit line shape expressions are derived characterizing linear or saturated absorption by two- or three-level "active" atoms which are undergoing collisions with perturber atoms. The line shapes may be broadened, shifted, narrowed, or distorted as a result of collisions which may be "phase-interrupting" or "velocity-changing" in nature. Systematic line shape studies can be used to obtain information on both the differential and total active atom-perturber scattering cross sections.

* This paper is written as part of a *Festschrift* for Professor Willis Lamb on the occasion of his 65th birthday.

1. Introduction

I had the opportunity of working with Professor Willis Lamb for a period of five years, 1966–1971. For three of those years, I was a graduate student and for the remaining two years an Instructor at Yale University. Professor Lamb not only guided me in research, but also left me with an imprint of his philosophy of physics. It is with sincere gratitude that I dedicate this article to him.

There is a certain mythology that has arisen concerning Professor Lamb. It has been rumored that one should never utter the word "photon" or words "Green's function" in his presence. In my relationship with Professor Lamb, I never found this to be the case. As long as the terminology clearly described the physical processes under discussion, there was never an objection to one word or another. However, I think it is fair to say that Professor Lamb is somewhat impatient with those who use terminology or formalism at the expense of physics.

Stressing the physical aspects of a given problem was always foremost in Professor Lamb's mind. He would often use classical or well known quantum-mechanical analogs to try to explain a new result, rather than simply accept the fact that "it follows from the mathematics". I should say that Professor Lamb's greatest influence on me was to convey this need to get "inside" a problem to understand the underlying physical principles.

If there is one interaction I shall never forget, it is the eight or nine month period that we spent going over my thesis. Each sentence was subjected to careful scrutiny and it was not uncommon to change a phrase two or three times before Professor Lamb found it acceptable. The general theme of his critical reading of the manuscript was "If it's worth putting in, it's worth explaining it clearly". While I admit that I have been guilty of not following this maxim from time to time, it is the type of philosophy I try to pass along to my students.

I have tried to incorporate Professor Lamb's philosophy (or, more precisely, my perception of Professor Lamb's philosophy) in writing this article. The article contains a summary of the research I have carried out over the past several years related to spectroscopic studies of collision effects in atomic and molecular systems. It is *not* a review article, but rather a personal view of the subject matter in which the physical aspects of the various problems are stressed. Extensive bibliographies may be found in two recent reviews of this subject area [1, 2].

A fundamental problem in atomic and molecular physics is the determination of differential and total cross sections for atom–atom, atom–molecule or molecule–molecule scattering. The traditional method for studying scattering phenomena involves the use of crossed atomic or molecular beams. Crossed beam experiments are usually restricted to ground or metastable levels; excited state densities are too small to give rise to detectable scattering signals. Recently, however, significant excited state population has been achieved by using a laser to excite atoms in the scattering region.

In this paper, I discuss an alternative method for studying atomic and molecular collisions. Consider a bulb containing a gas of classical oscillators ("active" atoms) and perturbers. The oscillators absorb or emit radiation. There is a characteristic profile associated with these processes having a width that reflects both the Doppler broadening and natural damping of the oscillators. When an oscillator collides with a perturber, its phase and velocity are altered. These effects give rise to a modification of the absorption or emission profile. Consequently, line shape studies can be used to implicitly monitor collision processes in the gas. One can determine the active atom-perturber collision rate and total cross section by this method.

Actually the situation is a bit different if one uses two-level atoms rather than classical atoms

to represent the active atoms. The linear superposition of the two states induced by an external field or the vacuum field produces a dipole moment in these atoms, in analogy with the dipole moment of the classical oscillators. However, the active atom-perturber scattering interaction may be state dependent for two-level atoms (i.e. dependent on which state the two-level atom is in) whereas it was state-independent for classical oscillators. When a two-level atomic dipole enters a collision, which trajectory should it follow? There is no classical answer to this question; the quantum-mechanical answer is discussed in section 2. The study of the linear absorption or emission profiles associated with two-level atoms can provide values for the state-dependent active atom-perturber collision rates and total cross sections.

Linear spectroscopy can provide information on total cross sections only. To learn something about *differential* scattering cross sections, one may use saturation spectroscopy. A monochromatic pump field excites only those atoms with a specified velocity component in the direction of the field's propagation vector. The excited atoms undergo collisions in which their velocities are altered, and these velocity changes can be observed by subjecting the atoms to a probe field acting on the same or a coupled transition. One does not obtain a true differential scattering cross section in such experiments, but rather a differential scattering cross section averaged over perturber velocities and those active atom velocities not selected by the pump field. Still, some semi-quantitative data on the excited state differential scattering cross section may be inferred from the line shape.

In light of the comments given above, it is reasonable to believe that linear and saturation spectroscopy should be effective probes of atomic and molecular collisions. The remainder of this paper outlines a systematic method that permits one to extract appropriate collision rates and cross sections from the line shapes associated with atomic and molecular systems. In section 2, an equation for the collisional time rate of change of atomic density matrix elements is derived. It is shown that for state dependent collision interactions, it is not possible to use a classical velocity to describe the atomic center-of-mass motion. In section 3 the linear absorption line shape for a two-level system is calculated and in section 4, the saturation spectroscopy profile for a three-level system is derived. Phenomena such as collision broadening, shifting, and narrowing are discussed in these sections. Section 4 also illustrates the way in which saturation spectroscopy can be used to provide information on excited state differential scattering cross sections. In section 5 additional problems relating to inelastic collisions, level degeneracy and resonant exchange collisions are discussed briefly.

2. Collisions

To study collisions between "A" and "P" atoms using spectroscopy as a collision probe, one starts with a bulb containing a mixture of A and P atoms. The A ("active") atoms are allowed to interact with some external fields while undergoing collisions with the P (perturber) atoms. One monitors the active atom-field interaction (e.g. absorption of an applied field) as a function of perturber pressure to obtain information on A–P collisions. It is assumed that the perturbers interact negligibly with the external fields.

The line shapes associated with the active atom-field interactions reflect all collisional processes occurring in the gas. It is possible, however, to choose the experimental parameters such that binary A–P collisions are the only type of collisions that contribute significantly in line shape

formation. First, a *dilute* ($\leq$ 500 Torr) gas must be used to insure that three-body collisions are not important. In this *binary collision* pressure region, the time between collisions is much greater than the duration of a collision. Second, a large ratio of perturbers to active atoms must be maintained to guarantee that it is A–P rather than A–A collisions which are dominant.

When the ratio of perturber to active atoms is large, there is an additional simplification; the perturbers' velocity distribution is essentially unaffected by the relatively few collisions they undergo with active atoms. The perturbers may be thought to constitute a thermal bath that is unchanged by collisions. In the presence of this thermal bath the evolution of the active atoms' velocity distribution may be described by a linear transport equation rather than the more general Boltzmann equation. The appropriate transport equation is derived below.

The situation can be more complicated if one wishes to study A–A collisions. In that case, it is possible for atoms to resonantly exchange excitation during a collision. Resonant collisions are discussed briefly in section 5. In sections 2–4, the discussion is limited to binary, elastic, foreign gas (non-resonant) collisions.

2.1. *One-level system*

The simplest system one can envision involves one-level active atoms. Physically, these one-level active atoms could correspond to ground state atoms which are injected with some non-equilibrium velocity distribution into the perturber bath. For these one-level active atoms, collisions result solely in a change of velocity (fig. 1). In fact, the system may be though of classically as a thermal classical gas of P atoms into which few non-thermal A atoms have been introduced. The velocity of A atoms is then governed by the linear transport equation

$$\partial f_{\mathrm{A}}(v, t)/\partial t = -\Gamma_{\mathrm{A}}(v) f_{\mathrm{A}}(v, t) + \int \mathrm{d}v' W_{\mathrm{A}}(v' \rightarrow v) f_{\mathrm{A}}(v', t), \tag{2.1}$$

where $f_{\mathrm{A}}(v, t)$ is the distribution function of the A atoms, $W_{\mathrm{A}}(v' \rightarrow v)$ is the collision kernel giving the probability density per unit time that an A atom undergoes a velocity change from v' to v and

$$\Gamma_{\mathrm{A}}(v) = \int \mathrm{d}v' W_{\mathrm{A}}(v \rightarrow v') \tag{2.2}$$

is the rate of collisions. Eq. (2.1) multiplied by $\mathrm{d}v$ describes the flow of A atoms out of and into the velocity range between v and $v + \mathrm{d}v$.

It is not too difficult to arrive at a quantum-mechanical transport equation analogous to eq. (2.1). Provided that the range of the collision interaction is much less than the collisional mean free path (binary collision approximation), collisions result solely in a change in the average velocity v of a wave packet associated with an active atom. The quantum mechanical collision kernel is

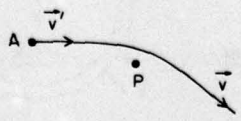

Fig. 1. Classical picture of a collision between a "one-level" active atom A and a perturber P. The atom's velocity is changed from v' to v as a result of the collision.

$\langle \mathcal{N} v_r | f_A(v_r' \to v_r)|^2 \rangle$ where $\mathcal{N}$ is the perturber density, v_r the active atom-perturber relative velocity, $f_A(v_r' \to v_r)$ the scattering amplitude for active atom-perturber collisions, and the average is over all possible perturber velocities consistent with conservation of momentum and energy. Explicitly

$$W_A(v' \to v) = \mathcal{N}\left(\frac{m}{\mu}\right)^3 \int dv_p' \, dv_r W_p(v_p') v_r^{-1} \delta\left[v_r + \frac{m}{m_p} v' - \frac{m}{\mu} v + v_p'\right] \delta(v_r' - v_r) \, f_A(v_r \to v_r)|^2, \tag{2.3}$$

$$v_r = v - v_p, \qquad v_r' = v' - v_p',$$

where v (or v') is the active atom velocity, v_p (or v_p') the perturber velocity, $W_p(v_p)$ the perturber velocity distribution, m the active atom mass, m_p the perturber mass and μ the reduced mass.

Similarly, the collision rate is given by $\langle \mathcal{N} v_r \sigma_A(v_r) \rangle$ where σ is the total elastic cross section for active atom-perturber scattering. As in eq. (2.2) one has

$$\Gamma_A(v) = \int dv' W_A(v \to v') = \mathcal{N} \int dv_p W_p(v_p) v_r \sigma_A(v_r). \tag{2.4}$$

The quantum mechanical transport equation has the same form as eq. (2.1), with the kernel and rate now given by eqs. (2.3) and (2.4), respectively, and the distribution function now describing a wave packet with average velocity v.

Since it will aid in one's understanding of collisions in two-level systems, I should like to outline a simple, non-rigorous quantum-mechanical derivation of eq. (2.1). Imagine an active atom wave packet of cross-sectional area σ and average momentum p' approaching a stationary perturber ($\sigma \ll$ square of the collision interaction range). This packet could be described by a wave function

$$\psi(R, t^-) = e^{(i/\hbar)p' \cdot R} A(R, t^-), \tag{2.5}$$

where $A(R, t^-)$ properly localizes the packet. Following the collision, the packet consists of an unscattered component $A(R, t^+)$ plus a spherically scattered wave $S(R, t^+)$ (fig. 2)

$$\psi(R, t^+) = e^{(i/\hbar)p' \cdot R} A(R, t^+) + \frac{f_A(v' \to v)}{R} e^{(i/\hbar)p'R} S(R, t^+), \tag{2.6}$$

where

$$A(R, t^+) = \exp\left[-(imv'^2/2\hbar)(t^+ - t^-)\right] A\left[R - v'(t^+ - t^-), t^-\right], \tag{2.7a}$$

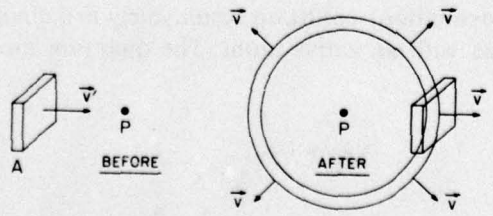

Fig. 2. Quantum-mechanical picture of a collision between an active atom A and a perturber P. The active atom is represented by a localized wave packet. Following a collision, the active atom consists of an unscattered component plus a spherical shell representing the scattered wave.

and

$$S(\boldsymbol{R}, t^+) = \exp\left[-(imv'^2/2\hbar)(t^+ - t^-)\right] A[R\hat{\boldsymbol{v}}' - \boldsymbol{v}'(t^+ - t^-), t^-], \tag{2.7b}$$

again give the proper localization of the packet. The change in probability density resulting from this collision is

$$\begin{aligned}\delta\rho(\boldsymbol{R}, t^+, t^-) &= |\psi(\boldsymbol{R}, t^+)|^2 - |\psi(\boldsymbol{R}, t^-)|^2 \\ &= \left[|A(\boldsymbol{R}, t^+)|^2 - |A(\boldsymbol{R}, t^-)|^2\right] + \frac{f_A(\boldsymbol{v}' \to \boldsymbol{v})^*}{R} e^{(i/\hbar)(\boldsymbol{p}' \cdot \boldsymbol{R} - p'R)} A(\boldsymbol{R}, t^+) S(\boldsymbol{R}, t^+)^* \\ &\quad + \frac{f_A(\boldsymbol{v}' \to \boldsymbol{v})}{R} e^{(i/\hbar)(p'R - \boldsymbol{p}' \cdot \boldsymbol{R})} A(\boldsymbol{R}, t^+)^* S(\boldsymbol{R}, t^+) + \frac{|f_A(\boldsymbol{v}' \to \boldsymbol{v})|^2}{R^2} |S(\boldsymbol{R}, t^+)|^2. \end{aligned} \tag{2.8}$$

In the limit that

$$\delta t = t^+ - t^-$$

goes to zero, the lead term in (2.8) will vanish, reflecting the fact that the atomic velocity is unchanged if no collision occurs.

The remaining terms specify the change in velocity from an initial value $\boldsymbol{v}' = \boldsymbol{p}'/m$ to a final value $\boldsymbol{v} = v'\hat{\boldsymbol{R}}$. For a perturber density $\mathcal{N}$, the density of particles scattered per unit time into a solid angle $d\Omega_v$ is

$$\begin{aligned}\left[\delta\rho(\boldsymbol{v}, \boldsymbol{v}', t, \delta t)/\delta\tau\right] d\Omega_v &= (\mathcal{N} v' \sigma \delta\tau)(R^2\, d\Omega_v/\sigma)\delta\rho(\boldsymbol{R}, t^+, t^-)/\delta\tau \\ &= \mathcal{N} v' \left[\frac{f_A(\boldsymbol{v}' \to \boldsymbol{v})^*}{R} e^{(i/\hbar)(\boldsymbol{p}' \cdot \boldsymbol{R} - p'R)} A(\boldsymbol{R}, t^+) S(\boldsymbol{R}, t^+)^*\right. \\ &\quad \left. + \frac{f_A(\boldsymbol{v}' \to \boldsymbol{v})}{R} e^{(i/\hbar)(p'R - \boldsymbol{p}' \cdot \boldsymbol{R})} A(\boldsymbol{R}, t^+)^* S(\boldsymbol{R}, t^+) + \frac{|f_A(\boldsymbol{v}' \to \boldsymbol{v})|^2}{R^2} |S(\boldsymbol{R}, t^+)|^2\right] R^2\, d\Omega_v. \end{aligned} \tag{2.9}$$

It is necessary to integrate eq. (2.9) over all possible incident velocity directions $d\Omega_{v'}$. In performing this integration, one uses the fact that $R \gg h/p'$ (i.e. in the binary collision pressure region, the (collisional mean free path) $\gg \lambda_B = h/p'$ – it follows that, for all but a negligible range of R, $R \gg \lambda_B$) to set

$$\int d\Omega_{v'} f(\boldsymbol{v}' \to \boldsymbol{v}) e^{(i/\hbar)(\boldsymbol{p}' \cdot \boldsymbol{R} - p'R)} \approx \frac{2\pi\hbar}{ipR} f(\boldsymbol{v} \to \boldsymbol{v}). \tag{2.10}$$

The rapid oscillation of the phase factor leads to destructive interference in all but the forward direction. Dropping the $d\Omega_v$ and integrating (2.9) over $d\Omega_{v'}$ making use of (2.10), one obtains

$$\begin{aligned}\frac{\delta\rho(\boldsymbol{v}, t, \delta t)}{\delta\tau} &= \mathcal{N} v \left(\frac{2\pi\hbar}{ip}\right)\left[f_A(\boldsymbol{v} \to \boldsymbol{v})^* A(\boldsymbol{R}, t^+) S(\boldsymbol{R}, t^+)^* - f_A(\boldsymbol{v} \to \boldsymbol{v}) A(\boldsymbol{R}, t^+)^* S(\boldsymbol{R}, t^+)\right] \\ &\quad + \mathcal{N} v \int d\Omega_{v'} |f_A(\boldsymbol{v}' \to \boldsymbol{v})|^2 |S(\boldsymbol{R}, t^+)|^2. \end{aligned} \tag{2.11}$$

Using (2.7) and taking the limit $\delta t \to 0$, $\delta\tau \to 0$, one arrives at the quantum mechanical transport

equation

$$\partial\rho(v,t)/\partial t\big|_{\text{coll}} = -\Gamma_A(v)\rho(v,t) + \int dv' W_A(v' \to v)\rho(v',t), \tag{2.12}$$

where

$$W_A(v' \to v) = \mathcal{N} v \,|\, f_A(v' \to v)|^2 v^{-2}\delta(v - v'), \tag{2.13}$$

$$\Gamma_A(v) = \mathcal{N} v\left(\frac{2\pi\hbar}{ip}\right)[f_A(v \to v) - f_A(v \to v)^*]. \tag{2.14}$$

The optical theorem can be used to transform (2.14) into

$$\Gamma_A(v) = \mathcal{N} v \sigma_A(v). \tag{2.15}$$

Eq. (2.12) with eqs. (2.13) and (2.15) generalized to allow for moving perturbers is seen to be equivalent to eq. (2.1) with the kernel and rate given by eqs. (2.3) and (2.4), respectively. In a classical or quantum-mechanical picture, collisions for one level systems can be described by a transport equation. Naturally, some measurement technique would be needed to monitor the active atom velocity distribution. It is implicitly assumed above that the time scale of the measurement is much greater than the collision time.

2.2. *Two-level system*

In contrast to beam experiments where scattering from one-level atoms is typical (i.e., ground state–ground state or ground state–metastable state collisions), bulk experiments generally involve scattering of active atoms which are in a linear superposition of internal states. In the beam experiments one directly measures the scattered particles; however in laser spectroscopic collisions studies, one uses absorption or emission profiles to indirectly monitor collisions in the gas. The radiation fields that are either absorbed or emitted by the gas produce a linear superposition state in the active atoms (i.e., an oscillating atomic dipole). Consequently, collisions involving two-level atoms must be analyzed to properly interpret spectroscopic line shapes.

Consider the two level atom of fig. 3 in which the frequency separation of levels 1 and 2 is ω. The atom is assumed to be in a coherent superposition state produced by a radiation field and undergoes collisions with ground state perturber atoms. For the present, I assume that collisions are *elastic* (inelastic collisions are discussed in section 5), not possessing sufficient frequency components or energy to induce transitions between states 1 and 2. Since the collision duration τ_c is typically $\approx 10^{-12}$ sec, collisions contain frequency components up to $\omega_c = (\tau_c)^{-1} \approx 10^{12}\,\text{sec}^{-1}$. The frequency ω_T corresponding to thermal energies is $\approx 10^{13}\,\text{sec}^{-1}$. Thus, the elastic or adiabatic assumption is

$$\omega > \text{Min}(\omega_c, \omega_T) = \omega_c \approx 10^{12}\,\text{sec}^{-1}. \tag{2.16}$$

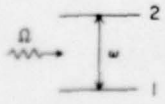

Fig. 3. A two-level atom. An external field creates a linear superposition of states 1 and 2.

Electronic, vibrational and some rotational energy level spacings are sufficiently large to ensure that the adiabatic approximation (2.16) is valid.

The atomic system is described by density matrix elements and we seek a transport equation describing their time evolution. Before a collision, the wave function is given by

$$\psi(\boldsymbol{R}, t^-) = e^{(i/\hbar)\boldsymbol{p}'\cdot\boldsymbol{R}}[A_1(\boldsymbol{R}, t^-)\psi_1(\boldsymbol{r}) + A_2(\boldsymbol{R}, t^-)\psi_2(\boldsymbol{r})], \tag{2.17}$$

where $\boldsymbol{R}$ is the center-of-mass coordinate, $\boldsymbol{r}$ the electronic coordinate, $A_i(\boldsymbol{R}, t)$ the state i probability amplitude and $\psi_i(\boldsymbol{r})$ the state i eigenfunction. Following the elastic collision, the wave function is given

$$\begin{aligned}\psi(\boldsymbol{R}, t^+) = &\left[e^{(i/\hbar)\boldsymbol{p}'\cdot\boldsymbol{R}}A_1(\boldsymbol{R}, t^+) + \frac{e^{(i/\hbar)p'R}}{R} f_1(\boldsymbol{v}' \to \boldsymbol{v})S_1(\boldsymbol{R}, t^+)\right]\psi_1(\boldsymbol{r}) \\ &+ \left[e^{(i/\hbar)\boldsymbol{p}'\cdot\boldsymbol{R}}A_2(\boldsymbol{R}, t^+) + \frac{e^{(i/\hbar)p'R}}{R} f_2(\boldsymbol{v}' \to \boldsymbol{v})S_2(\boldsymbol{R}, t^+)\right]\psi_2(\boldsymbol{r}),\end{aligned} \tag{2.18}$$

where $A_i(\boldsymbol{R}, t^+)$ and $S_i(\boldsymbol{R}, t^+)$ are obvious generalizations of (2.7a) and (2.7b), respectively. The change in the density matrix element ρ_{ij} resulting from a collision is

$$\begin{aligned}\delta\rho_{ij}(\boldsymbol{R}, t^+, t^-) = &\left[e^{(i/\hbar)\boldsymbol{p}'\cdot\boldsymbol{R}}A_i(\boldsymbol{R}, t^+) + \frac{e^{(i/\hbar)p'R}}{R} f_i(\boldsymbol{v}' \to \boldsymbol{v})S_i(\boldsymbol{R}, t^+)\right] \\ &\times \left[e^{(i/\hbar)\boldsymbol{p}'\cdot\boldsymbol{R}} + \frac{e^{(i/\hbar)p'R}}{R} f_j(\boldsymbol{v}' \to \boldsymbol{v})S_j(\boldsymbol{R}, t^+)\right]^* - A_i(\boldsymbol{R}, t^-)A_j(\boldsymbol{R}, t^-)^*.\end{aligned} \tag{2.19}$$

Following the same procedure that was used in going from (2.8) to (2.12), one arrives at the quantum-mechanical transport equation

$$\partial\rho_{ij}(\boldsymbol{v}, t)/\partial t\big|_{\text{coll}} = -\Gamma_{ij}(\boldsymbol{v})\rho_{ij}(\boldsymbol{v}, t) + \int d\boldsymbol{v}' W_{ij}(\boldsymbol{v}' \to \boldsymbol{v})\rho_{ij}(\boldsymbol{v}', t), \tag{2.20}$$

$$\begin{aligned}W_{ij}(\boldsymbol{v}' \to \boldsymbol{v}) = &\mathcal{N}(m/\mu)^3 \int d\boldsymbol{v}'_p\, d\boldsymbol{v}_r W_p(\boldsymbol{v}'_p)v_r^{-1}\delta[\boldsymbol{v}_r + (m/m_p)\boldsymbol{v}' - (m/\mu)\boldsymbol{v} + \boldsymbol{v}'_p] \\ &\times \delta(v_r - v'_r) f_i(\boldsymbol{v}'_r \to \boldsymbol{v}_r) f_j(\boldsymbol{v}'_r \to \boldsymbol{v}_r)^*,\end{aligned} \tag{2.21}$$

$$\Gamma_{ij}(\boldsymbol{v}) = \tfrac{1}{2}\mathcal{N}\int d\boldsymbol{v}_p W_p(\boldsymbol{v}_p)v_r\left(\frac{4\pi\hbar}{i\mu v_r}\right)[f_i(\boldsymbol{v}_r \to \boldsymbol{v}_r) - f_j(\boldsymbol{v}_r \to \boldsymbol{v}_r)^*]. \tag{2.22}$$

The contributions to $\partial\rho_{ij}(\boldsymbol{v}, t)/\partial t|_{\text{coll}}$ are easily understood in terms of quantum-mechanical scattering processes. The two terms appearing in (2.22) correspond to the interference of the unscattered j or i wave with the spherically scattered i or j wave, respectively. As in eq. (2.10), these terms contribute only in the forward direction. The contribution (2.21) represents the overlap of the i and j spherically scattered waves. The collision "kernel" (2.21) and "rate" (2.22) are now complex quantities so that a simple classical interpretation of the transport equation is no longer possible. The transport equation is best discussed by considering diagonal and off-diagonal elements separately.

1. *Diagonal elements* $i = j$. For $i = j$, the transport equation is

$$\partial\rho_{ii}(\boldsymbol{v}, t)/\partial t|_{\text{coll}} = -\Gamma_{ii}(\boldsymbol{v})\rho_{ii}(\boldsymbol{v}, t) + \int d\boldsymbol{v}' W_{ii}(\boldsymbol{v}' \to \boldsymbol{v})\rho_{ii}(\boldsymbol{v}', t), \tag{2.23}$$

with a real collision kernel

$$W_{ii}(\boldsymbol{v}' \to \boldsymbol{v}) = \mathcal{N}\left(\frac{m}{\mu}\right)^3 \int d\boldsymbol{v}'_{\text{p}}\, d\boldsymbol{v}_{\text{r}} W_{\text{p}}(\boldsymbol{v}'_{\text{p}}) v_{\text{r}}^{-1} \delta\left[\boldsymbol{v}_{\text{r}} + \frac{m}{m_{\text{p}}}\boldsymbol{v}' - \frac{m}{\mu}\boldsymbol{v} + \boldsymbol{v}'_{\text{p}}\right]$$
$$\times\, \delta(v_{\text{r}} - v'_{\text{r}})\,|\, f_i(\boldsymbol{v}'_{\text{r}} \to \boldsymbol{v}_{\text{r}})|^2 \tag{2.24}$$

and a real rate

$$\Gamma_{ii}(\boldsymbol{v}) = \mathcal{N}\int d\boldsymbol{v}_{\text{p}} W_{\text{p}}(\boldsymbol{v}_{\text{p}}) v_{\text{r}} \sigma_i(\boldsymbol{v}_{\text{r}}) = \int d\boldsymbol{v}' W_{ii}(\boldsymbol{v} \to \boldsymbol{v}'). \tag{2.25}$$

The first part of eq. (2.25) follows from eq. (2.22) and the optical theorem, while the second part of eq. (2.25) may be verified by direct integration of eq. (2.24). Thus, each population density $\rho_{ii}(\boldsymbol{v}, t)$ obeys a transport equation equivalent to that for the one-level problem. Since the kernel and rate are state dependent, the total population density $\sum_i \rho_{ii}(\boldsymbol{v}, t)$ does *not* obey a transport equation. In this sense one can not obtain a classical picture for scattering of the atom as a whole. Rather, it is possible to envision a classical limit for the scattering in each of the levels i. (This result is analogous to that of a Stern–Gerlach experiment where one may assign classical trajectories to each of the spin states.)

Additional simplifications of eqs. (2.23–2.24) are sometimes possible. If the ratio of perturber to active atom mass is small ($m_{\text{p}}/m \ll 1$), collisions produce a relatively small change in the active atom's velocity. Mathematically, this situation leads to a kernel $W_{ii}(\boldsymbol{v}' \to \boldsymbol{v})$ that is sharply peaked about $\boldsymbol{v}' = \boldsymbol{v}$ and enables one to expand $\rho_{ii}(\boldsymbol{v}', t)$ appearing in eq. (2.23) about $\boldsymbol{v}' = \boldsymbol{v}$. The limiting form of eq. (2.23) for this weak collision case is a Fokker–Planck equation

$$\partial\rho_{ii}(\boldsymbol{v}, t)/\partial t|_{\text{coll}} \approx [-\Gamma_{ii}(\boldsymbol{v}) + A_0(\boldsymbol{v})]\rho_{ii}(\boldsymbol{v}, t) + \boldsymbol{A}_1(\boldsymbol{v})\frac{\partial\rho_{ii}(\boldsymbol{v}, t)}{\partial\boldsymbol{v}} + \boldsymbol{A}_2(\boldsymbol{v})\frac{\partial^2\rho_{ii}(\boldsymbol{v}, t)}{\partial\boldsymbol{v}^2}, \tag{2.26}$$

with

$$\boldsymbol{A}_n(\boldsymbol{v}) = \frac{1}{n!}\int d\boldsymbol{v}'(\boldsymbol{v}' - \boldsymbol{v})^n W_{ii}(\boldsymbol{v}' \to \boldsymbol{v}). \tag{2.27}$$

The Fokker–Planck limit of the transport equation is valid only if $\rho_{ii}(\boldsymbol{v}, t)$ has a velocity width less than the kernel width, justifying the expansion of $\rho_{ii}(\boldsymbol{v}', t)$ about $\boldsymbol{v}' = \boldsymbol{v}$.*

The opposite limit, $m_{\text{p}}/m \gg 1$, corresponds to scattering by stationary perturbers with the kernel and rate given by eqs. (2.13) and (2.14), respectively.

2. *Off-diagonal elements* $i \neq j$. A picture of the scattering process is shown in fig. 4. As in a Stern–Gerlach experiment, one can associate a trajectory with ρ_{11} and ρ_{22} for an active atom that enters the collision in a linear superposition state. However, associating a classical trajectory

* For example, one may have a case of weak collisions $\Delta v_{\text{c}}/v \ll 1$ in which a radiation field excites a very narrow velocity distribution Δv_{f}. If $\Delta v_{\text{f}} \ll \Delta v_{\text{c}}$, the Fokker–Planck equation is not valid, even though the collisions are weak.

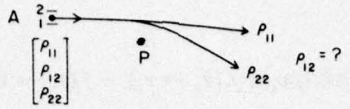

Fig. 4. An attempt to give a classical picture of a collision between a two-level active atom A and a perturber P. Before the collision, the atom is in a linear superposition of states 1 and 2. Following the collision, it is possible to assign classical trajectories to ρ_{11} and ρ_{22} but not to ρ_{12}. The quantum mechanical picture of this collision is again given by fig. 2, with an unscattered and a scattered component for each state amplitude.

with ρ_{12} is impossible just as it is impossible in the Stern–Gerlach case. A quantum-mechanical calculation of the scattering process is necessary and it is such a calculation that led to the quantum-mechanical transport equation (2.20).

The need for quantization of the atomic center-of-mass motion escaped notice for many years. The development of lasers and laser spectroscopy served as an impetus for a reevaluation of theories of pressure effects in atomic systems and led to the realization that a classical description of the atomic motion was inadequate. I remember when I came upon this idea in 1969 and discussed it with Professor Lamb. I was having some trouble formulating the problem quantum-mechanically and he suggested a reference to a 1930 article by Bethe [3]. I mention this incident because it is typical of Professor Lamb's ability to pinpoint appropriate references to the literature, even though the article may be 40 years old! I was able to generalize Bethe's method to solve the dilemma of what to do with the off-diagonal density matrix elements. The two articles emerging from that work [4, 5], while not presenting the results in the form of a transport equation, were straightforward, quantum-mechanical calculations of the type that Professor Lamb favors. I believe that he was pleased with these papers, owing to the basic nature of the calculations and the consequences of the results.

Although eqs. (2.20–2.22) are difficult to interpret owing to the presence of a complex kernel and rate, several limiting cases may be discussed:

Equal collision interactions. In the limit of equal scattering amplitudes for levels i and j, $f_i(\boldsymbol{v}_r' \to \boldsymbol{v}_r) = f_j(\boldsymbol{v}_r' \to \boldsymbol{v}_r)$, the *state independent* kernel $W(\boldsymbol{v}' \to \boldsymbol{v})$ and rate $\Gamma(\boldsymbol{v})$ are real and given by eqs. (2.24) and (2.25), respectively. With regards to collisions, the atom has no internal structure since the collision interaction is state independent. In this case, one can assign a velocity to the atom as a whole rather than to individual density matrix elements. The only effect of collisions on off-diagonal density matrix elements is to change the velocity associated with those elements. This velocity change leads to a subsequent change in the atom's Doppler phase factor and to *narrowing* of spectral profiles in linear spectroscopy (clearly, it is not appropriate to speak of pressure *broadening* in this limit) and to *either* broadening or narrowing in non-linear spectroscopic profiles. The limit of state-independent scattering may be found if levels 1 and 2 belong to the same hyperfine multiplet, fine structure multiplet, vibrational or electronic multiplet.

Light perturbers – $m_p/m \ll 1$. In this limit, the active atom's velocity is unchanged in collisions, to a first approximation. The expression for the kernel (2.21) reduces to

$$W_{ij}(\boldsymbol{v}' \to \boldsymbol{v}) = \mathcal{N}\delta(\boldsymbol{v} - \boldsymbol{v}') \int d\boldsymbol{v}_p \, d\Omega_{v_r} v_r W_p(\boldsymbol{v}_p) f_i(\boldsymbol{v}_r \to \boldsymbol{v}_r') f_j(\boldsymbol{v}_r \to \boldsymbol{v}_r')^*, \tag{2.28}$$

leading to a corresponding change of eqs. (2.20–2.22)

$$\partial\rho_{ij}(\boldsymbol{v}, t)/\partial t|_{\text{coll}} = -\bar{\gamma}_{ij}(\boldsymbol{v})\rho_{ij}(\boldsymbol{v}, t), \tag{2.29}$$

where

$$\bar{\gamma}_{ij}(v) = \mathcal{N}\int dv_p W_p(v_p) v_r \left\{ (2\pi\hbar/i\mu v_r)\left[f_i(v_r \to v_r) - f_j(v_r \to v_r)^* \right] \right.$$
$$\left. - \int d\Omega_{v_r'} f_i(v_r \to v_r') f_j(v_r \to v_r')^* \right\}. \tag{2.30}$$

The quantity $\bar{\gamma}_{ij}(v)$ is a complex decay parameter that appears in the quantum-mechanical pressure broadening theory of Baranger [6], in which all active atom velocity changes are neglected.

To interpret eq. (2.29) one need only consider the effect of a collision on ρ_{ij} when active atom velocity changes are neglected. For an elastic collision, only the phase of the atomic state probability amplitudes can change, leading to a change in ρ_{ij} for a single collision

$$\delta\rho_{ij} = (e^{i\theta} - 1)\rho_{ij}, \tag{2.31}$$

where θ is a relative phase change $(\theta_i - \theta_j)$ of the probability amplitudes. If this equation is averaged over collision histories one arrives at (2.29) with

$$\bar{\gamma}_{ij}(v) = \mathcal{N}\int dv_p W_p(v_p) v_r \int_0^\infty 2\pi b\, db[1 - e^{i\theta(b, v_r)}], \tag{2.32}$$

where b is the collision impact parameter. The correspondence between eqs. (2.30) and (2.32) is obtained if the scattering amplitudes in eq. (2.30) are expanded in partial waves and the partial wave phase shifts are evaluated in the WKB or eikonal approximations.

With the neglect of active-atom velocity changes, collisions are solely *phase-interrupting* in their effect on off-diagonal density matrix elements. Each collision produces an abrupt phase change for the atomic oscillator and this effect is translated into a shift and broadening in the spectral profile associated with the transition. Traditionally, one has used an equation of the form (2.29) to describe collision effects on spectral profiles; it is understandable that one talks of pressure *broadening* in this limit.

Scattering in one state only. If the collision interaction is much stronger in one of the levels than the other ($|f_1(v_r' \to v_r)| \ll |f_2(v_r' \to v_r)|$ or $|f_2(v_r' \to v_r)| \ll |f_1(v_r' \to v_r)|$), the scattering interaction in the weakly interacting state can be neglected to first approximation. In that limit, $W_{ij}(v' \to v) \approx 0$ and (2.20) becomes

$$\partial\rho_{ij}(v, t)|_{\text{coll}} = -\tilde{\gamma}_{ij}(v)\rho_{ij}(v, t), \tag{2.33}$$

with

$$\tilde{\gamma}_{ij}(v) = \tfrac{1}{2}\mathcal{N}\int dv_p W_p(v_p) v_r \left(\frac{4\pi\hbar}{i\mu v_r}\right)\left[f_i(v_r \to v_r)\delta_{i\alpha} - f_j(v_r \to v_r)^*\delta_{j\alpha} \right] \tag{2.34}$$

and α indicating the strongly interacting level.

Eq. (2.33) has the *same* form as (2.29), implying that collisions are phase-interrupting in their effect on $\rho_{ij}(v, t)$. However velocity-changing effects are absent in eqs. (2.29) and (2.33) for *different* reasons. In eq. (2.29), the presence of light perturbers led to negligible active atom velocity changes in collisions. In eq. (2.33) only the forward scattering direction contributed to the change in $\rho_{ij}(v, t)$ owing to quantum-mechanical interference effects. Whereas active atom velocity changes will be

small for the atom as a whole when eq. (2.29) is valid, it is possible to have significant velocity changes associated with the population $\rho_{\alpha\alpha}(v, t)$ of the strongly scattered α state when eq. (2.33) is applicable.

One might expect a strong state dependence of the scattering interaction if levels 1 and 2 correspond to different electronic or possibly to different vibrational states.

Although the origin of eqs. (2.29) and (2.33) are different as stressed above, they both lead to the same type of equation, which can be interpreted in terms of an effective phase interruption following each collision. In this spirit, I shall write

$$\partial\rho_{ij}(v, t)/\partial t\,|_{\text{coll}} = -\gamma_{ij}^{\text{ph}}(v)\rho_{ij}(v, t), \tag{2.36}$$

$$\gamma_{ij}^{\text{ph}}(v) = \begin{cases} \bar{\gamma}_{ij}(v) & m_p/m \ll 1, \\ \tilde{\gamma}_{ij}(v) & \text{single-state-scattering}, \end{cases} \tag{2.37}$$

to represent both cases where velocity-changing collision effects on $\rho_{ij}(v, t)$ are absent. The parameter $\gamma_{ij}^{\text{ph}}(v)$ is the phase-interrupting collision parameter.

Further approximations. It may be possible to carry out perturbation theory with one of the above limits as the zeroth order approximation. For example, if $|f_i(v_r' \to v_r)| \gg |f_j(v_r' \to v_r)|$, a solution to first order in $f_j(v_r' \to v_r)$ might be attempted. On the other hand, if $f_i \approx f_j$, collisions are velocity-changing in first approximation and ρ_{ij} follows a prescribed trajectory; the slight difference in f_i and f_j produces a correlated phase interruption calculated along this trajectory [7]. In still another scheme [8], larger impact parameter collisions are assumed to produce small velocity changes while close-in collisions are taken to be phase-interrupting in nature.

General case. If none of the above limits are realized, the "kernel" and "rate" are given by (2.21) and (2.22), respectively. Little progress has been made in their evaluation, although one might imagine that some semi-classical or eikonal approximations could be tried. A simple interpretation in terms of a velocity change and a phase-interruption occurring in each collision does not seem appropriate since the two effects are completely intermingled. One would expect asymmetric and distorted profiles when both velocity-changing and phase-interrupting effects are important.

2.3. Impact approximation

The quantum mechanical transport equation (2.20) provides a description of elastic scattering for any n level atomic or molecular system. This equation was derived on the implicit assumption that any external fields which are interacting with the system do not appreciably alter it during the collision duration $\tau_c \approx 10^{-12}$ sec. In other words, collisions occur "instantaneously" (impact approximation) with regards to other time scales in the problem.

The impact approximation will be valid (1) if the atom does not decay during a collision ($\gamma\tau_c \ll 1$, where γ is some decay rate), (2) if two collisions do not occur during a collision time (binary collision approximation), (3) if the field is not strong enough to induce transitions in a time τ_c (valid for field strengths $\lesssim 10^7$ W/cm^2), and (4) if the atom-field detuning Δ satisfies $|\Delta|\tau_c \ll 1$ (the atom-field interaction effectively takes place on a time scale $\tau_d \lesssim |\Delta|^{-1}$, as required by the uncertainty principle – one must have $\tau_d \gg \tau_c$ for the impact approximation to be valid).

The calculations are restricted to situations where the impact approximation is valid. For the case of a dilute gas interacting with weak external fields considered below, the only restriction from the impact approximation is that the detunings $|\Delta|$ must be $\lesssim 10^{12}$ sec^{-1}.

3. Linear spectroscopy

Both linear and non-linear spectroscopy can be used to probe collision effects in atomic and molecular systems. In section 4, the manner in which non-linear spectroscopy can be used to provide differential as well as total cross-section data is explored. In this section, it is shown that values for total collision cross sections may be extracted from linear spectroscopy line profiles.

In linear spectroscopy, one measures the absorption or emission profile associated with a given transition. The two-level system shown in fig. 5 serves to illustrate the essential features of linear spectroscopy. Atoms are incoherently pumped into level 1 with a rate density $\lambda(v)$ assumed to be independent of position. The population in levels 1 and 2 decay with rates γ_1 and γ_2, respectively, owing to spontaneous emission. A monochromatic field (propagation vector $k = k\hat{Z}$, frequency $\Omega = ck$)

$$\boldsymbol{E}(\boldsymbol{R}, t) = \hat{\imath}E \cos(kZ - \Omega t) \tag{3.1}$$

is applied to the atom and drives the 1–2 transition which has a natural frequency ω. The population of level 2 is a measure of the absorption of the external field by the atom. For weak external fields, the population ρ_{22} as a function of Ω yields the linear absorption spectral profile.

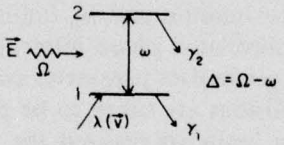

Fig. 5. The two-level system considered in this work.

To calculate ρ_{22}, one finds its equation of motion in the absence of collisions and adds to that the collisional contribution. The results depend critically on the velocity distribution in level 1 which, in turn, is a function of the excitation rate density $\lambda(v)$. To simplify the discussion, I shall assume that level 1 is a ground state with a thermal velocity distribution. This assumption corresponds to taking

$$\lambda(v) \sim 0, \qquad \gamma_1 \sim 0, \qquad \lambda(v)/\gamma_1 \sim N(v), \tag{3.2}$$

with

$$N(v) = NW_0(v), \tag{3.3}$$

$$W_0(v) = (\pi u^2)^{-3/2} e^{-v^2/u^2}, \tag{3.4}$$

where u is the most probable speed of the thermal distribution $W_0(v)$. The necessary modifications of the theory that arise when the pumping density $\lambda(v)$ can *not* be satisfactorily represented by an equilibrium velocity distribution (as might occur in emission or absorption from excited states) are discussed elsewhere [1].

3.1. Line shape – no collisions

In the absence of collisions, the Hamiltonian for the nth atom (neglecting pumping and decay terms which will be added later on) is

$$H(\boldsymbol{r}_n, \boldsymbol{R}_n, t) = H_0(\boldsymbol{r}_n) - (\hbar^2/2m)\nabla^2_{R_n} + V(\boldsymbol{r}_n, \boldsymbol{R}_n, t), \tag{3.5}$$

where $\boldsymbol{r}_n$ represents all electronic coordinates of atom n, $\boldsymbol{R}_n$ is the center-of-mass coordinate of atom n, $H_0(\boldsymbol{r}_n)$ is the free atom electronic Hamiltonian and $V(\boldsymbol{r}_n, \boldsymbol{R}_n, t)$ is the atom-field interation

$$V(\boldsymbol{r}_n, \boldsymbol{R}_n, t) = -\boldsymbol{\mu}_n \cdot \boldsymbol{E}(\boldsymbol{R}_n, t), \tag{3.6}$$

where $\boldsymbol{\mu}_n$ is the atomic dipole moment operator. The wave function of the nth atom can be expanded in terms of eigenfunctions $\psi_i(\boldsymbol{r}_n)$ of $H_0(\boldsymbol{r}_n)$ as

$$\psi(\boldsymbol{r}_n, \boldsymbol{R}_n, t) = \sum_i A_i^n(\boldsymbol{R}_n, t)\psi_i(\boldsymbol{r}_n). \tag{3.7}$$

Density matrix elements (diagonal in coordinate space) are defined by

$$\rho_{ij}^n(\boldsymbol{R}_n, t) = A_i^n(\boldsymbol{R}_n, t)A_j^n(\boldsymbol{R}_n, t)^*, \tag{3.8}$$

which obey an equation of motion

$$\partial\rho_{ij}^n(\boldsymbol{R}_n, t)/\partial t = -\mathrm{i}\omega_{ij}\rho_{ij}^n(\boldsymbol{R}_n, t) - \nabla \cdot \boldsymbol{J}_{ij}^n(\boldsymbol{R}_n, t) + (\mathrm{i}\hbar)^{-1}[V(\boldsymbol{R}_n, t), \rho^n(\boldsymbol{R}_n, t)]_{ij}, \tag{3.9}$$

where

$$\omega_{ij} = (E_i - E_j)/\hbar; \qquad \omega \equiv \omega_{21}. \tag{3.10}$$

E_i is the state i eigenenergy,

$$\boldsymbol{J}_{ij}^n(\boldsymbol{R}_n, t) = [\hbar/(2mi)]\left[A_j^n(\boldsymbol{R}_n, t)^*\nabla A_i^n(\boldsymbol{R}_n, t) - A_i^n(\boldsymbol{R}_n, t)\nabla A_j^n(\boldsymbol{R}_n, t)^*\right] \tag{3.11}$$

is a quantum-mechanical current, and matrix elements of $V(\boldsymbol{R}_n, t)$ are given by

$$V_{ij}(\boldsymbol{R}_n, t) = \int \mathrm{d}\boldsymbol{r}_n \psi_i(\boldsymbol{r}_n)^* V(\boldsymbol{r}_n, \boldsymbol{R}_n, t)\psi_i(\boldsymbol{r}_n) = (1 - \delta_{ij})\mu_{ij}E\cos(kZ - \Omega t), \tag{3.12}$$

with $\mu_{ij} = \mu_{ji}$ a matrix element of the x component of the dipole moment operator.

Provided that the external field does not alter the atomic center-of-mass motion, it is possible to obtain a classical limit for eq. (3.9) (classical with regards to the center-of-mass motion – the internal states are always treated quantum-mechanically). An external field *does* change the atomic velocity slightly owing to recoil effects resulting from the emission or absorption of radiation. If these recoil effects are neglected, however, one can associate a classical position $\boldsymbol{R}_n$ and velocity $\boldsymbol{v}_n$ to the average position and velocity, respectively, of a wave packet representing the atom. In this limit, the current becomes

$$\boldsymbol{J}_{ij}^n(\boldsymbol{R}_n, t) \to \boldsymbol{v}_n \cdot \nabla\rho_{ij}^n(\boldsymbol{R}_n, \boldsymbol{v}_n, t) \tag{3.13}$$

and eq. (3.9) goes over into

$$\partial\rho_{ij}^n(\boldsymbol{R}_n, \boldsymbol{v}_n, t)/\partial t = -\mathrm{i}\omega_{ij}\rho_{ij}^n(\boldsymbol{R}_n, \boldsymbol{v}_n, t) - \boldsymbol{v}_n \cdot \nabla\rho_{ij}^n(\boldsymbol{R}_n, \boldsymbol{v}_n, t) + (\mathrm{i}\hbar)^{-1}[V(\boldsymbol{R}_n, t), \rho^n(\boldsymbol{R}_n, \boldsymbol{v}_n, t)]_{ij}, \tag{3.14}$$

which now possesses a characteristic convective flow term $-\boldsymbol{v}_n \cdot \nabla\rho_{ij}^n$.

Macroscopic density matrix elements

$$\rho_{ij}(\boldsymbol{R}, \boldsymbol{v}, t) = \sum_n \int \mathrm{d}\boldsymbol{R}_n\, \mathrm{d}\boldsymbol{v}_n \rho_{ij}^n(\boldsymbol{R}_n, \boldsymbol{v}_n, t)\delta(\boldsymbol{R} - \boldsymbol{R}_n)\delta(\boldsymbol{v} - \boldsymbol{v}_n) = \sum_n \rho_{ij}^n(\boldsymbol{R}, \boldsymbol{v}, t) \tag{3.15}$$

are defined such that

$$N(\boldsymbol{R}, \boldsymbol{v}, t) = \sum_i \rho_{ii}(\boldsymbol{R}, \boldsymbol{v}, t) \tag{3.16}$$

is the density of active atoms in the sample. Density matrix elements $\rho_{ij}(\boldsymbol{R}, \boldsymbol{v}, t)$ also satisfy (3.14) since each atom interacts independently with the field. The pumping of level 1 can be introduced by the addition of a term $\lambda(\boldsymbol{v})\delta_{i1}\delta_{j1}$ and the decay by the addition of a term $-\gamma_{ij}\rho_{ij}(\boldsymbol{R}_n, \boldsymbol{v}_n, t)$,

$$\gamma_{ij} = (\gamma_i + \gamma_j)/2, \tag{3.17}$$

to the rhs of eq. (3.14). The resultant equation for the macroscopic density matrix elements is

$$\partial\rho_{ij}(\boldsymbol{R}, \boldsymbol{v}, t)/\partial t = -\boldsymbol{v}\cdot\nabla\rho_{ij}(\boldsymbol{R}, \boldsymbol{v}, t) - i\omega_{ij}\rho_{ij}(\boldsymbol{R}, \boldsymbol{v}, t) - \gamma_{ij}\rho_{ij}(\boldsymbol{R}, \boldsymbol{v}, t) + (i\hbar)^{-1}[(V(\boldsymbol{R}, t),\rho(\boldsymbol{R}, \boldsymbol{v}, t)]_{ij} + \lambda(\boldsymbol{v})\delta_{i1}\delta_{j1}, \tag{3.18}$$

which describes the time evolution of the system in the absence of collisions. A term corresponding to the spontaneous emission from level 2 serving to populate level 1 could be added to (3.18); however, this process does not lead to any modification of the line shapes in linear spectroscopy.

Although transient solutions of eqs. (3.18) are sometimes useful for collision studies, only steady-state solutions are considered in this work. Introducing the field interaction representation

$$\rho_{12}(\boldsymbol{R}, \boldsymbol{v}, t) = \tilde{\rho}_{12}(\boldsymbol{v})\exp[-i(kZ - \Omega t)], \tag{3.19a}$$

$$\rho_{ii}(\boldsymbol{R}, \boldsymbol{v}, t) = \tilde{\rho}_{ii}(\boldsymbol{v}), \tag{3.19b}$$

employing the rotating wave approximation (neglect of rapidly varying anti-resonance terms), and using eq. (3.12), one finds that the steady-state density matrix elements $\tilde{\rho}_{ij}(\boldsymbol{v})$ satisfy the following equations for the two-level system of fig. 5:

$$\gamma_1\tilde{\rho}_{11}(\boldsymbol{v}) = i\chi[\tilde{\rho}_{21}(\boldsymbol{v}) - \tilde{\rho}_{12}(\boldsymbol{v})] + \lambda(\boldsymbol{v}), \tag{3.20a}$$

$$\gamma_2\tilde{\rho}_{22}(\boldsymbol{v}) = i\chi[\tilde{\rho}_{12}(\boldsymbol{v}) - \tilde{\rho}_{21}(\boldsymbol{v})], \tag{3.20b}$$

$$(\eta_{12} - ikv_z)\tilde{\rho}_{12}(\boldsymbol{v}) = i\chi[\tilde{\rho}_{22}(\boldsymbol{v}) - \tilde{\rho}_{11}(\boldsymbol{v})], \tag{3.20c}$$

$$\tilde{\rho}_{21}(\boldsymbol{v}) = \tilde{\rho}_{12}(\boldsymbol{v})^*, \tag{3.20d}$$

where

$$\chi = \mu_{12}E/2\hbar, \tag{3.21}$$

$$\eta_{12} = \gamma_{12} + i\Delta, \tag{3.22}$$

and the detuning Δ is given by

$$\Delta = \Omega - \omega. \tag{3.23}$$

Eq. (3.20) may be solved exactly, but a perturbation solution of the equations is all that is needed in linear spectroscopy. The two perturbation chains leading to a value of $\tilde{\rho}_{22}(\boldsymbol{v})$ to second order in χ are

$$\rho_{11} \to \rho_{12} \to \rho_{22}, \tag{3.24a}$$

$$\rho_{11} \to \rho_{21} \to \rho_{22}. \tag{3.24b}$$

These chains are conveniently pictured in the Feynman type diagrams of fig. 6.*

Each horizontal line represents a history for a state amplitude, while density matrix elements are formed from a product of the amplitudes. The wavy lines represent atom-field interactions and the density matrix elements for each part of a history are indicated explicitly between the two lines. Figures 6a and 6b correspond to chains (3.24a) and (3.24b), respectively, but it is easy to see that they are really the same diagram with a different "time-ordering" for the fields (since the problem is time independent, the words "time-ordering" are used solely in analogy with Feynman diagrams). Diagrams of this type are especially useful when collisions are incorporated into the problem.

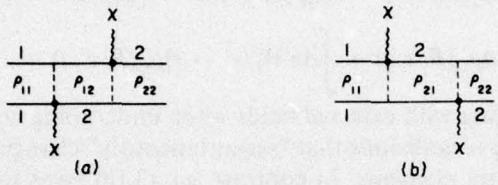

Fig. 6. Diagrams illustrating linear absorption of a field $\boldsymbol{E}$ (χ is the field strength in frequency units) taking an atom from state 1 to state 2. Each solid line represents a state amplitude and each wavy line an atom-field interaction. The numbers above or below the lines indicate the state the atom is in and the product of the two amplitudes gives rise to the density matrix elements indicated in the diagrams. Figures (a) and (b) correspond to chains (3.24a) and (3.24b), respectively.

The perturbation solution of (3.20) according to the chains (3.24) is straightforward and one obtains

$$\tilde{\rho}_{22}(v) = 2\chi^2 N W_0(v)\gamma_{12}\{\gamma_2[(\gamma_{12})^2 + (\Delta - kv_z)^2]\}^{-1}, \tag{3.25}$$

with $W_0(v)$ given by (3.4). The absorption line shape is defined as

$$I(\Delta) = \int dv\tilde{\rho}_{22}(v) = \frac{2\chi^2 N}{\gamma_2(\pi u^2)^{3/2}} \int_{-\infty}^{\infty} dv \frac{\gamma_{12}\exp[-(v/u)^2]}{(\gamma_{12})^2 + (\Delta - kv_z)^2} \tag{3.26}$$

and is the convolution of the Doppler shifted Lorentzian absorption profile associated with atoms having velocity v with the Gaussian distribution of atomic velocities $W_0(v)$. The line shape (3.26) is the so-called Voigt profile and may be expressed in terms of the plasma dispersion function $Z(\mu)$ as

$$I(\Delta) = \frac{2\chi^2 N}{\gamma_2 ku} Z_i\left(\frac{\Delta + i\gamma_{12}}{ku}\right) \tag{3.27}$$

where

$$Z(\mu) = Z_r(\mu) + iZ_i(\mu) = \frac{-1}{\pi^{1/2}} \int_{-\infty}^{\infty} dx \frac{e^{-x^2}}{\mu + x}, \tag{3.28}$$

* A similar idea was presented earlier [4, 5] with another pictorial format. Professor S. Stenholm suggested the more compact representation of fig. 6.

with $\mathrm{Im}(\mu) > 0$. Since γ_{12} is generally much less than the Doppler width* $ku[\ln 2]^{1/2}$, $I(\Delta)$ is essentially a Gaussian function, representing the well known "Doppler broadening" of spectral profiles.

3.2. Collisions – general considerations

In the impact approximation, the external fields and collisions contribute independently to $\partial\rho_{ij}(\boldsymbol{R}, \boldsymbol{v}, t)/\partial t$ allowing one to simply add eqs. (3.18) and (2.20). The resulting quantum mechanical transport equation

$$\partial\rho_{ij}(\boldsymbol{R}, \boldsymbol{v}, t)/\partial t = -\boldsymbol{v}\cdot\nabla\rho_{ij}(\boldsymbol{R}, \boldsymbol{v}, t) - \mathrm{i}\omega_{ij}\rho_{ij}(\boldsymbol{R}, \boldsymbol{v}, t) - \gamma_{ij}\rho_{ij}(\boldsymbol{R}, \boldsymbol{v}, t) + (\mathrm{i}\hbar)^{-1}[V(\boldsymbol{R}, t), \rho(\boldsymbol{R}, \boldsymbol{v}, t)]_{ij}$$
$$-\Gamma_{ij}(\boldsymbol{v})\rho_{ij}(\boldsymbol{R}, \boldsymbol{v}, t) + \int \mathrm{d}\boldsymbol{v}' W_{ij}(\boldsymbol{v}' \to \boldsymbol{v})\rho_{ij}(\boldsymbol{R}, \boldsymbol{v}', t) + \lambda(\boldsymbol{v})\delta_{i1}\delta_{j1} \tag{3.29}$$

characterizes atoms interacting with external fields while undergoing collisions. The contribution (2.20) gives the average effect of collisions that "instantaneously" change the velocity and/or phase associated with density matrix elements. In contrast, eq. (3.18) gives the change in $\rho_{ij}(\boldsymbol{R}, \boldsymbol{v}, t)$ for the time *between* collisions, in which the atomic center-of-mass motion associated with each density matrix element is that of a free particle.

Steady-state equations for the $\tilde{\rho}_{ij}(\boldsymbol{v})$ defined by eq. (3.19) may be obtained from (3.29) in the rotating wave approximation and are given by

$$[\gamma_1 + \Gamma_{11}(\boldsymbol{v})]\tilde{\rho}_{11}(\boldsymbol{v}) - \int \mathrm{d}\boldsymbol{v}' W_{11}(\boldsymbol{v}' \to \boldsymbol{v})\tilde{\rho}_{11}(\boldsymbol{v}') = \mathrm{i}\chi[\tilde{\rho}_{21}(\boldsymbol{v}) - \tilde{\rho}_{12}(\boldsymbol{v})] + \lambda(\boldsymbol{v}), \tag{3.30a}$$

$$[\gamma_2 + \Gamma_{22}(\boldsymbol{v})]\tilde{\rho}_{22}(\boldsymbol{v}) - \int \mathrm{d}\boldsymbol{v}' W_{22}(\boldsymbol{v}' \to \boldsymbol{v})\tilde{\rho}_{22}(\boldsymbol{v}') = \mathrm{i}\chi[\tilde{\rho}_{12}(\boldsymbol{v}) - \tilde{\rho}_{21}(\boldsymbol{v})], \tag{3.30b}$$

$$[\eta_{12} - \mathrm{i}kv_z + \Gamma_{12}(\boldsymbol{v})]\tilde{\rho}_{12}(\boldsymbol{v}) - \int \mathrm{d}\boldsymbol{v}' W_{12}(\boldsymbol{v}' \to \boldsymbol{v})\tilde{\rho}_{12}(\boldsymbol{v}') = \mathrm{i}\chi[\tilde{\rho}_{22}(\boldsymbol{v}) - \tilde{\rho}_{11}(\boldsymbol{v})], \tag{3.30c}$$

$$\tilde{\rho}_{21}(\boldsymbol{v}) = \tilde{\rho}_{12}(\boldsymbol{v})^*. \tag{3.30d}$$

Solutions of these linear coupled integral equations are very difficult to obtain for arbitrary collision kernels $W_{ij}(\boldsymbol{v}' \to \boldsymbol{v})$.

However, a formal solution of eqs. (3.30) can always be found that turns out to be specially useful for perturbation (in the external field) calculations. This solution to eqs. (3.30) is given by

$$\tilde{\rho}_{11}(\boldsymbol{v}) = \int \mathrm{d}\boldsymbol{v}' G_{11}(\boldsymbol{v}' \to \boldsymbol{v})\left[\mathrm{i}\chi\{\tilde{\rho}_{21}(\boldsymbol{v}') - \tilde{\rho}_{12}(\boldsymbol{v}')\} + \lambda(\boldsymbol{v}')\right],$$

$$\tilde{\rho}_{22}(\boldsymbol{v}) = \int \mathrm{d}\boldsymbol{v}' G_{22}(\boldsymbol{v}' \to \boldsymbol{v})\left[\mathrm{i}\chi\{\tilde{\rho}_{12}(\boldsymbol{v}') - \tilde{\rho}_{21}(\boldsymbol{v}')\}\right],$$

$$\tilde{\rho}_{12}(\boldsymbol{v}) = \int \mathrm{d}\boldsymbol{v}' G_{12}(\boldsymbol{v}' \to \boldsymbol{v})\left[\mathrm{i}\chi\{\tilde{\rho}_{22}(\boldsymbol{v}') - \tilde{\rho}_{11}(\boldsymbol{v}')\}\right],$$

$$\tilde{\rho}_{21}(\boldsymbol{v}) = \int \mathrm{d}\boldsymbol{v}' G_{21}(\boldsymbol{v}' \to \boldsymbol{v})\left[\mathrm{i}\chi\{\tilde{\rho}_{11}(\boldsymbol{v}') - \tilde{\rho}_{22}(\boldsymbol{v}')\}\right] = \tilde{\rho}_{12}(\boldsymbol{v})^*, \tag{3.31}$$

* By "width", I always refer to the half width at half maximum (HWHM).

where the propagators $G_{ij}(v' \to v)$ satisfy

$$[\eta_{ij}(v_z) + \Gamma_{ij}(v)]G_{ij}(v' \to v) - \int dv'' W_{ij}(v'' \to v)G_{ij}(v' \to v'') = \delta(v - v'), \tag{3.32}$$

with

$$\eta_{ii}(v_z) = \gamma_i; \qquad \eta_{12}(v_z) = \eta_{12} - ikv_z = \eta_{21}(v_z)^*. \tag{3.33}$$

All the effects of collisions are contained in the propagator equation (3.32) which, in general, is very difficult to solve.

Assuming one has a solution of eq. (3.32) for $G_{ij}(v' \to v)$, he can easily obtain an iterative solution of eq. (3.31). The perturbation chains leading to a value for $\tilde{\rho}_{22}(v)$ to second order in χ are completely analogous to those of (3.24). One obtains

$$\tilde{\rho}^a_{22}(v) = \chi^2 \int dv_2\, dv_1\, dv_0 G_{22}(v_2 \to v)G_{12}(v_1 \to v_2)G_{11}(v_0 \to v_1)\lambda(v_0), \tag{3.34a}$$

corresponding to chain (3.24a) and

$$\tilde{\rho}^b_{22}(v) = \chi^2 \int dv_2\, dv_1\, dv_0 G_{22}(v_2 \to v)G_{21}(v_1 \to v_2)G_{11}(v_0 \to v_1)\lambda(v_0), \tag{3.34b}$$

corresponding to chain (3.24b). These results have a simple interpretation in terms of the diagrams of fig. 6. For example, in fig. 6a and in (3.34a), one can think of the incoherent pumping as providing a $\lambda(v_0)$. The quantity $G_{11}(v_0 \to v_1)$ propagates this solution up to the first field interaction. Between the first and second field interaction the propagator $G_{12}(v_1 \to v_2)$ acts, and following the second field interaction the propagator $G_{22}(v_2 \to v)$ carries along the solution.

Thus, to solve (3.30) to any order in perturbation theory in the external field, one first draws all the appropriate diagrams of the type shown in fig. 6. At each field interaction, there is a multiplicative coupling constant ($\pm i\chi$) that enters the calculation. *Between* two successive field interactions the solution is propagated by the $G_{ij}(v' \to v)$ that corresponds to the $\tilde{\rho}_{ij}(v)$ which appears in the diagram between those field interactions (i.e., $\tilde{\rho}_{12}(v)$ appears between the first and second field interactions in fig. 6a). Before the first field interaction, $G_{11}(v_0 \to v_1)$ propagates the incoherent pumping $\lambda(v_0)$ and following the last field interaction $G_{22}(v_n \to v)$ propagates the solution to some final velocity v. Integrals over all intermediate velocities must be taken. This diagrammatic technique is used in section 4 to obtain results for a three-level problem.

By adding (3.34a) to (3.34b) and integrating the sum over all v, one determines the line shape in linear spectroscopy

$$I(\Delta) = \chi^2\gamma_1 N \int dv\, dv_2\, dv_1\, dv_0 G_{22}(v_2 \to v)[G_{12}(v_1 \to v_2) + G_{12}(v_1 \to v_2)^*]G_{11}(v_0 \to v_1)W(v_0), \tag{3.35}$$

where eqs. (3.2–3.4) have been used. This line shape may be simplified in two ways. First, collisions do not change $W_0(v)$ since it is already on equilibrium distribution so that

$$\int dv_0 G_{ii}(v_0 \to v_1)W_0(v_0) = W_0(v_1)/\gamma_i. \tag{3.36}$$

Second, diagonal propagators have the property, easily derived by integrating eq. (3.32) over

velocity, that

$$\int d\nu G_{ii}(\nu' \to \nu) = 1/\gamma_i. \tag{3.37}$$

Eq. (3.37) expresses the fact that the total population of any level, $\int d\nu \tilde{\rho}_{ii}(\nu)$, is unaffected by elastic velocity-changing collisions (collisions redistribute the velocities but do not change the total population). In terms of the diagrammatic solutions of fig. 6, eqs. (3.36) and (3.37) eliminate the need to consider collision effects before the first field interaction (when an equilibrium velocity distribution existed) and following the last field interaction (since the total population only of the final state is measured).

Using eqs. (3.36) and (3.37) in eq. (3.35), one obtains

$$I(\Delta) = \frac{\chi^2 N}{\gamma_2} \int d\nu_0 \, d\nu G_{12}(\nu_0 \to \nu) W_0(\nu_0) + \text{conjugate}, \tag{3.38}$$

which is the final form for the line shape in linear spectroscopy. Only collision effects on $\tilde{\rho}_{12}(\nu)$ enter in eq. (3.38) since the effects of collisions on populations have been eliminated by eqs. (3.36) and (3.37). Limiting forms for eq. (3.38) are discussed below corresponding to $G_{12}(\nu' \to \nu)$ determined by collisions that are either phase-interrupting or velocity-changing in their effect on $\tilde{\rho}_{12}(\nu)$.

3.3. Line shape – phase-interrupting collisions

When collisions are phase-interrupting in nature, the collisional time rate of change of $\rho_{12}(\nu, t)$ is given by eq. (2.36). Consequently, the collision terms in eq. (3.29) for $\rho_{12}(\boldsymbol{R}, \nu, t)$ are replaced by $-\gamma_{12}^{ph}(\nu)\rho_{12}(\boldsymbol{R}, \nu, t)$ and this change is reflected in eq. (3.32) as

$$[\eta_{12}(v_z) + \gamma_{12}^{ph}(\nu)] G_{12}^{ph}(\nu' \to \nu) = \delta(\nu - \nu'). \tag{3.39}$$

Recalling the definition (3.33) for $\eta_{12}(v_z)$, one obtains the propagator

$$G_{12}^{ph}(\nu' \to \nu) = \frac{\delta(\nu - \nu')}{[\gamma_{12} + \Gamma_{12}^{ph}(\nu)] + i[\Delta - kv_z + S_{12}^{ph}(\nu)]}, \tag{3.40}$$

where

$$\Gamma_{ij}^{ph}(\nu) = \text{Re}\,[\gamma_{ij}^{ph}(\nu)]; \qquad S_{ij}^{ph}(\nu) = \text{Im}\,[\gamma_{ij}^{ph}(\nu)] \tag{3.41}$$

are the phase-interrupting broadening and shift parameters, respectively. The propagator $G_{12}(\nu' \to \nu)$ is proportional to $\delta(\nu - \nu')$ for phase-interrupting collisions since there is no velocity change associated with off-diagonal density matrix elements for reasons discussed in subsection 2.2.2. The line shape obtained by combining eqs. (3.38) and (3.40) is

$$I(\Delta) = \frac{2\chi^2 N}{\gamma_2 (\pi u^2)^{3/2}} \int d\nu \frac{[\gamma_{12} + \Gamma_{12}^{ph}(\nu)] \, e^{-\nu^2/u^2}}{[\gamma_{12} + \Gamma_{12}^{ph}(\nu)]^2 + [\Delta - kv_z + S_{12}^{ph}(\nu)]^2}. \tag{3.42}$$

The absorption profile is broadened and shifted from the no-collision line shape (3.26); one can go from eq. (3.26) to (3.42) by the simple replacements

$$\gamma_{12} \to \gamma_{12} + \Gamma_{12}^{ph}(\nu); \qquad \Delta \to \Delta + S_{12}^{ph}(\nu). \tag{3.43}$$

The broadening and shift can be understood in terms of the phase-interrupting collision mechanism. Collisions interrupt the oscillator's coherence train and result in an effective decrease of the oscillator lifetime with a corresponding broadening of the absorption profile. The persistence of some phase memory following a collision (for collisions with large impact parameters) results in a shift of the line center. That distant collisions contribute to the shift is easily seen from eq. (2.31) which, when expanded for small phase shifts $|\theta| \ll 1$, leads to

$$\partial\rho_{12}(\boldsymbol{R}, \boldsymbol{v}, t)/\partial t|_{\text{coll}} = \mathrm{i}\langle\dot{\theta}\rangle\rho_{12}(\boldsymbol{R}, \boldsymbol{v}, t), \tag{3.44a}$$

with

$$\langle\dot{\theta}\rangle = \mathcal{N}\int \mathrm{d}\boldsymbol{v}_{\mathrm{p}} W_{\mathrm{p}}(\boldsymbol{v}_{\mathrm{p}}) v_{\mathrm{r}} \int_{b_{\min}}^{\infty} 2\pi b\, \mathrm{d}b\theta(b, v_{\mathrm{r}}). \tag{3.44b}$$

Thus, distant collisions lead to a shift, $\omega \to \omega + \langle\dot{\theta}\rangle$, of the oscillator's resonance frequency. For strong collisions ($|\theta| > 1$), the average value of $\rho_{12}(\boldsymbol{v}, t)$ after a collision is zero; these collisions give rise to a decay of $\rho_{12}(\boldsymbol{v}, t)$ (and to a broadening of the absorption profile), but do not contribute to the shift.

The line shape (3.42) has some interesting features. The broadening and shift parameters are given as functions of velocity, but, typically, they will be functions of speed only. This result follows from eqs. (2.37, 2.30, 2.34) provided that $f_i(\boldsymbol{v}_{\mathrm{r}} \to \boldsymbol{v}_{\mathrm{r}})$ depends only on the magnitude of $\boldsymbol{v}_{\mathrm{r}}$ and that $W_{\mathrm{p}}(\boldsymbol{v}_{\mathrm{p}})$ is an even function. Since these limits are generally realized, it is assumed that $\Gamma_{ij}^{\mathrm{ph}}$ and S_{ij}^{ph} are functions of v only. I shall call the resulting line shape (3.42) a Speed Dependent Voigt Profile (SDVP). The conditions under which the speed dependence is significant is discussed below.

The presence of a speed dependent shift leads to an asymmetry of the profile. To see how this asymmetry arises, replace $(v_x^2 + v_y^2)$ by some average u_{T}^2 and consider the contribution to the line shape from atoms moving with $\pm v_{z_0}$. This contribution,

$$\frac{2\chi^2 N}{\gamma_2(\pi u^2)^{1/2}} \exp\{-(u_{\mathrm{T}}^2 + v_{z_0}^2)/u^2\}\,\mathrm{d}v_{z_0}$$

$$\times\left\{\frac{[\gamma_{12} + \Gamma_{12}^{\mathrm{ph}}(u_{\mathrm{T}}^2 + v_{z_0}^2)]}{[\gamma_{12} + \Gamma_{12}^{\mathrm{ph}}(u_{\mathrm{T}}^2 + v_{z_0}^2)]^2 + [\Delta - kv_{z_0} + S_{12}^{\mathrm{ph}}(u_{\mathrm{T}}^2 + v_{z_0}^2)]^2}\right.$$

$$\left. + \frac{[\gamma_{12} + \Gamma_{12}^{\mathrm{ph}}(u_{\mathrm{T}}^2 + v_{z_0}^2)]}{[\gamma_{12} + \Gamma_{12}^{\mathrm{ph}}(u_{\mathrm{T}}^2 + v_{z_0}^2)]^2 + [\Delta + kv_{z_0} + S_{12}^{\mathrm{ph}}(u_{\mathrm{T}}^2 + v_{z_0}^2)]^2}\right\}, \tag{3.45}$$

is a symmetric function of Δ about $-S_{12}^{\mathrm{ph}}(v_{z_0}^2 + u_{\mathrm{T}}^2)$. If one next considers the contribution from atoms moving with $\pm v_{z_1}$, he finds it to be symmetric about $-S_{12}^{\mathrm{ph}}(v_{z_1}^2 + u_{\mathrm{T}}^2) \neq -S_{12}^{\mathrm{ph}}(v_{z_0}^2 + u_{\mathrm{T}}^2)$. Thus the sum of the two contributions is *asymmetric*. Since $W_0(\boldsymbol{v})$ is composed of $\pm v_z$ pairs, the line shape (3.42) is asymmetric. Furthermore, since the asymmetry will be pressure dependent, the shift of the line center will be a non-linear function of perturber pressure. It may also be noted that erroneous values for the broadening parameter will be obtained if one attempts to fit experimental data to a normal Voigt profile rather than a SDVP.

These effects are important only if the speed dependence of $\gamma_{12}^{\mathrm{ph}} = \Gamma_{ij}^{\mathrm{ph}} + \mathrm{i}S_{ij}^{\mathrm{ph}}$ is significant. If $m_{\mathrm{p}} \ll m$, $v_{\mathrm{r}} \approx v_{\mathrm{p}}$ and it follows from eqs. (2.37, 2.30, 2.34) that $\gamma_{ij}^{\mathrm{ph}}$ depends on the most probable perturber speed but *not* on the active atom speed v. Therefore, significant deviations from a Voigt

AD-A061 099 NEW YORK UNIV N Y DEPT OF PHYSICS F/G 7/4
THEORETICAL STUDIES RELATING TO THE INTERACTION OF RADIATION WI--ETC(U)
OCT 78 P R BERMAN, E J ROBINSON N00014-77-C-0553
UNCLASSIFIED NL

2 OF 2
ADA
061099

END
DATE FILMED
2-79
DDC

profile can occur only for $m_p \gtrsim m$. Since the condition $m_p \gtrsim m$ is not consistent with the phase-interrupting collision limit (2.30) requiring $m_p \ll m$, collisions involving negligible active atom velocity changes can lead only to normal Voigt profiles. On the other hand, deviations from a Voigt profile *could* occur in the quantum interference phase-interrupting collision limit (2.34), provided $m_p \gtrsim m$. Unless $m_p \gg m$, however, it is generally a good approximation to neglect the speed dependence of the shift and broadening parameters [9, 10].

A line shape analysis using (3.42) enables one to determine Γ_{12}^{ph} and S_{12}^{ph} which are related to the cross-section and real part of the forward scattering amplitudes in states 1 and 2. If one state is more strongly scattered than the other the total elastic scattering cross-section for that state may be found. In this manner, linear spectroscopy profiles can yield excited state total elastic cross section data.

The line width (HWHM) of (3.42) as a function of perturber pressure is shown in curve a of fig. 7 for $\gamma_{12} \ll ku$, neglecting the speed dependence of Γ_{12}^{ph} and Δ_{12}^{ph}. At low pressures the width is dominated by the Doppler contribution, but as the pressure is increased to the point where $\Gamma_{12}^{ph} \gg ku$, the line profile becomes Lorentzian with width Γ_{12}^{ph}. If the speed dependence of the line shape parameters is ignored, eq. (3.42) becomes

$$I(\Delta) = \frac{2\chi^2 N}{\gamma_2 ku} Z_i\left(\frac{(\Delta + S_{12}^{ph}) + i(\gamma_{12} + \Gamma_{12}^{ph})}{ku}\right).$$

3.4. *Line shape – velocity-changing collisions*

In contrast to phase-interrupting collisions, collisions which are velocity-changing in their effect on $\tilde{\rho}_{12}(v)$ give rise to a *narrowing* of the linear absorption or emission profiles associated

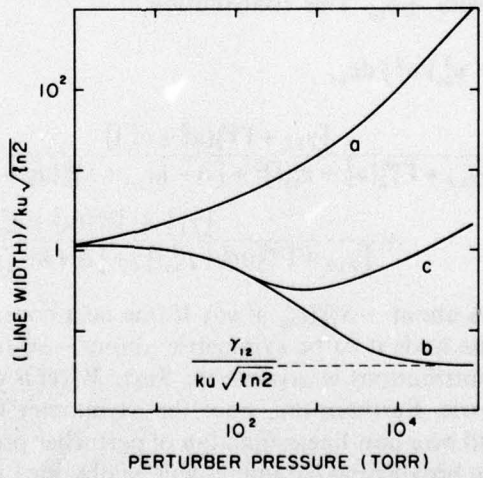

Fig. 7. Typical behavior of the line width (HWHM) as a function of pressure in linear absorption. At low pressures the width is approximately equal to the Doppler width $ku\,[\ln 2]^{1/2}$ (assuming $\gamma_{12} \ll ku$). (a) For phase-interrupting collisions the width increases monotonically with pressure, becoming linear with pressure for $\Gamma_{12}^{ph} \gg ku$. (b) For velocity-changing collisions, the line width decreases monotonically with pressure, ultimately reaching a value of γ_{12}. (c) When levels 1 and 2 experience nearly equal collision interactions the width decreases and then increases with increasing pressure.

with the 1–2 transition. While it is not difficult to understand the narrowing effect, it will aid the discussion to first introduce the concept of an effective collision rate.

Imagine that a velocity distribution $\rho_{ii}(v, t)$ is produced by some means. The velocity distribution is centered about $v_0 \approx u$ with a spread (Δu_0). Collisions will cause the velocity distribution to relax back towards a Maxwellian distribution centered at $v = 0$ with a width (HWHM) of $u(\ln 2)^{1/2}$. The rate at which this relaxation occurs is called the effective collision rate and is denoted by Γ'_{ii}. The effective collision rate can be much smaller than the velocity-changing rate Γ_{ii}, especially for weak collisions. If the rms velocity change per collision is (Δu), there must be *at least* $u/\Delta u$ collisions to restore the Maxwellian distribution. A more realistic estimate for the required number of collisions turns out to be $[u/(\Delta u)]^2$, taking into account that random nature of the collision process (that is, $\langle v \rangle$ undergoes something similar to a random walk from its initial value v_0 to its final value of zero).*

Thus, the relaxation time is $[u/(\Delta u)]^2/\Gamma_{ii}$ giving an effective collision rate

$$\Gamma'_{ii} = \Gamma_{ii}[(\Delta u)/u]^2. \tag{3.46}$$

For reasons to be discussed below, linear absorption experiments are sensitive mainly to Γ'_{ii} whereas non-linear spectroscopy may be used to determine both Γ_{ii} and (Δu).

The spectral profile is given by eq. (3.38) with the propagator $G^{vc}_{12}(v' \to v)$ satisfying eq. (3.32)

$$(\eta_{12} - kv_z)G^{vc}_{12}(v' \to v) + \Gamma^{vc}_{12}(v)G^{vc}_{12}(v' \to v) - \int dv'' W^{vc}_{12}(v'' \to v)G^{vc}_{12}(v' \to v'') = \delta(v - v'). \tag{3.47}$$

The collision kernel $W^{vc}_{12}(v' \to v)$ and rate $\Gamma^{vc}_{12}(v)$ are real and state independent since the collision interaction is state independent when collisions are velocity-changing in their effect on ρ_{12} (see discussion in subsection 2.2.2). Eq. (3.47) is difficult to solve for all but very simple collision kernels. However, one can explain most line shape features without explicit reference to a particular kernel.

To write the spectral profile (3.38) in a more suggestive fashion, I first rewrite the no-collision line shape (3.26) as

$$I(\Delta) = \frac{\chi^2 N}{\gamma_2(\pi u^2)^{3/2}} \int dv \int_0^\infty dt\, e^{-v^2/u^2} \exp\{-\gamma_{12}t - i(\Delta - kv_z)t\} + \text{conjugate}. \tag{3.48}$$

When collisions are present, one might expect that $\exp(i\boldsymbol{k} \cdot \boldsymbol{v}t)$ is replaced by $\langle \exp[i\boldsymbol{k} \cdot \int_0^t \boldsymbol{v}(t')\,dt'] \rangle$ where $\boldsymbol{v}(0) = \boldsymbol{v}_0$ and the average is over collision histories. With this clue, one writes (3.38) in the form

$$I(\Delta) = \frac{\chi^2 N}{\gamma_2} \int dv_0 \int_0^\infty dt C(t, v_0)\, e^{-(\gamma_{12} + i\Delta)t} W_0(v_0) + \text{conjugate}, \tag{3.49}$$

where $C(t, v_0)$, as obtained by iteration from eq. (3.47), is given by

* The factor $(u/\Delta u)^2$ is easily derived for the case of weak collisions by calculating the decay rate of $\langle v \rangle$ [11].

$$C(t, v_0) = \exp\{-\Gamma_{12}(v_0)t\}\exp(ik\cdot v_0 t) + \int dv \int_0^t dt_1 \exp\{-\Gamma_{12}^{vc}(v_0)t_1\}\exp(ik\cdot v_0 t_1)W_{12}^{vc}(v_0 \to v)$$

$$\times \exp\{-\Gamma_{12}^{vc}(v)(t-t_1)\}\exp\{ik\cdot v(t-t_1)\} + \int dv\, dv_1 \int_0^t dt_2 \int_0^{t_2} dt_1$$

$$\times \exp(-\Gamma_{12}^{vc}(v_0)t_1)\exp(ik\cdot v_0 t_1)W_{12}^{vc}(v_0 \to v_1)\exp\{-\Gamma_{12}^{vc}(v_1)(t_2-t_1)\}$$

$$\times \exp\{ik\cdot v_1(t_2-t_1)\}W_{12}^{vc}(v_1 \to v)\exp\{-\Gamma_{12}^{vc}(v)(t-t_2)\}\exp\{ik\cdot v(t-t_2)\} + \ldots$$

$$= \left\langle \exp\left\{ik\cdot\int_0^t v(t')\,dt'\right\}\right\rangle . \tag{3.50}$$

Eqs. (3.49, 3.50) provide the expected generalization of eq. (3.48) to include velocity-changing collision effects.

The collisional narrowing effect can now be understood as a randomization of the Doppler phase. In the absence of collisions, $C(t, v_0) = \exp(ik\cdot v_0 t)$ and the line width is on the order of ku (assuming $ku \gg \gamma_{12}$). To estimate $C(t, v_0)$ in the presence of collisions, it is useful to express it as

$$C(t, v_0) = \langle \exp[ik\cdot R(t)]\rangle \tag{3.51}$$

where $R(t)$ is the displacement undergone by an active atom in time t having a velocity $v = v_0$ at $t = 0$. Collisions result in active atoms altering their velocity by a significant amount in a time on the order of $[(\Gamma_{12}^{vc})']^{-1}$ (Γ' is the effective collision rate); consequently, a typical atom undergoes a type of random walk with a mean free path $\approx u/(\Gamma_{12}^{vc})'$. The mean square displacement of such a particle in time t is

$$\langle [R(t)]^2\rangle = [u/(\Gamma_{12}^{vc})']^2[(\Gamma_{12}^{vc})'t] = [u^2/(\Gamma_{12}^{vc})']t \tag{3.52}$$

valid for $(\Gamma_{12}^{vc})'t > 1$. The collisionally induced reduction of the Doppler phase from its no-collision value $k\cdot v_0 t$ to a value $\approx k\langle [R(t)]^2\rangle^{1/2}$ provides a narrowing mechanism for the line profile.

One can now trace the development of the line width as a function of pressure. For $(\Gamma_{12}^{vc})' < ku$, the atom does not undergo an effective collision in its "coherence" time $t_{coh} = (ku)^{-1}$ and the line width remains close to the Doppler width [t_{coh} is the largest time for which the integrand in eq. (3.49) contributes effectively to the integral]. For $(\Gamma_{12}^{vc})' > ku$ but $(ku)^2/(\Gamma_{12}^{vc})' > \gamma_{12}$, t_{coh} is determined by the $\langle k^2[R(t_{coh})]^2\rangle = 1$ giving a value equal to $t_{coh} = (\Gamma_{12}^{vc})'/(ku)^2$ and a line width of order

$$W = (ku)[ku/(\Gamma_{12}^{vc})']. \tag{3.53}$$

The Doppler width is reduced by a factor $[(ku)/(\Gamma_{12}^{vc})']$ at pressures where the effective mean free path $[u/(\Gamma_{12}^{vc})']$ is less than the atomic wavelength $(2\pi/k)$. At still higher pressures where $\langle k^2[R(t)]^2\rangle \ll \gamma_{12}t$, the Doppler phase may be totally neglected, and the line profile is a Lorentzian of width γ_{12}.

The line width as a function of pressure is shown schematically in curve b of fig. 7. At low pressures, the line is a Voigt profile with a width equal to slightly more than the Doppler width (assuming $\gamma_{12} \ll ku$). The width decreases monotonically with increasing pressure, ultimately reaching the value γ_{12}. In the infra-red or optical range, collisional narrowing becomes important

at pressures on the order of several hundred Torr and has been experimentally observed on vibrational and rotational transitions. Inelastic collisions may tend to obscure the narrowing effect by broadening the line with increasing pressure.

If the collision interaction for levels 1 and 2 differed slightly, one might still expect collisional narrowing over a wide range of pressures. For high enough pressures, however, $(ku)^2/(\Gamma_{12}^{vc})' < \Gamma_{12}^{ph}$, and collisional broadening of the line profile may be seen. This case is shown in curve c of fig. 7.

To this point, I have not discussed the detailed nature of the collision kernel. While the line profile *does* depend to some extent on the specific form of the kernel [12], it is not overly sensitive to either Γ_{12}^{vc} or Δu separately, but rather to the effective collision rate $(\Gamma_{12}^{vc})' = \Gamma_{12}^{vc}[(\Delta u)/u]^2$. The semiquantitative discussion of the narrowing effect given made no reference to Γ_{12}^{vc} or Δu; only $(\Gamma_{12}^{vc})'$ was mentioned. It should be noted, however, that a physically acceptable kernel (i.e., one that obeys detailed balancing) should be used if one wants to be assured of getting the narrowing effect. For example, a difference kernel $W(v' \to v) = W(v - v')$, commonly used to describe weak collisions, does not obey detailed balancing and does *not* lead to collisional narrowing. From the symmetry of such a kernel, it is easy to conclude that $\langle v \rangle = v_0$, implying that equilibrium is never reached. Consequently, $(\Gamma_{12}^{vc})' = 0$ and the effective mean free path is infinite.

4. Non-linear spectroscopy

At low pressures ($\lesssim$ 100 Torr), the Doppler effect provides the major contribution to the line width of absorption or emission profiles. The relatively large Doppler width tends to mask any collision induced modifications of the line profile, and it is therefore desirable to devise schemes in which the Doppler effect plays a minimal role in line shape formation. Any such schemes are also well suited for high resolution spectroscopic studies. In the past, the Doppler effect was reduced by using either cooled bulb samples or well-collimated atomic beams. The last few years, however, have witnessed the emergence of a large number of "Doppler-free" techniques involving the use of non-linear spectroscopy.

The manner in which non-linear spectroscopy can be used to eliminate the Doppler width is best illustrated by two specific examples. First, consider two-photon transitions between atomic levels separated by a frequency ω_{31}. If an atom is moving with velocity v and absorbs one photon each from fields E, E' having propagation vectors k, k', respectively, the resonance condition for two-photon absorption is

$$\Omega + \Omega' + (k + k') \cdot v = \omega_{31}. \tag{4.1}$$

If $k \approx -k'$, eq. (4.1) is independent of the atomic velocity and each atom contributes equally in the absorption process. In effect, the Doppler phase created by the first field is exactly compensated by the second. In this Doppler-free technique, all active atoms, regardless of velocity, contribute in line shape formation.

As a second example, consider any of the three-level configurations in fig. 8. Two photon transitions of the type discussed above are still possible for these level schemes. However, an additional resonant interaction is possible. If the field E with propagation vector $k = k\hat{Z}$ is tuned to be nearly resonant with the 1–2 transition in fig. 8, only those atoms for which

$$kv_z = \Omega - \omega \tag{4.2}$$

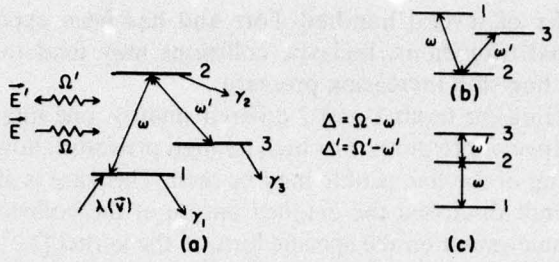

Fig. 8. The three-level systems considered in this work: (a) inverse V, (b) V, (c) upward cascade.

will be significantly excited by the field. A probe field $\boldsymbol{E}'$ with propagation vector $\boldsymbol{k}' = \pm k'\hat{\boldsymbol{Z}}$ and frequency $\Omega' = k'c$ will be resonant with the 2–3 transition provided

$$\Omega' = \omega' \pm k'v_z, \tag{4.3}$$

where ω' is the 2–3 transition frequency. Since v_z has been selected by the field $\boldsymbol{E}$ according to (4.2), the resonance condition (4.3) becomes

$$\Omega' = \omega' \pm (k'/k)(\Omega - \omega). \tag{4.4}$$

The atomic velocity does not appear in eq. (4.4), indicating that a measurement of the absorption of $\boldsymbol{E}'$ as a function of Ω' is a Doppler-free technique. In contrast to the two-photon Doppler free resonance condition (4.1), the Doppler free nature of the stepwise absorption of fields $\boldsymbol{E}$ and $\boldsymbol{E}'$ is due to the selective absorption of the field $\boldsymbol{E}$ by a narrow velocity subset of atoms. Only a fraction of the atoms are used in this Doppler-free technique whereas all the atoms are used in the two-photon Doppler free case in which a cancellation of the Doppler phase leads to the Doppler-free resonance.

Thus, non-linear spectroscopy offers the potential for achieving Doppler-free line shapes. Moreover, the modifications of these Doppler-free line shapes resulting from collision effects can be dramatic. As an example of the role collisions can play, reconsider the stepwise absorption chain (4.2)–(4.4). Atoms with a selected value of v_z given by eq. (4.2) are excited into state 2 by the field $\boldsymbol{E}$. Collisions result in a relaxation of this narrow velocity distribution towards a thermal equilibrium one. The absorption profile of $\boldsymbol{E}'$ measures the amount of velocity relaxation that has occurred. Since it is collision induced velocity changes that are directly monitored, one obtains information on the *differential* scattering cross section in level 2. (More precisely, one determines the differential scattering cross section averaged over perturber velocities and transverse active atom velocities.) A detailed discussion of this effect, as well as the collision induced line broadening, narrowing, shifting and line shape distortion that may occur in non-linear spectroscopy, is given below.

To illustrate the various aspects of collision effects in non-linear spectroscopy, I consider the three-level systems of fig. 8. The calculation is carried out for the inverted V of fig. 8a, with corresponding results for the V (fig. 8b) and upward cascade (fig. 8c) given at the end of this section. The field $\boldsymbol{E}$, pumping $\lambda(v)$ and excitation density $N(v)$ are the same as for the two-level system [eqs. (3.1), (3.2) and (3.3), respectively]. The field $\boldsymbol{E}$ drives only the 1–2 transition and a field

$$\boldsymbol{E}' = \hat{\boldsymbol{i}}E' \cos(\varepsilon k'Z - \Omega t) \tag{4.5}$$

either copropagating ($\varepsilon = +1$) or counterpropagating ($\varepsilon = -1$) with the field $\boldsymbol{E}$ drives only the

2–3 transition. The population of level 3 is monitored as a function of probe frequency Ω' for fixed Ω and serves to measure the probe field absorption in the presence of the "pump" field $\boldsymbol{E}$. The calculations will be carried out to lowest order in the fields $\boldsymbol{E}$ and $\boldsymbol{E}'$ since it is in the weak field limit that collision effects are most transparent.

4.1. *Line shape – no collisions*

In the absence of collisions, eq. (3.18) gives the equation of motion for density matrix elements with an atom-field interaction

$$V(\boldsymbol{r}, \boldsymbol{R}, t) = -\boldsymbol{\mu}\cdot(\boldsymbol{E} + \boldsymbol{E}'). \tag{4.6}$$

Steady state solutions of eq. (3.18) are obtained by introducing the field interaction representation,

$$\rho_{12}(\boldsymbol{R}, v, t) = \tilde{\rho}_{12}(v)\exp\left[-\mathrm{i}(kZ - \Omega t)\right], \tag{4.7a}$$

$$\rho_{23}(\boldsymbol{R}, v, t) = \tilde{\rho}_{23}(v)\exp\left[\mathrm{i}(\varepsilon k'Z - \Omega' t)\right], \tag{4.7b}$$

$$\rho_{13}(\boldsymbol{R}, v, t) = \tilde{\rho}_{13}(v)\exp\left\{-\mathrm{i}\left[(k - \varepsilon k')Z - (\Omega - \Omega')t\right]\right\}, \tag{4.7c}$$

$$\rho_{ii}(\boldsymbol{R}, v, t) = \tilde{\rho}_{ii}(v), \tag{4.7d}$$

making the rotating wave approximation, and recalling that $\boldsymbol{E}$ drives only the 1–2 transition and $\boldsymbol{E}'$ only the 2–3 transition. When eqs. (4.7) are substituted into eq. (3.18), one finds that the steady state density matrix elements $\tilde{\rho}_{ij}(v)$ satisfy

$$\gamma_1\tilde{\rho}_{11}(v) = \mathrm{i}\chi\left[\tilde{\rho}_{21}(v) - \tilde{\rho}_{12}(v)\right] + \lambda(v), \tag{4.8a}$$

$$\gamma_2\tilde{\rho}_{22}(v) = \mathrm{i}\chi\left[\tilde{\rho}_{12}(v) - \tilde{\rho}_{21}(v)\right] + \mathrm{i}\chi'\left[\tilde{\rho}_{32}(v) - \tilde{\rho}_{23}(v)\right], \tag{4.8b}$$

$$\gamma_3\tilde{\rho}_{33}(v) = \mathrm{i}\chi'\left[\tilde{\rho}_{23}(v) - \tilde{\rho}_{32}(v)\right], \tag{4.8c}$$

$$(\eta_{12} - \mathrm{i}kv_z)\tilde{\rho}_{12}(v) = \mathrm{i}\chi\left[\tilde{\rho}_{22}(v) - \tilde{\rho}_{11}(v)\right] - \mathrm{i}\chi'\tilde{\rho}_{13}(v), \tag{4.8d}$$

$$(\eta_{23} + \mathrm{i}\varepsilon k'v_z)\tilde{\rho}_{23}(v) = \mathrm{i}\chi'\left[\tilde{\rho}_{33}(v) - \tilde{\rho}_{22}(v)\right] + \mathrm{i}\chi\tilde{\rho}_{13}(v), \tag{4.8e}$$

$$\left[\eta_{13} - \mathrm{i}(k - \varepsilon k')v_z\right]\tilde{\rho}_{13}(v) = \mathrm{i}\chi\tilde{\rho}_{23}(v) - \mathrm{i}\chi'\tilde{\rho}_{12}(v), \tag{4.8f}$$

$$\tilde{\rho}_{ji}(v) = \left[\tilde{\rho}_{ij}(v)\right]^*, \tag{4.8g}$$

where

$$\chi = \mu_{12}E/2\hbar; \qquad \chi' = \mu_{23}E'/2\hbar, \tag{4.9}$$

$$\eta_{12} = \gamma_{12} + \mathrm{i}\Delta, \tag{4.10a}$$

$$\eta_{23} = \gamma_{23} - \mathrm{i}\Delta, \tag{4.10b}$$

$$\eta_{13} = \gamma_{13} + \mathrm{i}(\Delta - \Delta'), \tag{4.10c}$$

and the detunings Δ and Δ' are given by

$$\Delta = \Omega - \omega; \qquad \Delta' = \Omega' - \omega'. \tag{4.11}$$

Perturbations solutions of eqs. (4.8) are easily obtained. The six chains leading to a population

$\tilde{\rho}_{33}(v)$ of order $(\chi\chi')^2$ are

$$\tilde{\rho}_{11} \xrightarrow{\chi} \tilde{\rho}_{12} \xrightarrow{\chi} \tilde{\rho}_{22} \xrightarrow{\chi'} \tilde{\rho}_{23} \xrightarrow{\chi'} \tilde{\rho}_{33}, \tag{4.12a}$$

$$\tilde{\rho}_{11} \xrightarrow{\chi} \tilde{\rho}_{21} \xrightarrow{\chi} \tilde{\rho}_{22} \xrightarrow{\chi'} \tilde{\rho}_{23} \xrightarrow{\chi'} \tilde{\rho}_{33}, \tag{4.12b}$$

$$\tilde{\rho}_{11} \xrightarrow{\chi} \tilde{\rho}_{12} \xrightarrow{\chi} \tilde{\rho}_{22} \xrightarrow{\chi'} \tilde{\rho}_{32} \xrightarrow{\chi'} \rho_{33}, \tag{4.12c}$$

$$\tilde{\rho}_{11} \xrightarrow{\chi} \tilde{\rho}_{21} \xrightarrow{\chi} \tilde{\rho}_{22} \xrightarrow{\chi'} \tilde{\rho}_{32} \xrightarrow{\chi'} \tilde{\rho}_{33}, \tag{4.12d}$$

$$\tilde{\rho}_{11} \xrightarrow{\chi} \tilde{\rho}_{12} \xrightarrow{\chi'} \tilde{\rho}_{13} \xrightarrow{\chi} \tilde{\rho}_{23} \xrightarrow{\chi'} \tilde{\rho}_{33}, \tag{4.12e}$$

$$\tilde{\rho}_{11} \xrightarrow{\chi} \tilde{\rho}_{21} \xrightarrow{\chi'} \tilde{\rho}_{31} \xrightarrow{\chi} \tilde{\rho}_{32} \xrightarrow{\chi'} \tilde{\rho}_{33}, \tag{4.12f}$$

and the corresponding Feynman type diagrams are shown in fig. 9. Chains (4.12a–d) involve the intermediate state population $\tilde{\rho}_{22}(v)$ and may be grouped as

$$\begin{matrix} \nearrow \tilde{\rho}_{12} \searrow \\ \tilde{\rho}_{11} \qquad \tilde{\rho}_{22} \qquad \tilde{\rho}_{33} \\ \searrow \tilde{\rho}_{21} \nearrow \end{matrix} \quad \begin{matrix} \nearrow \tilde{\rho}_{23} \searrow \\ \qquad \tilde{\rho}_{22} \qquad \tilde{\rho}_{33} \\ \searrow \tilde{\rho}_{32} \nearrow \end{matrix} \qquad \underline{\text{SW}}. \tag{4.13}$$

I refer to the sum of these four terms as a stepwise (SW) contribution to the line shape. The term "stepwise" is used since (4.13) involves the sequential absorption of fields $\boldsymbol{E}$ and $\boldsymbol{E}'$. The remaining two terms (4.12e, f)

$$\begin{matrix} \nearrow \tilde{\rho}_{12} \rightarrow \tilde{\rho}_{13} \rightarrow \tilde{\rho}_{23} \searrow \\ \tilde{\rho}_{11} \qquad\qquad\qquad\qquad \tilde{\rho}_{33} \\ \searrow \tilde{\rho}_{21} \rightarrow \tilde{\rho}_{31} \rightarrow \tilde{\rho}_{32} \nearrow \end{matrix} \qquad \underline{\text{TQ}} \tag{4.14}$$

contain $\tilde{\rho}_{13}(v)$ [or $\tilde{\rho}_{31}(v)$] rather than $\tilde{\rho}_{22}(v)$. I refer to the sum of these two terms as a two-quanta (TQ) contribution to the line shape. While this label is somewhat arbitrary, it is meant to imply that TQ contributions are identically zero unless two quanta (one from each field) act on the system at the *same* time.

The break-up into TQ and SW chains will be particularly useful when collisions are included. For the no-collision steady-state calculation, it is artificial to distinguish the TQ and SW chains. The no-collision calculation can be carried out using probability *amplitudes* rather than density matrix elements. In the amplitude calculation, there is nothing to distinguish the TQ and SW

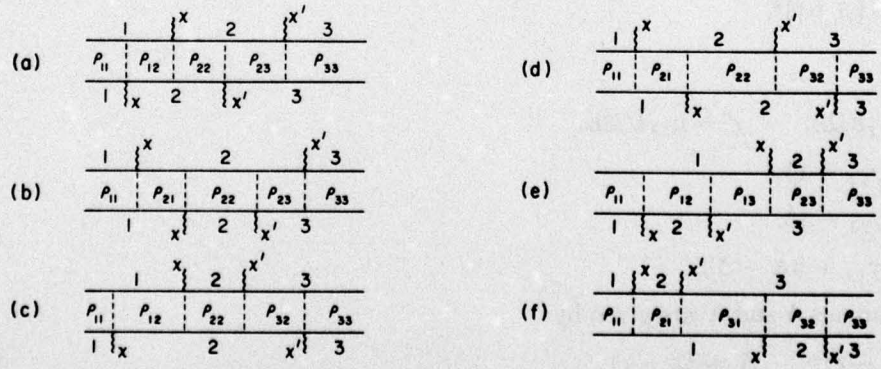

Fig. 9. Diagrams illustrating the absorption of fields $\boldsymbol{E}$ and $\boldsymbol{E}'$ taking an atom from level 1 to level 3. Each diagram is simply a different "time-ordering" of the same diagram.

chains. I shall return to this point in discussing the resonance conditions for the atom-field interactions. Note that each diagram of fig. 9 is simply a different "time-ordering" of the same diagram.

A straightforward solution of eqs. (4.8) according to the perturbation chains (4.13) and (4.14) yields a population density $\tilde{\rho}_{33}(v)$

$$\rho_{33}(v) = \tilde{\rho}_{33}^{SW}(v) + \tilde{\rho}_{33}^{TQ}(v), \tag{4.15a}$$

where

$$\tilde{\rho}_{33}^{SW}(v) = \frac{4(\chi\chi')^2 N W_0(v)}{\gamma_2\gamma_3} \frac{\gamma_{12}}{[(\gamma_{12})^2 + (\Delta - kv_z)^2]} \frac{\gamma_{23}}{[(\gamma_{23})^2 + (\Delta' - \varepsilon k v_z)^2]}, \tag{4.15b}$$

$$\tilde{\rho}_{33}^{TQ}(v) = \frac{(\chi\chi')^2 N W_0(v)}{\gamma_3} \frac{1}{[\gamma_{12} + i(\Delta - kv_z)]} \frac{1}{[\gamma_{23} - i(\Delta' - \varepsilon k' v_z)]}$$

$$\times \frac{1}{[\gamma_{13} + i\{(\Delta - \Delta') - (k - \varepsilon k')v_z\}]} + \text{conjugate} \tag{4.15c}$$

are the contributions from eqs. (4.13) and (4.14), respectively. The SW term (4.15b) is simply the product of absorption cross sections for the fields $\boldsymbol{E}$ and $\boldsymbol{E}'$. The resonance conditions are those for the individual absorptions,*

$$\Delta = kv_z \pm \gamma_2/2, \tag{4.16}$$

$$\Delta' = \varepsilon k' v_z \pm \gamma_{23}, \tag{4.17}$$

written for the case $\gamma_1 = 0$. For the TQ term (4.15c) there is a characteristic two photon resonance condition

$$\Delta' = \Delta - (k - \varepsilon k')v_z \pm \gamma_3/2, \tag{4.18a}$$

or

$$(\Omega - kv_z) - (\Omega' - \varepsilon k' v_z) = \omega - \omega' \pm \gamma_3/2. \tag{4.18b}$$

There are, in addition, resonances given by eqs. (4.16) and (4.17). At first glance, it seems that, for fixed Δ and v_z there should be *two* Δ' resonances, given by eqs. (4.17) and (4.18), respectively.

However, when state 1 has zero width ($\gamma_1 = 0$), eqs. (4.15b) and (4.15c) may be combined to give

$$\tilde{\rho}_{33}(v) = \frac{(\chi\chi')^2 N W_0(v)}{[(\gamma_2/2)^2 + (\Delta - kv_z)^2]\{(\gamma_3/2)^2 + [(\Delta - \Delta') - (k - \varepsilon k')v_z]^2\}}, \tag{4.19}$$

showing that there is only *one* Δ' resonance (4.18a). This result may be understood by considering the excitation as a single process rather than breaking it up into TQ and SW components. Starting from the ground state in fig. 10, the monochromatic field $\boldsymbol{E}$ adds an energy $\hbar\Omega[1 - (v_z/c)]$ in the atom's rest frame. The field $\boldsymbol{E}'$ must take the atom from this energy to the final state of the system (see fig. 10). For fixed Ω and v_z the process is resonant when $(\Omega - kv_z) - (\Omega' - \varepsilon k' v_z) = \omega - \omega'$, which is just condition (4.18). The width of level 2 is unimportant for the resonance condition on Ω' owing to the fact that the fixed frequency Ω brings the atom to a specific energy within level

* A resonance condition written in the form $\Delta = A \pm B$ is a shorthand notation for $|\Delta - A| \lesssim B$.

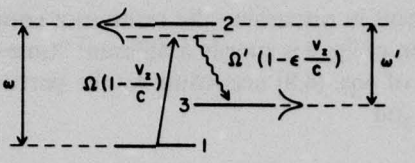

Fig. 10. Schematic representation of absorption of photons from fields E and E' taking an atom from a zero width ground state to a finite width final state. The curves alongside levels 2 and 3 symbolize the natural widths of those levels. For a fixed detuning $(\Omega - \omega)$ and longitudinal atomic velocity v_z, absorption is optimal when $(\Omega - kv_z) - (\Omega' - \varepsilon k'v_z) = \omega - \omega' \pm \gamma_3/2$.

2's width. There is no mechanism (i.e., collisions) to allow for a redistribution of the energy in level 2. The existence of a single resonance condition on Δ' is evidence that the break-up into TQ and SW chains is artificial in the no-collision case.

The line shape is obtained from (4.19) as

$$I(\Delta', \Delta) = \int dv \tilde{\rho}_{33}(v)$$

$$= \frac{(\chi\chi')^2 N}{\pi^{1/2} u} \int_{-\infty}^{\infty} dv_z \frac{\exp[-(v_z/u)^2]}{[(\gamma_2/2)^2 + (\Delta - kv_z)^2]} \frac{1}{\{(\gamma_3/2)^2 + [(\Delta - \Delta') - (k - \varepsilon k')v_z]^2\}}. \quad (4.20)$$

While it is possible to express eq. (4.20) in terms of plasma dispersion functions, the physics contained in eq. (4.20) becomes clearer if various limiting cases are considered. In all cases, the Doppler limit

$$\gamma_{ij} \ll ku \quad (4.21)$$

is assumed and the results are interpreted in terms of the resonance conditions (4.16) and (4.18).

1. $|\Delta| \gg ku$. For pump detunings larger than the Doppler width, eq. (4.16) is equally well satisfied for all v_z since the detuning Δ is large. Thus, the allowed range of contributing v_z is dictated by $W_0(v_z)$, a distribution centered at $v_z = 0$ with width $u(\ln 2)^{1/2}$. If this distribution of v_z is inserted into eq. (4.18a) one predicts a line shape centered at $\Delta' = \Delta$ with a width equal to the convolution of a Gaussian of width $(k - \varepsilon k')u(\ln 2)^{1/2}$ with a Lorentzian of width γ_{13} [the sum $\{(k - \varepsilon k')v_z \pm \gamma_{13}\}$ is represented in the line shape as a convolution]. The limiting form of eq. (4.20) for $|\Delta| \gg ku$ is

$$I(\Delta', \Delta) \sim \frac{(\chi\chi')^2 N}{\pi^{1/2} u \Delta^2} \int_{-\infty}^{\infty} dv_z \frac{\exp[-(v_z/u)^2]}{(\gamma_3/2)^2 + [(\Delta - \Delta') - (k - \varepsilon k')v_z]^2}$$

$$= \frac{2(\chi\chi')^2 N}{\gamma_3 |k - \varepsilon k'| u \Delta^2} Z_i\left(\frac{\Delta' - \Delta + \frac{1}{2}i\gamma_3}{|k - \varepsilon k'| u}\right), \quad (4.22)$$

which verifies the prediction.

2. $|\Delta| < ku$. For near resonant tuning in the Doppler limit (4.21), there is a velocity subset of atoms centered at $v_z = \Delta/k$ with width γ_{12}/k that is resonant with the field E and fulfills condition (4.16). Atoms with these velocities provide the major contribution to the line shape. Inserting this distribution of v_z in the resonance condition (4.18a), one predicts a line shape centered at $\Delta' = \varepsilon(k'/k)\Delta$ with a width $\{[|k - \varepsilon k'|/k]\gamma_2/2 + \gamma_3/2\}$. The limiting form of (4.20) for $|\Delta| < ku$,

$\gamma_{ij} \ll ku$ yields a Lorentzian line shape with precisely these features

$$I(\Delta', \Delta) = \frac{4\pi^{1/2}(\chi\chi')^2 N \exp[-(\Delta/ku)^2]}{\gamma_2\gamma_3 ku\bar{\Gamma}} \frac{\bar{\Gamma}^2}{\bar{\Gamma}^2 + \bar{\Delta}^2}, \tag{4.23a}$$

$$\bar{\Gamma} = \frac{|k - \varepsilon k'|}{k}\frac{\gamma_2}{2} + \frac{\gamma_3}{2}, \tag{4.23b}$$

$$\bar{\Delta} = \Delta' - \varepsilon(k'/k)\Delta. \tag{4.23c}$$

3. $|\Delta| \approx ku$. For $|\Delta| \approx 3ku$, the resonance condition (4.16) is satisfied in two ways. First, atoms having v_z within the central region of $W_0(v_z)$ contribute. These atoms are detuned by $|\Delta| > ku$ and give rise to a resonance as in the $|\Delta| \gg ku$ case. Second, there is a small number of atoms (weighting factor of $\exp[-(\Delta/ku)^2]$) having $v_z = \Delta/k$ that satisfy (4.16) and lead to a resonance as in the $|\Delta| < ku$ case. For $|\Delta| \approx (2\text{–}4)ku$ the two contributions are about equal and one sees two resonances [13], with the line shape given approximately by the sum of (4.22) and (4.23).

In fig. 11, the line shape for the three cases is illustrated for copropagating waves. The line widths for copropagating waves are smaller than the corresponding widths for counterpropagating waves, owing to the partial cancellation of Doppler phase shifts in the copropagating case.

4.2. Collisions – general considerations

A formal expression for the line shape incorporating collision effects can be written by inspection if one uses the techniques developed in section 3, along with the diagrams of fig. 9. In each diagram, one starts with $\tilde{\rho}_{11}(v_0) = \gamma_1 N W_0(v_0)$. The collision propagator $G_{11}(v_0 \to v_1)$ defined through eq. (3.32), propagates $\gamma_1 N W_0(v_0)$ to the first field interaction. The appropriate $G_{ij}(v_1 \to v_2)$ [G_{12} for diagrams 9a, c, e; G_{21} for diagrams 9b, d, f] propagates the solution between the first and second field interactions. The process continues through all the field interactions with $G_{33}(v' \to v)$ propagating the solution following the last field interaction. The $G_{ij}(v' \to v)$ are obtained as solutions of eq. (3.32) with the $\eta_{ij}(v_z)$ given by

$$\eta_{ii} = \gamma_i; \qquad \eta_{12}(v_z) = \eta_{21}(v_z)^* = \eta_{12} - ikv_z,$$
$$\eta_{23}(v_z) = \eta_{32}(v_z)^* = \eta_{23} + i\varepsilon k' v_z; \qquad \eta_{13}(v_z) = \eta_{31}(v_z)^* = \eta_{13} - i(k - \varepsilon k')v_z \tag{4.24}$$

and the η_{ij} defined by eq. (4.10).

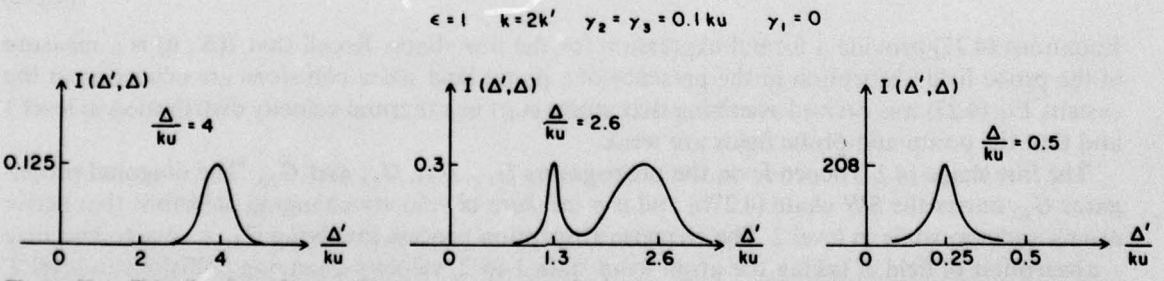

Fig. 11. No-collision line shapes for copropagating waves in a three-level system. For large detunings $\Delta \gtrsim 4ku$, the line shape is a Voigt profile centered near $\Delta' = \Delta$. For a detuning $\Delta \approx (2\text{–}3)ku$, the line shape consists of the sum of a Voigt profile centered near $\Delta' = \Delta$ *plus* a Lorentzian centered at $\Delta' = \varepsilon(k'/k)\Delta$. For $\Delta < ku$, the line shape is a Lorentzian centered at $\Delta' = \varepsilon(k'/k)\Delta$. The intensity is in arbitrary units, but the same scale is used for the three line shapes.

The line shape is obtained by associating a coupling constant ($\pm i\chi$, $\pm i\chi'$) with each field interaction and integrating the product of G_{ij}'s over initial, intermediate, and final velocities. Grouping the results according to eqs. (4.13) and (4.14), one finds

$$I(\Delta', \Delta) = \rho_{33}^{SW} + \rho_{33}^{TQ}, \tag{4.25a}$$

with

$$\rho_{33}^{SW} = (\chi\chi')^2 \int dv\, dv_4\, dv_3\, dv_2\, dv_1\, dv_0 G_{33}(v_4 \to v) \times [G_{23}(v_3 \to v_4) + G_{32}(v_3 \to v_4)] G_{22}(v_2 \to v_3) \times [G_{12}(v_1 \to v_2) + G_{21}(v_1 \to v_2)] G_{11}(v_0 \to v_1) [\gamma_1 N W_0(v_0)], \tag{4.25b}$$

$$\rho_{33}^{TQ} = (\chi\chi')^2 \int dv\, dv_4\, dv_3\, dv_2\, dv_1\, dv_0 G_{33}(v_4 \to v) \times [G_{23}(v_3 \to v_4) G_{13}(v_2 \to v_3) G_{12}(v_1 \to v_2) + G_{32}(v_3 \to v_4) G_{31}(v_2 \to v_3) G_{21}(v_1 \to v_2)] G_{11}(v_0 \to v_1) [\gamma_1 N W_0(v_0)]. \tag{4.25c}$$

There are six separate terms, one for each diagram of fig. 9.

By using eqs. (3.36) and (3.37) to perform the integrals over G_{11} and G_{33}, respectively, along with the fact that

$$G_{ij}(v' \to v) = G_{ji}(v' \to v)^*, \tag{4.26}$$

one reduces eq. (4.25) to the simplified form

$$I(\Delta', \Delta) = \rho_{33}^{SW} + \rho_{33}^{TQ} \tag{4.27a}$$

$$\rho_{33}^{SW} = \frac{(\chi\chi')^2 N}{\gamma_3} \int dv\, dv_2\, dv_1\, dv_0 [G_{23}(v_2 \to v) + G_{23}(v_2 \to v)^*] \times G_{22}(v_1 \to v_2) [G_{12}(v_0 \to v_1) + G_{12}(v_0 \to v_1)^*] W_0(v_0) \tag{4.27b}$$

$$\rho_{33}^{TQ} = \frac{(\chi\chi')^2 N}{\gamma_3} \int dv\, dv_2\, dv_1\, dv_0 G_{23}(v_2 \to v) G_{13}(v_1 \to v_2) G_{12}(v_0 \to v_1) W_0(v_0) + \text{conjugate}. \tag{4.27c}$$

Equations (4.27) provide a formal expression for the line shape. Recall that $I(\Delta', \Delta)$ is a measure of the probe field absorption in the presence of a pump field when collisions are occurring in the system. Eq. (4.27) was derived assuming that atoms start in a thermal velocity distribution in level 1 and that the pump and probe fields are weak.

The line shape (4.27) depends on the propagators G_{12}, G_{22}, G_{23} and G_{13}. The diagonal propagator G_{22} enters the SW chain (4.27b) and is a measure of velocity-changing collisions that active atoms undergo while in level 2. The stepwise absorption process involving G_{22} is easy to visualize – absorption of field $\boldsymbol{E}$ taking the atom from state 1 to 2, velocity-changing collisions in level 2, absorption of field $\boldsymbol{E}'$ taking the atom from level 2 to 3.

The off-diagonal propagators G_{12} and G_{23} appear in both the SW and TQ chains, while G_{13} appears only in the TQ chain. These propagators contain the effects of collisions on off-diagonal

density matrix elements. The line shape will take on different forms, depending upon whether collisions are phase-interrupting, velocity-changing, or both phase-interrupting and velocity-changing (in some inseparable combination) in their effect on the various off-diagonal density matrix elements. Rather than examine all the different combinations of either phase-interrupting or velocity-changing effects on each off-diagonal propagator, I consider only two specific collision models to illustrate the basic physical principles. In both models, collisions are assumed to be phase-interrupting in their effect on ρ_{12} and ρ_{23}, as would be the case if state 2 scattering is substantially different from state 1 and state 3 scattering. Consequently, $G_{12}(v' \to v)$ and $G_{23}(v' \to v)$ are given by equations similar to eq. (3.40). In *collision model 1*, $G_{12}(v' \to v)$ is also given by an equation similar to (3.40) – collisions are phase-interrupting in their effect on ρ_{13}. In *collision model 2*, collisions are velocity-changing in their effect on ρ_{13} (i.e., equal collision interaction for levels 1 and 3, as might be the case if they belonged to the same electronic configuration). In collision model 2, the propagator $G_{13}(v' \to v)$ is given as a solution of eq. (3.32) with a real kernel and rate.

One additional approximation is adopted in both models. As a good first approximation, the speed dependence of the Γ_{ij}'s is neglected. (Although neglected in this work, the speed dependence of the Γ_{ij}'s can play an interesting role in saturation spectroscopy. For near resonant pump fields $|\Delta| < ku$, atoms with a velocity component $v_z = \Delta/k$ are selected by the field. Since $|v_z| \propto \Delta$, the energy or temperature dependence of the Γ_{ij}'s and the corresponding cross sections may be determined by varying Δ. Thus, in a gas at a given temperature, one can measure cross sections as a function of temperature by choosing hot or cold atoms using a suitable pump detuning. The analysis is complicated by the fact that the transverse velocity components are *not* selected by the fields, so that the line shapes must be averaged over these components [14].)

4.3. *Line shape – collision model 1*

If collisions are phase-interrupting in their effect on off-diagonal density matrix elements, the off-diagonal propagators are given by

$$G_{ij}^{\mathrm{ph}}(v' \to v) = \frac{\delta(v - v')}{(\gamma_{ij} + \Gamma_{ij}^{\mathrm{ph}}) + \mathrm{i}(\Delta_{ij} + S_{ij}^{\mathrm{ph}})} \tag{4.28a}$$

$$\Delta_{12} = \Delta - kv_z; \qquad \Delta_{23} = -\Delta' + \varepsilon k' v_z; \qquad \Delta_{13} = \Delta_{12} + \Delta_{23} \tag{4.28b}$$

with $\Gamma_{ij}^{\mathrm{ph}}$ and S_{ij}^{ph} defined by eq. (3.41) (the speed dependence of these parameters is neglected). Inserting eq. (4.28) into (4.27), one obtains the line shape

$$I(\Delta', \Delta) = \rho_{33}^{\mathrm{SW}} + \rho_{33}^{\mathrm{TQ}} \tag{4.29a}$$

$$\rho_{33}^{\mathrm{SW}} = \frac{4(\chi\chi')^2 N}{\gamma_3} \int \mathrm{d}v\, \mathrm{d}v_0 \frac{\tilde{\Gamma}_{23}}{(\tilde{\Gamma}_{23})^2 + (\tilde{\Delta}' - \varepsilon k' v_z)^2} G_{22}(v_0 \to v) \frac{\tilde{\Gamma}_{12}}{(\tilde{\Gamma}_{12})^2 + (\tilde{\Delta} - kv_{z_0})^2} W_0(v_0), \tag{4.29b}$$

$$\rho_{33}^{\mathrm{TQ}} = \frac{(\chi\chi')^2 N}{\gamma_3} \int \mathrm{d}v \frac{1}{\tilde{\Gamma}_{23} - \mathrm{i}(\tilde{\Delta}' - \varepsilon k' v_z)} \frac{1}{\tilde{\Gamma}_{13} + \mathrm{i}[\tilde{\Delta} - \tilde{\Delta}' - (k - \varepsilon k')v_z]} \frac{1}{\tilde{\Gamma}_{12} + \mathrm{i}(\tilde{\Delta} - kv_z)} W_0(v) + \text{conjugate}, \tag{4.29c}$$

where

$$\tilde{\Gamma}_{ij} = \gamma_{ij} + \Gamma_{ij}^{ph}, \tag{4.30}$$

$$\tilde{\Delta} = \Delta + S_{12}^{ph}, \tag{4.31}$$

$$\tilde{\Delta}' = \Delta' - S_{23}^{ph}, \tag{4.32}$$

$$\overline{\Delta - \Delta'} = \Delta - \Delta' + S_{13}^{ph}. \tag{4.33}$$

Rather than analyze the line shape for the most general case, I shall consider (4.29) in the limits of large pumping detuning $|\Delta| \gg ku$ and near resonant tuning $|\Delta| < ku$.

In discussing the no-collision line shape for $\gamma_1 = 0$, I stressed that there was only one resonance condition for Δ' [(4.18)]. The conservation of energy argument regarding internal states used to arrive at that conclusion can no longer be maintained since internal energy can be transformed into translational energy during a collision. Thus, there are *two* resonance conditions for Δ'

$$\Delta' = \Delta - (k - \varepsilon k')v_z + S_{13}^{ph} \pm \tilde{\Gamma}_{13}, \tag{4.34}$$

$$\Delta' = \varepsilon k' v_z + S_{23}^{ph} \pm \tilde{\Gamma}_{23}, \tag{4.35}$$

along with the resonance condition on Δ

$$\Delta = kv_z - S_{12}^{ph} \pm \tilde{\Gamma}_{12}. \tag{4.36}$$

Eqs. (4.34) and (4.35) may be thought of as two-photon and single photon resonance conditions, respectively, although eq. (4.35) also enters the TQ chain.

1. $|\Delta| \gg ku$.

SW chain. The SW chain consists of the absorption of field $\boldsymbol{E}$, velocity-changing collisions in level 2, and the absorption of field $\boldsymbol{E}'$. For large detunings, the detunings $\Delta - kv_z \approx \Delta$ of different velocity subsets are approximately equal so that the entire Maxwellian velocity distribution of active atoms is equally excited into level 2 (albeit with small probability) by field $\boldsymbol{E}$. As previously noted, collisions do not alter an equilibrium velocity distribution; consequently, velocity-changing collisions in level 2 have no effect on the line shape. The absorption of $\boldsymbol{E}'$ takes place from a Maxwellian atomic velocity distribution. All these features are contained in the SW contribution (4.29b) which, for $|\Delta| \gg ku$ and $\tilde{\Gamma}_{12} \ll |\Delta|$ becomes

$$\rho_{33}^{SW} = \frac{4(\chi\chi')^2 N \tilde{\Gamma}_{12}}{\gamma_2\gamma_3\Delta^2} \int dv \frac{\tilde{\Gamma}_{23}}{(\tilde{\Gamma}_{23})^2 + (\tilde{\Delta}' - \varepsilon k' v_z)^2} W_0(v), \tag{4.37}$$

where eq. (3.36) has been used.

TQ chain. I can not offer a simple physical interpretation of the TQ chain. Since it is not positive definite, the TQ chain does not correspond to an excitation probability. Instead, it represents an interference term that contributes to the total level 3 population. The TQ contribution (4.29c) is a product containing all three resonance conditions (4.34)–(4.36). For large detunings, condition (4.36) can not be satisfied, condition (4.34) can be satisfied near $\Delta' = \Delta$ and condition (4.35) can be satisfied near $\Delta' = 0$. Thus (4.29c) exhibits two resonances in Δ', the one near $\Delta' = 0$ combining with the SW contribution. For large detunings, eq. (4.29c) reduces to

$$\rho_{33}^{TQ} = \frac{(\chi\chi')^2 N}{\gamma_3(i\Delta)} \int dv \frac{1}{\tilde{\Gamma}_{23} - i(\Delta' - \varepsilon k' v_z)} \frac{1}{\tilde{\Gamma}_{13} + i[\overline{\Delta - \Delta'} - (k - \varepsilon k')v_z]} W_0(v) + \text{conjugate}. \tag{4.38}$$

Line shape. Combining eqs. (4.37) and (4.38), one obtains the line shape

$$I(\Delta', \Delta) = \frac{(\chi\chi')^2 N}{\gamma_3} \int d\nu \left[\frac{4\tilde{\Gamma}_{12}\tilde{\Gamma}_{23}(\gamma_2)^{-1}}{(\tilde{\Gamma}_{23})^2 + (\tilde{\Delta}' - \varepsilon k' v_z)^2} + \left\{ \frac{(i\Delta)^{-1}}{\tilde{\Gamma}_{23} - i(\Delta' - \varepsilon k' v_z)} \frac{1}{\tilde{\Gamma}_{13} + i[\Delta - \Delta' - (k - \varepsilon k')v_z]} + \text{conjugate} \right\} \right] W_0(\nu), \tag{4.39}$$

which exhibits two resonances. At $\Delta' \approx \Delta$, only the TQ chain is important and (4.39) reduces to

$$I(\Delta', \Delta) \sim \frac{2(\chi\chi')^2 N}{\gamma_3 |k - \varepsilon k'| u \Delta^2} Z_i\left(\frac{\Delta' - \Delta - S_{13}^{ph} + i\tilde{\Gamma}_{13}}{|k - \varepsilon k'| u} \right) \quad \text{for} \quad \Delta' \approx \Delta, \tag{4.40}$$

while in the vicinity of $\Delta' = 0$ both the TQ and SW chains combine to give

$$I(\Delta', \Delta) \sim \frac{2(\chi\chi')^2 N}{\gamma_3 k' u \Delta^2} \left[\frac{2(\frac{1}{2}\gamma_2 + \Gamma_{12}^{ph})}{\gamma_2} - 1 \right] Z_i\left(\frac{\Delta' - S_{23}^{ph} + i\tilde{\Gamma}_{23}}{k' u} \right) \quad \text{for} \quad \Delta' \approx 0. \tag{4.41}$$

Near the two-photon resonance, $\Delta' \approx \Delta$, the line profile (4.40) is broadened and shifted from the corresponding resonance (4.22) of the no-collision case. Line shape studies in the region of $\Delta' \approx \Delta$ allow one to determine Γ_{13}^{ph} and S_{13}^{ph}.

As predicted, there is a *new* resonance at $\Delta' \approx 0$. In the no-collision limit, $\Gamma_{12}^{ph} = 0$, and the TQ and SW contributions cancel one another. With increasing perturber pressure (or, equivalently, increasing Γ_{12}^{ph}), the SW component grows relative to the TQ one leading to absorption near $\Delta' = 0$. For a fixed detuning Δ, the increase in the SW contribution reflects an additional absorption of the field E, owing to the collisional increase in the damping associated with that absorption. The amplitude of the resonance provides a measure of Γ_{12}^{ph} while the width and shift can be used to obtain values for Γ_{23}^{ph} and S_{23}^{ph}, respectively. A typical profile is shown in fig. 12.

It is interesting to note that the *integrated* profile $\int I(\Delta', \Delta)\, d\Delta'$ increases with pressure, owing to the presence of the new resonance at $\Delta' \approx 0$. Thus, if the probe frequency is swept through both resonance regions, the *total* number of atoms excited to level 3 will increase with pressure. More-

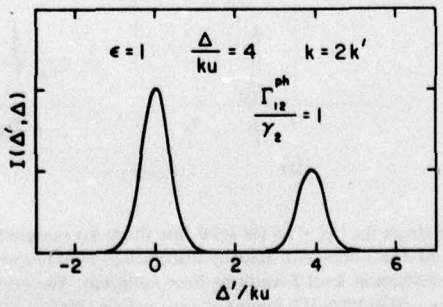

Fig. 12. Line shape (4.40, 4.41) for $\Delta = 4ku$ and copropagating waves when collisions are phase-interrupting in their effect on ρ_{13}. The profiles are drawn assuming $\gamma_1 = 0$, $|\gamma_{13}^{ph}| \ll (k - k')u$ and $|\gamma_{23}^{ph}| \ll k'u$. The line shape consists of Voigt profiles centered near $\Delta' = \Delta$ and $\Delta' = 0$. Compare this profile with the $\Delta = 4ku$ no-collision profile in fig. 11. Collisions give rise to a *new* resonance centered near $\Delta' = 0$.

over, excitation occurs in a new region ($\Delta' \approx 0$) of the probe frequency spectrum. Collisions give rise to an increased range of probe frequencies for which level 3 excitation is possible.

2. $|\Delta| < ku$.

In all cases, it is assumed that

$$S_{ij}^{ph}, \tilde{\Gamma}_{ij} \ll ku. \tag{4.42}$$

SW chain. For $|\Delta| < ku$, there is always a velocity subset of atoms resonant with field E and this field excites atoms having

$$v_z = (\Delta + S_{12}^{ph})/k \pm (\tilde{\Gamma}_{12}/k). \tag{4.43}$$

The population $\tilde{\rho}_{22}(v_z)$ excited by E is shown schematically in fig. 13a.

Velocity-changing collisions result in a relaxation of this distribution back towards an equilibrium one. Regardless of the detailed nature of the collision kernel $W_{22}(v' \to v)$ giving rise to this relaxation, the degree of relaxation is determined by the number of collisions

$$\langle n \rangle = \Gamma_{22}/\gamma_2, \tag{4.44}$$

occurring within the lifetime of level 2 and the root mean square change in velocity per collision (Δu). The distribution $\tilde{\rho}_{22}(v_z)$ following $\langle n \rangle$ collisions is shown schematically in fig. 13b as a

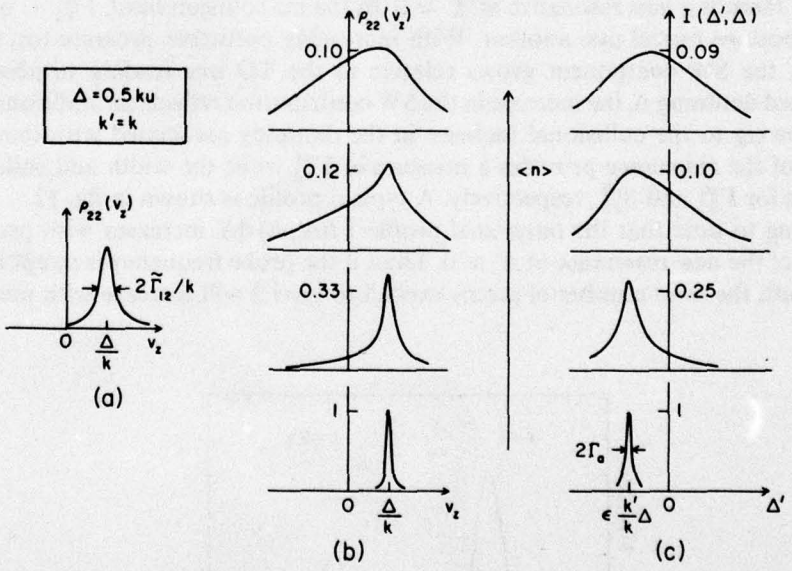

Fig. 13. Stepwise contribution to the line shape for $|\Delta| < ku$ (or total line shape for counterpropagating waves) when collisions are phase-interrupting in their effect on ρ_{13}. (a) The Lorentzian velocity distribution of atoms excited by field E is centered at $v_z = \Delta/k$ with width $\tilde{\Gamma}_{12}/k$. (b) Redistribution of velocities in level 2 resulting from collisions. These profiles were calculated using a collision kernel $W(v' \to v) = (0.6u\sqrt{\pi})^{-3} \exp\{-[(v - 0.8v')/0.6u]^2\}$ having a $(\Delta u) = 0.6u$. With increasing $\langle n \rangle = \Gamma_{22}/\gamma_2$ (or, equivalently, with increasing pressure), the velocity distribution tends towards thermal equilibrium. (c) Probe absorption line shapes as a function of $\langle n \rangle$. The line shapes represent the absorption of field E' from the level 2 population distributions shown in (b). The profile is a Lorentzian centered at $\Delta' = \varepsilon(k'/k)\Delta$ (ε is taken equal to -1 in the figure) at low pressures and tends towards a Voigt profile centered at $\Delta' = 0$ at high pressures. Vertical scales are in arbitray units, but the same scale is used for each diagram in (b) and in (c).

function of $\langle n \rangle$ assuming $k(\Delta u) > \tilde{\Gamma}_{12}$. (As long as $k(\Delta u) > \tilde{\Gamma}_{12}$, each collision is strong enough to be distinguished since it can remove an atom from the velocity distribution excited by field E. In this limit, it is the *true* rather than the effective collision rate that is pertinent to the discussion.) For low pressures ($\langle n \rangle \lesssim 1$), the distribution is a narrow Lorentzian, but with increasing pressure ($\langle n \rangle \gg 1$) the distribution tends towards a Maxwellian. (In many cases, at pressures required to thermalize level 2, the Doppler limit condition (4.42) no longer holds and the distributions will be somewhat more complicated than those shown in fig. 13b.)

The probe field absorption resonance condition is given by (4.35) with v_z obtained from the velocity distributions of fig. 13b. The corresponding line shapes are depicted in fig. 13c. For low pressures, v_z is determined by eq. (4.43), which, when substituted in eq. (4.35), shows that Δ' is resonant for

$$\Delta' = \varepsilon(k'/k)(\Delta + S_{12}^{\mathrm{ph}}) + S_{23}^{\mathrm{ph}} \pm (\tilde{\Gamma}_{23} + (k'/k)\tilde{\Gamma}_{12}). \tag{4.45}$$

For higher pressures, the probe absorption profile is the convolution of $\tilde{\rho}_{22}(v)$ with a Doppler shifted Lorentzian of width $\tilde{\Gamma}_{23}$; it becomes broader and its center shifts back towards $\tilde{\Delta}' = 0$, ultimately reaching the limit of a Voigt profile. There is no difficulty in understanding the SW contribution on the basis of simple physical arguments.

The form of the SW contribution depends on the specific nature of the kernel $W_{22}(v' \to v)$. For an arbitrary kernel, however, eq. (3.32) may be formally solved to give the propagator

$$G_{22}(v' \to v) = \delta(v - v')/(\gamma_2 + \Gamma_{22}) + \tilde{G}_{22}(v' \to v), \tag{4.46}$$

where

$$\tilde{G}_{22}(v' \to v) = \frac{1}{\gamma_2 + \Gamma_{22}} \int \mathrm{d}v'' W_{22}(v'' \to v) G_{22}(v' \to v''). \tag{4.47}$$

The first term in eq. (4.46) gives the contribution from atoms which have not undergone velocity-changing collisions in level 2 before being excited to level 3. The second term contains all the effects of velocity-changing collisions. By substituting eq. (4.46) into eq. (4.29b) and using eq. (4.42) one obtains the SW contribution

$$\begin{aligned} \rho_{33}^{\mathrm{SW}} = {} & \frac{4\pi^{1/2}(\chi\chi')^2 N \exp\left[-(\tilde{\Delta}/ku)^2\right]}{(\gamma_2 + \Gamma_{22})\gamma_3 ku \Gamma_a} \\ & \times \left\{ \frac{(\Gamma_a)^2}{(\Gamma_a)^2 + (\Delta_a)^2} + \frac{k(\gamma_2 + \Gamma_{22})\Gamma_a}{\pi^2 u^2} \int \mathrm{d}v\, \mathrm{d}v_0 \frac{\tilde{\Gamma}_{23}}{(\tilde{\Gamma}_{23})^2 + (\tilde{\Delta}' - \varepsilon k' v_z)^2} \right. \\ & \left. \times \tilde{G}_{22}(v_0 \to v) \frac{\tilde{\Gamma}_{12}}{(\tilde{\Gamma}_{12})^2 + (\tilde{\Delta} - k v_{z_0})^2} \exp\left[-\left(\frac{v_{x_0}^2 + v_{y_0}^2}{u^2} \right) \right] \right\}, \end{aligned} \tag{4.48}$$

where

$$\Gamma_a = \tilde{\Gamma}_{23} + (k'/k)\tilde{\Gamma}_{12}; \qquad \Delta_a = \tilde{\Delta}' - \varepsilon(k'/k)\tilde{\Delta}, \tag{4.49}$$

which contains a Lorentzian contribution from atoms that have not undergone velocity-changing collisions in level 2 plus a term reflecting the velocity relaxation in level 2. One may calculate $\tilde{G}_{22}(v' \to v)$ for specific collision kernels, but such calculations are not presented in this work. The general nature of the solution is shown in fig. 13c.

TQ chain. In the Doppler limit (4.42), $W_0(v)$ appearing in eq. (4.29c) is evaluated at $v_z = \tilde{\Delta}/k$ and the resulting TQ contribution to the line shape is

$$\rho_{33}^{TQ} = \frac{(\chi\chi')^2 N \exp[-(\tilde{\Delta}/ku)^2]}{\pi^{1/2} u\gamma_3} \int_{-\infty}^{\infty} dv_z \frac{1}{\tilde{\Gamma}_{23} - i(\tilde{\Delta}' - \varepsilon k' v_z)}$$

$$\times \frac{1}{\tilde{\Gamma}_{13} + i[\Delta - \Delta' - (k - \varepsilon k')v_z]} \frac{1}{\tilde{\Gamma}_{12} + i(\tilde{\Delta} - kv_z)} + \text{conjugate}. \tag{4.50}$$

For counterpropagating waves ($\varepsilon = -1$) all the poles are in the same half plane and the integral vanishes. For copropagating waves ($\varepsilon = +1$) and $k' > k$ the pole at

$$v_z = (\tilde{\Delta} - i\tilde{\Gamma}_{12})/k \tag{4.51}$$

contributes in the contour integration and corresponds to satisfying condition (4.36). When this value of v_z is substituted in the remaining conditions (4.34), (4.35), one finds Δ' resonances at

$$\Delta' = \frac{k'}{k}\Delta + \frac{k' - k}{k} S_{12}^{ph} + S_{13}^{ph} \pm \left[\tilde{\Gamma}_{13} + \frac{k' - k}{k}\tilde{\Gamma}_{12}\right] \tag{4.52}$$

$$\Delta' = \frac{k'}{k}\Delta + \frac{k'}{k} S_{12}^{ph} + S_{23}^{ph} \pm \left[\tilde{\Gamma}_{23} + \frac{k'}{k}\tilde{\Gamma}_{12}\right]. \tag{4.53}$$

Similarly, for $k > k'$, the pole at

$$v_z = (\tilde{\Delta}' + i\tilde{\Gamma}_{23})/k', \tag{4.54}$$

corresponding to condition (4.35), contributes in the integration and leads to resonance conditions

$$\Delta' = \frac{k'}{k}\Delta + \frac{k - k'}{k} S_{23}^{ph} + \frac{k'}{k} S_{13}^{ph} \pm \left[\frac{k'}{k}\tilde{\Gamma}_{13} + \frac{k - k'}{k}\tilde{\Gamma}_{23}\right], \tag{4.55}$$

$$\Delta' = \frac{k'}{k}\Delta + \frac{k'}{k} S_{12}^{ph} + S_{23}^{ph} \pm \left(\tilde{\Gamma}_{23} + \frac{k'}{k}\tilde{\Gamma}_{12}\right), \tag{4.56}$$

following from (4.34), (4.36). For each case ($k > k'$ or $k < k'$) there are two resonances with somewhat different central positions and widths.

On integrating (4.50) over v_z, one obtains the TQ contribution

$$\rho_{33}^{TQ} = \frac{4\pi^{1/2}(\chi\chi')^2 N \exp[-(\tilde{\Delta}/ku)^2]}{\gamma_3 ku} \frac{(\Gamma_a\Gamma_b - \Delta_a\Delta_b)}{[(\Gamma_a)^2 + (\Delta_a)^2][(\Gamma_b)^2 + (\Delta_b)^2]} \Theta(\varepsilon), \tag{4.57}$$

where

$$\Gamma_a = \tilde{\Gamma}_{23} + \frac{k'}{k}\tilde{\Gamma}_{12}; \qquad \Delta_a = \Delta' - \frac{k'}{k}(\Delta + S_{12}^{ph}) - S_{23}^{ph}, \tag{4.58a}$$

$$\Gamma_b = \frac{k}{k'}\left[\frac{k'}{k}\tilde{\Gamma}_{13} + \frac{k - k'}{k}\tilde{\Gamma}_{23}\right]\Theta(k - k') + \left[\tilde{\Gamma}_{13} + \frac{k' - k}{k}\tilde{\Gamma}_{12}\right]\Theta(k' - k), \tag{4.58b}$$

$$\Delta_b = \frac{k}{k'}\left[\Delta' - \frac{k'}{k}\Delta - \frac{k'}{k}S_{13}^{ph} - \frac{k-k'}{k}S_{23}^{ph}\right]\Theta(k-k') + \left[\Delta' - \frac{k'}{k}\Delta - S_{13}^{ph} - \frac{k'-k}{k}S_{12}^{ph}\right]\Theta(k'-k), \tag{4.58c}$$

$$\Theta(x) = \begin{cases} 1, & x > 0 \\ 0, & x < 0 \end{cases}. \tag{4.59}$$

This line shape possesses the resonance positions and widths predicted in eqs. (4.52–4.56).

To get some insight into this equation, one can multiply by $(\gamma_2 + \Gamma_{22})/(\gamma_2 + \Gamma_{22})$ and perform algebraic manipulations to obtain

$$\rho_{33}^{TQ} = \frac{4\pi^{1/2}(\chi\chi')^2 N \exp\left[-(\tilde{\Delta}/ku)^2\right]}{(\gamma_2 + \Gamma_{22})\gamma_3 ku\Gamma_a} \times \left\{-\frac{(\Gamma_a)^2}{(\Gamma_a)^2 + (\Delta_a)^2} + \frac{\Gamma_a\Gamma_b}{(\Gamma_b)^2 + (\Delta_b)^2} + \frac{\Gamma_a[(\delta\Gamma)(\Gamma_a\Gamma_b - \Delta_a\Delta_b) + (\delta S)(\Gamma_a\Delta_b + \Gamma_b\Delta_a)]}{[(\Gamma_a)^2 + (\Delta_a)^2][(\Gamma_b)^2 + (\Delta_b)^2]}\right\}, \tag{4.60}$$

where

$$(\delta\Gamma) = -(\Gamma_{12}^{ph} + \Gamma_{23}^{ph} - \Gamma_{13}^{ph} - \Gamma_{22})\left[\frac{k'}{k}\Theta(k-k') + \Theta(k'-k)\right], \tag{4.61a}$$

$$(\delta S) = -(S_{12}^{ph} + S_{23}^{ph} - S_{13}^{ph})\left[\frac{k'}{k}\Theta(k-k') + \Theta(k'-k)\right]. \tag{4.61b}$$

In this form, there are three contributions to the TQ contribution. The first term just cancels that part of the SW arising from atoms which have not undergone velocity-changing collisions in level 2 [first term of eq. (4.48)]. The second term is a Lorentzian with a narrower width than the first term, owing to a partial cancellation of the Doppler phases in the resonance condition (4.34) leading to this term. The third term results solely from collisions since $(\delta\Gamma)$ and (δS) vanish in the no-collision limit. By using eqs. (4.61, 3.41, 2.34) and the optical theorem, one can estimate that the magnitude of this term is relatively small and that it vanishes exactly when level 2 experiences the strongest collision interaction of the three levels. If the term is nonvanishingly small, it adds an asymmetry to the TQ contribution.

Line shape. The line shape obtained by combining eqs. (4.48) and (4.60) is

$$I(\Delta', \Delta) = \frac{4\pi^{1/2}(\chi\chi')^2 N \exp\left[-(\tilde{\Delta}/ku)^2\right]}{(\gamma_2 + \Gamma_{22})\gamma_3 ku\Gamma_a}\left\{\frac{(\Gamma_a)^2}{(\Gamma_a)^2 + (\Delta_a)^2}\Theta(-\varepsilon) + \frac{\Gamma_a\Gamma_b}{(\Gamma_b)^2 + (\Delta_b)^2}\Theta(\varepsilon) + \frac{k(\gamma_2 + \Gamma_{22})\Gamma_a}{\pi^2 u^2}\int d\mathbf{v}\, d\mathbf{v}_0 \frac{\bar{\Gamma}_{23}}{(\bar{\Gamma}_{23})^2 + (\tilde{\Delta}' - \varepsilon k' v_z)^2}\hat{G}_{22}(\mathbf{v}_0 \to \mathbf{v}) \times \frac{\bar{\Gamma}_{12}}{(\bar{\Gamma}_{12})^2 + (\Delta - kv_{z_0})^2}\exp\left[-\left(\frac{v_{x_0}^2 + v_{y_0}^2}{u^2}\right)\right] + \frac{\Gamma_a[(\delta\Gamma)(\Gamma_a\Gamma_b - \Delta_a\Delta_b) + (\delta S)(\Gamma_a\Delta_b + \Delta_a\Gamma_b)]}{[(\Gamma_a)^2 + (\Delta_a)^2][(\Gamma_b)^2 + (\Delta_b)^2]}\Theta(\varepsilon)\right\}. \tag{4.62}$$

For counterpropagating waves ($\varepsilon = -1$), the TQ chain does not contribute and the line shape is represented schematically in fig. 13c for various pressures. There is a Lorentzian contribution from atoms which have not undergone velocity-changing collisions in level 2 plus a "shoulder" arising from atoms which have been partially thermalized by velocity-changing collisions. Studies of the line shape as a function of pressure can provide values for S_{12}^{ph} and the characteristic kernel parameters (Δu) and $\langle n \rangle$, assuming that Γ_{23}^{ph}, Γ_{12}^{ph}, Γ_{13}^{ph}, S_{13}^{ph} and S_{23}^{ph} have been measured from large detuning experiments. There has been recent experimental verification of these line profiles [15].

Assuming that the third term in (4.62) is small, the line shape for copropagating waves ($\varepsilon = 1$) has the same general features as that for counterpropagating waves except that the copropagating Lorentzian is narrower than the counterpropagating one, owing to a partial cancellation of Doppler phases. The interpretation of the line shape is the same as that for the counterpropagating case and fig. 13c, with the Lorentzian components having somewhat narrower widths, again serves to illustrate the line shape as a function of pressure. If the third term in eq. (4.62) is non-negligible, there will be additional asymmetry added to the line shape.

(As an aside, I can mention that the line shape takes on a qualitatively different form than that shown in fig. 13c if velocity-changing collisions are "weak". Velocity-changing collisions are "weak" if the rms velocity change per collision (Δu) and the collision rate Γ_{22} are not sufficient to remove atoms from the velocity-profile (of width $\tilde{\Gamma}_{12}/k$) excited by field $\boldsymbol{E}$. In this limit, which can occur over a certain pressure range, the SW contribution remains Lorentzian with a width equal to Γ_a (4.49) (as if velocity-changing collisions were absent) plus a small pressure independent component owing to velocity-changing collisions. For counterpropagating waves, the line shape, as given by the SW chain, is Lorentzian; the line width extrapolated to zero pressure will yield an anomalously large value for the atomic state lifetimes, owing to the presence of the pressure independent velocity-changing collision contribution to the width. For copropagating waves, the line shape consists of a narrow Lorentzian given by the second term in the TQ contribution (4.60) *plus* line wings representing the effects of velocity-changing collisions in the SW chain.

For the counterpropagating case (or, equivalently, the SW chain), it is also possible to measure a line width that is a non-linear function of perturber density. To see how this effect arises, imagine that at low pressures, $(\Delta u) > \tilde{\Gamma}_{12}/k \approx \gamma_{12}/k$. Velocity-changing collisions remove atoms from the homogeneous width, but the total line shape remains nearly Lorentzian if $(\Delta u)/u \ll 1$. The width of this low pressure pseudolorentzian is the sum of *two* pressure dependent components – one from phase-interrupting collisions and one from velocity-changing collisions. However, as the pressure is increased, $\tilde{\Gamma}_{12}$ grows and collisions may become "weak" $[k(\Delta u) < \tilde{\Gamma}_{12}]$. In that pressure region, the only pressure dependent contribution to the line width comes from phase-interrupting collisions. Consequently the slope of a line width versus perturber density graph will be greater in the low pressure region than at higher pressures; i.e., the line width is a nonlinear function of perturber density [16, 2]. Such nonlinearities have been observed experimentally [17].)

4.4. *Line shape – collision model 2*

In collision model 2, the propagators $G_{12}(v' \to v)$ and $G_{23}(v' \to v)$ are still given by eq. (4.28) and the SW contribution is unchanged from (4.29b). For equal collision interactions in states 1 and 3, collisions are velocity-changing in their effect on $\tilde{\rho}_{13}(v)$ and the propagator G_{13}^{vc} is obtained as a solution of [see eq. (3.32)]

$$\{\gamma_{13}+\Gamma_{13}^{vc}+i[\Delta-\Delta'-(k-\varepsilon k')v_z]\}G_{13}^{vc}(v'\to v)-\int dv''W_{13}^{vc}(v''\to v)G_{13}^{vc}(v'\to v'')=\delta(v-v') \tag{4.63}$$

with a real collision kernel $W_{13}^{vc}(v'\to v)$ and rate Γ_{13}^{vc}. The line shape follows from (4.27) as

$$I(\Delta',\Delta)=\rho_{33}^{SW}+\rho_{33}^{TQ}, \tag{4.64a}$$

$$\rho_{33}^{SW}=\frac{4(\chi\chi')^2N}{\gamma_3}\int dv\,dv_0\frac{\tilde{\Gamma}_{23}}{(\tilde{\Gamma}_{23})^2+(\tilde{\Delta}'-\varepsilon k'v_z)^2}G_{22}(v_0\to v_z)\frac{\tilde{\Gamma}_{12}}{(\tilde{\Gamma}_{12})^2+(\tilde{\Delta}-kv_{z_0})^2}W_0(v_0), \tag{4.64b}$$

$$\rho_{33}^{TQ}=\frac{(\chi\chi')^2N}{\gamma_3}\int dv\,dv_0\frac{1}{\tilde{\Gamma}_{23}-i(\tilde{\Delta}'-\varepsilon k'v_z)}$$
$$\times G_{13}^{vc}(v_0\to v)\frac{1}{\tilde{\Gamma}_{12}+i(\tilde{\Delta}-kv_{z_0})}W_0(v_0)+\text{conjugate}. \tag{4.64c}$$

Again the discussion is limited to the large detuning and near resonant tuning limits. Only the TQ contribution and total line shape need be discussed since the SW contribution is the same as in collision model 1.

1. $|\Delta|\gg ku$. As for collision model 1, there are resonances near $\Delta'=0$ and $\Delta'=\Delta$. For $|\Delta|\gg ku$ and $\tilde{\Gamma}_{ij}\ll|\Delta|$ the propagator $G_{13}(v'\to v)$ in the vicinity of the $\Delta'=0$ resonance is independent of collision model, owing to the large value of $|\Delta|$; for either phase-interrupting (4.28) or velocity-changing (4.63) collisions, one obtains $G_{13}(v'\to v)\approx\delta(v-v')/i\Delta$. Thus, the line shape near $\Delta'=0$ is the same as in collision model 1 and is given again by eq. (4.41).

Near $\Delta'=\Delta$, the TQ contribution dominates and, for $|\Delta|\gg ku$ and $\tilde{\Gamma}_{ij}\ll|\Delta|$, (4.64) reduces to

$$I(\Delta',\Delta)\sim\frac{(\chi\chi')^2N}{\gamma_3\Delta^2}\int dv\,dv_0G_{13}^{vc}(v_0\to v)W_0(v_0)+\text{conjugate},\qquad \Delta'\approx\Delta, \tag{4.65}$$

which is similar in form to (3.38) with G_{13}^{vc} replacing G_{12}^{vc}. A discussion of the line shape parallels that of section 3.4. Collisions which are velocity-changing in their effect on ρ_{13} give rise to a narrowing of the two-photon resonance. The narrowing becomes significant when $(\Gamma_{13}^{vc})'>|k-\varepsilon k'|u$, where $(\Gamma_{13}^{vc})'$ is the effective collision rate discussed in section 3.4. For copropagating waves ($\varepsilon=1$), the onset of narrowing occurs at lower pressures than in linear spectroscopy while for counterpropagating waves ($\varepsilon=-1$), higher pressures are required to see the narrowing.

At low pressures, the line shape (4.65) is the convolution of a Gaussian of width $|k-\varepsilon k'|u(\ln 2)^{1/2}$ with a Lorentzian of width γ_{13}. The line width decreases monotonically with increasing pressure. For pressures where $(\Gamma_{13}^{vc})'>|k-\varepsilon k'|^2u^2/\gamma_{13}$, the line becomes a Lorentzian with width γ_{13}. (Note that the assumption $\tilde{\Gamma}_{ij}\ll|\Delta|$ probably fails at pressures where significant narrowing occurs; the line shape is modified slightly by this effect.) At all pressures, the line is centered at $\Delta'=\Delta$.

The large detuning limit in the region of $\Delta'\approx\Delta$ serves to test whether collisions are phase-interrupting or velocity-changing in their effect on ρ_{13}. If the two photon resonance *narrows* with increasing pressure, collisions are velocity-changing in nature and one may determine the effective collision rate $(\Gamma_{13}^{vc})'$. If the line broadens and shifts with increasing pressure (after any inelastic collision effects have been properly subtracted out), collisions are phase-interrupting in nature and one may determine Γ_{13}^{ph} and S_{13}^{ph}.

2. $|\Delta| < ku$. For near resonant tuning, the line shape *does* depend on the specific form of the collision kernel $W_{13}^{vc}(v' \to v)$. However, it is still possible to obtain a semiquantitative picture of the line profile without going into specific details of the kernel. The discussion is limited to "low" and "high" pressure regions.

a. *Low pressure* ($(\Gamma_{13}^{vc})' \ll |k - \varepsilon k'|u; \tilde{\Gamma}_{ij} \ll ku$). As in eqs. (4.46, 4.47) it is useful to write the propagator G_{13}^{vc} as

$$G_{13}^{vc}(v' \to v) = \frac{\delta(v - v')}{(\gamma_{13} + \Gamma_{13}^{vc}) + i[\Delta - \Delta' - (k - \varepsilon k')v_z]} + \tilde{G}_{13}^{vc}(v' \to v) \tag{4.66}$$

where

$$\tilde{G}_{13}^{vc}(v' \to v) = \frac{1}{\eta_{13}(v_z)} \int dv'' W_{13}^{vc}(v'' \to v) G_{13}^{vc}(v' \to v''). \tag{4.67}$$

The lead term in eq. (4.66) has the same form as the phase-interrupting collision propagator (4.28) with the substitutions $\Gamma_{13}^{ph} \leftrightarrow \Gamma_{13}^{vc}$, $S_{13}^{ph} \leftrightarrow 0$. Thus, taking into account only the contribution from the first term of eq. (4.66), one obtains the same line shape as in collision model 1 [eq. (4.62)] with Γ_{13}^{ph} replaced by Γ_{13}^{vc} and S_{13}^{ph} replaced by zero. There is however, an additional contribution to the line profile arising from the second term of (4.66). The total line shape is given by

$$\begin{aligned} I(\Delta', \Delta) = {} & \frac{4\pi^{1/2}(\chi\chi')^2 N \exp[-(\tilde{\Delta}/ku)^2]}{(\gamma_2 + \Gamma_{22})\gamma_3 ku\Gamma_a} \left\{ \frac{(\Gamma_a)^2}{(\Gamma_a)^2 + (\Delta_a)^2} \Theta(-\varepsilon) + \frac{\Gamma_a \Gamma_b'}{(\Gamma_b')^2 + (\Delta_b')^2} \Theta(\varepsilon) \right. \\ & + \left[\frac{k(\gamma_2 + \Gamma_{22})\Gamma_a}{4\pi^2 u^2} \int dv\, dv_0 \frac{1}{\tilde{\Gamma}_{23} - i(\tilde{\Delta}' - \varepsilon k'/v_z)} \right. \\ & \times \tilde{G}_{13}^{vc}(v_0 \to v) \frac{\exp[-(v_{x_0}^2 + v_{y_0}^2)/u^2]}{\tilde{\Gamma}_{12} + i(\Delta - kv_{z_0})} + \text{conjugate} \Big] \\ & + \frac{k(\gamma_2 + \Gamma_{22})\Gamma_a}{\pi^2 u^2} \int dv\, dv_0 \frac{\tilde{\Gamma}_{23}}{(\tilde{\Gamma}_{23})^2 + (\tilde{\Delta}' - \varepsilon k' v_z)^2} \\ & \times G_{22}(v_0 \to v) \frac{\tilde{\Gamma}_{12}}{(\tilde{\Gamma}_{12})^2 + (\Delta - kv_{z_0})^2} \exp\left[-\left(\frac{v_{x_0}^2 + v_{y_0}^2}{u^2} \right) \right] \\ & \left. + \frac{\Gamma_a[(\delta\Gamma')(\Gamma_a\Gamma_b' - \Delta_a\Delta_b') + (\delta S')(\Gamma_a\Delta_b' + \Gamma_b'\Delta_a)]}{[(\Gamma_a)^2 + (\Delta_a)^2][(\Gamma_b')^2 + (\Delta_b')^2]} \Theta(\varepsilon) \right\}, \end{aligned} \tag{4.68}$$

where

$$\Gamma_b' = \frac{k}{k'} \left[\frac{k'}{k} (\gamma_{13} + \Gamma_{13}^{vc}) + \frac{k - k'}{k} \tilde{\Gamma}_{23} \right] \Theta(k - k') + \left[\gamma_{13} + \Gamma_{13}^{vc} + \frac{k' - k}{k} \tilde{\Gamma}_{12} \right] \Theta(k' - k), \tag{4.69a}$$

$$\Delta_b' = \frac{k}{k'} \left[\Delta' - \frac{k'}{k} \Delta - \frac{k - k'}{k} S_{23}^{ph} \right] \Theta(k - k') + \left[\Delta' - \frac{k'}{k} \Delta - \frac{k' - k}{k} S_{12}^{ph} \right] \Theta(k' - k), \tag{4.69b}$$

$$(\delta\Gamma') = -(\Gamma_{12}^{ph} + \Gamma_{23}^{ph} - \Gamma_{13}^{vc} - \Gamma_{22}) \left[\frac{k'}{k} \Theta(k - k') + \Theta(k' - k) \right], \tag{4.70a}$$

$$(\delta S') = -(S_{12}^{ph} + S_{23}^{ph})\left[\frac{k'}{k}\Theta(k-k') + \Theta(k'-k)\right] \tag{4.70b}$$

and Γ_a and Δ_a are defined by eq. (4.58a). The third term in eq. (4.68) represents the contribution from collisions which are velocity-changing in their effect on ρ_{13} while the fourth term is the SW velocity redistribution resulting from collisions in level 2. The fifth term is assumed to be small.

The third term is the critical one for the present discussion. This term will take on a qualitatively different form depending upon whether collisions are "weak" or "strong" (in the sense described in section 4.3).

Copropagating waves ($\varepsilon = 1$). Any strong collision upsets the Doppler phase cancellation that characterizes the $\varepsilon = 1$ TQ chain. Thus, the third term in (4.68) is negligible for strong velocity-changing collisions in the low pressure region. Strong collisions broaden the narrow resonance of the TQ contribution [second term of eq. (4.68)]; these collisions have, in effect, decreased the coherence time associated with ρ_{13}. The narrow resonance is a Lorentzian centered near $\Delta' = (k'/k)\Delta$ with a width

$$\Gamma_b' = \left[\frac{\gamma_3}{2} + \frac{|k-k'|}{k}\frac{\gamma_2}{2} + \left(\frac{k'}{k}\Gamma_{13}^{vc} + \frac{k-k'}{k}\Gamma_{23}^{ph}\right)\Theta(k-k') + \left(\Gamma_{13}^{vc} + \frac{k'-k}{k}\Gamma_{12}^{ph}\right)\Theta(k'-k)\right] \tag{4.71}$$

For weak collisions, the Doppler phase cancellation is not significantly disturbed to render the third term in eq. (4.68) negligible. This term combines with the second to produce a non-Lorentzian line shape that broadens with increasing pressure. The specific form of the line shape will depend on the kernel $W_{13}^{vc}(v' \to v)$.

In addition to the narrow resonance of the TQ chain for either weak or strong collisions, there is a background [fourth term in eq. (4.68)] resulting from velocity-changing collisions in level 2.

Counterpropagating waves ($\varepsilon = -1$). In the absence of collisions, the TQ chain contribution vanishes. Mathematically, this result was obtained owing to the fact that all the poles in the velocity integration were in the same half-plane (physically, one might say that a cancellation of Doppler phase factors does not occur for counterpropagating waves). If weak velocity-changing collisions are present, the TQ chain still vanishes to first approximation since the velocity change is not sufficient to change the general nature of the solution. Even for strong collisions, the third term in eq. (4.68) does not contribute appreciably, as may be verified by using an iterative solution for $\tilde{G}_{13}^{vc}$ to estimate the importance of the term. At low pressures, the TQ contribution for counter-propagating waves remains small.

b. *High pressure* ($\Gamma_{12}^{ph} \gg ku$, $\Gamma_{23}^{ph} \gg k'u$, $(\Gamma_{13}^{vc})' \gg |k - \varepsilon k'|u$, $\Gamma_{22}' \gg \gamma_2$). In this limit the sample is completely thermalized by velocity-changing collisions. The probability that an atom has not undergone a velocity-changing collision in its lifetime is negligible and one can easily deduce from eqs. (3.32, 4.46, 4.47) and (4.63, 4.66, 4.67) that

$$G_{22}(v' \to v) \sim W_0(v)/\gamma_2 \approx \tilde{G}_{22}(v' \to v), \tag{4.72}$$

$$G_{13}^{vc}(v' \to v) \sim \frac{W_0(v)}{\gamma_{13} + i(\Delta - \Delta')} \approx \tilde{G}_{13}^{vc}(v' \to v). \tag{4.73}$$

Moreover, at these high pressures, it follows from (4.28a) that

$$G_{12}(v' \to v) \approx \delta(v - v')/\tilde{\Gamma}_{12}; \qquad G_{23}(v' - v) \approx \delta(v - v')/\tilde{\Gamma}_{23}. \tag{4.74}$$

By substituting eqs. (4.72–4.74) in (4.27), one obtains the high pressure line shape

$$I(\Delta', \Delta) \approx \frac{2(\chi\chi')^2 N}{\tilde{\Gamma}_{23}\tilde{\Gamma}_{12}\gamma_3\gamma_{13}}\left[\frac{2\gamma_{13}}{\gamma_2} + \frac{(\gamma_{13})^2}{(\gamma_{13})^2 + (\Delta' - \Delta)^2}\right]. \tag{4.75}$$

There is a nearly constant background from the SW chain plus a Lorentzian of width γ_{13} centered at $\Delta' = \Delta$ from the TQ chain. Velocity-changing collisions have narrowed the line [it is even narrower than the no-collision line width $\bar{\Gamma}$, given by eq. (4.23b)] and moved its center from $\Delta' \approx \varepsilon(k'/k)\Delta$ to $\Delta' = \Delta$. The line profile is the same for copropagating or counterpropagating waves (for $\tilde{\Gamma}_{ij} \gtrsim ku$, the counterpropagating wave TQ chain begins to contribute) and is shown schematically in fig. 14. Such a line profile has yet to be found experimentally.

Therefore, the line width of the narrow resonance for copropagating waves first broadens and then narrows with increasing pressure while its center shifts from $\Delta' = (k'/k)\Delta$ to $\Delta' = \Delta$. For counterpropagating waves the Lorentzian contribution of the SW chain [first term of eq. (4.68)] centered at $\Delta' = -(k'/k)\Delta$ diminishes with increasing pressure while a new narrow resonance arises from TQ chain [third term in eq. (4.68)], with the line shape ultimately reaching the form (4.75) at high pressures.

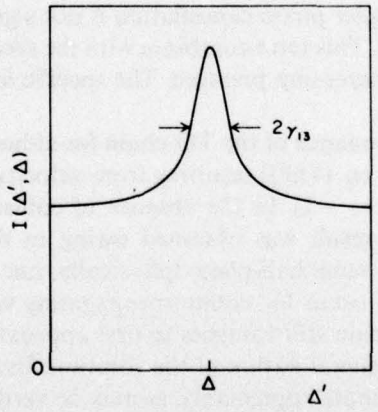

Fig. 14. High pressure limit of the collision line shape when collisions are velocity-changing in their effect on ρ_{13}. The collision narrowed profile is a Lorentzian of width γ_{13} centered at $\Delta' = \Delta$ superimposed on a broad background from the SW chain.

4.5. *Alternative level schemes*

The results of this section may be taken over directly to describe the alternative level schemes of fig. 8.

For the V, fig. 8b, $\Delta \to -\Delta$, $(\Delta - kv_z) \to -(\Delta - kv_z)$.

For the upward cascade, fig. 8c, $\Delta' \to -\Delta'$, and $(\Delta' - \varepsilon k'v_z) \to -(\Delta' - \varepsilon k'v_z)$.

5. Inelastic collisions, degeneracy, resonant collisions

The modifications of the theory needed to account for inelastic collisions, level degeneracy, and resonant excitation exchange collisions are discussed below. In some cases, there is no difficulty in extending the theory, in others, the generalization of the theory is by no means trivial.

5.1. Inelastic collisions

Inelastic collisions can be separated into two categories, *external* and *internal*.

External inelastic collisions. Quite often, levels 1 or 2 in fig. 5 or levels 1, 2 or 3 in fig. 8 are collisionally coupled to states not shown in these diagrams. An *external inelastic collision* is one that transfers population out of the two or three-level system under consideration. (Inelastic collisions that transfer population *into* the system can be incorporated into the problem by an appropriate generalization of the incoherent pumping terms $\lambda_i(v)$, $i = 1, 2, 3$.)

The effects of external inelastic collisions are easily calculated. In fact, the derivation of $\partial\rho_{ij}(v, t)/\partial t|_{\text{coll}}$ presented in section 2.2 is *unchanged* when external inelastic collisions are present. Eqs. (2.20–2.22), with *elastic* scattering amplitudes, are still valid. The forward elastic scattering amplitudes appearing in expression (2.22) for $\Gamma_{ij}(v)$ implicitly contain the effects of inelastic collisions, since these elastic amplitudes are related to the *total* (elastic + inelastic) scattering cross section via the optical theorem,

$$\sigma_i^{\text{TOTAL}}(v_r) = \frac{4\pi\hbar}{\mu v_r}\,\text{Im}\,[f_i(v_r \to v_r)]. \tag{5.1}$$

Since the form of $\Gamma_{ij}(v)$ is unchanged from the purely elastic collision case, it is clear that inelastic and elastic collisions affect the parameter $\Gamma_{ij}(v)$ in the same way. Thus, inelastic collisions provide additional channels for the decay of level population densities $\rho_{ii}(v)$, with a decay rate given by

$$\Gamma_{ii}(v) = \int dv' W_{ii}(v \to v') + \mathcal{N}\int dv_p W_p(v_p) v_r \sigma_i^Q(v_r) \tag{5.2}$$

where $W_{ii}(v' \to v)$ is the elastic collision kernel and $\sigma_i^Q(v)$ is the inelastic (or quenching) cross section. For *off-diagonal* density matrix elements, inelastic collisions add a contribution

$$\tfrac{1}{2}\mathcal{N}\int dv_p W_p(v_p)\,[\sigma_i^Q(v_r) + \sigma_j^Q(v_r)]$$

to the real part of $\Gamma_{ij}(v)$, providing a broadening mechanism in line shape formation. Since the imaginary part of $\Gamma_{ij}(v)$ is also affected by inelastic collisions, they give rise to a shift in line profiles. Inelastic collision broadening can often obscure the collisional narrowing effect.

Inelastic collisions can be studied by the four-level system shown in fig. 15. The pump field $\boldsymbol{E}$ with frequency Ω velocity selects a population $\rho_{22}(v_z)$. This population is transferred to level 3 by inelastic collisions with a corresponding velocity redistribution and the velocity profile $\rho_{33}(v_z)$ is probed by $\boldsymbol{E}'$ as a function of Ω'. This type of experiment provides information on the differential and total inelastic 2–3 scattering cross section and can be used to study the collision induced relaxation of fine structure or rotational levels. Note that the atom-probe field interaction is negligible in the absence of collisions.

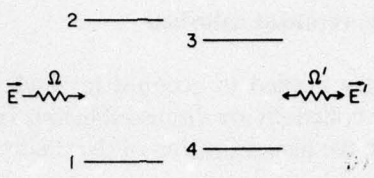

Fig. 15. A four-level system used to illustrate inelastic collision effects. Field $\boldsymbol{E}$ pumps the 1–2 transition and field $\boldsymbol{E}'$ probes any collisional transfer to levels 3 and 4.

Internal inelastic collisions. It may happen that the energy separations of the levels shown in fig. 5 or 8 are small enough to permit inelastic collisions between levels *within* the system under consideration. For the dipole allowed 1–2 and 2–3 transitions of figs. 5 and 8, inelastic collisions play a role only for transition frequencies $\lesssim 10^{12}$ Hz. Inelastic collisions between levels 1 and 3 of figs. 8a and 8b are likely to be important if these levels lie closely spaced in the same electronic subspace.

Incorporation of internal inelastic collision effects into the quantum mechanical transport equation for $\partial\rho_{ij}/\partial t|_{\text{coll}}$ is difficult, in general, owing to the collisional coupling of states with different total (internal plus center-of-mass) energy. I do not know of any treatment of this problem for arbitrary level separations. However, if the collisionally coupled states have frequency separations much less than $(\tau_c)^{-1}$ (τ_c = duration time of a collision), the impact approximation is still valid and the problem is greatly simplified. *In the impact limit*, using the techniques of section 2, it is easy to derive [18]

$$\partial\rho_{ij}(\boldsymbol{v},t)/\partial t|_{\text{coll}} = -\sum_{kn}\Gamma_{ij}^{kn}(\boldsymbol{v})\rho_{kn}(\boldsymbol{v},t) + \sum_{kn}\int d\boldsymbol{v}'\,W_{ij}^{kn}(\boldsymbol{v}'\to\boldsymbol{v})\rho_{kn}(\boldsymbol{v}',t), \tag{5.3}$$

where

$$\Gamma_{ij}^{kn}(\boldsymbol{v}) = \tfrac{1}{2}\mathcal{N}\int d\boldsymbol{v}_p W_p(\boldsymbol{v}_p)\left(\frac{4\pi\hbar}{i\mu v_r}\right)v_r\left[f_{ik}(\boldsymbol{v}_r\to\boldsymbol{v}_r)\delta_{jn} - f_{jn}(\boldsymbol{v}_r\to\boldsymbol{v}_r)^*\delta_{ik}\right]; \tag{5.4}$$

$W_{ij}^{kn}(\boldsymbol{v}'\to\boldsymbol{v})$ is an inelastic "kernel" given by (2.21) with the inelastic amplitudes $f_{ik}(\boldsymbol{v}'\to\boldsymbol{v})$ and $f_{jn}(\boldsymbol{v}'\to\boldsymbol{v})^*$ replacing the elastic amplitudes $f_i(\boldsymbol{v}'\to\boldsymbol{v})$ and $f_j(\boldsymbol{v}'\to\boldsymbol{v})^*$, respectively, appearing in that equation.

Inelastic collisions couple *different* density matrix elements, in contrast to elastic collisions. I have not yet analyzed the effects of internal elastic collisions on the line profiles derived in sections 3 and 4. The calculation is straightforward to any order of perturbation theory in the external fields. There may be some new line shape features introduced by the collision induced coupling of different density matrix elements.

The four level system of fig. 15 may also be used to probe inelastic collision effects. Imagine that levels 1 and 2 are collisionally coupled to levels 4 and 3, respectively. The field $\boldsymbol{E}'$ can monitor population transfer from levels 1 to 4 and 2 to 3 as well as any transfer of "coherence" from $\tilde{\rho}_{12}(\boldsymbol{v}')$ to $\tilde{\rho}_{34}(\boldsymbol{v})$ [19].

5.2. Degeneracy

Typically, each of the levels of the "two" or "three"-level systems contains several degenerate magnetic substates, leading to a corresponding increase in the number of states in the system. Inelastic collisions between magnetic substates of a given level are energetically allowed so that internal inelastic collisions can occur. For all but very strong external magnetic fields, the magnetic sublevel spacing is small enough for the impact approximation to be valid and the collisional time evoluation of density matrix elements is given by eq. (5.3).

Collisions result in the relaxation of both the populations and "coherences" (off-diagonal density matrix elements) of the magnetic substates within a given level. Transfers of the type $\rho_{1m,2m'} \rightarrow \rho_{1m'',2m'''}$ are also possible, in principle. The various "rates" $\Gamma^{km'',nm'''}_{im,jm'}$ and "kernels" $W^{km'',nm'''}_{im,jm'}$ are subject to certain selection rules and it is often useful to expand the density matrix in terms of its irreducible tensor components in order to exploit any symmetries in the problem.

Information on the *differential* as well as total cross sections associated with magnetic relaxation can be obtained by the saturation spectroscopy scheme indicated in fig. 15, in which levels 2 and 3 represent different magnetic substates of a given level. By choosing the polarization of fields $\boldsymbol{E}$ and $\boldsymbol{E}'$ properly, one is able to determine the rate at which collisions transfer population from level 2 to 3 and the associated change of velocity occurring in those collisions. It would be interesting to perform an analogous experiment to study the velocity changes associated with transfers of off-diagonal density matrix elements $\rho_{im,im'}(\boldsymbol{v}) \rightarrow \rho_{im'',im'''}(\boldsymbol{v})\,(m \neq m', m'' \neq m''')$, since there is as yet no simple physical picture to describe this process.

5.3. Resonant collisions

For the active atom and perturber level schemes of fig. 16 resonant exchange collisions may occur in which the perturber and active atom exchange roles. It is possible to transfer level population as well as off-diagonal density matrix elements from one atom to another.

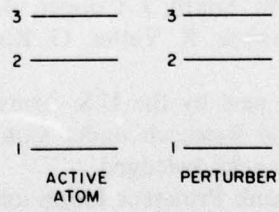

Fig. 16. Active atom and perturber energy level schemes in which resonant excitation exchange is possible. Collisions can transfer population or "coherence" (off-diagonal density matrix elements) from an active atom to a perturber.

The transfer of population is easy to understand. A pump field produces some velocity selected population in an active atom. Resonant exchange collisions can transfer this population to another atom. However, since the atom receiving the population transfer has an *arbitrary* velocity, the velocity selectivity created by the pump field is lost in the transfer process. In effect, each transfer collision completely thermalizes the active atom velocity distribution. Thus, in addition to the

probe absorption line shape features shown in fig. 13c arising from absorption from active atoms that have *not* transferred population to other atoms, there will be an additional broad (Doppler width) background signal owing to absorption from velocity thermalized atoms that have received population via excitation exchange collisions.

The transfer of off-diagonal density matrix elements is more difficult to analyze, since one is again faced with the problem of associating a velocity with off-diagonal density matrix elements. While I have not analyzed this process in any detail, I imagine that off-diagonal density matrix elements can not be transferred in strong collisions, owing to both the large phase shifts and quantum interference effects that characterize such collisions. There may be some possibility to observe this type of exchange in weak collisions. It is an interesting effect since phase information is transferred in the collision.

There is a complication that very often obscures resonant excitation exchange. For levels radiatively connected to the ground state, the exchange of real photons (radiation trapping) is possible. For example, an active atom may spontaneously emit a photon that is absorbed by another atom in the sample. This process gives rise to the same type of line shape modifications as does resonant excitation exchange. In practice, it is often impossible to distinguish the two effects, since the resonant excitation and radiative trapping exchange rates are both proportional to the active atom density over a broad pressure range.

6. Conclusion

I have described in general terms the way in which spectroscopic line shapes reflect the collisional processes occurring in atomic and molecular systems. Additional experiments are required to test the potential of these techniques and to determine whether or not linear and non-linear spectroscopy can provide a practical method of probing atomic and molecular collisions.

With the risk of omitting a name or two, I should like to take this opportunity to thank the following people who have provided me with information, encouragement and guidance (in chronological rather than alphabetical order): F. Zernike, M. Sargent, M. Scully, S. Stenholm, L. Menegozzi, S.P. Koutsoyannis, E.W. Smith, J. Cooper, B. Lippmann, R.G. Brewer, J. Hall, M. Feld, T. Hänsch, L. Klein, P. Toschek, R. Vetter, O. Robaux, P. Cahuzac, C. Brechignac, J. Le Gouet, S. Feneuille, A. Bambini.

My research was supported in the past by the U.S. Army Research Office and is currently supported by the U.S. Office of Naval Research under Contract No. N00014-77-C-0553. The support of these Agencies is gratefully acknowledged.

In closing, I should again like to thank Professor Lamb for the advice and encouragement he has given to me over the years. Many times when I went into his office to discuss a specific question that was troubling me, I did not leave with the answer to my problem. It was rare, however, to leave those discussions without some additional insight into the nature of physics.

References

[1] P.R. Berman, App. Phys. (Germany) 6 (1975) 283.
[2] P.R. Berman, in: Advances in atomic and molecular physics, eds. D.R. Bates and B. Bederson (Academic Press Inc., New York, 1977) Vol. 13, p. 57.
[3] H. Bethe, Ann. Physik 4 (1930) 443.
[4] P.R. Berman and W.E. Lamb Jr., Phys. Rev. A2 (1970) 2435.
[5] P.R. Berman and W.E. Lamb Jr., Phys. Rev. A4 (1971) 319.
[6] M. Baranger, Phys. Rev. 111 (1958) 481.
[7] G. Nienhuis, Physica 66 (1973) 245.
[8] J. Le Gouet and P.R. Berman, Phys. Rev. A17 (1977) 52.
[9] P.R. Berman, J. Quant. Spectr. Radiative Transfer 12 (1972) 1331.
[10] J. Ward, J. Cooper and E.W. Smith, J. Quant. Spectr. Radiative Transfer 14 (1974) 555.
[11] P.R. Berman, Phys. Rev. A9 (1974) 2170.
[12] S.G. Rautian and I.I. Sobelman, Soviet. Phys., Usp. 9 (1967) 701.
[13] J.E. Bjorkholm and P.F. Liao, Phys. Rev. A14 (1976) 751.
[14] L. Klein, M. Giraud and A. Ben-Reuven, Phys. Rev. A16 (1977) 289.
[15] W.K. Bischel and C.K. Rhodes, Phys. Rev. A14 (1976) 176;
M. Elbel, private communication;
C. Brechignac, R. Vetter and P.R. Berman, Phys. Rev. A (May, 1978).
[16] V.A. Alexseev, T.L. Andreeva, and I.I. Sobelman, Soviet. Phys., JETP 37 (1973) 413;
A.P. Kolchenko, A.A. Pukhov, S.G. Rautian and A.M. Shalagin, Soviet. Phys., JETP 36 (1973) 619.
[17] C.N. Bagaev, E.V. Baklanov and V.P. Chebotaev, JETP Letters 16 (1972) 9;
T.W. Meyer, C.K. Rhodes and H.A. Haus, Phys. Rev. A12 (1975) 1993;
P. Cahuzac, O. Robaux and R. Vetter, J. Phys. B9 (1976) 3165;
A.T. Mattick, N.A. Kurnit and A. Javan, Chem. Phys. Letters 38 (1976) 176;
P. Cahuzac, E. Marie, O. Robaux, R. Vetter and P.R. Berman, J. Phys. B. (1977).
[18] P.R. Berman, Phys. Rev. A6 (1972) 2157.
[19] S. Stenholm, J. Phys. B10 (1977) 761.

PHYSICS REPORTS
A review section of Physics Letters (Section C)

Volume 43C, number 3, July 1978

Single orders for this issue

PHYSICS REPORTS (Section C of PHYSICS LETTERS) 43, No. 3 (1978) 101–149.

Copies of this issue may be obtained at the price given below. All orders should be sent directly to the Publisher. Orders must be accompanied by check.

Single issue price Dfl. 23.00, postage included.

PHYSICAL REVIEW A VOLUME 17, NUMBER 1 JANUARY 1978

Effect of velocity-changing collisions upon optical coherences in a three-level system

J.-L. Le Gouët
Laboratoire Aimé Cotton, Centre National de la Recherche Scientifique II, Bâtiment 505, 91405 Orsay, France

P. R. Berman*
Physics Department, New York University, 4 Washington Place, New York, New York 10003
(Received 11 July 1977)

In this work, a theory of laser nonlinear spectroscopy and its application to the study of atomic collisions is developed. A three-level system (TLS) is considered in low-pressure gases. The effect of weak velocity-changing collisions (vcc) upon atomic coherences is introduced into the TLS equations established by Hänsch and Toschek. It appears that a TLS is suitable for the observation of the effect of vcc upon optical coherences.

I. INTRODUCTION

The fruitful development of nonlinear laser spectroscopic techniques during the last few years has provided new evidence for collision-induced homogeneous broadening, shifts, and even distortion of spectral lines in low-pressure gases. Saturated absorption[1-4] and two-photon[5] spectroscopy have been used for such studies.

The use of nonlinear spectroscopy to study collisional effects represents a marked improvement over linear spectroscopy in measuring the effects of velocity-changing collisions (vcc). In linear spectroscopy, one starts with a thermalized sample. Consequently, elastic collisions do not alter the velocity distribution of the various level populations of the atom, which are already in equilibrium. Collisions will affect only the coherence or off-diagonal density-matrix elements, leading to a disturbance of the phase of the atomic oscillators. In general this phase disturbance consists of an inseparable combination of velocity-changing and phase-interrupting effects, although, in certain limits (see below), one contribution can dominate. In linear spectroscopy, effects of vcc are easily lost in the large widths of spectral profiles arising from the Doppler effect. In some cases, the effect of vcc on atomic coherences can be detected by a narrowing of the Doppler profile, but, in general, vcc are difficult to detect in linear spectroscopy.

Nonlinear Doppler-free spectroscopy provides more promise for studying subtle collisional processes. In such experiments one excites a given velocity group of atoms. By probing the system, one can determine the rethermalization of this population velocity group resulting from collisions. Moreover, there are systems where one can attempt to study the effect of velocity-changing collisions on the atomic coherences.

In a three-level system, it is possible to have a saturated absorption signal arising solely from terms related to optical coherences and not dependent on populations. By examining the effect of collisions on these profiles, one eliminates any problems arising from velocity-changing collisions on populations which would tend to mask their effects on "coherences."

There exists a large literature of calculations of velocity-changing collision effects in both linear and nonlinear spectroscopy.[6-10] To our knowledge, no calculation exists in which the model of weak velocity-changing collisions affecting internal coherences in a three-level system (TLS) has been fully explored. In this work, such a model is adopted and may prove relevant to explain recent experimental results involving saturation spectroscopy in a three-level system.[11]

II. TLS UNIDIRECTIONAL SPECTROSCOPY

In a typical experiment, two cw monochromatic collinear laser beams interact with an atomic or molecular gas contained in a low-pressure cell (Fig. 1). The field $E(\omega, k)$ is resonant with and saturates the 1-2 transition alone, selectively exciting optical dipoles with an axial velocity close to zero. The field $E'(\omega', k')$ with a frequency ω' close to that of the 2-3 transition monitors the changes in the velocity distribution and phase coherences of the system, induced by the pump field in the presence or absence of collisions.

The parameter measured in typical experiments[11] is that part of the absorption coefficient of the probe beam containing saturation effects; the most interesting situation occurs with unidirectional beams and $k > k'$.

A theoretical description of this system was given by Hänsch and Toschek.[12] Using perturbation theory, neglecting collisions, and assuming

Supported by the U.S. Office of Naval Research under Contract No. N00014-77-C-0553.

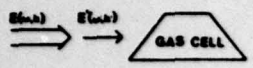

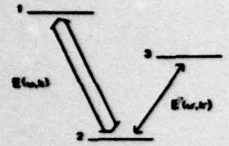

FIG. 1. Experimental situation and the energy-level scheme considered in this work. The frequencies of the fields E and E' are denoted by ω and ω', and the magnitudes of the propagation vectors by k and k'.

the Doppler limit (i.e., Doppler width much larger than decay rates), they obtained the term proportional to E'^2 in the absorption coefficient for the field E' as

$$\alpha_2 = 4\pi k' E'^2 \operatorname{Im}\chi_2,$$

where

$$\operatorname{Im}\chi_2 = 2\pi^{1/2}\hbar^{-2}\mu_{12}^2\mu_{23}^2(kv')^{-1}\exp\left(-\frac{(\omega-\omega_{12})^2}{(kv')^2}\right)$$
$$\times\left[N_{22}\left(\frac{1}{\gamma_{12}\Gamma_B^{vc}}\frac{1}{1+Y^2}+\frac{\omega_{23}}{\omega_{12}}\frac{1}{\Gamma_B^{vc}\Gamma_B^{vc}}\frac{1-XY}{(1+X^2)(1+Y^2)}\right)\right.$$
$$\left.+N_{33}\left(1-\frac{\omega_{23}}{\omega_{12}}\right)\frac{1}{(\Gamma_B^{vc})^2}\frac{1-X^2}{(1+X^2)^2}\right]. \quad (1)$$

N_{ij} is the population difference between i and j levels at equilibrium in the absence of all fields, γ_i is a level decay rate, γ_{ij} is the natural decay rate of the i–j coherence, ω_{ij} is a resonance frequency, μ_{ij} is the electric dipole moment of the i–j transition, Γ is the most probable atomic speed, and

$$\Gamma_B^{vc} = (1-\omega_{23}/\omega_{12})\gamma_{22}+(\omega_{23}/\omega_{12})\gamma_{13},$$
$$\Gamma_B^{vc} = \gamma_{33}+(\omega_{23}/\omega_{12})\gamma_{13},$$
$$X\Gamma_B^{vc} = Y\Gamma_B^{vc} = \omega'-\omega_{23}-(k'/k)(\omega-\omega_{12}).$$

Despite the apparent complexity of the expression for $\operatorname{Im}\chi_2$, it is possible to elucidate its physical content. The first term in square brackets is recognized as the usual saturation term resulting from the stepwise absorption of the fields E and E'. The second term is related with a two-quanta Raman-type transition connecting levels 1 and 3. The third term is another two-quanta contribution; it is noticeable that this term exists, even when the medium is transparent to the saturating field ($N_{21}=0$) contrary to the other two terms.

The third term corresponds, in atomic density-matrix formalism, to the following perturbative path:

$$\left.\begin{matrix}\rho_{22}^{(2)}\\ \rho_{33}^{(2)}\end{matrix}\right\} \xrightarrow{E'} \rho_{23}^{(1)} \xrightarrow{E} \rho_{13}^{(2)} \xrightarrow{E} \rho_{23}^{(1)}.$$

This path does not depend upon saturated diagonal matrix elements. Therefore, vcc effects on populations play no role in this chain, making it well suited for studying the effect of collisions on optical coherences. Consequently, an experimental situation of interest occurs when the population inversion N_{21}, prepared by suitable pumping procedure, is much smaller than N_{23}. In this paper we are concerned only with third term of (1).

The steady-state equations of motion giving rise to the contribution of the third term in (1) are given by

$$[\gamma_{23}-i(\Delta'-k'v_z)]\tilde\rho_{23}^{(1)}(\bar v) = -i\beta'[\rho_{22}^{(0)}(\bar v)-\rho_{33}^{(0)}(\bar v)],$$
$$\{\gamma_{13}+i[\Delta-\Delta'-(k-k')v_z]\}\tilde\rho_{13}^{(2)}(\bar v) = i\beta\tilde\rho_{23}^{(1)}(\bar v), \quad (2)$$
$$[\gamma_{23}-i(\Delta'-k'v_z)]\tilde\rho_{23}^{(1)}(\bar v) = i\beta\tilde\rho_{13}^{(2)}(\bar v),$$

where the pump and probe detunings are $\Delta=\omega-\omega_{12}$ and $\Delta'=\omega'-\omega_{23}$, respectively, $\tilde\rho_{ij}(\bar v)$ is a density-matrix element in a radiation interaction representation,

$$\tilde\rho_{13}(\bar v) = \rho_{13}(\bar v,z,t)\exp\{i[(k-k')z+(\omega'-\omega)t]\},$$
$$\tilde\rho_{23}(\bar v) = \rho_{23}(\bar v,z,t)\exp[i(\omega' t-k'z)],$$

and β and β' are the Rabi frequencies of the transitions and are assumed to be much smaller than γ_{ij} in order that the perturbation calculation be valid.

III. THE EFFECT OF ELASTIC COLLISIONS UPON OPTICAL COHERENCES: A REASONABLE MODEL

The problem of interaction with an electromagnetic field of atoms or molecules subjected to collisions in a gas has already given rise to considerable theoretical studies (a comprehensive bibliography can be found in Ref. 9). The dynamical as well as the internal aspects of collisions have been extensively investigated and totally quantum-mechanical treatments have been achieved.[7,8] However, a lack of information on the interatomic potential prevents one from determining the scattering amplitudes which play a prominent role in all these theoretical calculations. Especially, the angular dependence of these amplitudes seems to be very sensitive—at least in the medium-angle diffusion region—to the precise shape of the potential.

As a consequence, we shall choose a simple empirical model to take into account the effect of elastic collisions upon optical coherences (off-diagonal density-matrix elements).

We assume a separation of collisions into two groups:

(i) Those which occur in a "near region," where the interaction potentials of the two levels involved in the transition are very different. These collisions result in a large abrupt change in phase for the off-diagonal density-matrix elements and consequently in a destroying of the coherence. In other words, coherence cannot be drifted by such a collision from one velocity class to another.

(ii) Those which occur in a "far region," where the interaction potentials of the two levels are so close that the phase-interrupting effect is negligible These collisions result only in a change in the velocity associated with the atomic dipole. This change is necessarily small due to the size of the impact parameter but may still be detectable by laser-spectroscopy techniques. A consequence of these assumptions is a statistical independence of coherence-destroying and velocity-changing collisions. The small change in the velocity of the atom, enables us to use the so-called weak-collision approximation.

The model is expressed mathematically by the addition of a term $R_{ij}|_{coll}$ to the right-hand side of (2):

$$R_{ij}|_{coll} = -\gamma_{ij}^{pp}(\bar v)\tilde\rho_{ij}(\bar v)-\Gamma_{ij}^{vc}(\bar v)\tilde\rho_{ij}(\bar v)$$
$$+\int W_{ij}(\bar v'-\bar v)\tilde\rho_{ij}(\bar v')\,d\bar v', \quad (3)$$

where γ_{ij}^{pp} is the rate of phase-interrupting collisions, $W_{ij}(\bar v'-\bar v)$ is the collision kernel for vcc, and

$$\Gamma_{ij}^{vc}(\bar v) = \int d\bar v'\,W_{ij}(\bar v-\bar v')$$

is the rate of vcc. The collision kernel is assumed to be important in the region where $|\bar v'-\bar v|$ is much smaller than the mean atomic velocity.

IV. SOLUTION OF THE EQUATIONS OF MOTION

First, we can reduce the velocity dependence of the problem to one dimension by noticing that the orthogonal velocity distribution of the active atoms is hardly perturbed by the saturating beam (propagating along v_z). Therefore one can factorize density-matrix elements:

$$\tilde\rho_{ij}(\bar v) = \underline{\tilde\rho}_{ij}(v_z)W_M(\bar v_\perp),$$

where $W_M(\bar v_\perp)$ is the equilibrium velocity distribution for the transverse velocity components.

Including the collision terms in equation set (2) and summing it over $\bar v_\perp$, neglecting the velocity dependence of Γ^{vc} and γ^{pp}, one gets

$$[\Gamma_{23}-i(\Delta'-k'v_z)]\underline{\tilde\rho}_{23}^{(1)}(v_z)$$
$$= -i\beta' N_{23}(v_z)+\int W_{23}(v_z',v_z)\underline{\tilde\rho}_{23}^{(1)}(v_z')\,dv_z',$$
$$\{\Gamma_{13}+i[\Delta-\Delta'-(k-k')v_z]\}\underline{\tilde\rho}_{13}^{(2)}(v_z)$$
$$= i\beta\underline{\tilde\rho}_{23}^{(1)}+\int W_{13}(v_z',v_z)\underline{\tilde\rho}_{13}^{(2)}(v_z')\,dv_z', \quad (4)$$
$$[\Gamma_{23}-i(\Delta'-k'v_z)]\underline{\tilde\rho}_{23}^{(1)}(v_z)$$
$$= i\beta\underline{\tilde\rho}_{13}^{(2)}+\int W_{23}(v_z',v_z)\underline{\tilde\rho}_{23}^{(1)}(v_z')\,dv_z'$$

where

$$\Gamma_{ij} = \gamma_{ij}+\gamma_{ij}^{pp}+\Gamma_{ij}^{vc},$$
$$W_{ij}(v_z',v_z) = \int d\bar v_\perp\,d\bar v_\perp'\,W_M(\bar v_\perp')W_{ij}(\bar v'-\bar v),$$

and

$$N_{23}(v_z) = N_{23}W_M(v_z).$$

For weak collisions and low pressures, the collision kernels in (4) can be chosen to depend solely on the difference $|v_z-v_z'|$. While kernels of this nature do not satisfy detailed balancing and cannot give rise to collisional narrowing of spectral profiles, they may be used without significant error provided that the effective collisional mean free path is large compared with the appropriate wavelength in the problem. Specifically, one requires[13]

$$k\Gamma \gg \Gamma_{23}\beta_{23}^2/\Gamma^2,$$
$$|k-k'|\Gamma \gg \Gamma_{13}\beta_{13}^2/\Gamma^2,$$

where δ_{ij} is the width of the kernel $W_{ij}(v_z-v_z')$ and $\Gamma_{ij}\beta_{ij}^2/\Gamma^2$ is the effective[13] collision rate. In the frame of this approximation, the following equality holds:

$$\Gamma_{ij}^{vc} = \int_{-\infty}^{+\infty} W_{ij}(v_z,v_z')\,dv_z' = \int_{-\infty}^{+\infty} W_{ij}(v_z',v_z)\,dv_z'. \quad (5)$$

In what follows, we write

$$W_{ij}(|v_z-v_{z'}|) = W_{ij}(v).$$

The equations of motion are most easily solved by a Fourier-transform method.[7] The Fourier transform $\mathfrak{F}(\tau)$ of an arbitrary function $f(v_z)$ is defined as

$$\mathfrak{F}(\tau) = \left(\frac{k'}{2\pi}\right)^{1/2}\int_{-\infty}^{+\infty}\exp(ik'v_z\tau)f(v_z)\,dv_z.$$

Equation set (4) may be transformed into

$$[\Gamma_{22}-\mathcal{W}'_{22}(\tau)-i\Delta']\tilde{\underline{\rho}}^{(11)}_{22}(\tau)+\frac{d\tilde{\underline{\rho}}^{(11)}_{22}(\tau)}{d\tau}$$
$$=i\beta'\mathcal{R}_{22}(\tau)\,,$$
$$[\Gamma_{12}-\mathcal{W}'_{12}(\tau)+i(\Delta-\Delta')]\tilde{\underline{\rho}}^{(11)}_{12}(\tau)-\frac{k-k'}{k'}\frac{d\tilde{\underline{\rho}}^{(12)}_{12}(\tau)}{d\tau}$$
$$=i\beta\tilde{\underline{\rho}}^{(11)}_{12}(\tau)\,, \quad (6)$$
$$[\Gamma_{22}-\mathcal{W}'_{22}(\tau)-i\Delta']\tilde{\underline{\rho}}^{(12)}_{22}(\tau)+\frac{d\tilde{\underline{\rho}}^{(12)}_{22}(\tau)}{d\tau}$$
$$=i\beta\tilde{\underline{\rho}}^{(12)}_{12}(\tau)\,.$$

where $\mathcal{R}_{22}$, $\tilde{\underline{\rho}}_{ij}$, and $\mathcal{W}$ are the Fourier transforms of N_{22}, $\underline{\rho}_{ij}$, and W_{ij}, with

$$\mathcal{W}'_{ij}(\tau)=(2\pi/k')^{1/2}\mathcal{W}_{ij}(\tau)\,.$$

This system is solved as follows:

$$\tilde{\underline{\rho}}^{(11)}_{22}(\tau)=-i\beta'\int_{-\infty}^{\tau}\mathcal{R}_{22}(\tau'')$$
$$\times\exp\left(\int_{\tau}^{\tau''}[-i\Delta'+\Gamma_{22}-\mathcal{W}'_{22}(\tau^{iv})]\,d\tau^{iv}\right)d\tau''\,, \quad (7)$$

$$\tilde{\underline{\rho}}^{(11)}_{12}(\tau)=i\frac{k'}{k-k'}\beta\int_{\tau}^{\infty}d\tau'\tilde{\underline{\rho}}^{(11)}_{12}(\tau')\exp\left(-\int_{\tau}^{\tau'}d\tau''\frac{k'}{k-k'}[i(\Delta-\Delta')+\Gamma_{12}-\mathcal{W}'_{12}(\tau'')]\right), \quad (8)$$

$$\tilde{\underline{\rho}}^{(12)}_{22}(\tau)=i\beta\int_{-\infty}^{\tau}\tilde{\underline{\rho}}^{(11)}_{12}(\tau')\exp\left(\int_{\tau}^{\tau'}d\tau''[-i\Delta'+\Gamma_{22}-\mathcal{W}'_{22}(\tau'')]\right)d\tau'\,. \quad (9)$$

Each of the exponential factors acts as a propagator containing collision and natural damping. Each one drives a density-matrix element from its creation at time τ' due to a field interaction, up to time τ.

Bringing (7) into (8), and (8) into (9), one obtains

$$\tilde{\underline{\rho}}^{(12)}_{22}(\tau)=-i\beta^2\beta'\frac{k'}{k-k'}\int_{-\infty}^{\tau}d\tau'\int_{\tau'}^{\tau}d\tau''\int_{-\infty}^{\tau''}d\tau'''\,\mathcal{R}_{22}(\tau''')$$
$$\times\exp\left(\left(-i\Delta'+\Gamma_{22}\right)(\tau'-\tau)-\tilde{\mathcal{W}}_{22}(\tau')+\tilde{\mathcal{W}}_{22}(\tau)-\frac{k'}{k-k'}[i(\Delta-\Delta')+\Gamma_{12}](\tau''-\tau')\right.$$
$$\left.+\frac{k'}{k-k'}[\tilde{\mathcal{W}}_{12}(\tau'')-\tilde{\mathcal{W}}_{12}(\tau')]+\left(-i\Delta'+\Gamma_{22}\right)(\tau'''-\tau'')-\tilde{\mathcal{W}}_{22}(\tau''')+\tilde{\mathcal{W}}_{22}(\tau'')\right), \quad (10)$$

with

$$\tilde{\mathcal{W}}_{ij}(\tau)=\int_{0}^{\tau}d\tau''\mathcal{W}_{ij}(\tau')=\int_{-\infty}^{+\infty}dv_z\frac{\sin(k'v_z\tau)}{k'v_z}W_{ij}(v_z)\,, \quad (11)$$

where we have used the fact that $W_{ij}(v_z)$ is an even function.

We are interested in the integral of $\tilde{\underline{\rho}}^{(12)}_{22}(v_z)$ over velocity, since

$$E^0E'\operatorname{Im}\chi_3=\mu_{23}\operatorname{Im}\int_{-\infty}^{+\infty}dv_z\,\tilde{\underline{\rho}}^{(12)}_{23}(v_z)\,. \quad (12)$$

The transformation back to velocity space is performed using

$$\int_{-\infty}^{+\infty}\tilde{\underline{\rho}}^{(12)}_{22}(v_z)\,dv_z=i\beta^2\beta'\frac{k'}{k-k'}N_{22}\left(\frac{\Delta}{k}\right)\frac{2\pi}{k'}\left[\int_{0}^{\infty}d\tau\exp\left(\left(i\Omega'-\Gamma_\mu\right)\frac{k}{k-k'}\tau+\frac{k'}{k-k'}\tilde{\mathcal{W}}_{12}(\tau)+\tilde{\mathcal{W}}_{22}(\tau)\right)\right]^2, \quad (14)$$

where

$$\Gamma_\mu=(1-\omega_{22}/\omega_{12})\Gamma_{22}+(\omega_{22}/\omega_{12})\Gamma_{12}$$

and

$$\Omega'=\omega'-\omega_{22}-(k'/k)(\omega-\omega_{12})\,.$$

$$\int_{-\infty}^{+\infty}dv_z\,\tilde{\underline{\rho}}^{(12)}_{22}(v_z)=\left(\frac{2\pi}{k'}\right)^{1/2}\tilde{\underline{\rho}}^{(12)}_{22}(0)\,. \quad (13)$$

Additional approximations provide a more tractable expression. First, as has been done in arriving at (1), we may assume that the Doppler limit is fulfilled. Consequently, we approximate $N_{22}(v_z)$ by $N_{22}(\Delta/k)$ leading to a value

$$\mathcal{R}_{22}(\tau)=(2\pi/k')^{1/2}N_{22}(\Delta/k)\delta(\tau)$$

and the result

To go further, one needs an explicit form for the collision kernel. Keeping in mind that we have assumed that only distant collisions contribute to the velocity-changing collision kernel, we may conclude that the semiclassical approximation conditions are fulfilled in that region. Then, a Gaussian kernel can be obtained as has been shown by Kolchenko *et al.*[14]

Taking

$$W_{ij}(v_z)=(\Gamma^{vc}_{ij}/\sqrt{\pi}\,\bar{u}_{ij})\exp(v_z^2/\bar{u}_{ij}^2)\,,$$

using (10), and doing a little algebra, one finally gets

$$\tilde{\mathcal{W}}_{ij}(\tau)=\sqrt{\pi}\,\frac{\Gamma^{vc}_{ij}}{k'\bar{u}_{ij}}E_2\left(\frac{k'\bar{u}_{ij}\tau}{2}\right),$$

where $E_2(x)$ stands for the error function,

$$E_2(x)=\frac{2}{\sqrt{\pi}}\int_0^x e^{-t^2}dt\,.$$

The resulting contribution to the imaginary part of χ_3 is now in a form well suited for a computer calculation:

$$\operatorname{Im}\chi_3=\frac{2\pi}{k}\left(1-\frac{\omega_{23}}{\omega_{13}}\right)N^{-3}\mu_{13}^2\mu_{23}^2N_{23}\left(\frac{\Delta}{k}\right)$$
$$\times\operatorname{Re}\left\{\int_0^\infty d\tau\exp\left[\left(i\Omega'-\Gamma_\mu\right)\tau+\frac{\omega_{23}}{\omega_{13}}\sqrt{\pi}\,\frac{\Gamma^{vc}_{13}}{k'\bar{u}_{13}}E_2\left(\frac{k'\bar{u}_{13}\tau}{2}\right)+\left(1-\frac{\omega_{23}}{\omega_{13}}\right)\sqrt{\pi}\,\frac{\Gamma^{vc}_{23}}{k'\bar{u}_{23}}E_2\left(\frac{k'\bar{u}_{23}\tau}{2}\right)\right]\right\}^2. \quad (15)$$

This is the final expression that we obtain in this paper, taking into account the effect of vcc. When $\Gamma^{vc}_{13}\simeq\Gamma^{vc}_{23}=0$, one can easily identify (15) with the third term in (1).

V. DISCUSSION

In this section, we emphasize that the effect of vcc depends strongly upon the size of the width of the collision kernel relative to the atomic decay rates. In a characteristic situation, the shape of the signal profile may be noticeably distorted due to the effect of vcc.

In order to isolate the effect of vcc in a single term in Eq. (14), we make use of (5) and obtain an alternative form for (14):

$$\int_{-\infty}^{+\infty}\tilde{\underline{\rho}}^{(12)}_{22}(v_z)\,dv_z=i\beta^2\beta'\frac{k'}{k-k'}N_{22}\left(\frac{\Delta'}{k'}\right)\frac{2\pi}{k}\left[\int_0^\infty d\tau\exp\left(i\Omega'-\Gamma^0_\mu-\Gamma^{ph}_\mu\right)\frac{k}{k-k'}\tau+\frac{k}{k-k'}V(\tau)\right)\right]^2, \quad (16)$$

where

$$V(\tau)=\int_{-\infty}^{+\infty}dv_z\left(\frac{\sin(k'v_z\tau)}{k'v_z}-\tau\right)W_\mu(v_z) \quad (17)$$

and

$$W_\mu(v_z)=(k'/k)W_{13}(v_z)+[(k-k')/k]W_{23}(v_z)\,.$$

The entire effect of vcc is contained in $V(\tau)$. To analyze (16) and (17), a parameter of physical interest is the coherence time Γ_c^{-1}, the time at which the real part of the exponential argument in (16) is unity. Depending on the relative size of $k\bar{u}$ and Γ_c, two extreme situations occur [$\bar{u}^2$ is a mean-square change of velocity during a collision associated with the kernel $W_\mu(v_z)$].

(i) $\Gamma_c\gg k\bar{u}$. In this limit, the sine function in (17) can be expanded in a power series, and the first nonvanishing contribution leads to an exponential in (16) of the form[15]

$$\exp[i(\Omega'-\Gamma^0_\mu-\Gamma^{ph}_\mu)\frac{k}{k-k'}\tau-\frac{k}{k-k'}\frac{\Gamma^{vc}_\mu}{6}\tau(k'\bar{u}\tau)^2]\,.$$

The presence of a cubic term in τ indicates that vcc can give rise to line shape different in form from that obtained assuming either no collisions or only phase-interrupting collisions. The *coherence time* Γ_c^{-1} *is the solution of the cubic equation*

$$(\Gamma^0_\mu+\Gamma^{ph}_\mu)/\Gamma_c+\tfrac{1}{6}\,\Gamma^{vc}_\mu(k'\bar{u})^2/\Gamma_c^3\simeq 1\,.$$

The relative values of $k\bar{u}$, $\Gamma^0_\mu+\Gamma^{ph}_\mu$, Γ^{vc}_μ determine the specific effect of the vcc.

For example, if $\Gamma^{vc}_\mu(k'\bar{u})^2\ll(\Gamma^0_\mu+\Gamma^{ph}_\mu)^3$, the vcc will not significantly alter the phase of the off-diagonal density matrix elements during the coherence time $\Gamma_c^{-1}\simeq(\Gamma^0_\mu+\Gamma^{ph}_\mu)^{-1}$. On the other hand, if $\Gamma^{vc}_\mu(k'\bar{u})^2\gg(\Gamma^0_\mu+\Gamma^{ph}_\mu)^3$, it is the vcc which effectively determine coherence time Γ_c^{-1} $\simeq[\Gamma^{vc}_\mu(k'\bar{u})^2]^{-1/3}$. In this case, the vcc lead to a change in the functional form of the line shape resulting from phase excursions caused by a number of weak vcc with $k\bar{u}<\Gamma_c$.

(ii) $\Gamma_c\ll k'\bar{u}$. The sine function in (17) is rapidly varying for all τ of interest and may be neglected leading to an exponential in (16) of the form

$$\exp[i(\Omega'-\Gamma^0_\mu-\Gamma^{ph}_\mu-\Gamma^{vc}_\mu)\tau k/(k-k')]\,.$$

The net effect of the vcc in this case is to add an

additional rate Γ_g^{vc} to the destruction of atomic coherence. The inverse coherence time is now

$$\Gamma_c = \Gamma_g^0 + \Gamma_g^{ab} + \Gamma_g^{vc} .$$

Therefore, this situation occurs when $k'\bar{u} \gg \Gamma_g^0 + \Gamma_g^{ab} + \Gamma_g^{vc}$ so that each collision is strong enough to cause a total phase destruction of the coherences.

When none of the above limits are realized, (15) and (17) should be used. To have an insight into the physical meaning of these results it is useful to remember the case of level populations (i.e., diagonal matrix elements) on which the effects of vcc is simply understood as a redistribution of the atoms over the velocity space, approaching thermal equilibrium. The vcc act in a pure-classical kinetic way and do not affect the total population of a level (integrated over velocity).

On the contrary, a change of velocity induces a change in the translation or Doppler phase of the off-diagonal density matrix element, which results in an additional decay term of this matrix element.[10] Consequently, the vcc affect the total atomic coherence between two levels (i.e., the coherence integrated over the velocity) and, at the same time, the signal profile.

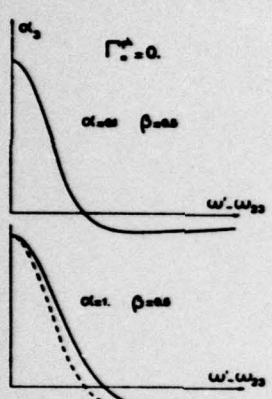

FIG. 2. Saturated absorption profiles for two values of the vcc kernel width. The dashed line represents α_s in the absence of collisions, and the solid line represents it in the presence of vcc. The parameter α denotes the ratio of the kernel widths of Γ_g^0/b'. In this figure one assumes that there is no effect of phase-interrupting collisions.

We have illustrated these results of Figs. 2 and 3, where Γ^{ab} and N_{12} are fixed to zero, and the following parameters are used:

$$\alpha = k'\bar{u}\ 2\Gamma_g^0 , \quad \beta = \Gamma_g^{vc}/\Gamma_g^0 .$$

Dashed lines represent the absorption coefficient α_s in the absence of collisions, and solid lines represent it in the presence of vcc.

Figure 2 shows the evolution of the profile with increasing kernel width, from $k'\bar{u} \ll \Gamma_g^0$ to $k'\bar{u} \sim \Gamma_g^0$. In Fig. 3, this width is constant and two different vcc rates are used. In the absence of vcc the ratio $\alpha_{2\,max}/\alpha_{2\,min}$ is a constant. In the presence of vcc, in addition to a broadening of the curve, the most interesting feature is a change in the value of $\alpha_{2\,max}/\alpha_{2\,min}$, providing a unique signature for the presence of vcc on optical coherences.

These results could be considered as complementary to those of Barantsov et al.[16] who have already pointed out the interest of observing the effect of the vcc upon the interference terms in a three-level system; they focused their calculations upon the study of the Dicke effect associated with a microwave transition between two levels connected to a third one by an optical transition and used a strong collision model.

Laser spectroscopy of molecular two-level systems (saturated absorption[17] and photon echo[18])

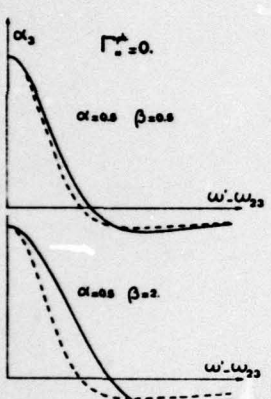

FIG. 3. Saturated absorption profiles for two values of the vcc rate. The parameter β denotes the ratio of the vcc rate to the decay rate Γ_g^0. The dashed and solid lines have the same meaning as in Fig. 2.

has already proved an efficient tool for observing the effect of vcc on optical coherences. On the other hand, observations of collision effects in a three-level system[15,19] have been consistent with an effect of vcc on level populations only; these studies have dealt mainly with the usual saturated contribution resulting from the stepwise absorption of the saturating and probe beams. In this paper, we have shown that TLS experiments, such as that referred to in Ref. 11, can also be used to search for the effect of vcc on optical coherences.

Note added in proof. An article[20] containing a similar calculational method for studying the effects of vcc on coherences using saturated absorption in a two-level system has recently appeared.

ACKNOWLEDGMENT

We are pleased to acknowledge stimulating discussions with Professor P. Toschek.

---

*Supported in part by the U. S. Office of Naval Research under Contract No. N00014-77-C-0553.

[1] S. N. Bagaev, E. V. Baklanov, and V. I. Chebotaev, Pis'ma Red. Zh. Eksp. Teor. Fiz. 16, 15 (1972); 16, 344 (1972) [Sov. Phys. JETP Lett. 16, 9 (1972); 16, 242 (1972)].

[2] P. W. Smith and T. W. Hänsch, Phys. Rev. Lett. 26, 740 (1971).

[3] Ph. Cahuzac, O. Robaux, and R. Vetter, J. Phys. B 9, 3165 (1976).

[4] A. T. Mattick, N. A. Kurnit, and A. Javan, Chem. Phys. Lett. 38, 176 (1976).

[5] F. Biraben, B. Cagnac, and G. Grynberg, J. Phys. (Paris) Lett. 36, 41 (1975).

[6] S. G. Rautian and I. I. Sobel'man, Usp. Fiz. Nauk 90, 209 (1966) [Sov. Phys. Usp. 9, 701 (1967)].

[7] V. A. Alekseev, T. L. Andreeva, and I. I. Sobel'man, Zh. Eksp. Teor. Fiz. 62, 614 (1972); 64, 813 (1973) [Sov. Phys. JETP 35, 325 (1972); 37, 413 (1973)].

[8] P. R. Berman, Phys. Rev. A 5, 927 (1972); 6, 2157 (1972).

[9] P. R. Berman, Appl. Phys. 6, 283 (1975).

[10] A. P. Kolchenko, A. A. Pukhov, S. G. Rautian, and A. M. Shalagin, Zh. Eksp. Teor. Fiz. 63, 1173 (1972) [Sov. Phys. JETP 36, 619 (1973)].

[11] Ph. Cahuzac, R. Vetter, and T. E. Toschek, Abstracts of the Fifth International Conference on Atomic Physics, Berkeley, Calif., 1976 (unpublished).

[12] T. W. Hänsch and P. E. Toschek, Z. Phys. 236, 213 (1970).

[13] P. R. Berman, J. M. Levy, and R. G. Brewer, Phys. Rev. A 11, 1668 (1975).

[14] A. P. Kolchenko, S. G. Rautian, and A. M. Shalagin, Rep. Nucl. Phys. Inst. Inst. Semicond. Phys. USSR Acad. Sci. I. A. F. 46–72 (1972).

[15] The integral in Eq. (16) may be expressed in terms of the Hardy integral

$$E_{13}(Z) = \int_0^\infty \exp(-t^3 - 3Zt)\,dt,$$

which, for any complex value of Z is represented by the series

$$E_{13}(Z) = \frac{\pi}{3}\frac{Z^2}{\cos(\pi/6)}\sum_{m=0}^{\infty}\frac{(-)^m Z^{3m}}{\Gamma(m+\frac{1}{3})\Gamma(m+\frac{2}{3})} + \frac{\pi}{3\sin(\pi/3)}\left(\sum_{m=0}^{\infty}\frac{(-)^m Z^{3m}}{m!\,\Gamma(m+\frac{2}{3})} - Z\sum_{m=0}^{\infty}\frac{(-)^m Z^{3m}}{m!\,\Gamma(m+\frac{4}{3})}\right)$$

[G. N. Watson, A Treatise on the Theory of Bessel Functions (Cambridge University, Cambridge, England, 1966).]

[16] V. I. Barantsov, L. T. Boltskikh, and A. K. Popov, Zh. Eksp. Teor. Fiz. 66, 866 (1974) [Sov. Phys. JETP 39, 419 (1974)].

[17] L. S. Vasilenko, V. P. Kochanov, and V. P. Chebotaev, Opt. Commun. 20, 409 (1977).

[18] T. W. Hänsch and P. E. Toschek, IEEE J. Quantum Electron. 5, 61 (1969).

[19] R. Keil, A. Schabert, and P. E. Toschek, Z. Phys. 261, 71 (1975).

[20] C. J. Bordé, S. Avrillier, and M. Gorlicki, J. Phys. Lett. (Paris) 38, 13 (1977).

HEATING OR COOLING USING COLLISIONALLY AIDED FLUORESCENCE

Paul R. BERMAN*
Physics Department, New York University, New York, N.Y. 10003, USA

and

Stig STENHOLM
Department of Technical Physics, Helsinki University of Technology, SF-02150 Espoo 15, Finland and Research Institute for Theoretical Physics, University of Helsinki, SF-00170 Helsinki 17, Finland

Received 2 November 1977

Collisionally aided redistribution of scattered laser light is suggested as a method to cool or heat gaseous samples. The efficiency is evaluated and restricting conditions are considered. Some potential applications are given.

Many recent treatments of laser light scattering (e.g. refs. [1–5]) imply that the process can be utilized to heat or cool an atomic sample. To our knowledge, there has been no explicit discussion of the phenomenon, hence we shall try to explain the mechanism and estimate its potentialities.

The effect is easily explained with reference to fig. 1. Weak monochromatic light of frequency Ω acts on a two-level atomic system with a stable lower level (i.e. a zero width eigenstate). For the preliminary discussion the atoms are assumed stationary, and no Doppler shifts occur. Without collisions, energy conservation requires, that any fluorescence (or Rayleigh scattering if you prefer) has to occur at the frequency Ω [6]. The scattering process first absorbs energy to a specific position inside the frequency band of the natural line width, and reemission must start from this point; the result is the delta function spectrum of fig. 1b.

With collision events present, the atoms can exchange energy during excitation and fluorescence acquires a new frequency component centered at the atomic level spacing [1–5] ω as shown in fig. 1c. Collisions provide a mechanism to redistribute the excited state population over the natural width of the upper level, γ say. This effect we shall call collisionally aided fluorescence (CAF). Since each scattering event transfers a photon from the frequency Ω to another frequency, the energy difference must be compensated by the translational energy of the colliding atoms, and we have to consider moving atoms, with the Doppler width

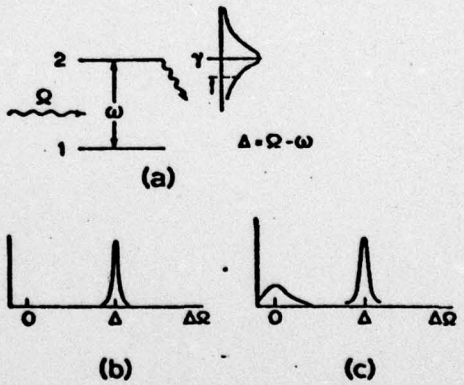

Fig. 1. (a) Two-level system, with the energy difference $\hbar\omega$, coupled by the field at frequency Ω. The lower level is sharp, the upper one has the natural width γ. (b) Without collisions energy conservation requires the scattered light to have the frequency, $\Omega' = \omega + \Delta\Omega$, centered at Ω. (c) Collision event provide Fourier components in the range τ_c^{-1}, allowing the population to settle on the excited level before decay. Hence there appears a component centered at $\Omega' \simeq \omega$ in the scattered light.

* Supported by the U.S. Office of Naval Research under contract number N00014-77-C-0553.

Supported by the U.S. Office of Naval Research under Contract No. N00014-77-C-0553.

$\omega_D \sim (\Omega/c)(k_B T/M)^{1/2}$.

Tuning with $\Omega > \omega$ produces heating and that with $\Omega < \omega$ cooling of the gas. The magnitude of the effect depends strongly on the ratio of the detuning $\Delta = \Omega - \omega$ to the Doppler width ω_D, the total energy per particle $W_T \propto k_B T$ and the duration of a collision τ_c; the Rabi frequency $\chi = \mu E/2\hbar$, the upper state lifetime γ^{-1} and the collision rate Γ. Here μ is the transition dipole and E is the field strength. We only need to consider phase-interrupting collision effects. We want to choose $|\Delta|$ large enough to have a considerable energy change per CAF event, but too large detunings will produce no upper state population to act as the source for the fluorescence. For common values of the parameters of a gas sample, we can choose the tuning such that

$$W_T/\hbar > \tau_c^{-1} > |\Delta| > \omega_D > \Gamma, \tag{1}$$

which also provides the advantage that collisions can be treated by the impact approximation as $|\Delta|\,\tau_c < 1$.

Each collision event which gives rise to CAF changes the translation energy of the system by an amount $\hbar|\Delta|$. If we want spontaneous emission to dominate we must assume a small population probability for the upper state, $n_2 \ll 1$. The rate of CAF events is then given by [4]

$$\dot{n}_2 = \frac{2\chi^2\Gamma}{\Delta^2 + (\Gamma + \gamma/2)^2} \simeq 2\chi^2\Gamma/\Delta^2. \tag{2}$$

Hence the total rate is the product of a collisional rate and the excitation probability. The population of the upper level decays at the rate γ and in steady-state we have

$$n_2 = 2\chi^2\Gamma/\gamma\Delta^2. \tag{3}$$

Requiring this to be much smaller than one we find the condition

$$2\chi^2\Gamma/\Delta^2 \ll \gamma_2. \tag{4}$$

This also implies that each excitation event will immediately be followed by spontaneous emission, which is necessary for optimum energy exchange.

The fractional rate of energy exchange per active atom is

$$\frac{dW_T/dt}{W_T} = \left(\frac{\hbar\Delta}{W_T}\right)\frac{2\chi^2\Gamma}{\Delta^2}. \tag{5}$$

Assume we have a sample of N active atoms and N' perturbers per unit volume, and the laser illuminates a volume V_T, which is less than the total volume V. Then the fractional energy (temperature) change per unit time is

$$f_T = \frac{d\log T}{dt} = \left(\frac{NV_L}{(N+N')V}\right)\left(\frac{dW_T/dt}{W_T}\right)$$

$$= \frac{2\chi^2\Gamma}{\Delta^2}\frac{\hbar\Delta}{W_T}\frac{NV_L}{(N+N')V}. \tag{6}$$

Eq. (6) is valid only when eq. (4) is satisfied. With typical values $W_T/\hbar = 10^{13}\ s^{-1}$, $\tau_c^{-1} = 10^{12}\ s^{-1}$ and $\omega_D = 10^{10}\ s^{-1}$, we can choose $|\Delta| = 10^{11}\ s^{-1}$ satisfying eq. (1). With moderate power requirements (e.g. W/cm^2) one can achieve values of $\chi^2/\Delta^2 \simeq 10^{-5}$. For simplicity we can take the collision rate to be $(N+N')v_r\sigma \simeq (N+N')\ 10^{-10}\ cm^3\ s^{-1}$, where v_r is the relative perturber-active atom velocity and σ is the collision cross section. Setting $V_L \simeq V$ we obtain from eq. (6) an attainable value of

$$f_T = 10^{-17}N \quad (cm^3\ s^{-1}) \tag{7}$$

subject to the restriction (eq. 4)

$$10^{-15}\,(N+N') \ll \gamma \quad (s\ cm^{-3}). \tag{8}$$

An increase of foreign gas perturbers is seen to leave the effect unchanged, since f_T depends on the active atoms only. The enhancement of the rate of CAF events is counteracted by the growth of the total energy reservoir to be cooled or heated. Total compensation occurs.

Eq. (7) suggests, that potentially large heating or cooling effects may occur. At 1.0 torr the time scale in which the energy of the gas is removed or doubled is 1.0 s(sic!). The condition (8) can, however, be quite restrictive when radiation trapping occurs. Then γ approaches zero for densities of the order of 10^{13} cm^{-3}, giving an upper limit of $f_T = 10^{-4}\ s^{-1}$. Even in this case heating or cooling is bound to occur for long enough interaction times. To enhance the heating or cooling one should try to avoid radiation trapping. If the upper state has a cascade decay branch back to the ground state no problem will arise. It may be possible to depopulate the upper level to some high lying state by optical pumping, and the atom would cascade back to the ground state by different routes. If, however, we empty the lower level, each

atom can be processed at most once and the upper limit of the temperature change is restricted by

$$\frac{\Delta T}{T} < \frac{N}{N+N'} \frac{\hbar|\Delta|}{W_T}. \quad (9)$$

Other limits to the heating or cooling attainable are wall collisions, and for long samples, depleting of the laser pump beam.

Experimentally the heating or cooling may be detected by observing the Doppler profile of any fluorescence which is not radiatively trapped. All transitions of the sample can be used, including those of the perturber atoms. The mechanism ought to be very efficient because each CAF event exchanges the energy $\hbar|\Delta|$ directly with the thermal reservoir, in contrast to the recently proposed schemes [7] using photon recoil, which can cool or heat only one component of the velocity in each scattering event.

Another interesting feature of CAF processes is, that the collision rate usually depends on some power of the atomic velocities‡. Thus in collisionally aided heating, the rate increases and the effect escalates. On the other hand, in the cooling process, the collision rate decreases and the cooling efficiency deteriorates.

‡ To a first approximation resonant collision rates *do not* depend on relative velocities. For cooling this provides the optimum conditions. For heating foreign gas perturbers should be used.

If the collision process is utilized to selectively channel energy in or out of a specific mechanical energy mode, only the effective temperature of this mode is changed immediately. In addition to the change of translational energy for a selected species, the vibrational energy of colliding molecules could be affected. Thus the process may be utilized to enhance selective chemical reactions in the sample. One could also envisage using two lasers to heat and cool different spatial regions of a gas in order to study the subsequent mixing and turbulence of the system. The two lasers could also act on different species to produce phenomena of energy exchange and reactions.

References

[1] D.L. Huber, Phys. Rev. 178 (1969) 93.
[2] A. Omont, E.W. Smith and J. Cooper, Astrophys. J. 175 (1972) 185.
[3] V.S. Lisitsa and S.I. Yakovlenko, Soviet Phys. JETP 41 (1975) 233.
[4] P.R. Berman, Phys. Rev. A13 (1976) 2191.
[5] J.L. Carlsten, A. Szöke and M.G. Raymer, Phys. Rev. A15 (1977) 1029.
[6] W. Heitler, The quantum theory of radiation, 3rd Edition (Oxford Univ. Press, Oxford, 1954) sec. V-20.
[7] T.W. Hänsch and A.L. Schawlow, Opt. Commun. 13 (1975) 68.